5-2013

Design and Fundamental Understanding of Minimum Quantity Lubrication (MQL) Assisted Grinding Using Advanced Nanolubricants

Parash Kalita
University of Arkansas, Fayetteville

DESIGN AND FUNDAMENTAL UNDERSTANDING OF MINIMUM QUANTITY LUBRICATION (MQL) ASSISTED GRINDING USING ADVANCED NANOLUBRICANTS

DESIGN AND FUNDAMENTAL UNDERSTANDING OF MINIMUM QUANTITY LUBRICATION (MQL) ASSISTED GRINDING USING ADVANCED NANOLUBRICANTS

A dissertation submitted in partial fulfillment
of the requirements for the degree of
Doctor of Philosophy in Microelectronics-Photonics

By

Parash Kalita
Bhavnagar University
Bachelor of Engineering in Production Engineering, 2006
University of Arkansas
Master of Science in Mechanical Engineering, 2009

May 2013
University of Arkansas

ABSTRACT

Abrasive grinding is widely used across manufacturing industry for finishing parts and components requiring smooth superficial textures and precise dimensional tolerances and accuracy. Unlike any other machining operations, the complex thermo-mechanical processes during grinding produce excessive friction-induced energy consumption, heat, and intense contact seizures. Lubrication and cooling from grinding fluids is crucial in minimizing the deleterious effects of friction and heat to maximize the output part quality and process efficiency. The conventional flood grinding approach of an uneconomical application of large quantities of chemically active fluids has been found ineffective to provide sufficient lubrication and produces waste streams and pollutants that are hazardous to human health and environment. Application of Minimum Quantity Lubrication (MQL) that cuts the volumetric fluid consumption by 3-4 orders of magnitude have been extensively researched in grinding as a high-productivity and environmentally-sustainable alternative to the conventional flood method. However, the lubrication performance and productivity of MQL technique with current fluids has been critically challenged by the extreme thermo-mechanical conditions of abrasive grinding.

In this research, an MQL system based on advanced nanolubricants has been proposed to address the current thermo-mechanical challenges of MQL grinding and improve its productivity. The nanolubricants were composed of inorganic MoS_2 nanoparticles (≈ 200 nm) intercalated with organic macromolecules of EP/AW property, dispersed in straight (base) oils – mineral-based paraffin and vegetable-based soybean oil. After feasibility investigations into the grindability of cast iron using MQL with nanolubricants, this research focused on the fundamental understanding of tribological behavior and lubricating mechanisms of nanolubricants as a

method to improve the productivity of MQL-assisted surface grinding of ductile iron and alloy steel.

An extensive investigation on MQL-assisted grinding using vitrified aluminum oxide wheel under varied infeed and lubrication condition was carried out with the scope of documenting the process efficiency and lubrication mechanisms of the nanolubricants. Experimental results showed that MQL grinding with nanolubricants minimized the non-productive outputs of the grinding process by reducing frictional losses at the abrasive grain-workpiece interfaces, energy consumption, wheel wear, grinding zone temperatures, and friction-induced heat generation. Use of nanolubricants in MQL yielded superior productivity by producing surface roughness as low as 0.35 μm and grinding efficiencies that were four times higher as compared to those obtained from flood grinding. Repeatable formation of tribochemical films of antifriction, antiwear, and extreme pressure chemical species in between the contact asperities of abrasive crystals and work material was identified with nanolubricants. The tribological behavior was characterized by this synergistic effect of the antiwear, antifriction, and load carrying chemical species that endured grain-workpiece seizures and reduced adhesion friction between the contact surfaces. Delivery of organic coated MoS_2 nanoparticles by anchoring on the natural porosity of the abrasive wheel and eventually, sliding-induced interfacial deformation into tribolayers and alignment at the grinding zone were established as the lubrication mechanisms of the nanolubricants. These mechanisms were further validated from tribological evaluations of lubricated cubic boron nitride (cBN) superabrasives-1045 steel sliding pairs on a reciprocating tribotest rig resembling the tool-lubricant-workpiece interactions of MQL-assisted grinding.

This dissertation is approved for recommendation
to the Graduate Council

Dissertation Director:

_____
Dr. Ajay P. Malshe

Dissertation Committee:

_____
Dr. Gregory Salamo

_____
Dr. Douglas P. Spearot

_____
Dr. Rian Tian

_____
Prof. Ken Vickers (*ex officio*)

_____
Dr. Wenping Jiang

The following signatories attest that all software used in this dissertation was legally licensed for use by Mr. Parash Kalita for research purposes and publication.

_____ _____
Mr. Parash Kalita, Student Dr. Ajay P. Malshe, Dissertation Director

This dissertation was submitted to http://www.turnitin.com for plagiarism review by the TurnItIn company's software. The signatories have examined the report on this dissertation that was returned by TurnItIn and attest that, in their opinion, the items highlighted by the software are incidental to common usage and are not plagiarized material.

_____ _____
Prof. Ken Vickers, Program Director Dr. Ajay P. Malshe, Dissertation Director

DISSERTATION DUPLICATION RELEASE

I hereby authorize the University of Arkansas Libraries to duplicate this dissertation when needed for research and/or scholarship.

Agreed _____

Parash Kalita

Refused _____

Parash Kalita

ACKNOWLEDGEMENTS

Firstly, I would like to express my sincere thanks to my advisor Dr. Ajay P. Malshe for all the academic guidance and support throughout the course of my graduate studies and research. I would also like to thank my dissertation committee members, Dr. Greg Salamo, Dr. Douglas Spearot, Dr. Rian Tian, Prof. Ken Vickers, and Dr. Wenping Jiang for their contribution and constructive feedback on the dissertation topics. I would also like to express my sincere gratitude to all the members of the MicroEP community, especially Prof. Ken Vickers for academic guidance and Ms. Renee Jones-Hearon for providing organizational assistance.

I would like to acknowledge my colleagues at Materials and Manufacturing Research Laboratories (MMRL), for their assistance with equipment and experiments throughout my research.

I would like to thank the Materials Characterization Facility at the Institute of NanoScience and Engineering of the University of Arkansas for electron-optical equipment. I would also like to thank the Central Manufacturing Technology Institute (CMTI) for providing testing facilities for this research. This program was financially supported by the National Science Foundation (NSF), under CMMI GOALI Grant No. 0927541. Any opinions, findings, and conclusions or recommendations expressed in this material are those of the author and do not necessarily reflect the views of the National Science Foundation.

Finally, I would especially like to thank my parents and my wife for their encouragement throughout the course of my doctoral studies. The completion of this dissertation would not have been possible without their support and assistance.

TABLE OF CONTENTS

I. INTRODUCTION 1
A. Background 1
B. Tribological System of Grinding Process 2
C. Problem Statement 4
D. Research Objectives 10
II. LITERATURE REVIEW 11
A. Overview of Grinding Process 11
B. Friction, Wear, and Lubrication in Grinding 12
C. Energy Transformations in Grinding and Influence of Lubrication 17
D. Lubrication Methods and Challenges 22
1. Grinding Fluids- Advantages and Limitations 22
2. Grinding Fluid Application Systems and Challenges 25
E. Summary 31
III. PROPOSED SOLUTION, HYPOTHESIS AND TECHNICAL OBJECTIVES 35
A. Solution and Hypothesis 35
B. Technical Objectives 37
IV. DESIGN AND SYNTHESIS OF NANOLUBRICANT 40
A. Nanolubricant Composition and Material Selection 40
B. Manufacturing of Nanoparticle-Based Additive Package 44
1. Process and Equipment 44
1. Nanoparticle-Based Additive Synthesis 46
2. Organic Mediums- Triglycerides and Phospholipids 46
C. Synthesis of Nanolubricant Formulations 48
D. Chemo-Physical Characterization 50
1. Analytical Techniques 50
2. Particle Size, Shape and Surface Area 51
3. Thermal Conductivity of Nanolubricants 57
V. EXPERIMENTAL APPROACH AND TECHNIQUES 58
A. Surface Grinding Tests 58
1. Surface Grinding and MQL Setup 58
2. Grinding Lubricants 62
3. Measurement Parameters and Methods 63
B. Tribological Testing 76
1. Lubricants 76
2. Tribological Test Rig 78
3. Measurement Parameters 81
VI. RESULTS AND DISCUSSION - SURFACE GRINDING NONPRODUCTIVE OUTPUTS 83
A. Tangential Grinding Force 83
B. Force Ratio (Coefficient of Friction) 87
1. Force Ratio- 10 and 20 μm Infeed Grinding of Ductile Cast Iron 87
2. Force Ratio- 20 μm Infeed Grinding of EN 24 Steel 92
C. G- Ratio 94
1. G-Ratio - Grinding of Ductile Cast Iron 94

2. G-Ratio - Grinding of EN 24 Steel 95
D. Specific Grinding Energy 97
1. Specific Grinding Energy- 10 μm Infeed Grinding of Ductile Cast Iron 97
2. Specific Grinding Energy - 20 μm Infeed Grinding of Ductile Iron and EN 24 Steel 99
E. Grinding Temperature and Thermal Analysis 102
VII. RESULTS AND DISCUSSION- SURFACE GRINDING PRODUCTIVE OUTPUTS 110
A. Surface Integrity Of Ground Workpiece 110
1. Surface Roughness of Cast Iron Workpieces 112
2. Surface Roughness of EN 24 Steel Workpieces 110
3. Summary of Surface Roughness 114
4. Surface Topography 115
B. Grinding Efficiency 121
VIII. RESULTS AND DISCUSSION- MECHANISMS OF LUBRICATION DURING GRINDING 125
A. Tribolayers On Workpiece Surface And Abrasive Grains 125
1. Tribolayers on Ground Workpiece Surface 125
2. Tribolayers on Abrasive Grains of Grinding Wheel 130
B. Chemical Integrity Of Tribochemical Films 132
C. Formation And Deformation Mechanisms Of Tribolayers 135
IX RESULTS AND DISCUSSION- TRIBOLOGICAL TESTING 139
A. Coefficient of Friction (COF) 139
B. Surface Topography 142
C. Tribochemical Films 147
D. Effect of Nanolubricant Films on Material Removal 149
E. Evolution And Lubrication Mechanism Of Nanolubricant Films 151
X. CONCLUSION AND FUTURE WORK 155
A. Conclusion 155
B. Recommendations for Future Study 157
REFERENCES 159
APPENDICES 169
A. Tribological Performance Comparison of Solid Lubricants 166
B. Description of Research for Popular Publication 178
C. Executive Summary of Intellectual Property And Potential Patent and Commercialization Aspects 181
D. Microsoft Project for PhD MicroEP Degree Plan 182
E. Identification of All Software Used in Research and Dissertation Generation 185
F. List of Publications 186

LIST OF FIGURES

Figure 1.1	Precision grinding from standard flat grinding to complex forms	1
Figure 1.2	Tribological grinding system	2
Figure 1.3	Inputs and outputs of abrasive machining processes	3
Figure 1.4	Flood application of metalworking (MWF)/lubricant	5
Figure 1.5	Environmental impact during lubricant lifecycle	6
Figure 1.6	Distribution of cooling/lubricant costs in machining operations in the automotive industry	7
Figure 1.7	Advantages of MQL over flood and challenges of energy-intensive MQL machining	9
Figure 2.1	An example of surface grinding (left) and motions of wheel-workpiece in plunge surface grinding	12
Figure 2.2	Interaction of abrasive grains with workpiece during grinding	13
Figure 2.3	Abrasive grains engaged in rubbing, ploughing, and shearing	13
Figure 2.4	Various stages of grinding with grit depth of cut	14
Figure 2.5	Effect of grinding depth of cut on contact arc length	18
Figure 2.6	Heat flow during the grinding of metallic materials	20
Figure 2.7	Tribology system ‘Machining’	22
Figure 2.8	An example of flood (wet) grinding (left) and MQL grinding (right)	26
Figure 3.1	Proposed process of precise MQL-assisted delivery of nanolubricant at the grinding zone	36
Figure 3.2	Proposed tribological functions of nanolubricant leading to productivity enhancement of MQL grinding	37
Figure 4.1	Crystal structure of Molybdenum Disulphide	42
Figure 4.2	High-energy ball milling equipment and stainless steel vial and impact media	44
Figure 4.3	Deformations in the material trapped between two colliding balls during ball milling	45

Figure 4.4	Synthesis process of oil-based nanolubricants	49
Figure 4.5	SEM-EDS microanalysis of MoS_2 particles after 48 hours of dry milling	52
Figure 4.6	XRD spectra of the as received and 48 h dry-milled MoS_2 particles	53
Figure 4.7	TEM images of MoS_2 nanoparticles after (a) 24 hours, (b) 36 hours, and (c) 48 hours of wet (hybrid) milling	54
Figure 4.8	D50 (median) particle size distribution of dry and wet milled MoS_2 particles	55
Figure 4.9	The BET specific surface area (SSA) versus average particle size (μm) of MoS_2 particles after different stages and periods of ball milling	56
Figure 4.10	Thermal conductivity of the base oils and oil-based nanolubricants with varying concentration of MoS_2 nanoparticles	57
Figure 5.1	Surface grinding setup (left) and MQL fluid delivery system (right)	59
Figure 5.2	Microstructures of ductile cast iron (Durabar 100-70-3), a) before heat treatment b) after heat treatment	62
Figure 5.3	Mechanisms of abrasive grain wear	65
Figure 5.4	Wear groove generated on the wheel's peripheral surface during grinding	67
Figure 5.5	Embedded thermocouple method of temperature measurement	69
Figure 5.6	Schematic drawing of heat transfer during grinding	71
Figure 5.7	A ground and hardened steel surface	72
Figure 5.8	AFM images of tribofilms generated from 1.0 wt% ZDDP under different rubbing time	74
Figure 5.9	Reciprocating tribotest rig (left), (b) Lubricant delivery during tribological testing (right	79
Figure 5.10	(a) and (b) cBN-abrasive mounted pin (150 grit) and polished AISI 1045 steel workpieces, respectively, (c) and (d) SEM micrograph of new electroplated cBN pin surface and polished workpiece surface, respectively	80

Figure 6.1	Tangential force vs. passes for flood and MQL with paraffin-based lubricants, obtained during grinding of ductile iron at 10 μm wheel-infeed	84
Figure 6.2	Tangential force vs. passes for flood and MQL with soybean-based lubricants, obtained during grinding of ductile iron at 10 μm wheel-infeed	85
Figure 6.3	Force ratios (μ) for (a) flood and MQL with paraffin-based lubricants, and (b) flood and MQL with soybean-based lubricants obtained during grinding of ductile iron	88
Figure 6.4	Reduction in force ratio (μ) by 8 wt.% loaded nanolubricants as compared to 2 wt.% loaded nanolubricants and pure base oils	91
Figure 6.5	Force ratio (μ) obtained during grinding of EN 24 steel at 20 μm wheel-infeed	93
Figure 6.6	G-ratio values obtained after grinding of ductile cast iron with (a) flood and MQL with paraffin-based lubricants, and (b) Flood and MQL with soybean-based lubricants	94
Figure 6.7	G-ratio values obtained after 100 passes of grinding of EN 24 alloy steel	96
Figure 6.8	Specific grinding energy obtained during grinding of ductile iron at 10 μm wheel-infeed	98
Figure 6.9	Specific grinding energy obtained during grinding of ductile iron and at 20 μm wheel-infeed	100
Figure 6.10	Specific grinding energy obtained during grinding of EN 24 steel at 20 μm wheel-infeed	102
Figure 6.11	Maximum rise in grinding temperatures at the workpiece surface (h = 0) as function of lubrication conditions obtained during grinding of ductile iron at 10 μm wheel-infeed	103
Figure 6.12	Lubrication and cooling behavior of the tribological system of grinding with different lubrication conditions	107
Figure 7.1	Average surface roughness (R_a) measurements of ductile iron obtained after grinding with, (a) 10-μm infeed and, (b) 20-μm feed using different lubrication conditions	111

Figure 7.2 Mean surface roughness (R_a) values of EN 24 steel workpieces obtained after 100 passes of conventional (flood) grinding and MQL grinding at 20 μm infeed/pass 113

Figure 7.3 Surface profiles of ground workpiece surface obtained after 100 passes of grinding with flood application of water-soluble synthetic fluid and MQL using pure base oils 116

Figure 7.4 Surface profile of ground workpiece surfaces obtained after 100 passes of grinding with MQL using paraffin-based lubricants (micro- 8 wt.% and nano- 2 and 8 wt.%) 118

Figure 7.5 Surface profile of ground workpiece surfaces obtained after 100 passes of grinding with MQL using soybean-based lubricants (micro- 8 wt.% and nano- 2 and 8 wt.%) 119

Figure 7.6 SEM micrographs of steel surface obtained after MQL grinding with nanolubricant and pure base oil 120

Figure 7.7 Grinding-efficiency obtained during grinding of cast iron with, (a) flood and MQL with paraffin-based lubricants and, (b) flood and MQL with soybean-based lubricants 122

Figure 7.8 Grinding-efficiency obtained during grinding of EN 24 steel at 20 μm wheel-infeed using different lubrication conditions 122

Figure 8.1 SEM-EDS microanalysis of workpiece surface after 100 passes of flood grinding with synthetic MWF and MQL-assisted grinding with pure base oil (without nanoparticles) 126

Figure 8.2 SEM-EDS microanalysis of ground workpiece (ductile iron) surfaces lubricated with 2 wt.% and 8 wt.% loaded nanolubricants 127

Figure 8.3 Debris accumulations over workpiece and its surroundings during MQL grinding of ductile cast iron and EN 24 steel with soybean-based nanolubricant 128

Figure 8.4 Optical images of nanolubricant-lubricated vitrified-bond Al_2O_3 wheel showing retention and entrapment of nanolubricant in the wheel porosity 130

Figure 8.5 SEM-EDS microanalysis of abrasive grains from vitrified-bond Al_2O_3 wheel, (a) before grinding and (b) after MQL grinding of ductile iron with nanolubricant 128

Figure 8.6	Raman characterizations of tribochemical films derived from 8 wt.%- loaded soybean and paraffin-based nanolubricant during MQL grinding of ferrous workpiece	133
Figure 8.7	Raman characterization of tribochemical films derived from 8 wt.%- loaded nanolubricant during MQL grinding of ferrous workpiece at 10 and 20 μm depth of cut	134
Figure 8.8	SEM-EDS microanalysis of 8 wt.%-loaded nanolubricant tribofilms formed during MQL grinding at (a, b) 10 and, (c, d) 20 μm wheel-infeed	136
Figure 8.9	Cross-sectional microstructure of nanolubricant tribofilm; EDS line scan confirms the presence of Molybdenum and Sulphur especially in zones where no iron debris was detected	138
Figure 9.1	Coefficient of friction vs. sliding time plots for (a) base oils and (b) MoS_2 nanoparticles-based lubricants	140
Figure 9.2	Average values of friction coefficient obtained after 1 h tribotest or 6070 sliding cycles with different lubrication conditions	141
Figure 9.3	Surface profiles of workpieces, obtained after 1-hour tribotest or 6070 sliding cycles with different lubrication conditions	143
Figure 9.4	SEM micrographs of cBN pin surfaces, obtained after 1 h tribotest or 6070 sliding cycles with different lubrication conditions	144
Figure 9.5	SEM micrographs of workpieces, obtained after 1 h tribotest or 6070 sliding cycles with different lubrication conditions; arrows indicate sliding direction	145
Figure 9.6	SEM-EDS microanalyses of tribochemical films formed on workpiece weartracks after 1 h (6070 sliding cycles) of tribotest	147
Figure 9.7	Workpiece material loss (in grams) vs. lubrication condition	150
Figure 9.8	SEM micrographs of tribochemical films derived from nanoparticles integrated lubricant	152
Figure 9.9	SEM micrograph showing multi-layer structure of tribofilm derived from organic-coated MoS_2 microparticles	153

LIST OF TABLES

Table 2.1	Grinding fluids characteristics (1-worst; 4-best)	24
Table 2.2	Summary of MQL-assisted grinding studies	34
Table 4.1	Smoke and flash temperatures of triglyceride sources	47
Table 4.2	Compositions of the nanolubricants	48
Table 4.3	Physical properties of base oils	50
Table 5.1	Surface grinding process parameters	60
Table 5.2	Workpiece material specifications	61
Table 5.3	List of lubricants	63
Table 5.4	Typical G-ratio values for different abrasive wheel types during grinding of various workpiece materials	67
Table 5.5	Grinding parameters used for temperature measurements and thermal analysis	71
Table 5.6	List of lubricants for tribological testing	77
Table 5.7	The chemo-physical properties of the base fluids	77
Table 5.8	Tribological test parameters	79
Table 6.1	Summary of heat transfer analysis in grinding experiments	105

LIST OF SYMBOLS

MoS_2	Molybdenum Disulphide
Al_2O_3	Aluminum oxide
cBN	Cubic boron nitride
MQL	Minimum quantity lubrication
MWF	Metal working fluid
EP	Extreme-pressure
AW	Antiwear
U	Specific grinding energy
$U_{chip\text{-}formation}$	Specific grinding energy for chip formation
$U_{ploughing}$	Specific grinding energy for ploughing
$U_{sliding}$	Specific grinding energy for sliding
μ	Coefficient of friction
V_s	Wheel peripheral speed
V_w	Workpiece speed
F_t	Tangential grinding force
F_n	Normal grinding force
F_{ts}	Sliding component of tangential grinding force
F_{ns}	Sliding component of normal grinding force
q	Total power flux
a_e	Depth of cut (infeed)
l_c	Grinding arc contact length
b, b_w	Grinding width
Q_w	Volumetric material removal rate
D_m	Mean wheel diameter
ΔR	Decrease in wheel radius
V_{rw}	Volume of radial wheel wear
V_{mr}	Volume of material removed
θ_{max}	Maximum temperature rise
q_w	Heat flux entering into workpiece
k	Thermal conductivity of the workpiece
α	Thermal diffusivity of the workpiece
d_s	Grinding wheel diameter
P	Grinding power
ε	Energy partition
R_a	Arithmetic average roughness
Micro (8%)	Lubricant containing 8 wt./vol% of MoS_2 microparticles
Nano (2%)	Nanolubricant with 2 wt.% loading of organic coated nanoparticles
Nano (8%)	Nanolubricant with 8 wt.% loading of organic coated nanoparticles

I. INTRODUCTION

A. BACKGROUND

Grinding is an abrasive surface generation process widely used for shaping and finishing parts and components requiring smooth surface textures and precise dimensional tolerances. In comparison to other material removal processes, grinding can machine harder materials with extremely high dimensional accuracy and low superficial roughness. Grinding has been reported to produce flatness tolerances of less than ± 0.0001 in. [1] and surface finish of upto 0.1 μm, which is about ten times better than turning or milling processes [2]. Furthermore, it can machine surfaces of different shapes and contour, including, flat, vertical, slot, and angular surfaces as well as radius grinding, as shown in Figure 1.1. As a result, it has been reported for upto 25% of total machining expenditures and almost every machined part or product are either finished or shaped by grinding or by machines that owes their accuracy to grinding processes [3]. From delicate precision slicing of silicon wafers to high accuracy finishing of piston pins, crankshafts, bearings, valves and heavy-duty stock removal of castings, abrasive grinding finds extensive applications in almost every manufacturing industry.

Figure 1.1 Precision grinding from standard flat grinding to complex forms [4]

B. TRIBOLOGICAL SYSTEM OF GRINDING PROCESS

By definition, tribology is the science and engineering of contact surfaces in motion and primarily studies friction, wear, and lubrication [5]. A tribological grinding system is an abrasive material removal process that functions by removing chip from the workpiece fed against a bonded abrasive wheel rotating at very high speeds (20-140 m/s). The elements of tribological system of grinding are shown in Figure 1.2. It includes the bonded abrasive wheel (abrasive ceramic grains), workpiece material, process fluid (lubricant), and materials from the environment, such as, air, dust, swarf, etc. The tribological relationships between these elements define the thermo-mechanical processes occurring at the grinding zone. These thermo-mechanical processes play a decisive role in friction, heat transfer, and lubrication during grinding [6], which are discussed in the next chapter.

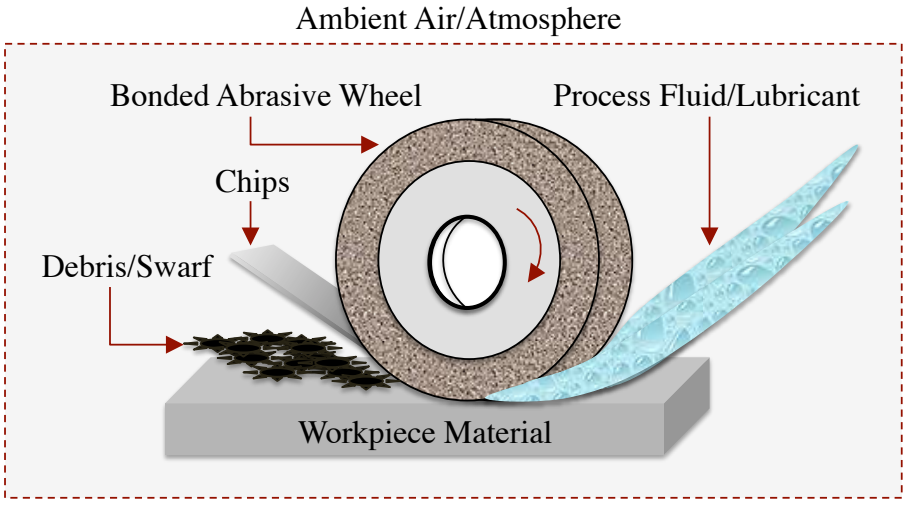

Figure 1.2 Tribological grinding system

The various inputs and outputs of the tribological grinding system are shown in Figure 1.3.

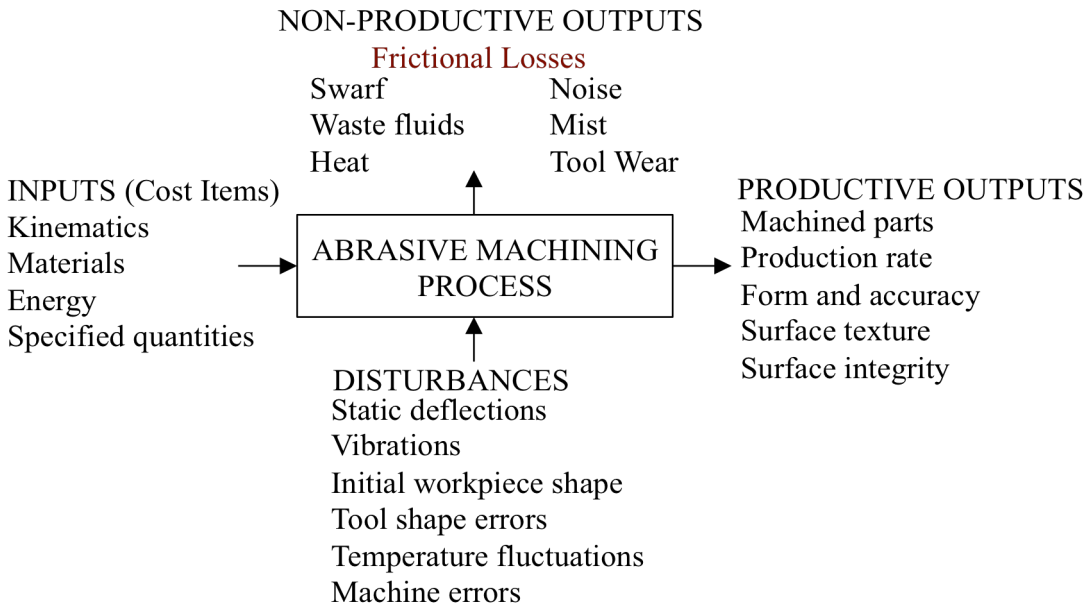

Figure 1.3 Inputs and outputs of abrasive machining processes [7]

The input parameters consist of the kinematics or interactive motions between the abrasive grains and workpiece, process parameters, consumable materials including tools, workpiece, process fluid or lubricant, etc., and energy input. The productive output of the grinding process is the ground part and its required qualities such as, production rate, from and accuracy, and surface finish and integrity. The process also consists of a number of modes of controllable and unavoidable disturbances. Like any other intrinsic input-output system, a grinding system also has process losses that include frictional losses, wear products, and waste fluids. Excessive frictional loss during abrasive grain-workpiece interaction is the major nonproductive output of grinding process. Severe sliding friction results in higher forces, wheel wear, and energy requirement for material removal. Nearly all the energy concentrated at the grinding zone is dissipated as heat that leads to high grinding temperatures (reaching upto 500-700°C) capable of causing thermal damage and distortions to the workpiece [8]. Lubrication and cooling from

grinding fluids is crucial in minimizing the non-productive outputs of friction and heat and increase the production efficiency of the tribological system of grinding.

C. PROBLEM STATEMENT

Use of metalworking fluids (MWFs) or lubricants is extremely important in grinding because it influences the productive outputs of the process, such as part quality, surface integrity, wheel life, and material removal by:

- Reducing friction and hence, specific energy and wear by lubricating the chip-grain and grain-workpiece contact interfaces.
- Cooling the grinding zone by removing heat from the grain-workpiece interfaces.
- Maintaining clean surfaces by flushing the chips and debris away from the grinding zone.
- Inhibiting in-process corrosion.

The type of grinding process, workpiece and wheel material, and specified part quality levels guides the selection of grinding fluids/lubricants. The type of fluid (oil or water-based) and its chemical additive composition and fluid application method determines the lubrication and cooling efficiency of a grinding fluid. A sufficient quantity of right composition of fluid should be delivered at the point of cut or the grinding zone in order to achieve optimum performance during grinding. Despite such important considerations, the decisions related to the selection and application of grinding fluids has been based on traditional beliefs and industrial customs rather than knowledge-based quantitative analysis. Flood grinding, i.e., flooding the grinding area with a large volume of MWFs is one such conventional approach as shown in Figure 1.4. Such heavy and wasteful application of MWFs has adverse technical, environmental and economic effects, which must be solved or minimized to achieve energy-efficient and sustainable manufacturing.

Scientific studies have reported the inability during flood application of fluid to penetrate into the high hydrodynamic pressure-grinding zone, resulting in a major volume of the fluid being deflected away from the point of cut without yielding sufficient lubrication [9].

Figure 1.4 Flood application of metalworking fluid (MWF)/lubricant [10]

The second and the foremost effect is the health and safety concerns of millions of workers exposed to chemically active MWFs during grinding operations. Flood application of MWFs generates excessive amount of waste streams and airborne mist that causes dermatitis, hypersensitivity pneumonitis, respiratory illness, and several types of cancer [11]. Typical lubricant mist concentration from conventional flood application in US automotive parts manufacturing is 20-90 mg/m^3 [12], as compared to permissible exposure limits of 5 mg/m^3 and 0.5 mg/m^3 as per as OSHA and NIOSH [12]. Waste streams of MWF promote microbial infestation and their disposal after the end of useful life lead to environmental pollution, such as soil and water contamination. The environmental impact during the lifecycle of a lubricant (MWF) in machining operations is shown in Figure 1.5.

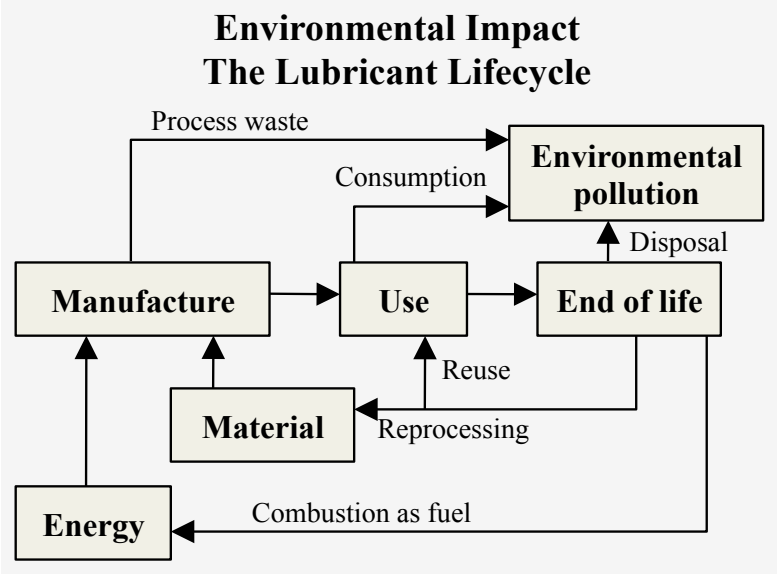

Figure 1.5 Environmental impact during lubricant lifecycle [13]

Apart from health and environmental concerns, flood grinding has serious economic concerns as well. Strict environmental laws and protocols require special handling and processing of fluids before disposal, such as chemical pretreatment. The costs associated with such treatments, along with the cost of application and recirculation of high-volume of MWFs, is usually higher than the cost of the fluid [14,15]. The costs of MWF consumption in machining operations has been reported to constitute about 7-17% of the total cost of production, which exceeds the tooling costs (approximately 4% of total production cost) [13]. Figure 1.6 shows an exemplary industrial data on the lubricant related costs in machining operations.

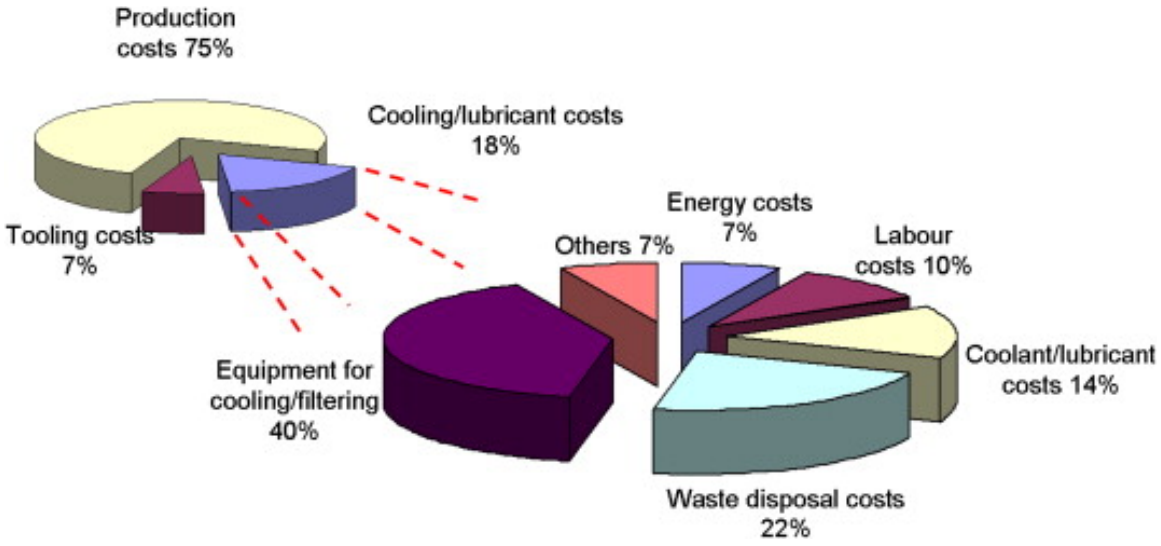

Figure 1.6 Distribution of cooling/lubricant costs in machining operations in the automotive industry (data from a Danobat-Ideko internal report, updated on March 2010) [15]

Serious efforts have been made in the last decade to develop advanced environmentally conscious machining processes that utilize less or no lubricants. Dry machining (coolant-less) and minimum quantity lubrication (MQL) have emerged as the feasible alternatives to conventional flood machining. Dry machining that completely eliminates the use of MWFs has been extensively studied. Although it has showed feasibility in certain machining processes, there are still many issues that limit its productivity. The critical issues include requirement of special tools and coatings, concerns related to tool life, lubrication, and thermal distortion and damage to the machined parts and components [16-26]. In such conditions, minimum quantity lubrication (MQL) becomes an attractive alternative for sustainable machining.

MQL refers to the precision delivery method of lubricant (in the form of droplets or mist using compressed air) directly at the tool-workpiece point of contact and the consumption of lubricant is 3-4 orders of magnitude lower than that of conventional flood application method [27-28]. MQL has been extensively researched in the past decade and has been successfully implemented

in machining operations with well-defined cutting edge geometry, including, turning [29-33], milling [34-38], and drilling [25, 39-41]. Successful cases of industrial application of MQL include Ford's Advanced Manufacturing Technical Development (AMTD) in automotive powertrain component production and General Motors Powertrain Division. A recent report has revealed that by implementing MQL in powertrain manufacturing, Ford is anticipating annual cost savings of upto $ 2.80 million [42] The key benefit of MQL is good lubrication that reduces tool-workpiece friction during machining and provides some internal cooling. MQL provides significant cost savings due to the reduction of fluid use and disposal while maintaining similar or better level of output part quality as compared to flood machining, which suggest viability of high-productivity and environmentally-sustainable machining with a well-designed MQL process.

After the extensive development of MQL technology in the past years, the current imposing challenge is its successful implementation in energy-intensive abrasive grinding processes. Due to the overwhelming importance of grinding processes in industrial manufacturing, MQL has been widely researched in grinding. However, its lubrication performance has been critically challenged by the extreme thermo-mechanical conditions of abrasive grinding as shown in Figure 1.7. In depth discussions on these conditions are given in the chapter II. Figure 1.7 also summarizes the unique advantages of MQL over flood machining.

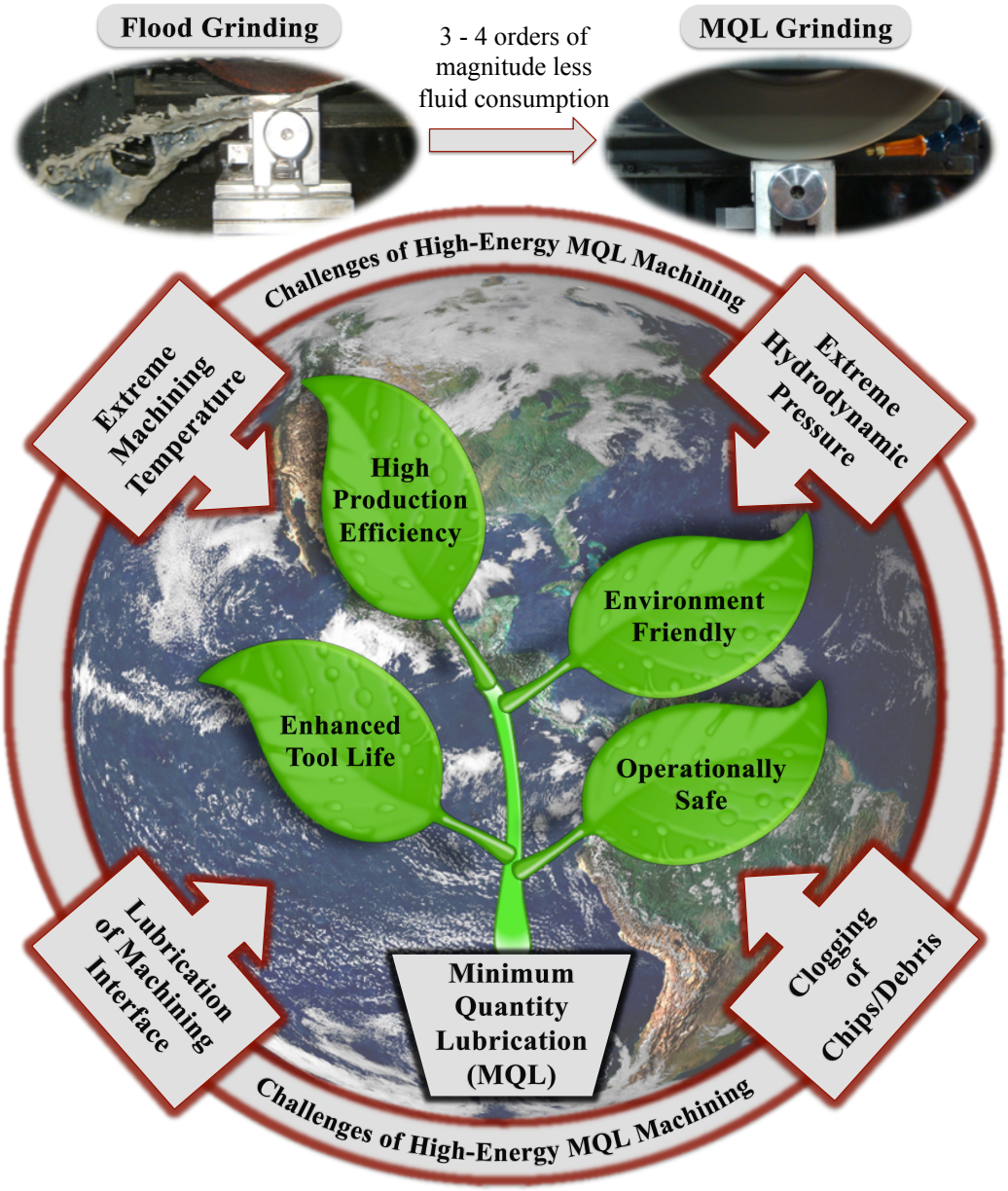

Figure 1.7 Advantages of MQL over flood and challenges of energy-intensive MQL machining

The goal of this research was to address the current thermo-mechanical challenges of MQL grinding and improve its process productivity. This research focused on developing an effective MQL system based on advanced nanolubricants. Nanolubricants proposed in this research were

advanced oil-based formulations for MQL machining, developed by integrating multiple organic-inorganic material chemistries at nanoscale.

D. RESEARCH OBJECTIVES

To understand the tribological behavior and the lubricating mechanisms of nanolubricants as a method to improve the process performance of MQL-assisted surface grinding of ductile iron and alloy steel, the following research objectives were addressed in this study:

1. Design and synthesis of nanolubricant compositions for MQL
2. MQL-assisted surface grinding with conventional Al_2O_3 wheels under varying downfeed conditions to study the lubrication effectiveness of nanolubricants by quantifying and analyzing the non-productive and productive outputs of the process
3. Evaluation of the state and mechanisms of lubrication in the grinding zone from structural and chemical microanalysis of tribochemical films formed at the contact surfaces of workpiece and Al_2O_3 abrasive grains
4. Evaluation of friction and wear in the tribosystem of nanolubricant-lubricated cubic boron nitride (cBN) superabrasives-1045 steel sliding pair on a reciprocating tribotest rig resembling the tool-lubricant-workpiece interactions of MQL-assisted grinding

II. LITERATURE REVIEW

This chapter presents a review of scientific literature relevant to the tribological and lubrication fundamentals of grinding systems. The literature review is divided into four sections including, (A) overview of grinding process, (B) friction, wear, and lubrication in grinding, (C) energy transformations in grinding and influence of lubrication, (D) existing lubrication methods and challenges.

A. OVERVIEW OF GRINDING PROCESS

Grinding is an abrasive material removal process that employs numerous abrasive grains contained in a bonded wheel for material removal and surface generation [2]. During grinding, fresh surfaces of workpiece are continuously fed against the bonded abrasive wheel that rotates at very high surface speeds (20-140 m/s) as compared to other machining operations. Also unlike other machining processes, grinding is an energy-intensive process that involves large energy transformation and concentration into workpiece. Several types grinding operations exists depending on wheel-workpiece configuration including, surface grinding, cylindrical grinding, and centerless grinding. Each of these grinding process is carried out using either conventional abrasive wheels (aluminum oxide, silicon carbide) or superabrasive wheels (cBN, diamond). This research utilized reciprocating surface grinding with a conventional aluminum oxide wheel. As shown in Figure 2.1, the workpiece traversed (reciprocating linear motion) in a plane relative to the grinding wheel. Upon contact with the grinding wheel, a minute quantity of material was cut from the workpiece thereby creating a plain flat surface. The traversing speed of the workpiece was 300-500 times lower than the surface speed of the rotary wheel. For continuous material removal, the grinding wheel was given a small downfeed after the end of each grinding

pass or cycle to make contact with the reciprocating work material. The downfeed motion of the grinding wheel was precisely controlled to cut a specified depth of workpiece material.

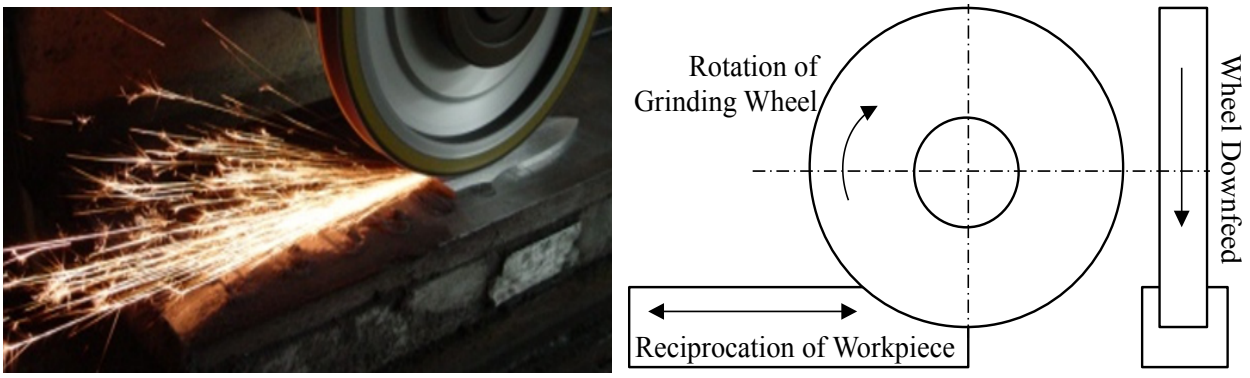

Figure 2.1 An example of surface grinding [43] (left) and motions of wheel-workpiece in plunge surface grinding (right)

B. FRICTION, WEAR AND LUBRICATION IN GRINDING

Friction and wear conditions of a tribological process are dependent on the interaction of the system components. In grinding, the interacting system components include the tool (bonded abrasive wheel), workpiece, and the state of lubrication. The tool-workpiece contact geometry and interaction of grinding is complex as compared to other machining processes. The bonded wheels consist of numerous abrasive crystals of undefined geometries (rake angle varying from + 45 ° to - 60 ° or more) and are randomly scattered on the wheel periphery [44]. As a result, the process of grinding is characterized by relatively large and geometrically varying wheel-workpiece contact area. Due to this unique grain-workpiece contact, grinding-generated chips are of relatively smaller thicknesses (0.25-25 μm) as compared to continuous (several millimeter thick) chips of other machining processes [45]. During grinding, the abrasive crystals engage with the workpiece surface at random orientations and locations as shown in Figure 2.2.

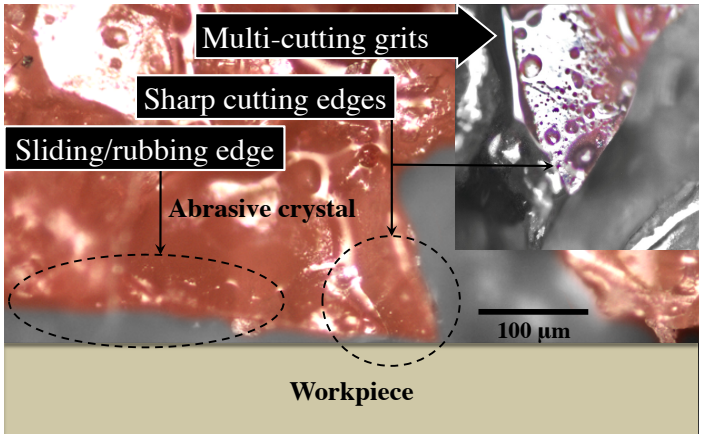

Figure 2.2 Interaction of abrasive grains with workpiece during grinding [46]

At microscopic levels, the complex grain-workpiece interaction of chip formation has been simplified to micro cutting (shearing), rubbing, and ploughing [7], as shown in Figure 2.3. These interactions are determined by the grain geometry, penetration of grains into the workpiece, and workpiece material characteristics. Abrasive grains with favorable sharp geometries and penetration produce chips by shearing the work material, while abrasive grains with large –ve rake angles or rounded edges lead to rubbing and ploughing that does not contribute in chip formation [47].

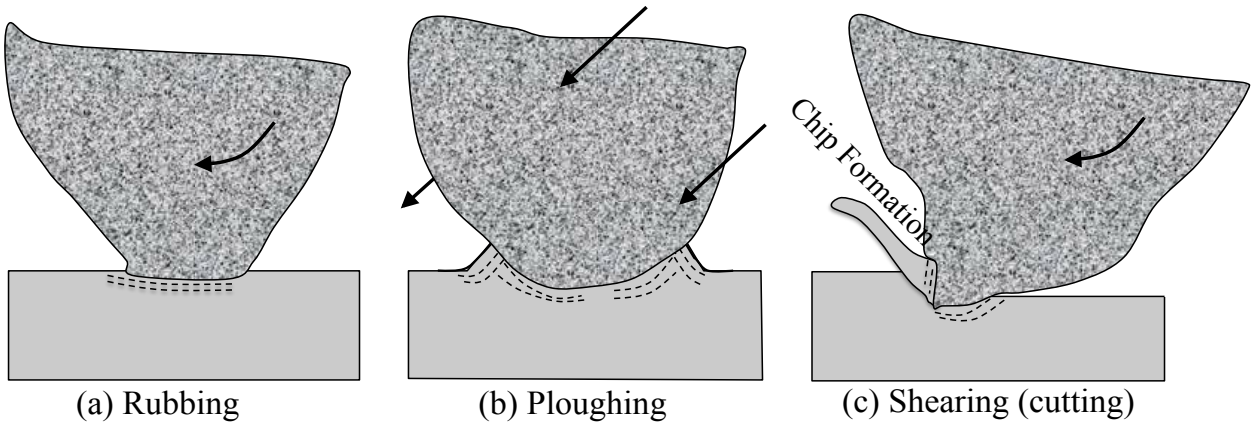

Figure 2.3 Abrasive grains engaged in rubbing, ploughing, and shearing

Figure 2.4 shows the three stages of material deformation as a function of grinding force and grain penetration depth.

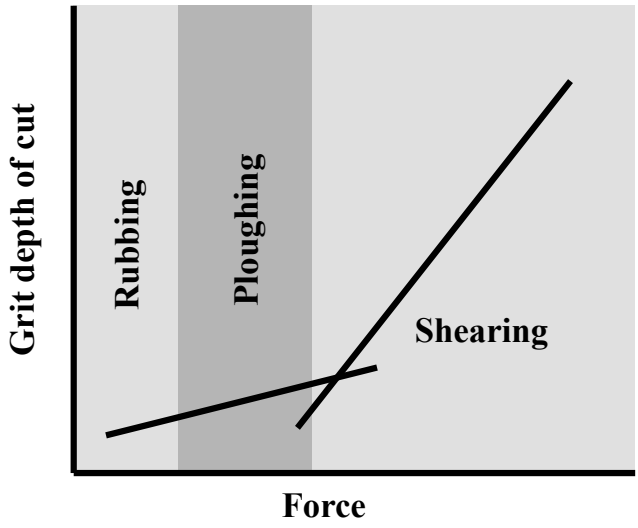

Figure 2.4 Various stages of grinding with grit depth of cut [46]

In the sliding stage, the abrasive grains pass through the workpiece with small penetration without forming any chips. With further increase in grain penetration, the abrasive grains plows through the workpiece that pushes the work material upward and sideways to form ridges or lateral pile up. This process also does not contribute in chip formation, as the ploughed material remains adhered to the workpiece. With further increase in penetration depth, the abrasive grains cuts through the workpiece material in the form of chips. As seen from Figure 2.4, the rate of increase of grinding force with an increase in grain penetration depth is much less during cutting as compared to the non-productive stages of rubbing and ploughing. Even though rubbing and ploughing do not contribute in chip formation, they increase frictional losses and hence, force requirement, energy consumption and wear of abrasive grains [48]. During rubbing and ploughing modes, the hard abrasive grains causes plastic-flow of the relatively soft workpiece

material that eventually leads to adhesion friction. Adhesive friction due to the severe surface deformation in abrasive-workpiece contact leads to tribochemical reactions that are responsible for attritious wear of abrasive grains [3,7]. These reactions involve constant formation and separation of atomic bonds between the molecules of interacting surfaces (grains and workpiece) and between the interacting surfaces and the environment. In conventional grinding with Al_2O_3 wheels, tribochemical reactions between abrasives and metal oxides (of workpiece) have been reported to cause rapid grain wear by forming spinel type complexes [3,7],

FeO (ferrous oxide) + Al_2O_3 (aluminum oxide) → $FeAl_2O_4$ (Hercynite- spinel mineral)

Equation 1

Another wear-causing tribochemical reaction is between the grain-workpiece contact surfaces, catalyzed by water molecules that are absorbed from the surrounding environment during grinding [8],

$$2Fe + O_2 + 2Al_2O_3 \xrightarrow{H_2O} 2FeAl_2O_4 \qquad \text{Equation 2}$$

Attritious wear from tribochemical reactions wear out the sharp edges of abrasive grains that eventually leads to the formation of new or enlarged wearflats on the wheel periphery. Sliding of wearflats against a workpiece without any material removal accounts for undesirable expenditure of grinding energy, as discussed in the next section II.C

The state of lubrication can play a decisive role in lessening or aggravating adhesive sliding friction and the related tribochemical reactions. Friction prevails as the contact or the grinding zone is deprived of, or insufficiently supplied, with lubrication. Effective lubrication can reduce adhesive friction (and tribochemical reactions) by forming protective tribolayers at the contact

zone. Primary lubrication mechanisms that can lead to the formation of protective as well as lubricating tribochemical films/layers in a grinding process include:

- Physisorption- Physisorbed tribolayers are weakly bonded to the friction surfaces by van der Waal forces without any material transfer [7]. The performance of such layers is limited to low temperature and loading (pressure) conditions. Surface temperatures higher than 100 °C causes desorption of such tribolayers. Metal Disulphide and oil films are typical examples of physisorbed tribolayers.
- Chemisorption- Chemisorbed tribolayers are formed by chemical bonding (electron transfer) between the molecules of adsorbate and active friction surface (e.g. freshly machined reactive metallic surface) [7]. These films are stable and stronger than physisorbed layers. However, high surface temperatures (greater than the characteristic desorption point of a layer) lead to their release or desorption from the workpiece surface [8]. Friction modifier (FM) additives in lubricants form chemisorbed layers.
- Chemical triboreaction- Triboreaction layers are directly formed on the workpiece surface by either internal reaction within the lubricant additives or tribochemical reaction between additives and metallic surface. These layers are sacrificial that inhibit material transfer between the contact surfaces and can withstand moderate temperatures [7]. Example of such tribolayers includes those formed by antiwear (AW) and extreme-pressure (EP) lubricant additives [7].

Abrasive grinding is an extreme-pressure and temperature process with an undefined tool-workpiece contact geometry [2]. Therefore, the effectiveness of a lubrication system in grinding will strictly depend on:

- Thermally stable lubricant composition with enhanced tribological properties.

- A precise and sufficient supply of lubricant at the grinding zone.
- The formation of protective (load carrying) low-friction tribolayers at the grinding zone by synergistic mechanisms including, physisorption, chemisorption, and triboreaction.

C. ENERGY TRANSFORMATIONS IN GRINDING AND INFLUENCE OF LUBRICATION

Material removal during grinding is accompanied by a high consumption of energy, nearly 100 times higher than other material removal processes [45]. It has been found that the specific grinding energy consists of three components corresponding to the three stages or mechanisms of material deformation [3]:

$$\text{Specific grinding energy, } U = U_{\text{chip-formation}} + U_{\text{ploughing}} + U_{\text{sliding}} \qquad \text{Equation 3}$$

For material removal, only chip-formation energy is actually consumed and hence, it represents the minimum energy requirement. As mentioned before, much of the grinding energy is consumed by the non-productive mechanisms- ploughing and sliding. The later largely consists of sliding of wearflats against the workpiece without any material removal. The sliding component of specific grinding energy has been found proportional to A_a, which is the effective contact area of the abrasive wearflats with the workpiece [3].

$$U_{\text{sliding}} = \mu \cdot (F_{ns}) \cdot V_s = \mu \cdot (\bar{p} \cdot A_a) \cdot V_s \qquad \text{Equation 4}$$

Where,

- μ- Coefficient of friction between the wearflats and the workpiece
- F_{ns}- Normal grinding force proportional to grain wear flat area (A_a)
- $\bar{p}$- Average contact pressure
- V_s- Wheel peripheral speed

The effective wearflat area (A_a) of the grinding wheel increases with grinding passes (or time). The material properties of interacting abrasive and workpiece, wheel dressing conditions, and grinding parameters such as infeed or depth of cut also affect the growth rate of wearflat area [3]. Increment in depth of cut extends the length of contact arc and hence, the area between the grinding wheel and the workpiece as shown in Fig 2.5 and thus, increases the possibilities of growth of wearflat areas.

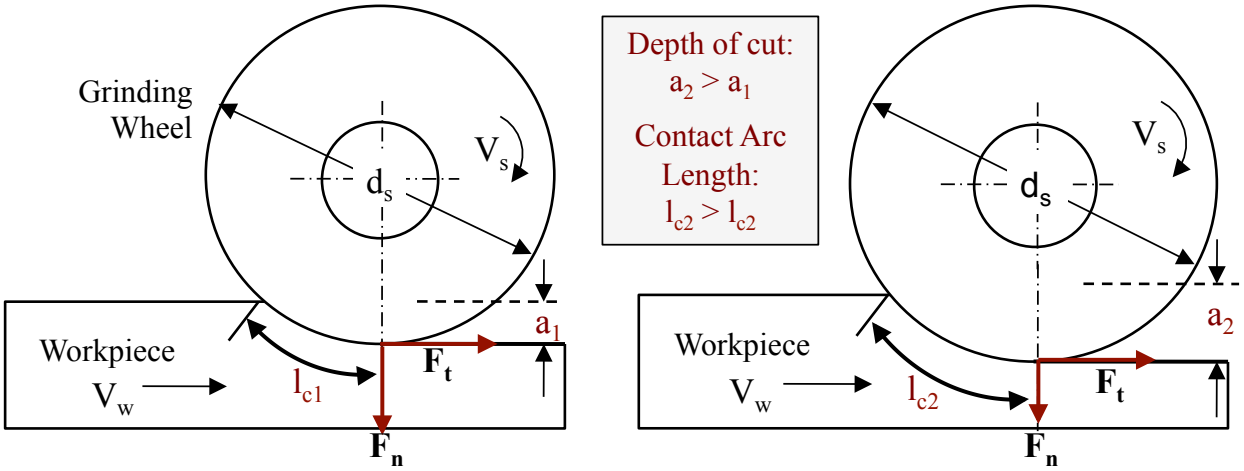

Figure 2.5 Effect of grinding depth of cut on contact arc length

In Equation 2,

$$\mu \cdot F_{ns} = \mu \cdot \bar{p} \cdot A_a = F_{ts} \qquad \text{Equation 5}$$

Where, F_{ts} is the fraction of total tangential force (F_t) that is required to overpower sliding friction during grinding.

Thus, based on Equations 4 and 5, the sliding component of specific energy can be written in terms of tangential force component as,

$$U_{sliding} = F_{ts} \cdot V_s \qquad \text{Equation 6}$$

Grinding forces can be expressed in terms of chip-formation and sliding components [3]:

$$\text{Tangential Force } (F_t) = F_{t\cdot\text{chip-formation}} + F_{ts} \qquad \text{Equation 7}$$

$$\text{Normal Force } (F_n) = F_{n\cdot\text{chip-formation}} + F_{ns} \qquad \text{Equation 8}$$

Equations 7 and 8 can be rewritten as,

$$\text{Tangential Force } (F_t) = F_{t\cdot\text{chip-formation}} + \mu\cdot\bar{a}\cdot A_a \qquad \text{Equation 9}$$

$$\text{Normal Force } (F_n) = F_{n\cdot\text{chip-formation}} + \bar{a}\cdot A_a \qquad \text{Equation 10}$$

Combining Equations 9 and 10,

$$F_n = \frac{1}{\mu} F_t + \frac{\mu\cdot F_{n.\text{chip-formation}} - F_{t.\text{chip-formation}}}{\mu} \qquad \text{Equation 11}$$

For a given set of grinding conditions, the cutting (chip-formation) components of forces remain constant [3]. Hence, the graph of F_t vs. F_n would yield a straight line with μ (coefficient of friction) as its slope. Based on Equation 9, a decline in sliding friction (drop in μ) and wearflat area (A_a) would reduce tangential force requirement. The grinding forces have a direct influence on power consumption ($P = F_t.V_s$) and specific grinding energy (from Equation 4 and 3). Such reductions in grinding forces and specific energy by reducing friction and wear are feasible through effective lubrication at the sliding interfaces of abrasive grains and the workpiece. Hence, from friction and wear point of view, suggestive influences of effective lubrication in grinding are:

- Reduction in sliding frictional losses at the contact zone of abrasive grains (in particularly wearflats) and workpiece.

- Reduction in the growth of wearflats- reduction in attritious wear of grains (of wheel) by forming reaction layers that prevent material transfer between the abrasive grains and metal surface.
- Reduction of friction between the chip surface and the abrasive grains as well as wheel bond, as shown in Figure 2.6 and friction between the wheel bond and the workpiece surface, resulting in a decline in bond abrasion and hence, grain wear [49].
- Increase in elasto-plastic deformation of the workpiece material underneath the abrasive grains, resulting in a better surface finish of the ground parts and components [49].

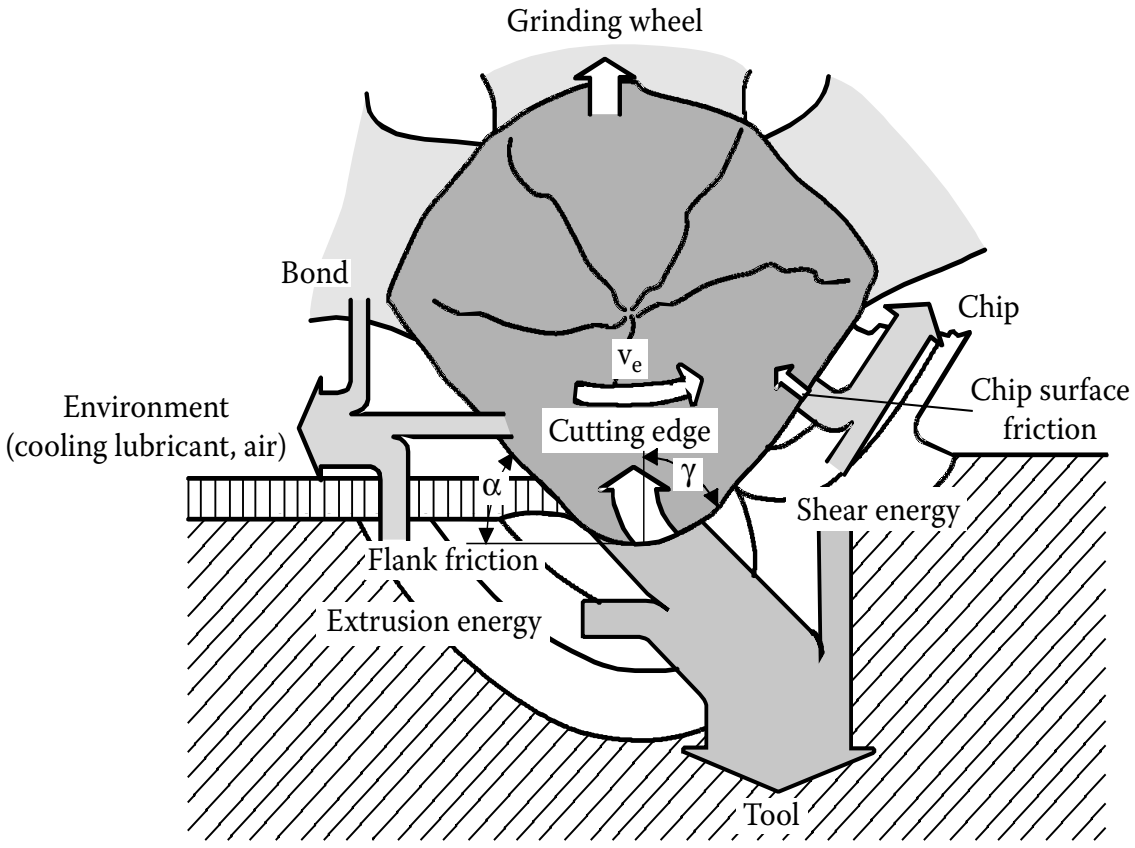

Figure 2.6 Heat flow during the grinding of metallic materials [49]

Sliding friction between the abrasive grains and the workpiece has a direct effect on the power or energy flux (power generated per unit area) at the grinding zone. The total power flux (q) generated at the grinding zone is given by [50],

$$q = {}^{F_t \cdot V_s}\!/_{l_c \cdot b} \qquad \text{Equation 12}$$

Where, the numerator is the grinding power that is proportional to the tangential force and hence, sliding friction, μ (from Equations 7 and 5) and the denominator is the grinding contact area (contact arc length, l_c × grinding width, b).

The energy concentrated at the grinding zone is primarily transformed into heat. As compared to cBN superabrasives, the conventional ceramic wheels made of Al_2O_3 and SiC, have poor thermal conductivities. As a result, a high percentage (upto 60-85%) of the total heat flux dissipates into the metal workpiece. This leads to a substantial rise in localized surface temperatures, reaching upto 400°C- 500°C [8], and is capable of causing serious thermal damage and distortions of the surface layers of the ground workpieces. Many external friction (sliding) and internal friction processes have been found contributing to friction heat generation and flow during grinding [49]. The external processes include grain-workpiece, grain-chip, and wheel bond-workpiece contact friction during grinding (Figure 2.6.). Internal processes include friction through plastic deformation and displacement of material during grinding [49]. A precise and sufficient supply of lubricants can provide thermal relief by:

- Reducing friction between the various contact parts, resulting in reduced heat flux generation and hence, easy thermal damage-free dissipation through the workpiece.
- Convection cooling of the grinding zone and its surroundings including the bulk workpiece area.

Figure 2.7 summarizes the overall lubrication and cooling effects of a lubricant on the tribological grinding system.

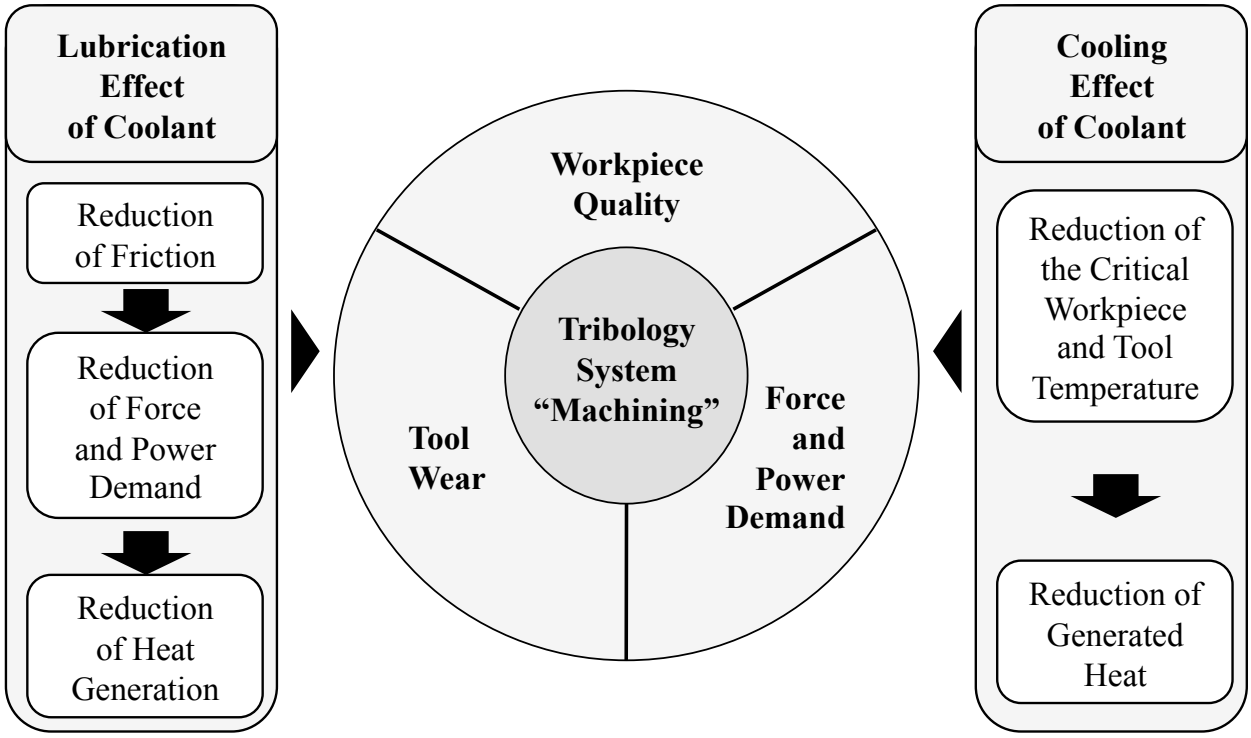

Figure 2.7 Tribology system 'Machining' [6]

D. LUBRICATION METHODS AND CHALLENGES

Grinding Fluids- Advantages and Limitations

According to Silva et al. [51], selection of an effective grinding fluid is an important part of the optimization of grinding process that can provide optimum productivity, tool life, and workpiece quality. The resultant tribological properties from the type and composition of the fluids play a decisive role in lubrication and cooling performance during grinding. Most of the conventional grinding fluids can be categorized into straight (neat) cutting oils and water-miscible fluids. Straight grinding oils are either mineral-based (paraffin) oils or natural fatty oils. They are

compounded with polar (fatty) additives for lubrication and/or chemically active additives/compounds based on sulfur and/or chlorine for antiwear performance [8]. The water-miscible fluids are emulsifiable (soluble) oil, semisynthetic (semi chemical-based) fluids or synthetic (chemically formulated fluids). These water-soluble fluids are compounded with many chemical additives such as emulsifiers, surfactants, rust inhibitors, water conditioners, foam inhibitors, EP additives (sulfur and chlorine-based compounds), biocides, and many others [52]. Out of all chemical additives, the correct composition and properties of friction modifiers, antiwear (AW), and extreme-pressure (EP) additives are very important for the tribochemical functioning of a grinding fluid. Existent grinding fluids contain polar compounds, such as fatty acids or their derivatives, as friction modifiers that have strong affinities for metals and form low-friction films at the sliding interfaces [53]. EP and AW additives develop reaction layers on the surface asperities of the workpiece to prevent contact seizure and adhesion or loading of metallic particles on abrasive wheel. They are typically organic compounds based on Phosphorus, Chlorine, and/or Sulfur [8]. Chlorinated additives are under scrutiny for potential health concerns while heavy presence of sulphurized compounds causes metal staining and rancidity [54].

Table 2.1 (adapted from [53]) lists the characteristics of the major types of grinding fluids.

Table 2.1 Grinding fluids characteristics (1-worst; 4-best) [53]

Properties	Synthetics	Semi-Synthetics	Soluble Oils	Straight Cutting Oils
Heat removal	4	3	2	1
Lubricity	1	2	3	4
Maintenance	3	2	1	4
Filterability	4	3	2	1
Environmental	4	3	2	1
Cost	4	3	2	1
Wheel life	1	2	3	4

In grinding, straight cutting oils have been found to be better lubricants than the water-miscible fluids. The straight oils that are used without any dilution have been reported to yield good lubrication (friction reduction) performances in grinding different workpiece materials. The key advantages of straight oil lubrication include lower grinding forces, low specific energies, lower wheel wear, and better surface quality. At the same time, the poor cooling property of straight oils often limits their production rates as compared to the water-miscible fluids. Other disadvantages of straight oils include, their messy or sticky nature, the fire hazard, and high cost [55]. During grinding, straight oils tend to produce mist and fumes that are considered health hazards [53] and often require solvent-assisted removal from the ground parts [55]. Due to these disadvantages, the use of straight oils is mostly restricted to heavy-duty grinding operations involving cBN wheels as compared to conventional grinding with Al_2O_3 or SiC wheels. This is primarily due to the low cooling requirements of cBN grinding, where water-based fluids fail to provide effective lubrication.

Despite superior lubricity, water miscible fluids (especially soluble oils) outperform straight oils in commercial and industrial use. Unlike straight oils, these fluids are diluted in water at different

proportions depending on the type of grinding application. The key advantages water-based fluid is their superior transfer coefficient [53], which helps to control bulk workpiece temperature and prevent thermal damage and distortion of the ground workpiece [3]. In limitations, water-miscible fluids have extremely poor lubricity and many of its additives are known to cause skin diseases from frequent handling and contact irritation [56]. After poor lubrication, the biggest disadvantage of water miscible fluids is biodeterioration from bacterial and fungal attack [56,57]. A wide range of organic additives in water-based coolants serves as nutrient sources for microorganisms. Microbial infestation causes degradation of fluid components that leads to technical as well as hygienic and allergic problems [56, 57].

Based on the above analysis, it can be concluded that no fluid in its current form has the ability to provide optimum lubrication and cooling during grinding and hence, needs formulation development.

Grinding Fluid Application Systems and Challenges

Like any other machining process, grinding continuously generates new surfaces. With each grinding pass, lubricant-derived tribochemical films are virtually removed from the workpiece surface. To sustain lubrication and cooling in such conditions, a precise and sufficient supply of fluid is continuously required at the grinding zone that is characterized by high contact pressure and temperatures. Therefore, the effectiveness of a fluid application system is unarguably important for achieving desirable performance from the grinding fluids.

The conventional and still the most widely used fluid application method in grinding is flood (wet) application. As shown in Figure 2.8, this method floods the workpiece with grinding fluids by means of nozzles.

Figure 2.8 An example of flood (wet) grinding (left) and MQL grinding (right)

The flooding nozzles are typically pointed tangentially at the grinding zone and utilize different cross-sectional designs to manipulate the velocities/pressure of the coolant (fluid) jet. This method typically uses water-miscible fluids (largely, soluble oils diluted in water) at very high volumetric flow rates, typically ranging between 5-13 l/min. Flood grinding provides superior convection cooling of the bulk workpiece and flushing of machining swarf/debris. However, despite high-volume application of grinding fluids, its lubrication performance is generally poor. The key techno-economic challenges and limitations of conventional flood grinding are as follows:

- The high-rotational speeds of grinding wheel have been reported to introduce an air barrier at the wheel circumference that restricts the fluid penetration into the grinding zone [6,9]. To penetrate the air barrier, special jet nozzles are often employed to increase the pressure and velocities of the coolant jet. The use of such high-pressure jet application is very limited and its ability to penetrate into the high hydrodynamic pressure-grinding zone has been reported to vary [9].
- The costs associated with pressurized jet type delivery of fluids is usually high and causes high levels of aerosol mists that are hazardous to human health and environment [6].

- The energy consumption for fluid delivery due to hydrodynamic effect, system cooling and electric-operated air filter has been reported to be about 19% of overall energy consumption [56].
- The fluids are continuously filtered and recirculated during grinding operation to reduce volumetric usage, and that adds to the total production cost.
- The use and disposal of the water-based fluids accounts for about 7-17% of the total machining costs because of the fluid's short working life [58].
- The disposal of the fluids has several biological and environmental problems and often encounters strict government regulations for treatment and waste disposal.

In order to completely eliminate the use of MWFs and the related problems, the feasibility of dry (coolant-less) machining has been researched [16-26]. Generation of high forces, tool wear, superficial roughness, and temperatures have been reported with dry grinding [6,59], which indicated severe technical and production-related challenges of this manufacturing technique.

Near-dry lubrication or minimum quantity lubrication (MQL) offers a technologically and environmentally feasible bridge between flood and dry machining. MQL has been found to yield numerous advantages, in terms of both productivity and environment-friendliness, as compared to flood application. Some of the prominent advantages of MQL over flood application were shown earlier in Figure 1.7. MQL combines the functionality of lubrication and cooling the machining zone with an extremely low consumption of fluids, 3-4 orders of magnitude less than that of flood application [60]. MQL system delivers a targeted stream of lubricant mist at the machining zone with flow rates ranging between 10-500 ml/h and air pressure between 4-6.5 psi [51]. In MQL, straight-cutting oils (mostly mineral-based oils) are generally used due to their better lubricity than the water-miscible fluids. After successful implementation and performance

validation in machining processes such as turning, drilling, and milling, the use of MQL in grinding has been a subject of current research. The feasibility of MQL in grinding has been extensively studied using many combinations of grinding oils/fluids, workpiece materials, and grinding wheels. The following two sections discuss the current state-of-the-art studies of MQL grinding using conventional Al_2O_3 and cBN wheels.

1. **MQL grinding with conventional Al_2O_3 wheels**- In their keynote review, Brinksmeier et al. [6] has reported MQL studies with conventional Al_2O_3 grinding wheels dating back to 1997. Based on the reviewed results of low grinding forces but high wheel wear and superficial roughness with MQL as compared to flood grinding, it was concluded that MQL is only feasible in fine grinding with a proper selection of type and composition of fluid. Hafenbraedl and Malkin [61] demonstrated feasibility of MQL (12 ml/h flow rate) with ester oil by producing power, specific grinding energy, and tool wear that were comparable or superior to those obtained from flood grinding (5.3 l/min flow rate). However, MQL showed higher surface roughness as compared to flood grinding. Similar results were also reported by Sadeghi et al. [62] in shallow cut grinding of titanium alloy, where MQL (15-140 ml/h flow rate) showed reduction in tangential forces but produced high surface roughness in comparison to flood condition (8.4 l/min flow rate). By optimizing the design and positioning of the MQL nozzle and the lubricant-air flow rate, Silva et al. [51] showed that MQL (40-60 ml/h flow rate) with chlorinated MWF (LB 1000) reduces tangential forces, diametral wheel wear, and surface roughness as compared to 8400 ml/min of flood application. Investigation by Tawakoli et al. [63] confirmed these results by showing low tangential forces and surface roughness by optimizing the MQL-specific process parameters. Results of improved superficial

roughness of ground workpieces with MQL were also reported in investigations mentioned elsewhere in [9, 64, 65]. Use of MQL has also been reported to produce higher residual stresses in ground workpieces [9, 51]. Residual compressive stress is always beneficial as it improves the fatigue and fracture strength and hence, life of ground parts and components. Improvements in material cutting have been observed from superior lubrication of MQL technique [11, 65]. Studies on chip morphology during surface grinding of AISI 1060 steel showed shearing and fracture type chip formation with MQL (vegetable oil at 120ml/h) as opposed to shearing, ploughing, and rubbing modes with flood (using soluble oil) and dry grinding [11]. As compared to flood grinding, MQL with vegetable oil also showed some relative reduction in grinding zone temperature. But the measured temperatures were in the high ranges of 300-600 °C (for 10-40 μm infeed). Such elevated temperatures are capable of producing surface and subsurface thermal damage to the workpiece [3].

Ineffectiveness of MQL in providing direct cooling was also confirmed by Shen et al. [8] and Hadad et al. [66]. During surface grinding of ductile iron, Shen et al. [8] reported grinding temperatures of 444 °C and 106 °C for MQL (15 ml/min) and flood application (5400 ml/min), respectively, using water-based synthetic fluid for both cases. Measurement of energy partitions showed 84% of grinding heat flux entering into workpiece during MQL grinding, as compared to 24% with flood application. While thermal analysis of grinding processes by Hadad et al. [66] showed average convection heat transfer coefficients of 3.7×10^4 – 4.3×10^4 W/m^2 and 900-1500 W/m^{2}K for flood and MQL grinding, respectively. To improve cooling performance of MQL fluids by enhancing their thermal conductivity, the use of nanofluids containing solid particles of

Al_2O_3 (40 nm) and diamond (200 nm) has been reported in grinding [67]. MQL application of nanofluids (5 ml/min) showed some reduction in grinding forces and wheel wear, but showed no improvement in grinding temperatures as well as surface roughness as compared to flood cooling.

Hence, consistency in superficial roughness of ground workpieces and control of heat flux and temperatures at the grinding zone are the key challenges of MQL grinding with conventional Al_2O_3 wheels.

2. **MQL grinding with cBN superabrasives-** The feasibility of MQL has also been studied in grinding with cBN superabrasive wheels that have low fluid cooling requirements due to their high thermal conductivity (about 55 times higher than Al_2O_3). Also, cBN superabrasive wheels are extensively used for high-productivity grinding of high-speed and super-alloy due to their higher abrasive resistance and hardness as compared to Al_2O_3 wheels [68]. In a comprehensive study of MQL using Al_2O_3 and cBN wheels, Silva et al. [51] found mixed grinding performance of MQL with cBN wheels. Use of MQL yielded low tangential forces and high compressive residual stresses, but produced high diametral wheel wear and workpiece surface roughness as compared to flood condition. Alves et al. [69] reported high surficial roughness with MQL grinding using cBN wheel due to internal surface damage caused by the accumulation of slurry in the grinding zone. Some improvements in surface roughness have been reported by using special MQL arrangements, such as, additional compressed air jet for cBN wheel cleaning [70] and hybrid MQL with low-temperature CO_2 gas [71].

Using MQL application of soybean oil (5 ml/min), Shen et al. [72] reported low force

ratios and equivalent tangential forces as compared to flood cooling (5400 ml/min), suggesting better lubricity of soybean oil in cBN grinding. However, MQL was unable to reduce superficial roughness, even though grinding temperatures and workpiece energy partitions were relatively higher than flood cooling, but were low as compared to those obtained from MQL grinding with Al_2O_3 wheel. Similar thermal conditions were also reported by Hadad et al. [73], where grinding with cBN and Al_2O_3 wheels showed workpiece energy partitions of 46-48% and 73-77%, respectively, for MQL as compared to respective measurements of 14% and 36% with flood grinding.

Hence, grinding with cBN wheels can address the problem of insufficient cooling capacity of MQL. However, reduction of workpiece surface roughness and the wear of expensive cBN wheels from high strength and sustenance of lubricant films at the grinding zone remains a key challenge of MQL-assisted cBN grinding.

E. SUMMARY

Based on the analysis of available literatures, including tribological interactions in grinding, and state-of-the-art grinding fluids and application methods, the MQL-specific lubrication challenges are summarized below:

- Tribological property- High-hydrodynamic pressure at the machining interface inhibits liquid lubricant from reaching the grinding zone and the extreme grain-workpiece contact pressure at the grinding zone tends to desorb the lubricant films from the surface asperities. Tribological properties of lubricant composition must be able to sustain these conditions to deliver sufficient lubrication effect at the grinding zone with minimal fluid consumption.

- Thermal stability- Low flow rates and low thermal conductivities of oil-based fluids used during MQL are unable to produce sufficient cooling effect within the grinding zone. Therefore, the MQL-delivered lubricant system must yield effective lubrication to reduce heat producing grinding power in the machining zone for convenient dissipation without causing any thermal damage.
- Consistent superficial finish- The grinding-generated chips and abrasive debris become trapped at the contact asperities due to low flushing capacity of MQL and deteriorates the quality of ground surfaces by increasing friction and abrasion. MQL-delivered lubricant films must inhibit such detrimental material transfer for productivity enhancement of the grinding process.
- Environmental sustainability- Though fluid consumption of MQL is 3-4 orders of magnitude less than flood application, but it mostly uses mineral-based oils delivered by pressurized streams of air. During grinding, it forms hydrocarbon mist, smoke and vapors that are harmful for human inhalation [51]. Due to this, non-hazardous vegetable-based oils have been increasingly used in MQL. However, based on the available reports, these oils need improvement in their tribological properties for able to deliver effective lubrication in MQL grinding.

The goal of this research was to address these challenges by developing a new paradigm in MQL grinding. As a part of this process, a new lubricant formulation was developed for MQL by adding base (straight) oils with solid lubricant particles and organic precursors of friction polymers. The integral part of this lubricant composition was the functionalization of solid lubricant nanoparticles, which is discussed at greater length in the following chapters.

Solid lubricants have made great inroads in applications involving high loads and contact stresses, such as gear oils, antiseize grease, and metal deformation processes. The use of solid lubricants is particularly favored in applications where sliding surface asperities are of rough texture, e.g. the abrasive grain-workpiece sliding contact motion during grinding. Under such conditions, where liquid lubricants are squeezed out, solid lubricants effectively cover the surface asperities of the contact surfaces and shield against adhesive as well as abrasive friction and wear [74]. Despite apparent advantages, the exploration and prior use of solid lubricants in grinding fluids or MWFs are surprisingly very limited. Few investigations on the direct application of graphite and MoS_2 microparticles (without any carrier fluid) have been reported in grinding [75-77]. The experimental findings were encouraging, showing some reductions in grinding forces and energy. Performance comparisons showed improved lubrication by MoS_2 as compared to graphite [76]. In another investigation, slotted Al_2O_3 wheels impregnated with graphite were used for surface grinding of bearing steel that showed improvements in wheel-workpiece friction with an increase in the number of lubricant-filled slots [77]. Special wheel and apparatus design, wheel cleaning, and swarf removal are key issues of such direct applications of solid lubricants and are limited to interrupted grinding operations only. Alberts et al. [78] applied fluids containing graphite nanoplatelets by spraying and coating methods and studied their grinding performance as a function of form, size and concentration of nanoplatelets and carrier media. Table 2.2 shows the values of relevant input and output (performance) parameters used by some prominent researches in MQL grinding using Al_2O_3 wheels. These values were considered as benchmarks for the selection of input process parameters and performance evaluation of the proposed MQL exploration and fundamental understanding.

Table 2.2 Summary of MQL-assisted grinding studies

Ref.	Lubricant		Grinding Process	Input Parameters	Flow Rate		Performance Parameters (MQL vs. Flood)		
	MQL	Flood			MQL	Flood	Condition of Forces and Energy	Max. G-Ratio (MQL)	Min. Surface Roughness (MQL)
Feasi. Research [27,28]	MoS_2-based nanolubricants (oil-based)	Water-based synthetic fluid (5% conc.)	Plunge surface grinding	V_S = 30 m/s, a_e = 10 µm, V_w = 2400 mm/ min, Passes = 200, Wheel- Al_2O_3 (32A46-HVEP) Workpiece- Cast iron (50 HRc)	300 ml/h	5.4 l/min	$F_{MQL} < F_{flood}$ $U_{MQL} < U_{flood}$	42	-
[61]	Ester-based oil MQL+ cold air (- 2 C)	Soluble oil (at 5% conc.)	Internal cylindrical grinding	V_S=37m/s, V_w= 6600mm/min a_e = 300 µm, Passes = 5, Wheel- Al_2O_3 (32 A80- J5VBE) Workpiece- AISI 52100 steel (60 HRc)	12 ml/h	5.3 l/min	$U_{MQL} < U_{flood}$	40	0.49-0.87 µm
[51]	LB 1000 (chlorinated MWF) Air Vel.- 20,30,40 m/s	Soluble oil (at 5% conc.)	Plunge cylindrical grinding	V_S = 30 m/s, V_w= 20000 mm/min , Passes = 90, a_e = 100 µm, Wheel- Al_2O_3 (FE 38A60KV), Workpiece- ABNT 4340 steel (54 HRc)	40-60 ml/h	8.4 l/min	$F_{MQL} < F_{flood}$		0.41 µm (lowest) (MQL- 60 ml/min Air velocity- 20 m/s)
[67]	Nanofluids (Al_2O_3 and diamond nanoparticles in water) Water-based fluid (5%)	Water-based synthetic fluid (5% conc.)	Plunge surface grinding	V_S = 30 m/s, a_e = 10 µm, V_w = 2400 mm/ min, Passes = 155, Wheel- Al_2O_3 (32A46-HVEP) Workpiece- Ductile cast iron (50 HRc)	300 ml/h	5.4 l/min	$F_{MQL} < F_{flood}$	33 (MQL- 4% Al_2O_3 nps in water)	0.58 µm (water-based fluid) $Ra_{MQL} > Ra_{flood}$

Ref.	Lubricant		Grinding Process	Input Parameters	Flow Rate		Performance Parameters (MQL vs. Flood)			
	MQL	Flood			MQL	Flood	Forces Roughness (Ra)	Max. Temp. Rise	Max. Heat Flux into Workpiece	Max. Energy Partition
[7]	Water-based synthetic fluid (5% conc.)	Water-based synthetic fluid (5% conc.)	Plunge surface grinding	V_S = 30 m/s, a_e = 10 µm, V_w = 2400 mm/min, Wheel- Al_2O_3 (32A46-HVEP) Workpiece- Ductile cast iron (50 HRc)	900 ml/h	5.4 l/min	-	444 °C (MQL) 106 °C (Flood)	34.5 W/mm² (MQL) 8.3 W/mm² (Flood)	83 % (MQL) 24 % (Flood)
[64]	Mineral-based oil Air- 4 bar)	Water-miscible synthetic (5% conc.)	Plunge surface grinding	V_S = 30 m/s, a_e = 30 µm, V_w= 2000 mm/min, Wheel- Al_2O_3 (89A60I6V217) Workpiece- Hardened steel (50 ± 2 HRc)	100 ml/h		$F_{MQL} = F_{flood}$ Ra_{MQL}= 1.0 µm	123 °C (MQL) 55 °C (Flood)	-	73% (MQL) 36 % (Flood)

Solid Lubricants in Grinding						
[78]	Graphite nanoplatelets in different liquid media	Surface grinding	Application Method: Spraying and Coating	Min. Tangential Force = 28 N	Min. Specific Energy = 780 MPa	Min. Surface Roughness = 0.28 µm

III. PROPOSED SOLUTION, HYPOTHESIS AND TECHNICAL OBJECTIVES

A. SOLUTION AND HYPOTHESIS

Advanced nanolubricant-additized straight oil was proposed as a solution to address the current lubrication-related challenges and enhance the productivity of MQL grinding. Nanolubricant proposed in this research was a unique combination of multi-constituent nanomaterial additives in mineral and vegetable-based oils. The architecture of the nanoadditive package consisted of chalcogenide *hcp* layered MoS_2 nanoparticles (< 100 nm) with intercalated as well as capping layers of organic triglycerides and phospholipid macromolecules of antiwear/extreme-pressure property. This unique combination was anticipated to offer immediate opportunity for MQL-assisted ready delivery and prolonged residence of tribo-enhanced lubricant additives at the aggressive grinding interfaces. The following tribological mechanisms were hypothesized for nanolubricants to improve the efficiency and productivity of MQL-assisted grinding:

- **Accurate delivery at the grinding zone**- Assisted by the precise fluid delivery of MQL and due to their nano size and high surface energy, the organic coated nanoparticles would anchor and reside within the porosity, micro cavities, and capillary networks of the grinding wheel, as shown in Figure 3.1. This would lead to assured penetration and delivery of nanolubricants at the micro interfaces between the abrasive grains and the workpiece at the grinding zone.
- **Decomposition into tribochemical films**- The synergistic effect of polarity of organic molecules and high surface energy of inorganic nanoparticles was believed to enhance the chemo-physical absorption of nanolubricants on the reactive ferrous (workpiece) surface. Sliding motion between the abrasive grains (including wearflats) and the workpiece under extreme pressure conditions during grinding would lead to the plastic

deformation of the low strength shearing MoS_2 nanoparticles to deliver low-friction tribolayers, as shown in Figure 3.2. Simultaneously, the organic macromolecules of nanolubricant would react with the metallic surface to yield antiwear/extreme-pressure films.

- **Evolution of sacrificial tribofilms**- This would reduce frictional losses at the sliding interfaces, while EP/AW tribofilms would reduce contact seizure and attritious wear of the abrasive grains. These collective mechanisms would eventually lead to increased material cutting and less ploughing and rubbing, which would reduce grinding forces, energy/power requirements, and heat flux for easy dissipation and increase the useful life of grinding wheel.
- **Adhesion to the metallic chips**- The nanolubricant films would adhere to the chips to prevent material transfer and scuffing damage to the ground surface and yield better surface quality.

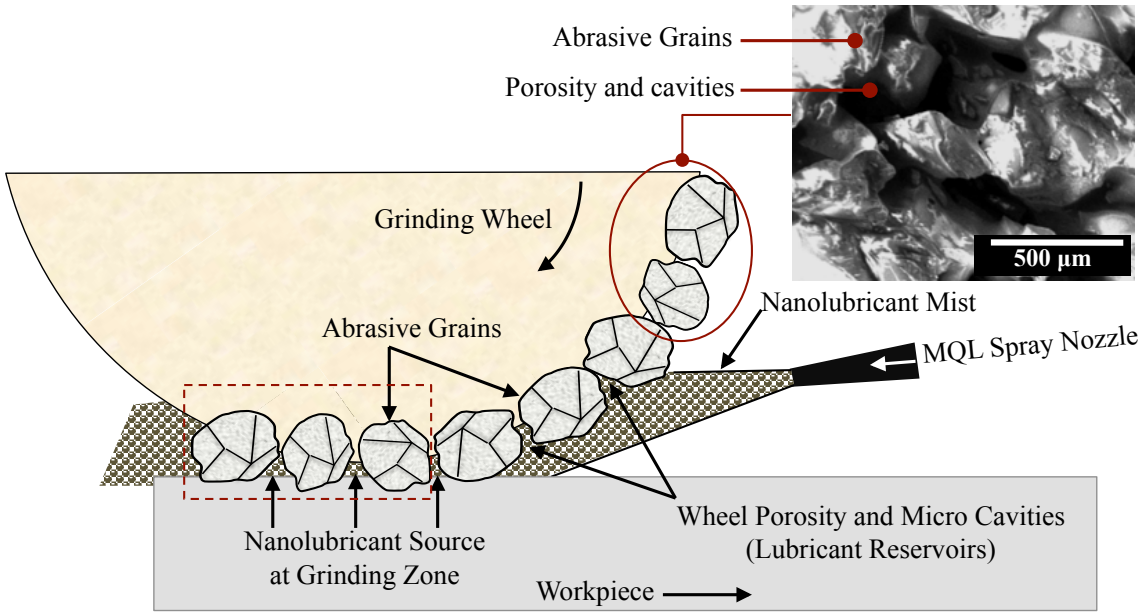

Figure 3.1 Proposed process of precise MQL-assisted delivery of nanolubricant at the grinding zone

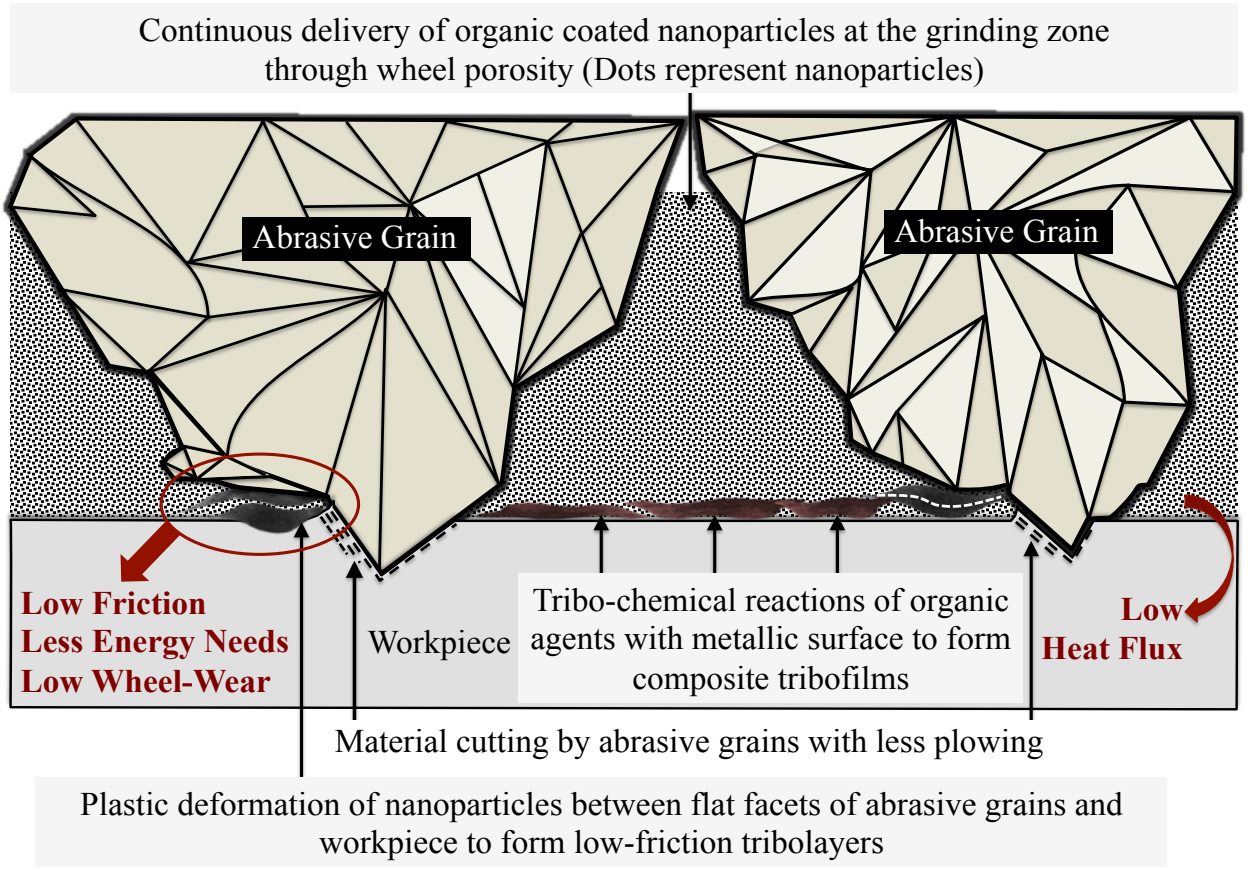

Figure 3.2 Proposed tribological functions of nanolubricant leading to productivity enhancement of MQL grinding (figure not to scale)

B. TECHNICAL OBJECTIVES

To experimentally validate the research hypotheses, following technical objectives were set and addressed in this study:

1. Design and synthesis of nanolubricant compositions for MQL
    a. Nanolubricant composition and material selection
    b. Synthesis of nanoparticle-based additive package and oil-based nanolubricant formulations
    c. Chemo-physical characterization of nanoparticles and nanolubricants, including

particle size, shape (morphology), surface area, and thermal conductivity measurement

2. Surface grinding studies with different lubrication conditions (flood, MQL with base fluids, and MQL with oil-based nanolubricants)
    a. Designing of MQL application test bed, selection of grinding process parameters, wheel and workpiece materials, and analytical tools
    b. MQL-assisted surface grinding with conventional Al_2O_3 wheels under varying downfeed conditions to study and compare the lubrication effectiveness of nanolubricants with other lubrication conditions by quantifying and analyzing:
        - Grinding forces and force ratios (coefficient of friction)
        - Specific grinding energy
        - G-ratio
        - Grinding zone temperature measurement and thermal analysis
        - Workpiece surface integrity
        - Grinding efficiency
3. Study the mechanisms of lubrication during grinding by analyzing:
    a. Structural and chemical microanalysis of lubricant derived tribolayers formed on the workpiece surface and the abrasive grains
    b. Chemical integrity of the tribochemical films formed at the contact interfaces of the abrasive grain and the workpiece during grinding
    c. Physical formation and deformation of tribolayers at the at the contact interfaces of the abrasive grain and the workpiece during grinding

4. Evaluate wear and friction in the tribosystem of nanolubricant-lubricated cubic boron nitride (cBN) superabrasives-1045 steel sliding pairs
    a. Design reciprocating tribotest rig resembling the tool-lubricant-workpiece interactions of MQL-assisted grinding with cBN superabrasives
    b. Tribological testing of nanolubricant compositions to verify their antifriction and antiwear characteristics with those obtained from the MQL grinding experiments by quantifying:
        - Coefficient of sliding friction,
        - Surface characteristics of workpiece wear tracks and cBN grains
        - Structural and chemical microanalysis of tribochemical films and other reaction products deposited on the contact surfaces of workpiece and cBN grains

IV. DESIGN AND SYNTHESIS OF NANOLUBRICANT

This chapter describes the design and composition details of the organic-inorganic additive package and nanolubricants, methods and equipment used for the synthesis of additive and nanolubricants, and the various characterization methods that were used to measure the chemo-physical properties of nanoparticles and nanolubricant compositions. The chapter is divided into four sections, A) nanolubricant composition and material selection, B) manufacturing of nanoparticle-based additive package, C) synthesis of nanolubricant formulations, and D) chemo-physical characterization.

A. NANOLUBRICANT COMPOSITION AND MATERIAL SELECTION

To effectively lubricate the elasto-plastic hydrodynamic regime of grinding zone, an oil-based nanolubricant composition was designed. It consisted of a multi-functional lubricant additive package in commercially available off-the-shelf straight (base) oils- mineral based paraffin oil and vegetable based soybean oil. The lubricant additive package was composed of inorganic solid-lubricant nanoparticles that were functionalized with organic precursors of triglycerides and phospholipids. Organic functionalization was in the form of intercalation and capping layers that led to encapsulation of inorganic nanoparticles in polar media as well as amphiphilic emulsification. This multicomponent-based single additive package offered key tribochemical characteristics to nanolubricants including antifriction, antiwear, and extreme-pressure properties. The following section describes the rationale of selection of solid lubricant nanoparticles, while descriptions of organic media and base oils are given in the next sections.

Solid Lubricant Nanoparticles

Three solid lubricant nanoparticles- Molybdenum Disulphide (MoS_2), Graphite, and Hexagonal Boron Nitride (hBN) were considered as potential candidates in this research. They all belong to the class of lamellar structured inorganic lubricants and have their own advantages and limitations. Owing to the excellent friction reduction performance in abrasive contacts, quasi-spherical MoS_2 nanoparticles (≈ 200 nm) was selected for use as solid lubricant particles in the nanoadditive package. The comparison of the properties and friction test results of the solid lubricant nanoparticles are discussed in Appendix I.

In the proposed nanolubricant, MoS_2 nanoparticles functioned as extreme-pressure (EP) bearing friction modifiers. The following are the unique properties of MoS_2 that validated its suitability as lubricant additive for abrasive grinding:

- **Load carrying lubrication** - MoS_2 is a lamellar solid with intrinsic low-friction properties. Exceptional low-friction of MoS_2 is due to the weakly bonded hexagonal planes of its crystal structure as shown in Figure 4.1. The hexagonal (basal) planes are held together by weak sulfur-sulfur bonds (van der Waal bonds) that imparts low-shear strength in the direction of sliding motion. However, strong interplaner sulfur-molybdenum-sulfur bonds impart high-compressive strength against forces applied perpendicular to the hexagonal planes. This load carrying (EP) capacity of MoS_2 resists penetration by surface asperities. Unlike graphite or any other solid lubricant, the lubrication effectiveness of MoS_2 has been reported to improve with an increase in contact forces [74].

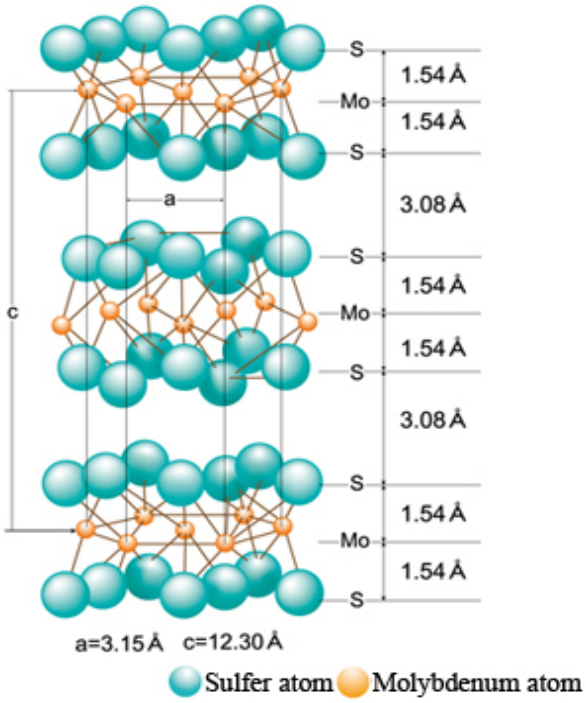

Figure 4.1 *hcp* layered crystal structure of Molybdenum Disulphide [82], weak S-S bonds between hexagonal planes result in low-friction

- **Film-forming capacity** - MoS_2 is known to form strong cohesive tribofilms on the metal surfaces. When smeared between sliding contact surfaces, the shear (friction) forces cause sliding induced deformation and orientation of MoS_2 layers and formation of thin lubricating films. The presence of large number of oleophilic tails provides MoS_2 films with good adhesion to metal surfaces [80]. Such films have been reported to have low coefficient of friction, ranging between 0.025-0.2 [74,81,82] and high load carrying (EP) capacity of 5×10^5 psi, which is higher than the yield strength of metals [80]. Along with physisorbed tribolayers, MoS_2 also forms chemisorbed tribofilms on metal surfaces. Decomposition of MoS_2 releases sulfur that reacts with metallic surfaces to form low-friction metal sulfide species.
- **Dispersion compatibility**- MoS_2 particles are chemically inert and do not produce any

undesirable cross interactions when added to different base fluids/oils and other chemical additives at room temperature [80].

The selection of nanostructured particles was based on the enhancement of tribological properties of MoS_2 with a reduction in particle size and shape modification. This was well supported by previous feasibility research on the machinability of lubricants containing MoS_2 nanoparticles [28].

1. **Nanosize effect** - The proposed advantages of the use of nanoparticles in the lubricants were enhanced confinement at the wheel porosity/micro cavities and the small-tolerance asperities of the contact surfaces and the subsequent release and furnishing of nanoparticles at the grinding zone. Other advantages included high dispersion stability and more active lubricant particles per unit volume of lubricant as compared to micro sized particles. Many tribological studies of lubricant films derived from MoS_2 nanoparticles have reported low coefficient of friction at boundary lubrication regimes [81-83]. A study on shock-absorption and failure mechanisms of MoS_2 nanoparticles (inorganic fullerenes, IF) by Zhu et al. [84] has reported survival of MoS_2 nanoparticles under 25 GPa of shock load and concurrent temperatures of 1000 °C with trivial structural damage.
2. **Shape effect** - The preference on quasi-spherical over commercially available platelets type nanoparticles was based on literature-reported thermo-mechanical advantages of the former in sliding friction contacts [83,85]. Quasi-spherical (IF) nanoparticles have been reported to facilitate their sliding mechanisms between rubbing contacts [83]. Experimental tribological studies under high contact loads and humid atmosphere have suggested shorter lubricant lifetime of 2H-MoS_2 particles as compared to IF particles

[85]. With a decrease in the size MoS_2 platelets, the number of reactive dangling bonds (Mo-S atoms on *hk0* faces) increases due to an increase in the surface area. This increases the reactive binding of MoS_2 platelets to the metal surfaces instead of parallel alignment of basal planes, resulting in rapid oxidation deterioration. Whereas, the close structure of quasi-spherical nanoparticles have been suggested for their high mechanical and oxidation stability [85].

B. MANUFATURING OF NANOPARTICLE-BASED ADDITIVE PACKAGE

Process and Equipment

Organic-encapsulated and intercalated MoS_2 nanoparticles were manufactured using a top-down approach in a tabletop high-energy ball milling apparatus (SPEX 8000D dual mixer/mill) as shown in Figure 4.2.

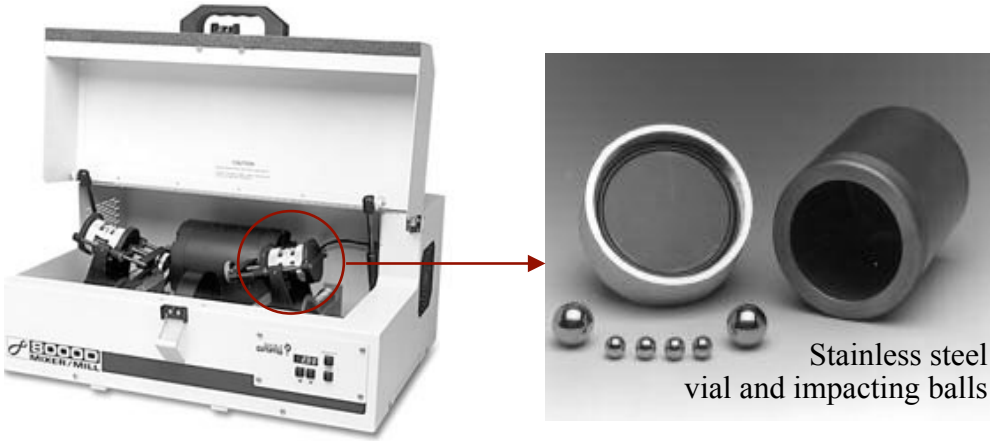

Figure 4.2 Ball milling apparatus- SPEX 8000D mixer/mill (left) and stainless steel vial and impact media (right)

Stainless steel grinding containers and balls (impacting media) were used during milling process. Comminution of the feed material particles was achieved from the high rpm shaking and lateral

movements of the grinding containers and the impacting balls. Further details on the shaking motions and mechanisms of the apparatus can be found elsewhere in [28,86]. The kinetic energy transfer from the impacting balls to powder resulted in grain-size reduction of the particles. The underlying mechanism of high-energy ball milling is mechanical milling and alloying as shown in Figure 4.3.

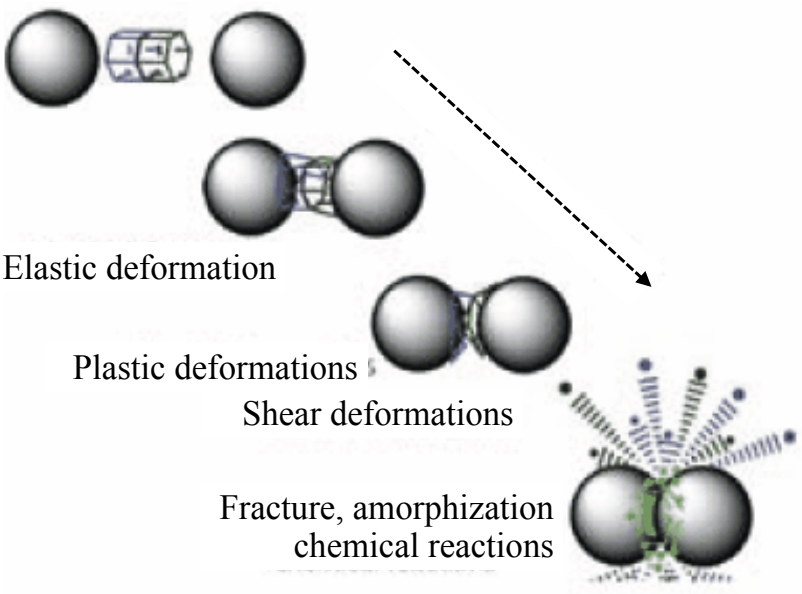

Figure 4.3 Deformations in the material trapped between two colliding balls during ball milling [90]

These mechanisms shown in Figure 4.3 allow various competing processes that are thermodynamically metastable such as, alloying, strain hardening of particles, particulate shearing, elastoplastic deformation, particulate-to-particulate welding, surface activation, etc. [87-89]. These processes occur in conjunction with grain-size reduction and chemical reactivity with the surrounding medium (such as organic molecules) as new reactive surfaces continuously evolve during milling. Mechanical alloying and milling are differentiated in terms of involvement of material transfer. Mechanical alloying refers to milling of mixtures of powders or

compounds to form homogeneous alloy and involve material transfer. Whereas, milling of pure powders or compounds without any material transfer is referred to as mechanical milling. Evolution of various equilibrium and non-equilibrium phases including, metastable and quasi-crystalline phases, amorphous alloys, nanostructured materials, and solid solutions have been reported with mechanical milling and alloying [89].

Nanoparticle-Based Additive Synthesis

The organic-inorganic additive was synthesized using a patent pending process discussed elsewhere in [79]. The first step of additive synthesis was the size reduction of MoS_2 particles via mechanical milling. Micro-sized MoS_2 particles (98 % pure, 3-5 μm average particle size from Alfa Aesar) were ball milled for 48 hours in a dry ambient environment. A ball to powder loading ratio of 2:1 was used during dry milling. To manufacture the additive package, dry milled MoS_2 particles were milled in a wet organic environment of triglyceride vegetable oil and emulsifying phospholipids. The ball-to-powder ratio was kept constant during the wet milling process, however milling time was varied at 24, 36, and 48 hours. Wet mechanical alloying yielded nanoscopic structures of MoS_2 intercalated and overlayered with the organic molecular mediums. The resultant organic-inorganic hybrid additive was the primary material of interest in this research and is referred to as MoS_2 nanoparticles from here onwards. Two nanoadditive compositions- A and B were manufactured by varying the source of triglycerides. The organic mediums- triglycerides and phospholipids used in formulating nanoadditives are discussed below.

Organic Mediums - Triglycerides and Phospholipids

1. **Triglycerides** - Triglycerides are esters composed of glycerol and three fatty acids and are the major constituent of vegetable oil**.** Canola oil (Spectrum) and soybean oil (STE oil

company) were used as the sources of triglycerides in nanoadditive-A and nanoadditive-B, respectively Soybean and canola oil are bio-based lubricants with high-level lubricity and smoke and flash points that are excellent attributes to withstand high friction and extreme temperatures during grinding processes. The smoke and flash temperatures of soybean and canola oils are listed in Table 4.1. The most distinctive advantage of triglyceride vegetable oil is the polar affinity to the metal surfaces. The polar functional group of triglyceride molecules of vegetable oil form strong bonds with the metallic surfaces [86]. Hence, the presence of polar capping layers led to stronger adsorption of MoS_2 nanoparticles on metal surfaces to yield low-friction tribolayers.

Table 4.1 Smoke and flash temperatures of triglyceride sources [91,92]

Triglyceride Source	Smoke Point (°C)	Flash Point (°C)
Canola Oil	240	327
Soybean Oil	241	327

2. **Phospholipids** - Phospholipids are fat derivatives that contains phosphate group. Phospholipid molecules are amphipathic, which means that they contain both hydrophobic and hydrophilic molecules having affinity for fats/oils and water, respectively. Soy lecithin (ALCOLEC® S, American Lecithin Company) derived from soybean oil was used as the high-level source of functional phospholipids in the nanoadditives (A and B). Intercalated and capping layers of soy-phospholipids offered following complimentary properties to the MoS_2 nanoparticles:
    - EP/AW bearing phosphate molecules known to form durable glassy films at the sliding interfaces.

- Emulsifying, dispersing, and stabilizing agent for MoS_2 nanoparticles in oil medium.
- Wettability enhancement of solid surfaces.

C. SYNTHESIS OF NANOLUBRICANT FORMULATIONS

Mineral and vegetable oil-based nanolubricants were formulated by homogenizing emulsified nanoadditive-A and nanoadditive-B in paraffin oil and soybean oil, respectively. Nanoadditive-B with soybean as triglyceride source was developed for synergistic combination with soybean base oil. The nanoadditive packages were added to the base fluids in two different concentrations- 2.0 and 8.0 wt.%. Homogenization of emulsified nanoparticles in base oils was achieved by ultrasonicating the lubricant mixtures for 4 hours. A 500-watt ultrasonic processor (VC 505, Sonics) was used for ultrasonicating the 2.0 wt.% and 8.0 wt.% nanolubricants at 25% and 30% ultrasonic amplitude, respectively. After ultrasonication, the nanolubricant compositions were further dispersed using high-shear mixing. During high-shear mixing stage, a MoS_2-specific dispersant (NA-SUL 729, King Industries) was added to enhance dispersion uniformity and colloidal stability of the nanolubricants. Table 4.2 summarizes the composition of the nanolubricants, while Figure 4.4 shows the overall process of nanolubricant synthesis.

Table 4.2 Compositions of the nanolubricants

Nanolubricant	Base Oil	MoS_2 Nanoadditive Type	MoS_2 Nanoadditive concentration	Dispersant Concentration*
1	Paraffin	Nanoadditive-A	2.0 wt./wt.%	0.1 wt./wt.%
2	Paraffin	Nanoadditive-A	8.0 wt./wt.%	0.4 wt./wt.%
3	Soybean	Nanoadditive-B	2.0 wt./wt.%	0.1 wt./wt.%
4	Soybean	Nanoadditive-B	8.0 wt./wt.%	0.4 wt./wt.%

*Dispersant concentration based on manufacturer's recommended treatment level

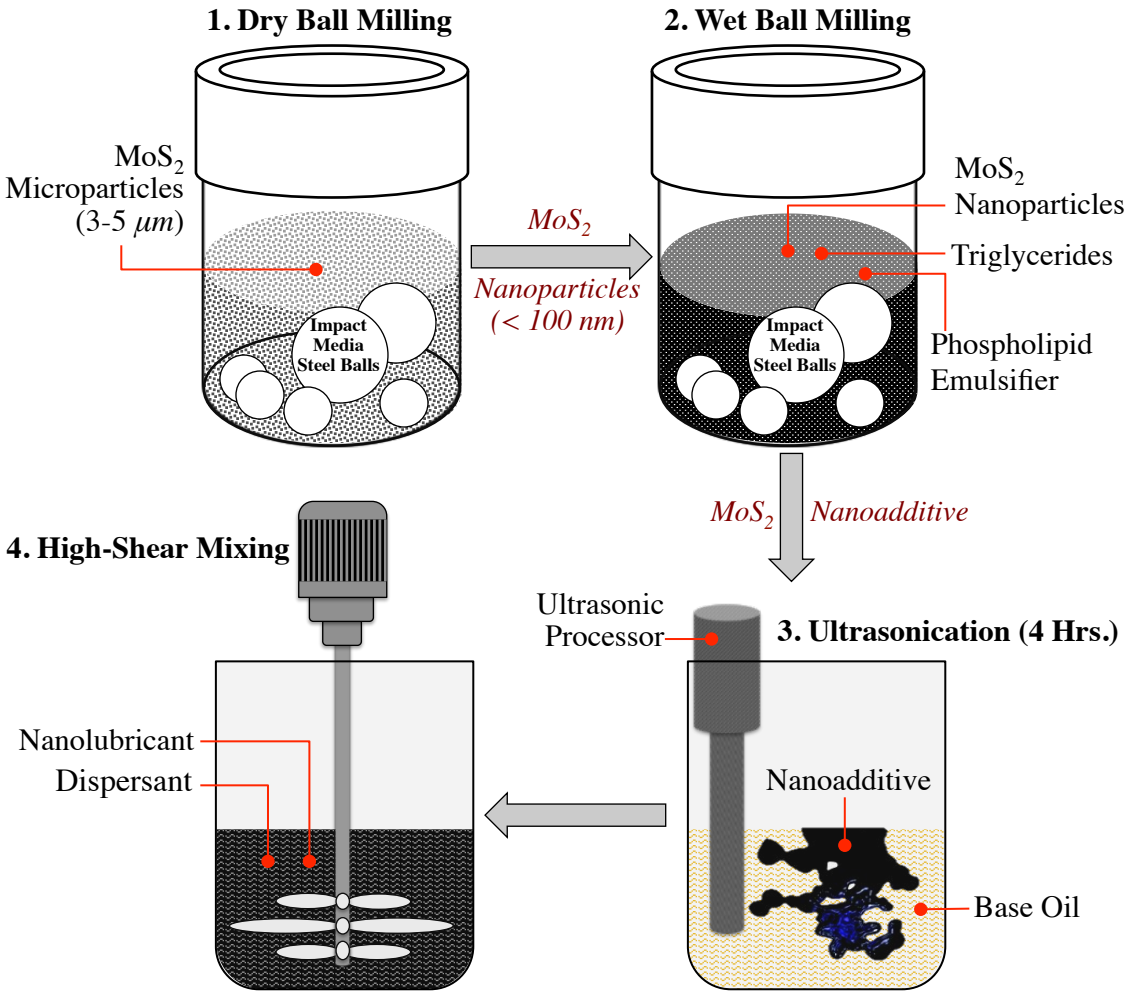

Figure 4.4 Synthesis process of oil-based nanolubricants

The concentrations of nanoadditive in base oils were varied to study the concentration effect of MoS_2 nanoparticles on the performance of MQL-assisted grinding. The selection of concentration levels was based on the results and analysis of prior research [28]. In this feasibility research, nanolubricants containing 5.0 and 20.0 wt.% of MoS_2 nanoadditive (canola oil as triglyceride source) were used in MQL grinding experiments. Mineral-based paraffin and vegetable-based soybean oil were selected as base oils to evaluate the performance of nanolubricants in MQL grinding as a function of base composition (hydrocarbon and triglyceride

based compositions). The chemical and physical properties of the base oils are listed in Table 4.3. Despite many differences in properties, paraffin and soybean-derived base oils are widely used in commercial MWFs. Examples include, Tru Cut 203NC- a paraffin based MWF and ELM SoyEasy NuCut Lite™- a soy-based biodegradable MWF.

Table 4.3 Physical properties of base oils

Base Oil	Type	Chemical Ingredient	Viscosity (at 20 °C)	Flash Temperature	Auto Ignition Temperature
Paraffin oil	Mineral oil	Saturated hydrocarbons	2.4 cST	195°C	338°C
Soybean oil	Vegetable oil	Triglycerides	75 cST	327°C	365°C

D. CHEMO-PHYSICAL CHARACTERIZATION

This section describes the structural and chemical analysis of nanostructures and organic-inorganic interfaces of nanolubricants. These analysis included 1) size, shape, and surface area of the MoS_2 nanoparticles, 2) chemical analysis of ball-milled MoS_2 particles, and 3) thermal conductivity of base oils and nanolubricant compositions.

Analytical Techniques

A nanostructural analysis of the MoS_2 particles was carried out using transmission electron microscopy (FEI - TITAN 80-300 S/TEM) and scanning electron microscopy (FEI-Philips XL 30 FEG). The median particle size distribution (D50) of dry and wet milled MoS_2 particles was measured using a laser scattering particle size analyzer (HORIBA LA-950). The D50 particle diameter splits the size distribution with half of the particle sizes above and below the diameter. BET surface area analyzer (Quantachrome- Quadrasorb SI) was used to measure the specific

surface area of the nanoparticles. X-ray diffraction (Rigaku D/Max) using Cu-Kα radiation was performed for the phase shift analysis and size estimation of MoS_2 particles after dry milling. To investigate the concentration-dependent conductivity of MoS_2 nanoparticles, thermal conductivity of nanolubricants and base fluids were measured. A transient hot wire setup was used for thermal conductivity measurements. This transient technique measured the temperature rise (ΔT) as a function of time over a defined length from a heated wire (hot wire) embedded in the test fluid. By assuming constant and uniform output from the hot wire over the sample length, thermal conductivity of the fluid was derived from the measured change in temperature over a defined time interval. The details of the setup and measurement method and calculations could be found elsewhere in [93].

Samples of nanosized MoS_2 were prepared by dissolution and precipitation in an organic solvent (acetone, C_3H_6O). Wet milled MoS_2 additive was homogeneously dispersed in acetone using ultrasonication. The resultant mix was centrifuged to separate and precipitate MoS_2 from the organic solvent and other dissolved organic matter. The MoS_2 precipitate was collected and dried in a contamination-free environment. The dried particles were directly used for surface area analysis, but were dispersed in fresh acetone for TEM (a thin film deposited and dried on carbon grid) and particle size analysis.

Particle Size, Shape and Surface Area

Figure 4.5 shows the SEM micrograph of MoS_2 particles after 48 hours of dry milling. Agglomerated particles of irregular shape and size were observed from the micrograph. Corresponding EDS elemental mapping of the particles showed chemical signatures of Mo and S with negligible traces of Fe, which indicated very low levels of iron contamination from steel-to-steel impaction during ball milling process.

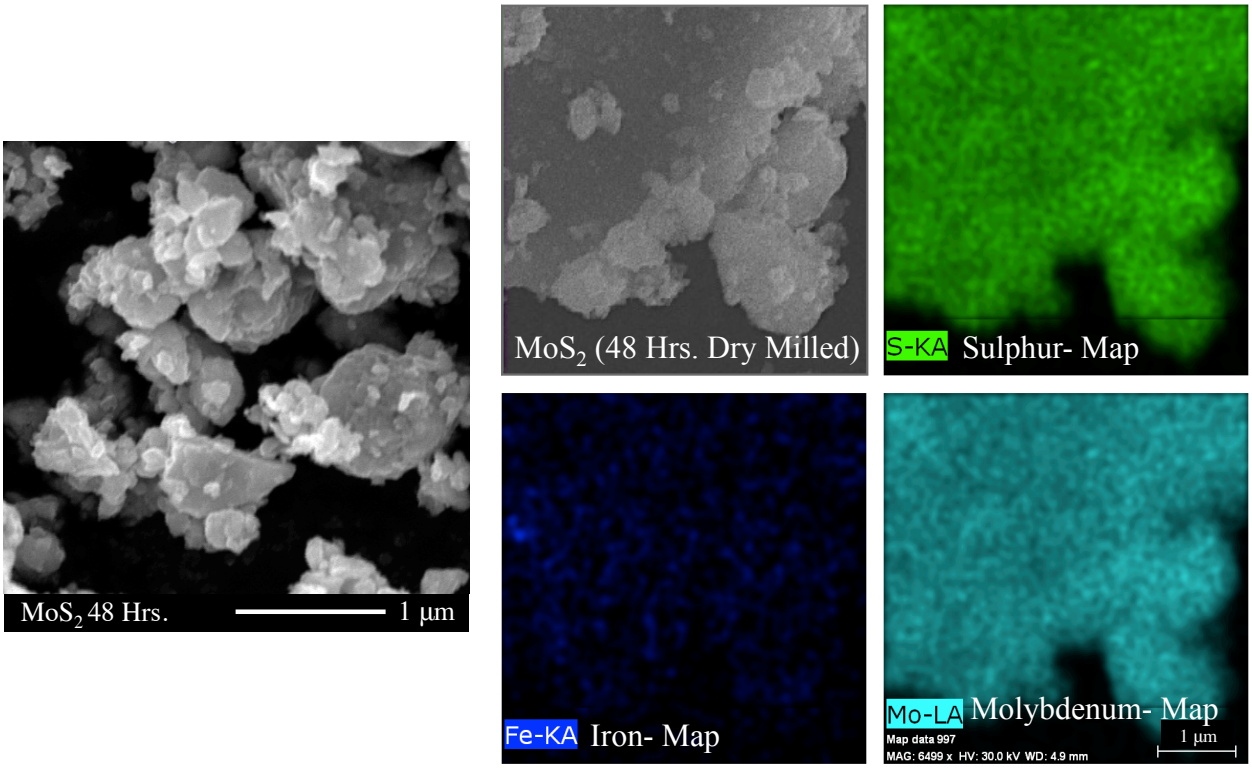

Figure 4.5 SEM-EDS microanalysis of MoS_2 particles after 48 hours of dry milling

Figure 4.6 shows the XRD spectra of the as received and 48 hours dry-milled MoS_2 particles. Similar diffraction peak patterns with no phase shift were observed for as-received and dry-milled MoS_2, suggesting similar material composition. This further confirmed the contamination-free ball milling of MoS_2 particles. The broadening of peak widths (002) was attributed to the formation of nanocrystallites by the size reduction of MoS_2 particles during ball milling. Diffraction peak width varies inversely with crystallite size, such that peak broadening corresponds to reduction in crystallite size. An average crystallite size of 33 nm of dry-milled MoS_2 particles was obtained using XRD The observed peak broadening was also suggestive of non-uniform lattice strains and defects induced by the mechanisms of mechanical milling/alloying.

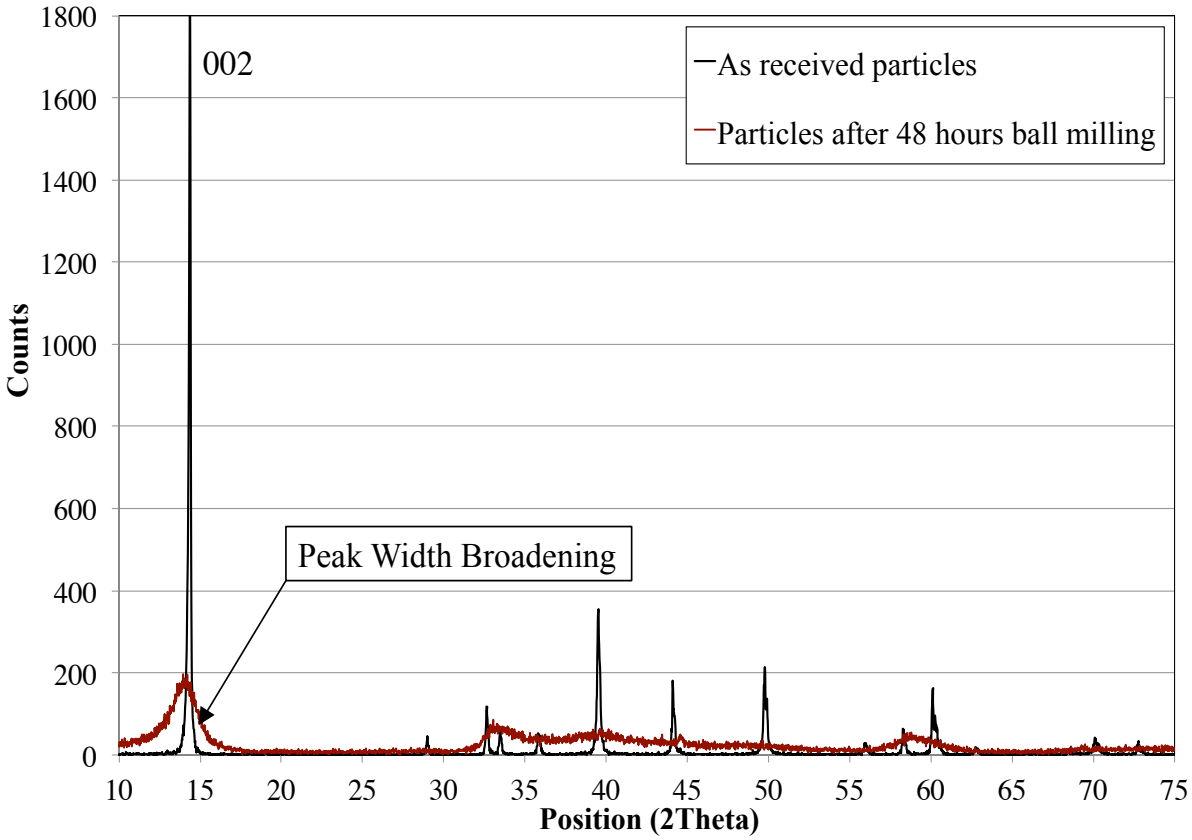

Figure 4.6 XRD spectra of the as received and 48 hours dry-milled MoS_2 particles

Figure 4.7 shows the TEM images of MoS_2 nanoparticles after 24, 36, and 48 hours of wet (hybrid) milling. Evolution of clustered elongated-shaped nanoparticles was seen after 24 hours of wet milling (Figure 4.7a). Less agglomeration of wet milled nanoparticles was observed as compared to the dry milled particles. This was attributed to the dispersion and emulsification effect of oil medium (triglycerides) and lecithin (phospholipids), respectively. Shape transformation from elongated to quasi-spherical morphology and particle deagglomeration was observed with an increase in wet milling time. High-resolution TEM (Figure 4.7b and c) showed that the resultant wet-milled MoS_2 particles were oval-shaped like slightly elongated coconuts with parallelly oriented atomic shear planes.

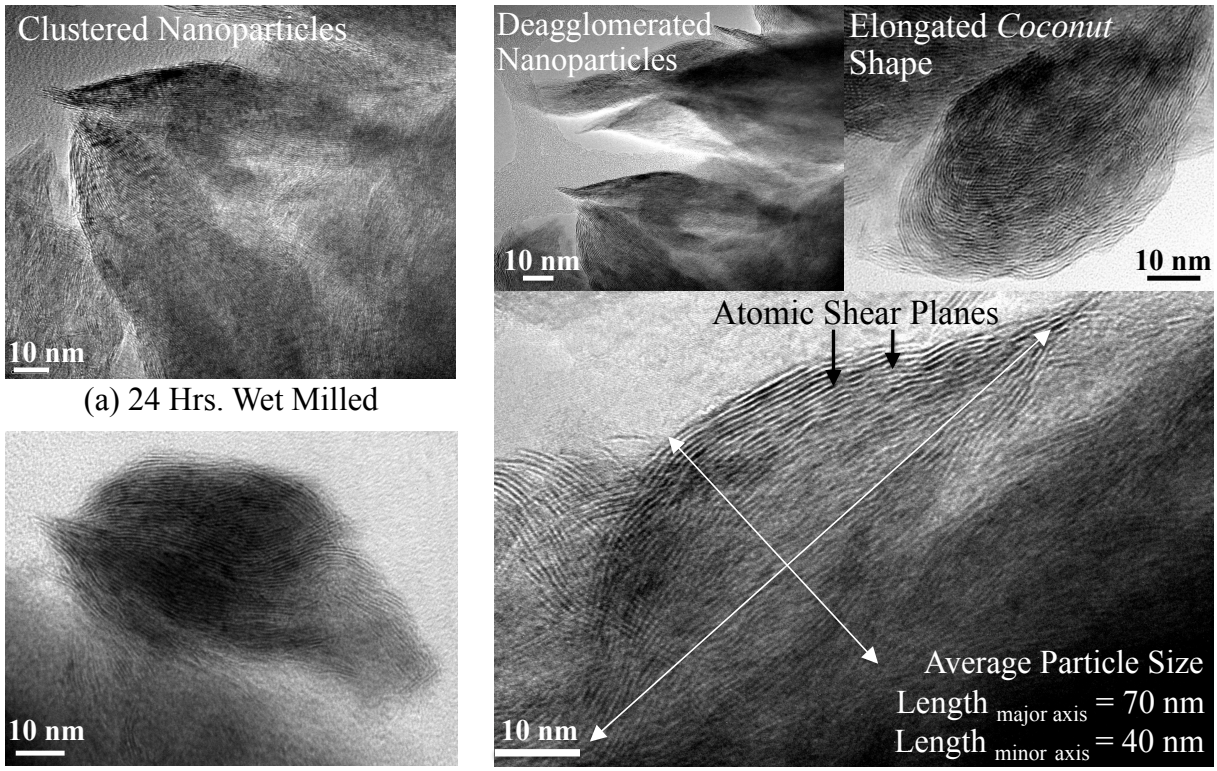

Figure 4.7 TEM images of MoS_2 nanoparticles after (a) 24 hours, (b) 36 hours, and (c) 48 hours of wet (hybrid) milling [94]

The size of a lamellar-structured MoS_2 nanoparticle was measured as 70 nm and 40 nm along the major and minor axes, respectively. Though shape and size transformation occurred with an increase in wet milling time from 24 to 36 hours, the morphology of nanoparticles remained the same after 36 hours and 48 hours of wet milling. Due to this repetitive observation, the wet milling time was set at 36 hours to obtain predictable and uniform particle size as well as homogenization consistency of organic-inorganic constituents.

The D50 (median) particle size distribution of ball-milled (dry and wet) particles is shown in Figure 4.8. Each plotted size was acquired by averaging the median particle sizes of 4 batches of each ball-milling condition. The ball milling parameters and environment were kept constant

during similar-condition milling batches.

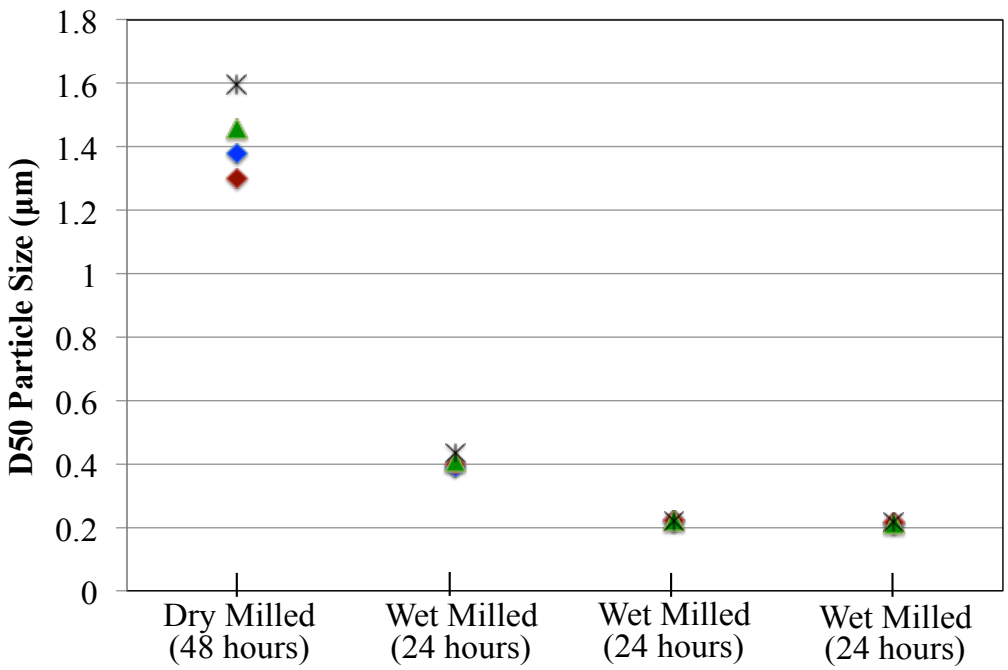

Figure 4.8 D50 (median) particle size distribution of dry and wet milled MoS_2 particles

An average median size of 1.435 µm was measured for the dry MoS_2 agglomerates after 48 hours of milling. With 24 hours of wet milling, the average particle diameter showed further reduction to 0.408 µm. Correlating with TEM observations, average particle size of 48 hours milled particles (0.215 µm) showed a narrow 1.8% reduction as compared to 36 hours of wet milling (0.219 µm). With progression from dry milling to increase in wet milling time, a decrease in the variation of the median particle sizes was observed. The reduction in the size variation was correlated to increasing uniformity in the size distribution of the particles.

The BET specific surface area (SSA) versus average particle size of MoS_2 particles at different stages of ball milling is shown in Figure 4.9.

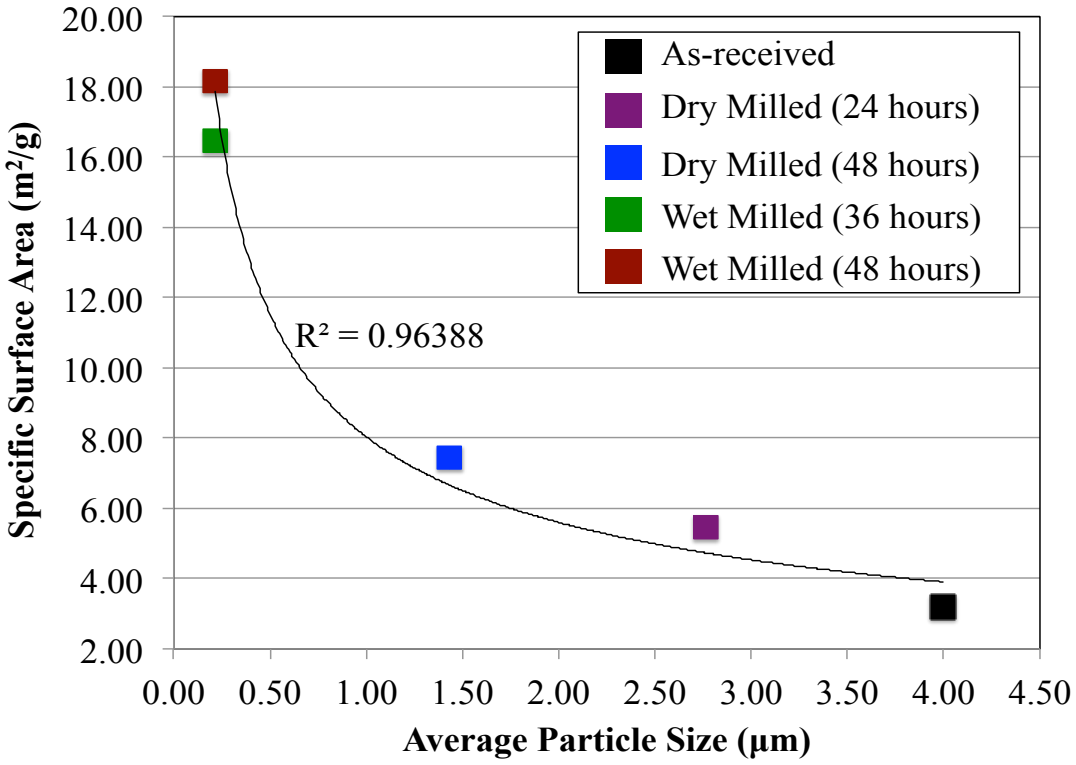

Figure 4.9 The BET specific surface area (SSA) versus average particle size (µm) of MoS_2 particles after different stages and periods of ball milling

As anticipated, the SSA of MoS_2 particles increased with an increment in dry milling time (reduction in particle size). 48 hours of dry milling yielded particles with surface area of 7.45 m^2/g, as compared to 3.20 m^2/g of as-received MoS_2 microparticles. A steep increase in surface area was observed after 36 hours of wet milling, confirming deagglomerated nanosized MoS_2 particles. The high-surface area of wet-milled nanoparticles (16-18 m^2/g) was anticipated to escalate their physisorption onto the micro cavities of abrasive grains and workpiece during grinding to deliver low-friction films of MoS_2.

Based on the cumulative results of TEM, particle size and surface area analysis, it was concluded that the evolved MoS_2 particles after 48 hours of dry milling followed by 36 hours of wet milling were nanostructured particles kept well dispersed by the organic medium.

Thermal Conductivity of Nanolubricants

Figure 4.10 shows the measured values of thermal conductivity of paraffin and soybean oil-based nanolubricants (with varying concentration of MoS_2 nanoparticles) and pure base oils (without nanoparticles).

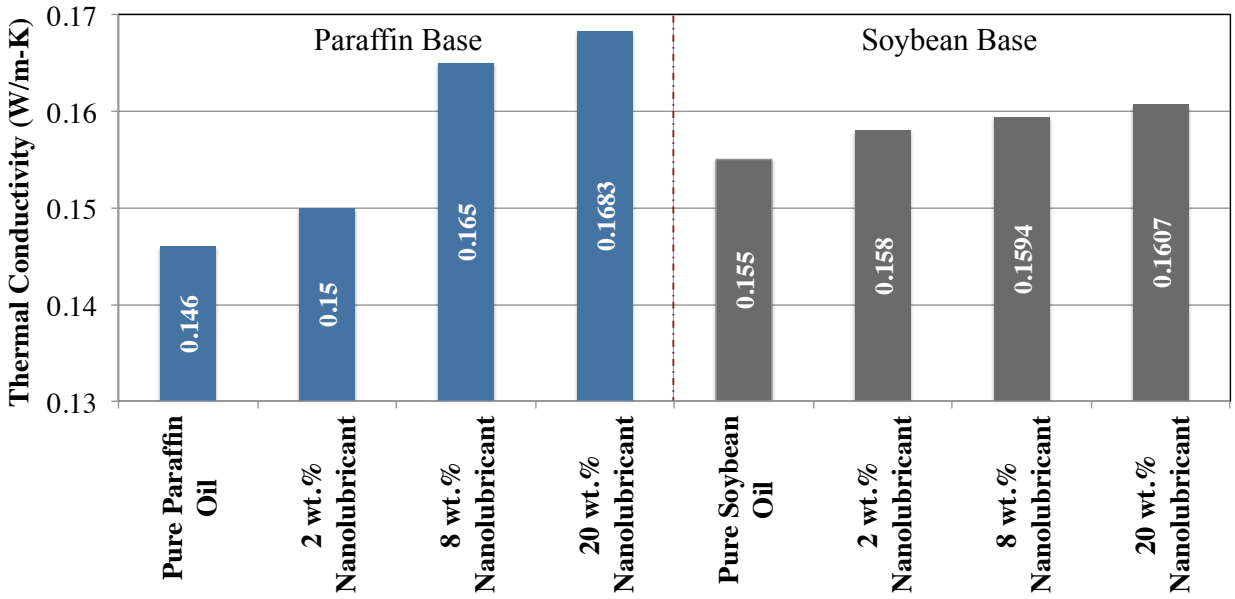

Figure 4.10. Thermal conductivity of the base oils and oil-based nanolubricants with varying concentration of MoS_2 nanoparticles

Thermal conductivity of pure soybean oil was measured at 0.155 W/m-K, which was slightly higher than pure paraffin oil (0.146 W/m-K). Addition and subsequent increase in the concentration of MoS_2 nanoparticles increased the thermal conductivities of both base oils (paraffin and soybean oil). 8 wt.% paraffin and soybean-based nanolubricant showed an increase of 13% and 3% in thermal conductivity as compared to that of the respective base fluids (without nanoparticles). Of all the test lubricants, the paraffin-based nanolubricant containing 20 wt.% of nanoparticles showed the highest thermal conductivity of 0.168 W/m-K measuring a 15% increment over pure paraffin oil.

V. EXPERIMENTAL APPROACH AND TECHNIQUES

This chapter describes the various experimental approach and analytical techniques that were used for studying the tribological and lubrication mechanisms of nanolubricants in MQL grinding. The chapter is divided in two sections, A) surface grinding tests and B) simulated tribological tests. Each section is subdivided into three sections that explain, 1) machine/equipment setup and parameters, 2) test lubricants, and 3) measurement parameters and methods.

A. SURFACE GRINDING TESTS

Plunge surface grinding tests were carried out with the goal of documenting the process efficiency of nanolubricants as well as the mechanisms of nanolubricant impingement in MQL-assisted grinding. The friction coefficient in grinding, tangential forces, specific energy, G-ratio, grinding zone temperature measurements and thermal analysis, and surface roughness and texture profile of ground workpieces were used as measurands for determining the efficiency and role of nanolubricants under various process conditions, as discussed below.

Surface Grinding and MQL Setup

All grinding experiments were performed on a mechanically controlled surface grinder (MFP 100- Magerle) in reciprocating plunge grinding mode (no cross feed). The grinding setup is shown in Figure 5.1. Surface grinding experiments were carried out under wet (flood) and MQL conditions. The conventional coolant supply system provided in the grinding machine was used for flood grinding. An external fluid delivery system (precision dispenser- AMCOL Corp.) was used for MQL assisted grinding, as shown in Figure 5.1.

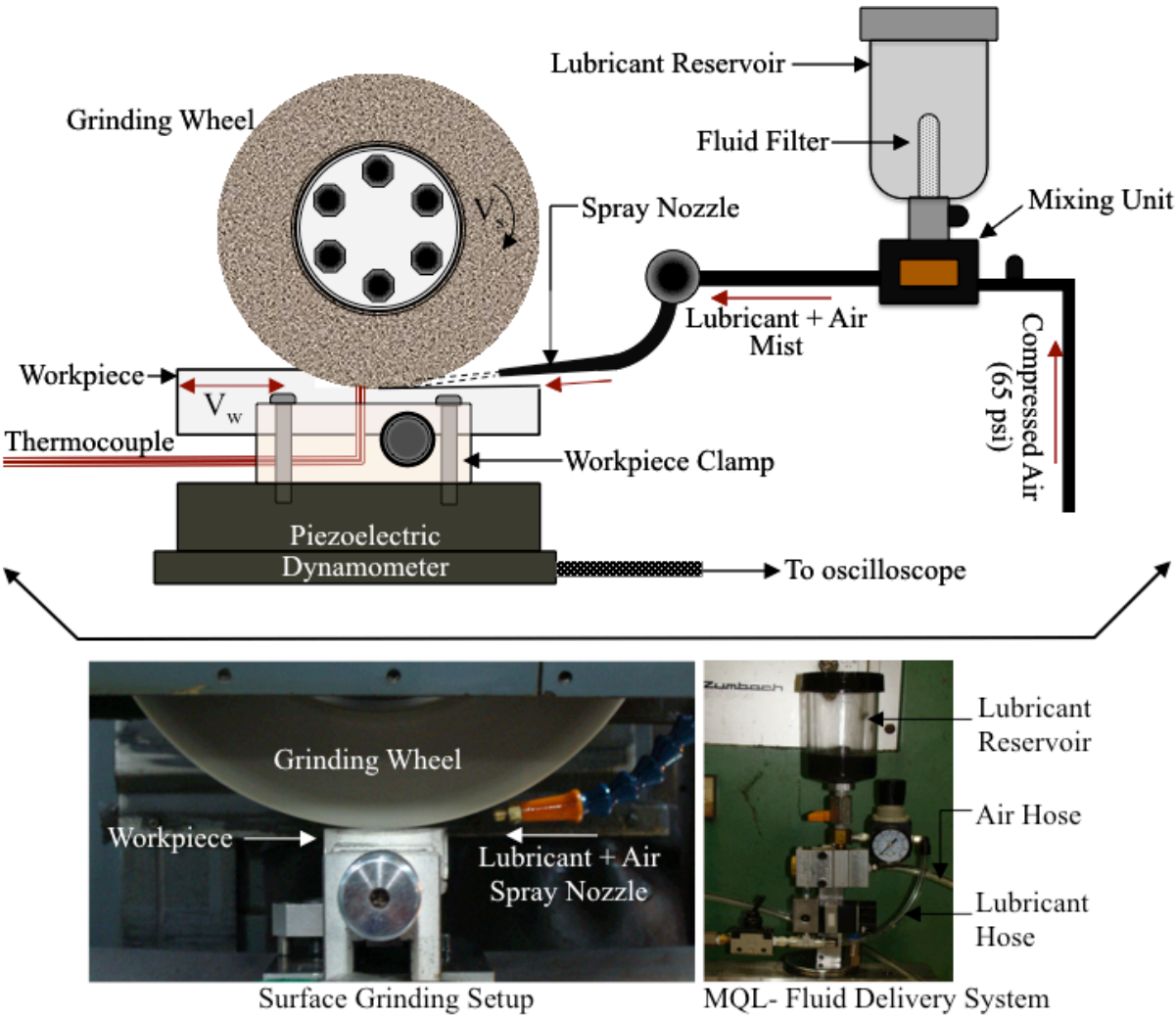

Figure 5.1 Surface grinding setup (left) and MQL fluid delivery system (right) [94]

In this system, the lubricant from the fluid reservoir was suctioned into a pressurized air stream (65 psi) coming from a compressed air source. The lubricant-air mixture was then propelled to the grinding zone by air pulses through a tube-nozzle system. The MQL jet impinged the grinding zone in the direction of rotation of the abrasive wheel. For precise lubricant impingement, the MQL spray nozzle was positioned at a distance of 70 mm from the grinding zone contact line and aligned at an angle of 15° to the workpiece surface. The precise location and positioning of spray nozzle along with air pressure adjustments were vital factors concerning

the effective MQL-assisted application of lubricants and its effect on grinding forces and surface roughness [95]. Workpiece material removal occurred throughout the grinding pass in up and down grinding modes. The grinding experiments were carried out with different depths of cut (infeeds) and work speeds, while other parameters were kept constant as listed in Table 5.1. The grinding parameters and combinations were selected based on guidance from previous research [27,28], available literature, and industrial collaborations.

Table 5.1 Surface grinding process parameters

Grinding Conditions		
Grinding mode	Reciprocating plunge surface grinding (no crossfeed)	
Infeed control	Automatic, up-grinding and down-grinding	
Grinding wheel	Vitrified aluminum oxide (32A46-HVBEP)	
Wheel diameter and thickness	300 mm and 25.4 mm	
Parameters	**Ductile Cast Iron**	**EN 24 Steel**
Wheel peripheral speed (m/s)	30	30
Workpiece traverse speed (m/s)	0.06	0.1
Depth of cut or Infeed (μm)	10, 20	20
Grinding passes (n)	100	100
Grinding width, b_w (mm)	7.2	7.5
MQL flow rate (ml/minute)	2.5	2.5
Flood flow rate (ml/minute)	8450	8450

A vitrified aluminum oxide (Al_2O_3) wheel (Saint Gobain-Norton Abrasives: 32A46-HVBEP, average grain size 356 μm) was used as the abrasive tool. After each grinding test, the wheel was dressed to resharpen the bonded abrasive grains. Dressing was carried out by crossfeeding the grinding wheel at 0.008 m/s against a diamond rotary dresser. An infeed of 10 μm and speed ratio of 0.4 was maintained during wheel dressing. Camshaft material- ASTM A536 grade 100-70-03 ductile cast iron and industrial alloy steel- EN 24 were used as workpiece materials. The

workpiece specifications are listed in Table 5.2. Before each grinding experiment, the workpiece surface was sparked out to eliminate inconsistencies, such as residual material and oxide layers.

Table 5.2 Workpiece material specifications

Workpiece material			Ductile cast iron
Grade			100-70-03
Hardness			50 ± 2 HRC (case hardened)
Composition			[Durabar, Inc.]
Element	Mass [%]	Element	Mass [%]
Carbon	3.5	Silicon	2.25
Manganese	0.15	Sulphur	0.025
Phosphorus	0.05		
Workpiece material			EN 24 alloy steel
Hardness			50 ± 2 (case hardened)
Composition			
Element	Mass [%]	Element	Mass [%]
Carbon	0.44	Silicon	0.35
Manganese	0.70	Sulphur	0.04
Chromium	1.40	Molybdenum	0.35
Phosphorus	0.035	Nickel	1.70

Both, ductile iron (Durabar 100-70-3) and EN 24 workpieces were case hardened to 50 ± 2 HRc, as per as manufacturer's heat treatment recommendations Typical microstructures of ductile cast iron before and after heat treatment are shown in Figure 5.2. Nodular graphite in a pearlitic matrix was seen in both the microstructures. Though pearlite dominates the matrix of ductile iron, it also contains some small quantities of ferrite.

(a) Ductile Iron- microstructure before heat treatment (b) Ductile Iron- microstructure after heat treatment

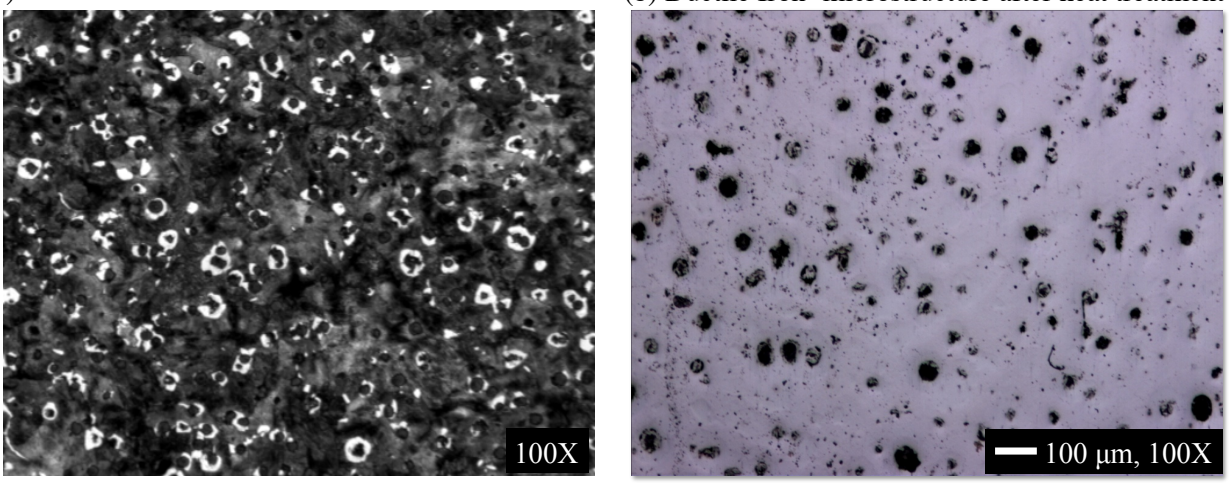

Figure 5.2 Microstructures of ductile cast iron (Durabar 100-70-3), a) before heat treatment (http://www.dura-bar.com/products/100-70-03.cfm), b) after heat treatment

Grinding Lubricants

The lubricating efficiency of MoS_2-based nanolubricants was compared against three lubrication conditions- flood (wet) lubrication, MQL with pure base fluids (without nanoparticles), and MQL with base fluids containing emulsified MoS_2 microparticles (3-5 μm). As mentioned earlier, two nanoadditive concentrations in two nanolubricant compositions were tested in this research. This group of test lubricants included mineral (paraffin) and vegetable (soybean) oil-based nanolubricants containing 2.0 and 8.0 wt./wt.% of nanoadditives. For particle size driven performance comparison, microparticles-based lubricants were formulated by dispersing 8 wt./wt.% of emulsified MoS_2 microparticles in base oils (paraffin and soybean oil). Grinding with flood lubrication or cooling was carried out with a synthetic water-soluble cutting fluid. The synthetic cutting fluid was mixed with DI water at 5 vol.% as specified by the manufacturer. Table 5.3 summarizes the lubricants applied in this research.

Table 5.3. List of lubricants

Nanolubricants	Fluid Delivery method
Paraffin-based (2 wt./wt.% nanoadditive A)	MQL
Paraffin-based (8 wt./wt.% nanoadditive A	MQL
Soybean based (2 wt./wt.% nanoadditive B)	MQL
Soybean-based (8 wt./wt.% nanoadditive B)	MQL
Lubricants containing MoS_2 microparticles (3-5 µm)	**Fluid Delivery method**
Paraffin-based (8 wt./wt.% emulsified MoS_2 microparticles)	MQL
Soybean-based (8 wt./wt.% emulsified MoS_2 microparticles)	MQL
Pure base fluids	**Fluid Delivery method**
Pure paraffin oil	MQL
Pure soybean oil	MQL
Water-based coolant	**Fluid Delivery method**
Water-based synthetic grinding fluid	Flood

Measurement Parameters and Methods

1. **Friction Coefficient and Specific Grinding Energy -** A piezoelectric dynamometer (Kistler 9275 A) and oscilloscope arrangement was used for in-process measurement of forces (tangential and normal force) during grinding. The dynamometer measured the reaction forces on the workpiece that was mounted on the dynamometer's cover plate. The grinding forces were recorded at 1 kHz sampling rate. The as measured grinding forces were used for calculations of the friction coefficient in grinding and specific energy, as discussed in Section 1.1 and Section 1.2.

   1.1. Friction coefficient in grinding (µ). In abrasive grinding, the ratio of tangential force (F_t) and normal force (F_n) is known as the friction coefficient or the force ratio in grinding.

$$\text{Coefficient of friction, } \mu = {F_t}/{F_n} \qquad \text{Equation 13}$$

In abrasive grinding, the values of μ typically range from 0.2 to 0.7 [7]. A low value of μ corresponds to well-lubricated blunt abrasive grains in contact with the workpiece surface. In case of blunt asperity contact, the hard abrasive grains rub or slide against the workpiece surface without or with small grain penetration. This results in the plastic deformation of soft workpiece material and therefore, high adhesive friction (μ). Well-lubricated conditions reduce adhesive friction, and hence tangential grinding forces (Equations 5 and 7). In this research, the coefficient of friction (force ratio) was computed from the measured values of forces and plotted against each lubrication condition to determine the antifriction performance of each lubricant.

1.2. Specific grinding energy. In abrasive grinding, specific energy is defined as the energy required or consumed for the removal of a unit volume of workpiece material [3]. It is directly proportional to tangential grinding force and is expressed as follows [3]:

$$\text{Specific grinding energy, } U = {P}/{Q_w} = {F_t \cdot V_s}/{b_w \cdot a_e \cdot V_w} \qquad \text{Equation 14}$$

Where, P - total machining power, Q_w - volumetric material removal rate, F_t - tangential grinding force, V_s - wheel peripheral speed, V_w - workpiece traverse speed, b_w - grinding width and, a_e - depth of cut

Specific energy is a measure of grinding process efficiency. A low value of specific energy means a reduction in the sliding frictional losses (Equation 3 and 4), which is an indicative of prevalence of material cutting instead of rubbing and ploughing during grinding. Like force ratio, specific energy values were computed and plotted against each lubrication condition.

This was done to correlate the friction reduction efficacy of each lubricant to energy efficiency of the grinding process.

2. **Grinding wheel wear -** Multi-asperity scuffing during grinding results in abrasive grain wear. A number of wear mechanisms are involved during grinding, including attrition, grain fracture, and grain pullout from the bond posts, as shown in Figure 5.3. Low wheel wear tends to reduce total perishable tooling costs and changeover time and hence, extended wheel life is a decisive factor in the economics of grinding.

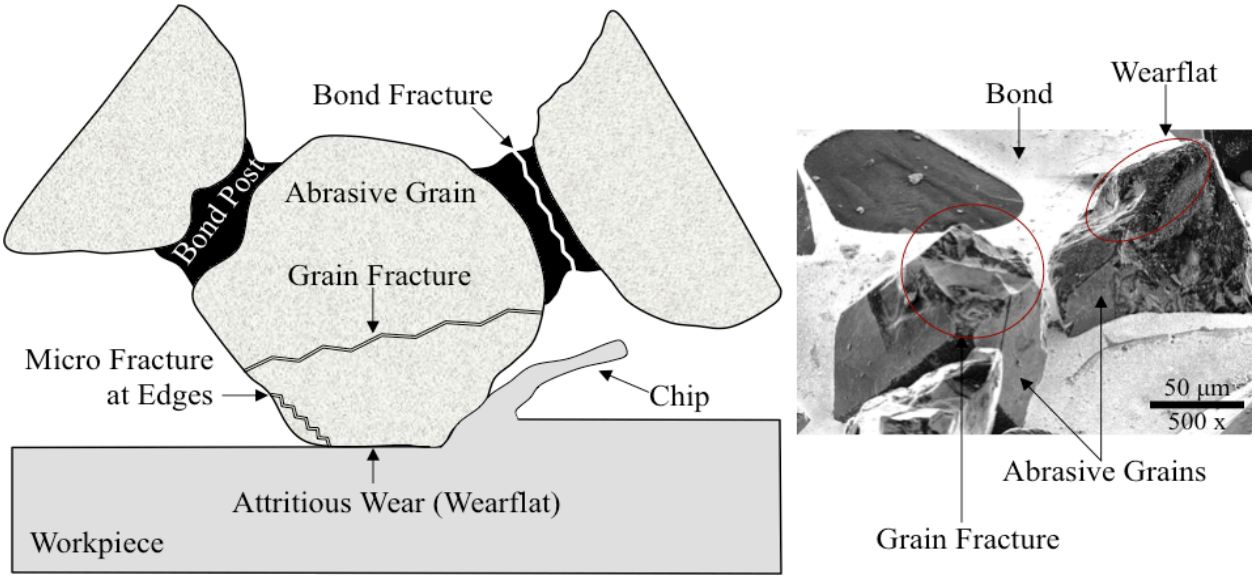

Figure 5.3 Mechanisms of abrasive grain wear

2.1. Grinding (G) Ratio. G-ratio is often used as a performance parameter to characterize wheel wear resistance. By definition, it is the ratio of the volume of material removed from the workpiece and volume of grinding wheel wear.

$$\text{G-Ratio} = \frac{\text{Volume of material removed } (V_{mr})}{\text{Volume of wheel wear } (V_{rw})} \qquad \text{Equation 15}$$

In order to measure the volume of material removed (V_{mr}) in Equation 15, the mass difference of the workpiece before and after grinding was precisely measured using an electronic balance and then multiplied with the pre-known density of work material.

V_{mr} = {Mass before grinding (M_1) - Mass before grinding (M_2)} × Mass density (ρ_w)

The volume of wheel wear was measured using expression [3]:

$$V_{rw} = \pi \cdot D_m \cdot \Delta R \cdot b_w \qquad \text{Equation 16}$$

Where, D_m is the mean wheel diameter before and after plunge grinding, ΔR is the decrease in wheel radius, and b_w the grinding width.

An indirect measurement method for ΔR was used due to the difference in the widths of wheel and workpiece. Due to this difference in widths, a wear groove was produced on the wheel's periphery during grinding, as shown in Figure 5.4. After each grinding test, a flat non-hardened steel part was precisely ground to imprint the wear groove on its surface and the depth of this groove (ΔR) in the surface replica was measured using a surface profilometer (Taylor Hobson Talysurf profilometer). Depending on the physical characteristics of the abrasive wheel and workpiece material, G-ratios exhibits a wide range of values, from 1 to several thousands [49].

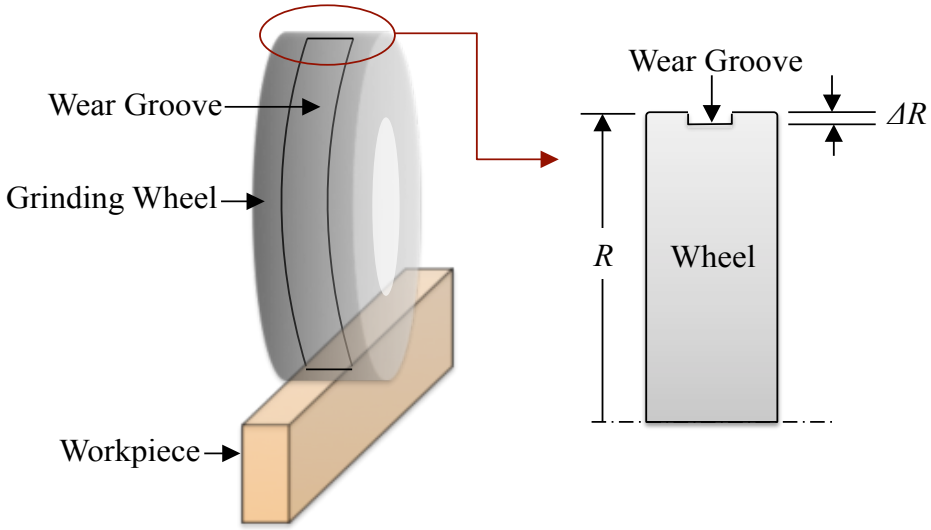

Figure 5.4 Wear groove produced on the Al_2O_3 wheel's peripheral surface after grinding

Table 5.4 lists and compares the G-ratio values for different abrasive wheel types during grinding of various workpiece materials. In general, high values of G-ratio represent high wear resistance (low-wheel wear) and hence, extended wheel life. As explained before, low interfacial friction from advanced lubrication can extend wheel life by reducing attritious wear and fracture of abrasive grains from bond posts [3]. To validate this correlation between lubrication efficacy and prolonged wheel life, G-ratio values were measured during each lubricated grinding condition and plotted.

Table 5.4 Typical G-ratio values for abrasive wheel types during grinding of various workpiece materials [96]

	Grinding Alumina	Grinding Steel	Grinding Nickel	Grinding Titanium
Diamond 9,000 Hv	100,000	1,000	100	50
CBN 4,500 Hv	1,000	10,000	5,000	100
Al_2O_3 1,800 Hv	<1	5-10	10	1
SiC 2,800 Hv	10	1-5	1	10

3. **Grinding Temperatures and Thermal Analysis -** Grinding involves high expenditure of energy during material removal. Dissipation of all of this energy into heat at the grinding zone leads to the generation of high temperatures, ranging between 500-700 °C. Such elevated temperatures adversely affect the efficiency and productivity of grinding process by causing thermal damage to the workpiece. Therefore, in process measurement and monitoring of temperature and thermal analysis is extremely important in grinding. In this research, the maximum temperature rise and grinding power were measured against each lubrication condition. These measured parameters were then used for heat-transfer analysis to evaluate the internal cooling effect of each lubrication condition.

3.1. Grinding Temperature Measurement. Measurement of grinding temperatures is an essential part of heat-transfer analysis in grinding. Numerous methods have been developed for the measurement of grinding temperature including, thermocouple embedded in the workpiece, thermocouple embedded in grinding wheel, foil/workpiece thermocouple, spectral radiance thermometry, IR films and PbS detectors, optical fiber, and thermal imaging [7, 96]. The embedded thermocouple method has found wide application in grinding due to its simple installation and high accuracy and reliability at a low cost [8].

In this study, the grinding temperature rise was measured through a dynamic thermocouple (grindable thermocouple) embedded in the workpiece using standard protocols [8,93]. As shown in Figure 5.5, a blind hole was drilled in the workpiece with its end located approximately at 0.5 mm below the surface. A 30 gauge K-type thermocouple (with grounded welded junction) was fixed in the drilled hole using high temperature alumina adhesive (Resbond™ 989 FS). The diameter of the drilled hole was matched with that of welded junction of the thermocouple to obtain a tight fit.

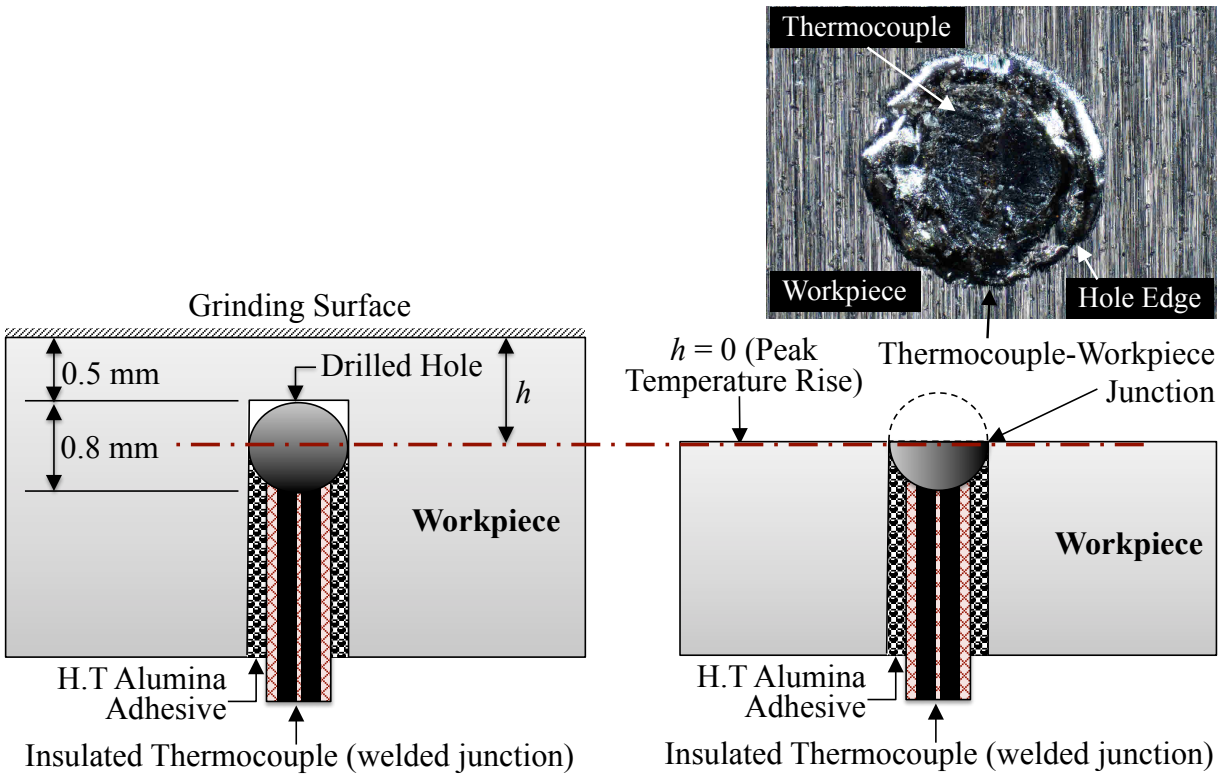

Figure 5.5 Embedded thermocouple method for temperature measurement

The thermocouple-workpiece system was calibrated in a furnace for temperatures up to 900°C. The embedded thermocouple was exposed during grinding and a hot junction was formed when the grinding wheel brazed the thermocouple junction to the workpiece, as shown in Figure 5.5. The measured temperatures showed progressive increases with each grinding pass until the exposure of the workpiece-thermocouple junction (h = 0) where the peak temperature remained almost constant for a series of grinding passes and then started dropping. This peak temperature at the workpiece-thermocouple junction (position h = 0) was considered to be the maximum grinding temperature rise at the workpiece surface.

By using a similar embedded thermocouple method, Shen et al. [7] measured the maximum temperature rise during surface grinding of cast iron by conventional alumina wheel at 10 μm

depth of cut. They suggested a maximum temperature rise of 566°C, 110°C, and 444°C for dry, flood (wet), and MQL conditions, respectively. For flood and MQL, a water-based synthetic grinding fluid was used at flow rates of 5400 ml/min and 15 ml/min, respectively.

3.2. Thermal Analysis. In this research, a moving heat source model was used for thermal analysis of the grinding process. This model considers the heated area in the grinding zone as a plane band source of heat that moves along the work surface at the workpiece traverse velocity (V_w) [50]. The grinding energy dissipation or the grinding heat flux (q_w) into the work material can be considered as uniformly distributed [3] or triangularly distributed [8] over the grinding zone (arc length of contact), as shown in Figure 5.6. For this two-dimensional model, the heat flux to the workpiece at the grinding zone was expressed as [98]:

$$q_w = \frac{kV_w^{1/2}}{\beta\alpha^{1/2}a_e^{1/4}d_s^{1/4}}\theta_{max} \qquad \text{Equation 14}$$

Where θ_{max} is the maximum temperature rise above ambient, k and α is the thermal conductivity and thermal diffusivity of the workpiece, respectively, a_e is the depth of cut, d_s is the grinding wheel diameter, and $\beta = 1.13$ (for uniformly distributed heat source) or 1.06 (for triangularly distributed heat source) [3]. In this study, $\beta = 1.06$ was used for a triangularly distributed heat source.

Out of the total heat flux generated at the grinding zone, only a fraction is dissipated to the workpiece material. This fraction is known as energy partition (ε) and is related to the workpiece heat flux (q_w) as [3]:

$$\varepsilon = q_w \frac{l_c b_w}{P} \qquad \text{Equation 15}$$

Where, l_c is the arc length of contact, b_w is the grinding width, and P is the grinding power. Power and l_c were determined using following expressions [3]:

$$P = \text{Tangential force } (F_t) \times \text{ Wheel peripheral speed } (v_s) \quad \text{Equation 16}$$

$$l_c = (a_e d_s)^{1/2} \quad \text{Equation 17}$$

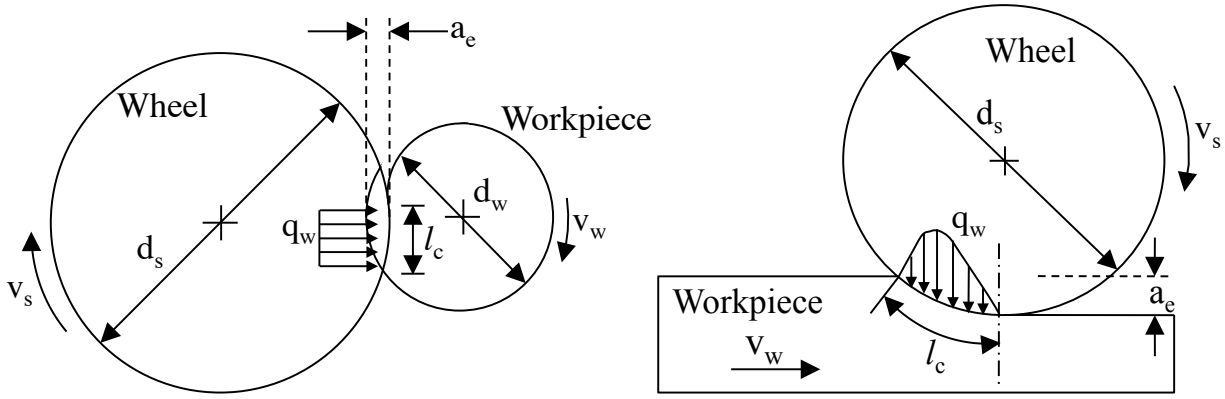

Figure 5.6 Schematic drawing of heat transfer during grinding [3]

The maximum rise in grinding temperature and heat flux into the workpiece was measured against each lubrication condition using grinding parameters listed in Table 5.5.

Table 5.5 Grinding parameters used for temperature measurements and thermal analysis

Grinding Conditions	
Grinding wheel	Vitrified aluminum oxide (32A46-HVBEP)
Wheel diameter (d_s)	300 mm
Workpiece	Ductile cast iron (100-70-03)
Parameters	**Values**
Wheel peripheral speed, V_s (m/s)	30
Workpiece traverse speed, V_w (m/s)	0.06
Depth of cut or Infeed, a_e (μm)	10
Grinding width, b_w (mm)	7.2
Thermal conductivity of workpiece, k (W/mK)	32.3
Thermal diffusivity of workpiece, α (m^2/s)	9.6×10^{-6}

4. **Surface integrity** - Surface grinding is exclusively used to shape and finish parts and components requiring superior dimensional and geometrical tolerances and surface finish. The quality of machined surface plays a decisive role in the reliability of many structural components for high-strength application. Therefore, the quality and integrity of the finished surface is the most critical productive output of a surface grinding process.

   For production operations, typical arithmetic average roughness (R_a) of a ground workpiece surface ranges from 0.1-0.15 μm to 1.5-1.6 μm [99]. Even though the accuracy and surface finish of ground parts is far better (almost 10 times) than turning and milling processes, the morphology of the ground surface is complicated by various mechanisms. Typical surface morphology of a ground surface consists of overlapping scratches formed as a result of slide ploughing of the workpiece material by abrasive cutting points, as shown in Figure 5.7.

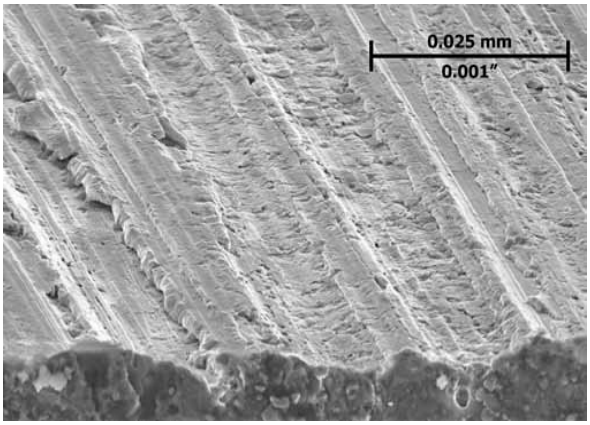

Figure 5.7 A ground and hardened steel surface. At the grit/ workpiece interface there are three possible interactions: rubbing, side and front plowing and chip formation. Side plowing creates grinding scratches. This image shows plowing that caused the material to fold onto itself [100]

   The level of side ploughing is dependent on the type of workpiece material and lubrication. Adhesive metals exhibit more side ploughing and further degrade the surface condition of workpiece by redepositing metallic particles/swarf adhered to the abrasive grains [3]. Film-

forming properties of advanced lubricants have been found to be highly effective in reducing ploughing by decreasing abrasive grain-workpiece adhesion [3]. Apart from workpiece material properties and lubrication, the type of wheel and its condition, wheel dressing, feed rate, and machine rigidity also influence the quality of grinding-generated surfaces.

In this research, the surface integrity of ground ductile iron and EN 24 steel specimens was characterized by superficial roughness, profile of surface texture, and surface microstructure. These parameters were measured and compared against each lubrication condition. Arithmetic average roughness (R_a) across the grinding direction was used as a measure of surface roughness. The characteristic peak-to-valley pattern of ground surfaces was analyzed using 3-d profile of surface texture. A Wyko NT9100 optical profiler from Veeco was used for roughness measurement (R_a) and 3-d surface profiling. The surface microstructure of the ground workpiece was studied using high-resolution scanning electron microscopy (SEM). All SEM studies were performed on an FEI- XL30 ESEM.

5. **Tribochemical Films -** In sliding (frictional) interfaces, chemo-physical reaction between the molecules of lubricant additives and the metallic work surface form protective films of low-shear strength. Such chemically derived films are known as tribochemical films or tribofilms. Figure 5.8 shows typical pad-structured tribofilms on steel surface derived from ZDDP lubricant additives. The chemical and physical structure and morphology of tribofilms determine their extreme-pressure carrying ability, antifrictional and antiwear properties. To understand the lubrication mechanisms at the grinding zone, the nanolubricant-derived tribochemical films were studied in depth. The studies included:
    - The reaction intermediates formed from thermal decomposition of nanolubricant chemistries at the grinding zone

- The formation and deformation of tribochemical films due to grinding process
- The location and morphology of the tribochemical films in the contact surfaces

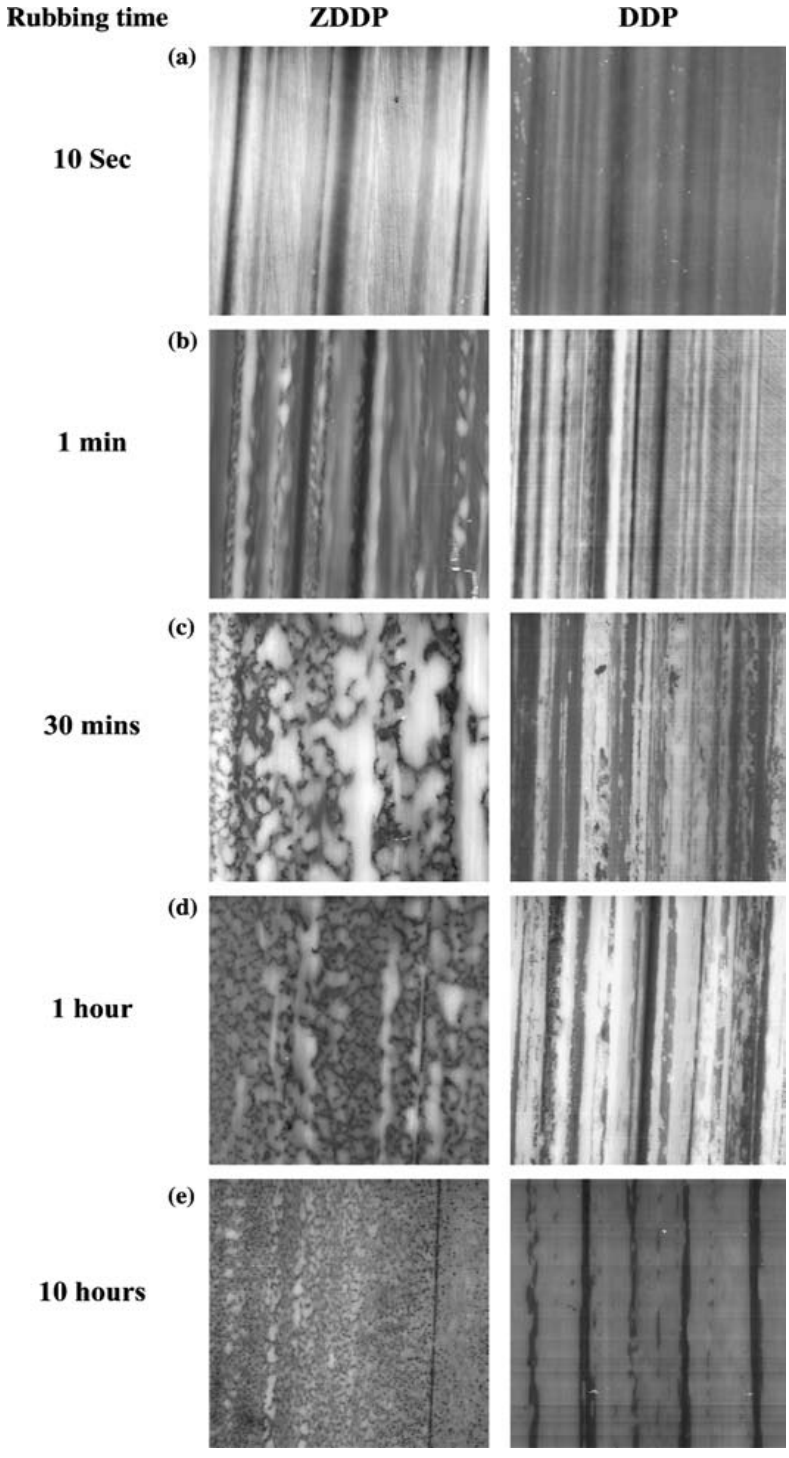

Figure 5.8 AFM of tribofilms generated from 1 wt.% ZDDP under different rubbing [101]

The microstructural analysis of tribochemical films was carried out on the ground surfaces of cast iron and steel workpieces as well as on abrasive grains of the grinding wheel using electron microscopy - TEM (FEI- TITAN 80-300S/TEM) and SEM (FEI- XL30 ESEM). Focused Ion Beam (FIB) milling was used to prepare cross-sectional samples for analyzing the sub-surface microstructure of tribochemical films evolved on workpiece surface. Before SEM and TEM analysis of oil coated workpiece samples, organic solvents were used to dissolve the weakly bonded oil molecules from the metallic surfaces. Further information on the implemented techniques of sample preparation for electron microscopy can be found elsewhere in [28]. Energy Dispersive X-Ray Spectroscopy (EDS) and Raman Spectroscopy were used for the chemical characterization of the tribofilms. To obtain Raman spectrum of tribofilms, a high-sensitivity and high-resolution confocal microscope (inVia-Renishaw) was used. Measurements were taken using 10x and 20x objective and 150 mW of 785 nm laser power. The structural characteristics of nanolubricant particles exposed to severe thermo-mechanical conditions during abrasive grinding were analyzed with TEM. For this analysis, the nanolubricant-covered grinding debris was collected from the machine bed after grinding. The metallic and other heavy particles were carefully removed from the debris by magnetic separation and centrifugation and the remnant liquid sample was used for TEM analysis.

B. TRIBOLOGICAL TESTING

The lubrication mechanisms of nanolubricants in grain-workpiece contact interface were studied from the tribological evaluations of nanolubricant-lubricated cubic boron nitride (cBN) superabrasives-1045 steel sliding pairs on a reciprocating tribotest rig resembling the tool-lubricant-workpiece interactions of MQL-assisted grinding. In this study, the interfacial sliding friction between electroplated cBN superabrasives and AISI 1045 steel workpieces, wear of cBN grains, and surface topography of workpieces were investigated and correlated to the tribological performance and lubricating mechanisms of the test lubricants. These tests also served to verify and correlate the antifriction and antiwear characteristics of nanolubricant compositions with those obtained from MQL-assisted surface grinding tests. During tribological testing, the tool-lubricant-workpiece interaction was simulated to resemble the contact and wear mechanisms of MQL-assisted grinding. The tests were carried out under varying experimental conditions as discussed below.

Lubricants

Six lubricants were applied in this study as summarized in Table 5.6 and were categorized into two groups. The first group consisted of three different base fluids, including vegetable oil, a water-based emulsion, and a biodegradable ester-based cutting fluid. The first two were unformulated base fluids without any additives, whereas the biodegradable ester-based cutting fluid was a commercial fluid containing Sulfur (S)-Phosphorus (P)- based additives. The second group included nanoparticle-based lubricants (nanolubricants) that were formulated by homogenizing MoS_2 nanoadditive (2.0 wt./wt.%) in the base fluids. The base fluids were selected to formulate high-performance grinding fluids with high lubrication ability (oil-based) and lubricity combined with high thermal conductivity (water-based).

Table 5.6 List of lubricants for tribological testing

Lubricant Composition	
Group 1	MoS_2 nanoadditive (2 wt.%) + Ester-based MWF
	MoS_2 nanoadditive (2 wt.%) + Vegetable oil
	MoS_2 nanoadditive (2 wt.%) + Water-based emulsion
Group 2	Ester-based MWF (pure base fluid)
	Vegetable oil (pure base fluid)
	Water-based emulsion (pure base fluid)

The variation in the type of base fluids was also intended to characterize the affect of base composition and chemistry on the performance of nanolubricants (friction, wear, and film-formation). The chemo-physical properties of the base fluids are listed in Table 5.7.

Table 5.7 The chemo-physical properties of the base fluids

Base Fluid	Viscosity (v), 40°C
Biodegradable ester-based MWF	28 cSt
Vegetable-based oil	37 cSt
Water-based emulsion	0.66 cSt

In addition to MoS_2 nanoparticles, hBN and graphite nanoparticles was also used to formulate test lubricants. This was done to compare the tribological performance of MoS_2 nanoparticles as solid lubricant additive with that of hBN and graphite nanoparticles. The friction and wear results from the comparative tribological testing were used to select the solid lubricant additive

for formulating nanolubricants for MQL grinding. The lubricant compositions and comparative tribotest results are discussed in Appendix I.

Tribological Test Rig

The wear and friction characteristics of cubic boron nitride (cBN) superabrasives-1045 steel sliding pairs in the presence of lubricant were investigated on a reciprocating tribotest rig. The sliding friction-wear tests were performed at room temperature using a pin-on-flat arrangement on an instrumented tribometer (Model- TRB, CSM Instruments). A reciprocating module, as shown in Figure 5.9, was attached to the tribometer to reciprocate the workpiece linearly with respect to the static cBN pin. This setup was designed to simulate the material removal mechanism of reciprocating surface grinding (no cross feed) where the workpiece is traversed past the static abrasive wheel rotating at a high speed. During sliding tests, the system acquired friction force data at a frequency of 5 Hz. The test parameters were typical of abrasive tribotesting and are listed in Table 5.8.

Lubricant was delivered to the pin-workpiece sliding zone in the form of droplets by using an injection syringe as shown in Figure 5.8. The syringe was positioned to drop lubricant from the front end of the cBN pin, so that the lubricant and its additives were carried to the sliding interfaces in the pores of the abrasive pin. This approach of fluid delivery closely resembled MQL in surface grinding. The only difference is the absence of compressed air in the former case. More details of the fluid delivery technique in MQL grinding can be found elsewhere in [28, 51]. During each 60-minute tribotest, a 3.0 ml volume of lubricant was delivered onto the sliding zone. A pre-measured volume of 0.5 ml lubricant was dispensed accurately in the beginning of the test and thereafter, reproducibly at every 10^{th} minute of the test.

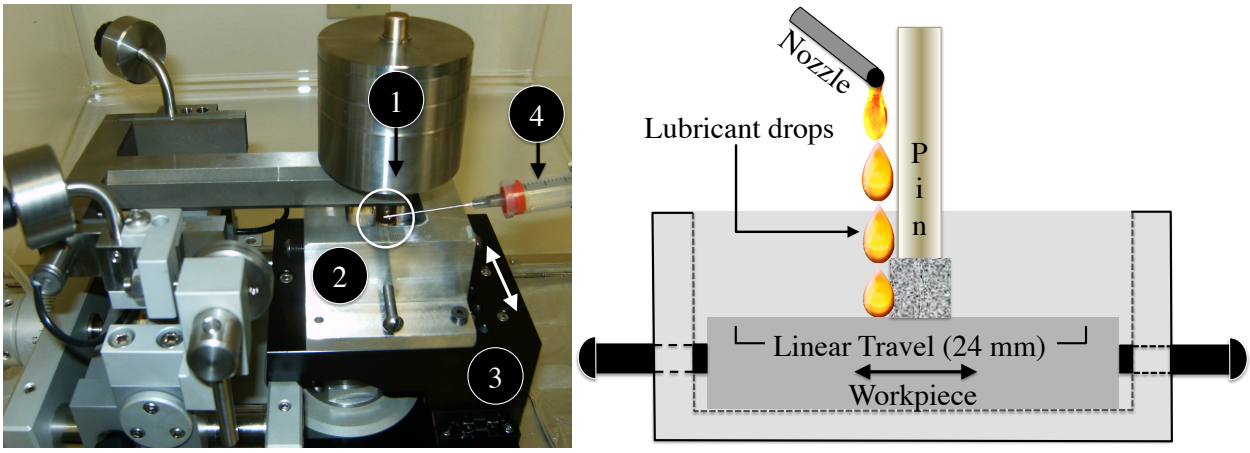

1. Load 2. Lubricant cup 3. Reciprocating module 4. Lubricant delivery injection syringe

Figure 5.9 Reciprocating tribotest rig (left) and lubricant delivery during tribological testing (right)

Table 5.8 Tribological test parameters

Test Parameters	Values
Normal Load	10 N
Linear speed	200 mm/s
Test duration	60 min
Linear passes	6070
Sliding distance/pass	24 mm

AISI 1045 carbon steel workpieces were used in the tests, which had nominal composition of 0.45 wt.% C; 0.25 wt.% Si; 0.75 wt.% Mn; 0.05 wt.% P; 0.05 wt.% S; and the base metal Fe. The workpieces were case hardened to 50 HRC and the test surfaces were mirror polished (R_a - 0.3 μm. The dimension and microstructure of a polished workpiece is shown in Figure 5.10(b) and 5.10(d). Electroplated cBN-superabrasive mounted pins (Saint Gobain/Norton abrasives) with grit size of 150 were used as the static partner in the sliding tests. The mounted pins

consisted a single layer of cBN superabrasive grains (of irregular shapes) held on the pin hub by an electroplated nickel bond, as shown in Figure 5.10(a) and 5.10(c).

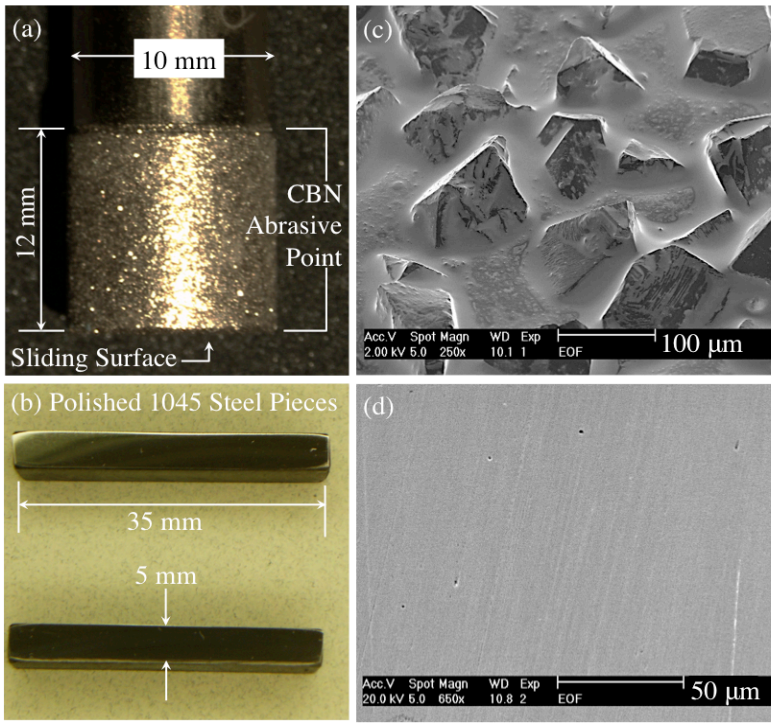

Figure 5.10 (a) and (b) cBN-abrasive mounted pin (150 grit) and polished AISI 1045 steel workpieces, respectively, (c) and (d) SEM micrograph of new electroplated cBN pin surface and polished workpiece surface, respectively

The selection of cBN superabrasive as tool (pin) material in tribological testing was guided by the importance of, as well as lubrication-related challenges of, grinding with cBN superabrasive wheel. Favored by the high thermal conductivity, vitrified as well as electroplated cBN superabrasive wheels are being increasingly used for grinding steels in automotive and heavy machinery industries. Reduced workpiece thermal damage has been reported with cBN superabrasive wheels as compared to the Al_2O_3 wheels [102]. Reports of lower energy partition with vitrified and electroplated cBN wheels have led to the conclusion that bulk cooling of machining zone by the grinding fluids is less of a factor of concern [103-105]. Thus, elimination

of frictional losses by lubrication becomes the primary role of the grinding fluids. To achieve better lubricity, application of oil-based fluids is by far the most common practice in cBN grinding. Application of straight cutting oils, synthetic fluids, and concentrated solutions of vegetable oil in water has been reported in the literature [106-108]. In addition to the inherent thermo-mechanical extremities of grinding process, the surface structure of the grinding wheel also influences lubrication. The unique structural porosity of an abrasive wheel serves as mini reservoirs for lubricants during grinding. However, single layered electroplated cBN wheels have limited surface porosity that tends to disfavor lubrication, particularly during minimal quantity application. Therefore, a single-layered cBN-superabrasive pin was ideally suited to test the effectiveness of the higher surface energy of nanoparticles (of nanolubricants) that was hypothesized to enhance their anchoring to the wheel porosities.

Measurement Parameters

Tribological performance and mechanisms of organic-coated MoS_2 nanoparticles were evaluated as a function of variation in chemo-physical properties of the base fluids using:

1. **Coefficient of sliding friction (μ) -** The ratio F_t/F_n is defined as the coefficient of friction, where F_t and F_n represents force tangential (frictional force) and normal to the tool surface, respectively [8]. The tribometer measured friction coefficient and the software produced friction coefficient versus time for both forward and backward displacement motions. μ versus time and mean coefficient of friction ($\mu_{average}$) was measured for each lubricant to quantify their antifriction (lubricating) property between cBN superabrasives-1045 steel sliding pairs.

2. **Surface characteristics of workpiece weartracks and abrasive grains -** Like grinding, pin-on-flat engagement of cBN superabrasives and workpiece produced weartracks on

the soft metal surface and caused wearing of cBN grains. Occurrence of abrasive wear including attritious wear (wearflat), grain fracture, and grain pullout were evaluated against lubrication condition and were correlated to the surface features of workpiece. SEM was used to characterize the worn surfaces of workpieces and cBN pins after 6070 abrasion cycles. The roughness profiles of the workpiece surfaces were measured using a Veeco Dektak 6M profilometer (scan length- 2.0 mm) and were compared against trials with different lubricants. The underlying objective was to evaluate the affect of lubricant on the level and depth of side ploughing of workpiece.

3. **Microstructure and chemical composition of tribochemical films -** The prime objective of simulating grinding tool-lubricant-workpiece interaction in tribological tests was to reproduce and study the nanolubricant-derived tribochemical films in MQL conditions. The microstructural and chemical characteristics of the tribochemical films were studied to understand the lubricating mechanisms of the nanolubricants at the cBN grain-workpiece contact interfaces. All microanalyses, including chemical identification of lubricant tribofilm, were carried out on a Philips XL-30 ESEM system equipped with Energy Dispersive Spectroscopy (EDS). Similar microanalyses were also performed on the worn surfaces of cBN grains of abrasive pin.

VI. RESULTS AND DISCUSSION- SURFACE GRINDING NONPRODUCTIVE OUTPUTS

This chapter presents the results and discussion of the nonproductive outputs obtained from surface grinding tests. These results assisted in the study of the lubrication (friction and wear reduction) effectiveness of nanolubricants in minimizing the non-productive outputs of the MQL-assisted grinding process. The chapter is divided into five sections that present the obtained results and discussion on, A) tangential grinding force, B) force ratio (coefficient of friction), C) G-ratio, D) specific grinding energy, and E) grinding temperature and thermal analysis.

A. TANGENTIAL GRINDING FORCE

This section presents the results of tangential forces versus grinding passes obtained during grinding of ductile cast iron at 10 μm wheel-infeed using different lubrication conditions. As recalled from Equation 9, a decline in wear (effective wearflat area- A_a) and friction (coefficient of friction- μ) causes a reduction in tangential grinding forces. Illustrative reduction and steadiness in tangential grinding force as a result of decline in friction and wear from effective lubrication of nanoparticle-integrated oils (nanolubricants) is shown in Figure 6.1 and Figure 6.2. Steadiness was assessed from the slope of the linearly fitted tangential force lines.

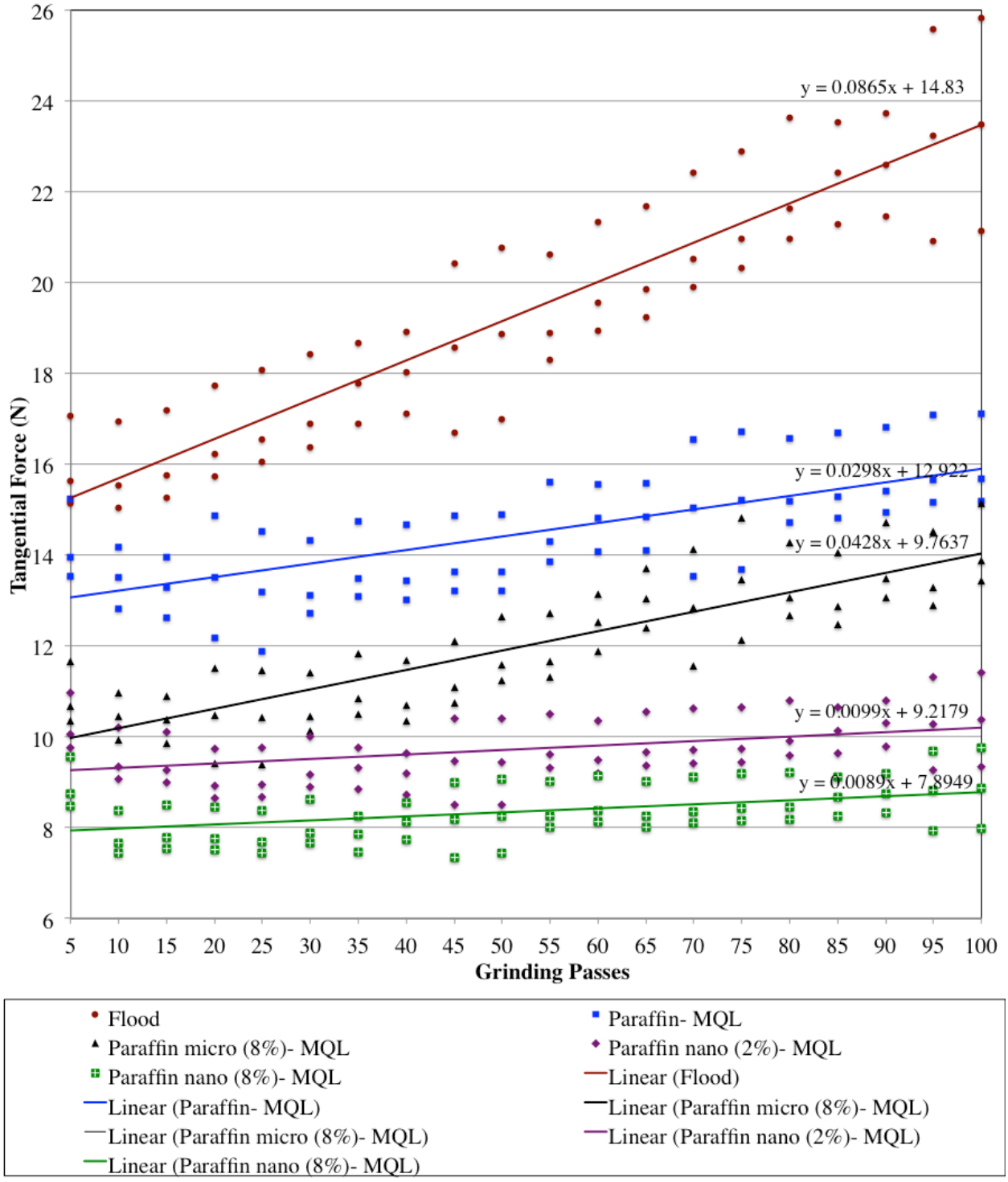

Figure 6.1 Tangential force vs. passes for flood and MQL with paraffin-based lubricants, obtained during grinding of ductile iron at 10 μm wheel-infeed (nano- nanolubricant, micro- microparticles)

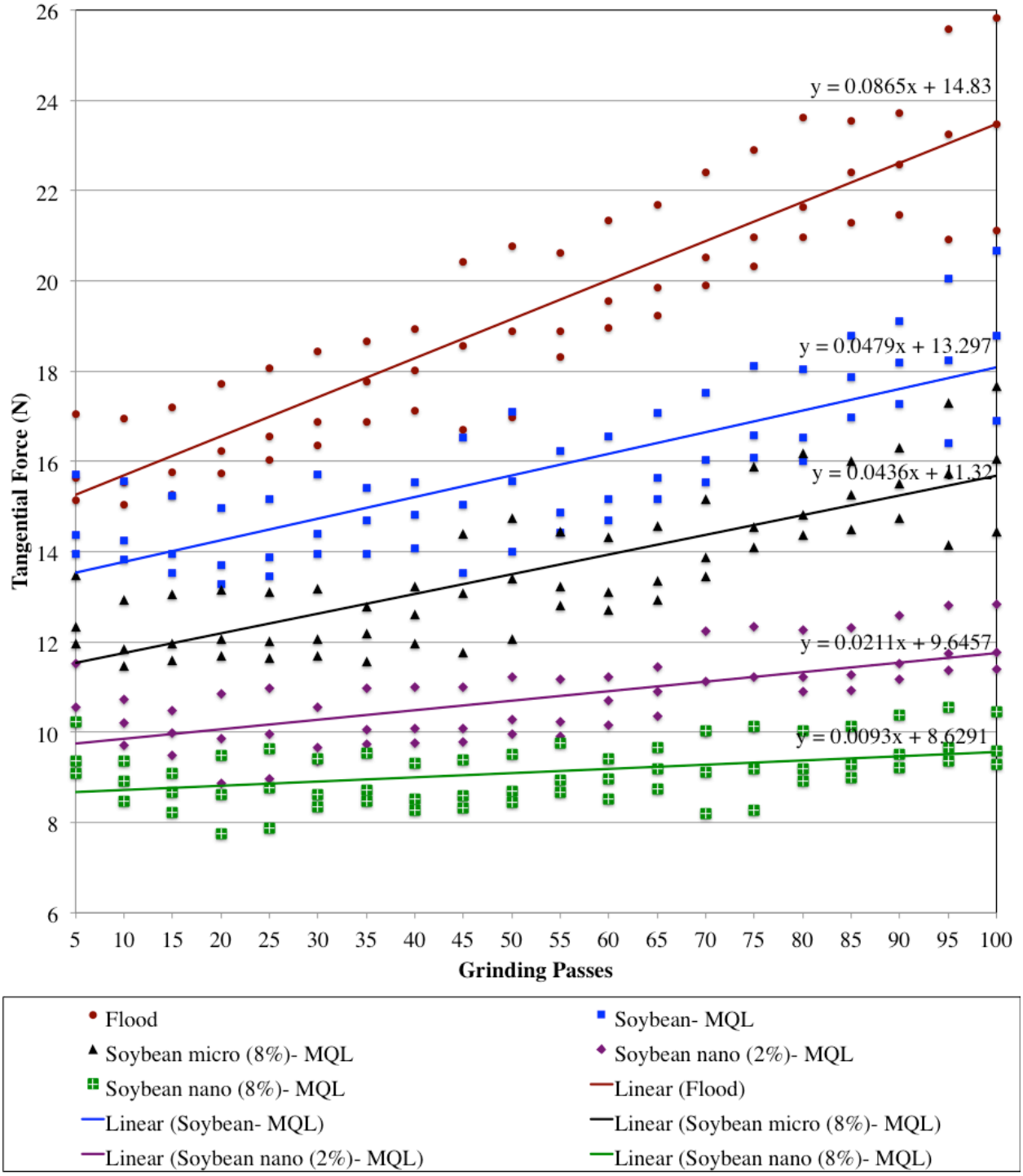

Figure 6.2 Tangential force vs. passes for flood and MQL with soybean-based lubricants, obtained during grinding of ductile iron at 10 μm wheel-infeed (nano- nanolubricant, micro- microparticles)

Lowest average tangential forces of 8.4 N and 9.1 N were measured for 8 wt.% loaded paraffin and soybean-based nanolubricants, respectively. In comparison, high tangential forces ($F_{tAvg.}$ = 19.4 N) were measured during flood grinding and the forces continued to increase steeply with grinding passes (slope- 0.0865). The effective wearflat area of abrasive wheel increased with grinding passes that caused grain-workpiece sliding friction and hence, tangential forces to increase and fluctuate. Therefore, continuous increase in the force values indicated that the synthetic water-based fluid was unable to reduce the growth of wearflats and friction between the grain wearflats and the workpiece.

MQL grinding with base lubricants (paraffin and soybean oil) showed comparative reduction in tangential forces. MQL use of paraffin and soybean oil measured average tangential forces of 14.5 N and 15.8 N, respectively. However, continuous increase in tangential forces with grinding passes suggested an inability of the lubricants to form durable antifriction films at the aggressive grinding zone. Similar observations were made in MQL grinding with paraffin and soy-based lubricants containing MoS_2 microparticles.

MQL grinding with 2 wt.% nanolubricants produced average tangential forces that were 32% lower than the pure base fluids. Slopes of 0.01-0.02 of the linear-fit lines demonstrated near-steady tangential forces throughout the 100 grinding passes. A slight increment in tangential forces, especially with soybean-based nanolubricant (slope- 0.02), was noticed towards later grinding passes. The tangential grinding forces were further reduced and steadied (slope- 0.009) during MQL grinding with 8 wt.% nanolubricants. The ability of nanolubricants to form antifriction and antiwear films at the sliding interfaces of abrasive grains and workpiece was suggested as the cause of the steady reduction in friction and wear and hence, tangential forces during grinding. To evaluate friction and wear between the abrasive grains (including wearflats)

and the workpiece during grinding, coefficient of friction (μ) and G-ratio were measured for all the lubrication conditions, as discussed in the following sections VI.B and VI.C.

B. FORCE RATIO (COEFFICIENT OF FRICTION)

This section presents the results of force ratio or friction coefficient (F_t/F_n or μ) obtained during grinding of cast iron (at 10 and 20 μm wheel-infeed) and EN 24 steel (at 20 μm wheel-infeed) using different lubrication conditions. The measured values of the friction coefficient were used to quantify the frictional losses during grinding with each lubrication condition and to determine the antifriction performance of the lubricants.

Force Ratio – 10 and 20 μm Infeed Grinding of Ductile Cast Iron

The results of force ratio or friction coefficient as a function of lubrication condition, obtained during grinding of ductile iron are shown in Figure 6.3(a) and (b). The plotted data for each lubrication condition was acquired by averaging the force ratio values of 100 grinding passes from three surface grinding tests.

Under the investigated process conditions, flood (wet) grinding using synthetic fluid showed the highest values of μ = 0.38 and 0.78 for 10 and 20 μm infeed, respectively. In comparison to flood lubrication, MQL-assisted grinding with pure base oils (paraffin and soybean) showed reductions in friction (μ_{para} = 0.26 and 0.46, μ_{soy} = 0.27 and 0.47, for 10 and 20 μm infeeds, respectively). Addition of emulsified microparticles to the base oils showed some improvement in the values of force ratio. Microparticles integrated paraffin oil measured μ = 0.22 (10 μm infeed) and 0.34 (20 μm infeed), while soybean oil-based counterpart measured μ = 0.25 (10 μm infeed) and 0.45 (20 μm infeed).

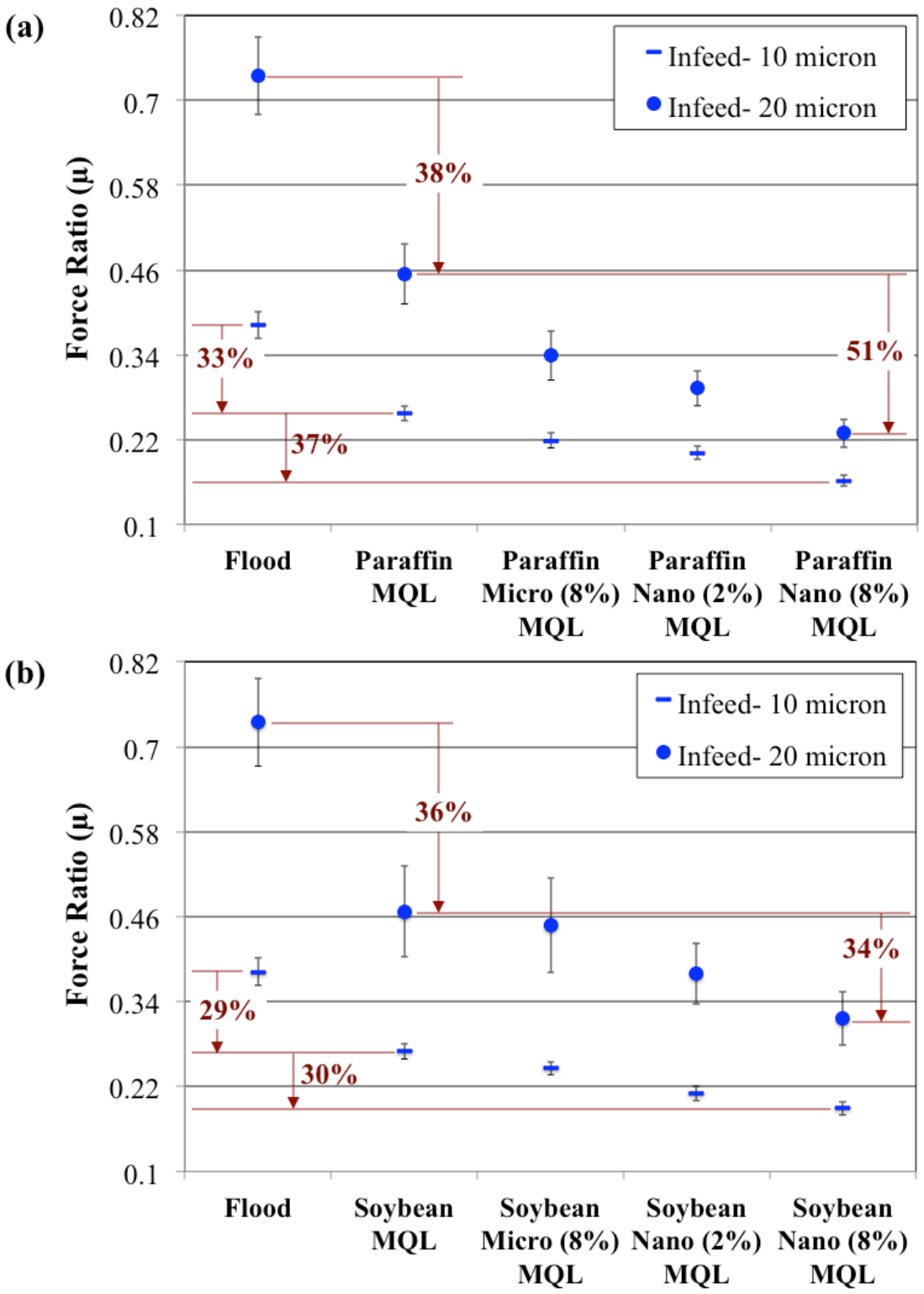

Figure 6.3 Force ratios (μ) for (a) flood and MQL with paraffin-based lubricants, and (b) flood and MQL with soybean-based lubricants obtained during grinding of ductile iron (average values of 100 measurements, error bars represent standard deviation about the mean specific energy measured over the 100 grinding passes)

Further reductions in the values of μ were observed during MQL-assisted grinding of ductile iron with oil-based nanolubricants. With 2.0 wt.% paraffin and soybean-based nanolubricants, force ratio values were reduced to 0.20 and 0.21, respectively for 10 μm infeed condition. While grinding with a 20 μm wheel infeed, 2.0 wt.% paraffin and soybean-based nanolubricants measured μ = 0.29 and 0.38, respectively. The lowest force ratios were attained during grinding with 8 wt.% nanolubricants. Force ratio values of 0.16 and 0.23 were recorded for paraffin-based nanolubricants during grinding with 10 and 20-μm wheel-infeed, respectively. For similar grinding conditions, soybean-based nanolubricants measured μ = 0.19 and 0.32, respectively.

As stated earlier, the force ratio or μ is a quantitative measurement of friction at the grain-workpiece sliding/rubbing interfaces during grinding. Hence, it can be considered as quantitative assessment of friction reducing (antifriction or lubricity) performance of the applied lubricants. High force ratios with flood grinding were typical of conditions involving limited availability of lubricants at the grinding zone. Such conditions were further worsened by the low lubricity of the applied water-based fluid. Observed reduction in friction with pure base oils was attributed to the enhanced penetration with pressurized fluid delivery of MQL and better lubricity of mineral and vegetable oils as compared to water-soluble synthetic fluid. Improvement in antifrictional properties of base oils was evident with the addition of microparticulated MoS_2 as solid lubricant. However, the friction reducing performances of microparticles containing lubricants were lower than the nanolubricants owing to their comparatively high viscosity and poor dispersibility. A debris-clogged cutting zone was observed during MQL grinding with viscous and heavy microparticles bearing paraffin and soybean oil. Third-body abrasion from excessive loose debris is known to exacerbate friction and wear conditions of abrasive processes [5]. Debris clogging was found more intense during grinding with a higher wheel infeed of 20 μm.

Compared to nanolubricants, microparticles had poor dispersibility in base oils despite equivalent emulsification and sonication. Rapid settling/separation of microparticles was observed in the fluid reservoir during MQL fluid application, which reduced the delivery of intrinsically lubricating MoS_2 particles to the grinding zone. This wasn't the case with enhanced penetration of well-dispersed and high-surface area nanoparticles of MoS_2, enabling targeted delivery through the grinding zone. It was evident from the results of low force ratios or friction coefficients attained during MQL grinding with nanolubricants. Low-friction results with nanolubricants were attributed to the synergistic effect of the polarity and lubricity of organic molecules and intrinsic low-friction property of lamellar structured MoS_2 nanoparticles well dispersed within base oils. The measured values of force ratio (μ) with paraffin and soybean-based nanolubricants corresponded to literature reported well-lubricated dulled/flattened abrasive grains (wearflats) in sliding contact with the workpiece surface [7].

In Figure 6.3, an increase in force ratio was observed with an increment in the depth of cut (infeed) during grinding with similar lubrication conditions. This was due to an increase in tangential (cutting) grinding forces at higher infeed conditions. An increase in depth of cut results in additional material removal per unit time and hence, increases the energy requirements of the process. This causes a proportional increase in the tangential forces if other parameters remain constant (Equations 14 and 6). In an interesting observation, an increase in grinding depth of cut from 10 to 20 μm showed greater percentage increments in force ratio for flood grinding (92% increase) as well as MQL grinding with pure base oils and with microparticles. MQL grinding with pure and microparticles bearing paraffin oil measured respective increments of 80% and 61% in force ratio as a function of increase in wheel-infeed, whereas soybean oil-based counterparts measured an approximate increment of 80%. In comparison, MQL grinding

with 2 and 8 wt.% loaded paraffin nanolubricant measured less than 45% increment in force ratio values due to increase in depth of cut from 10 to 20 µm. This was supportive of the suggested extreme-pressure (EP) property of the nanolubricants. Due to this load carrying capacity, nanolubricant-derived tribofilms continued to provide excellent protection against sliding friction despite exposure to high-contact pressures during MQL grinding.

Figure 6.4 lists the percentage reduction in the force ratio values during MQL grinding with 8 wt.%-loaded nanolubricants as compared to 2 wt.% loaded nanolubricants and pure base oils. Based on the measured % reduction values following conclusions were derived:

1. Effective friction reducing capability of nanolubricants in energy intensive grinding conditions due to increase in depth of cut (a_e- 20 µm).
2. Better performance (antifriction) control with a quantitative increase in the concentration of nanoadditive chemistries.

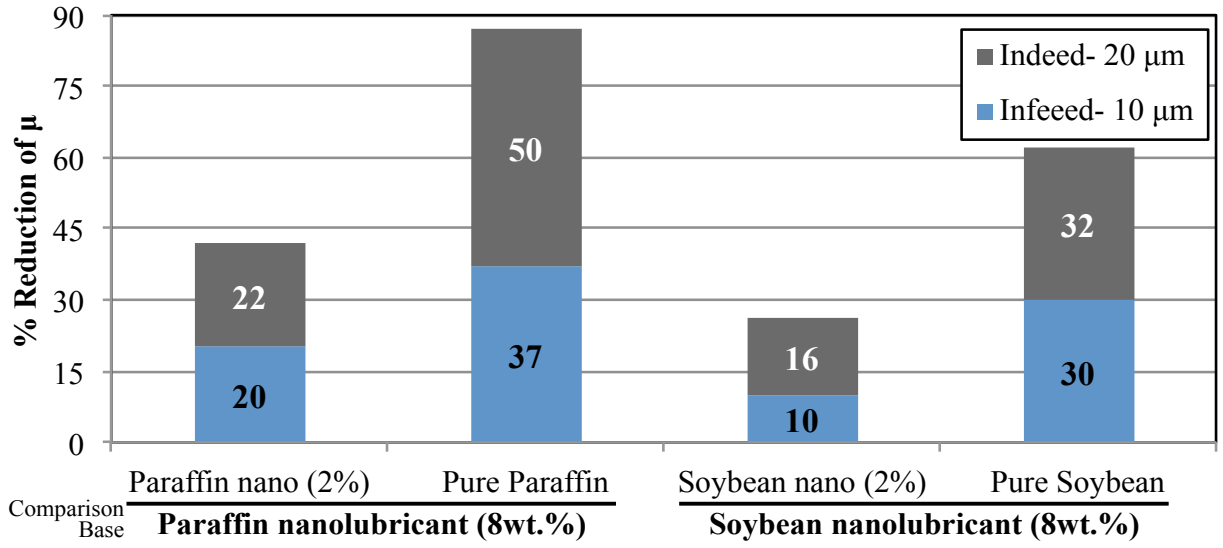

Figure 6.4 Reduction in force ratio (µ) by 8 wt.% loaded nanolubricants as compared to 2 wt.% loaded nanolubricants and pure base oils

Paraffin-based nanolubricants showed better friction reduction performance during MQL grinding of ductile iron as compared to soy-based counterparts. The workpiece-lubricant compositional relationship was further investigated by measuring and comparing the force ratios during grinding of EN 24 alloy steel, as discussed below.

Force Ratio - 20 µm Infeed Grinding of EN 24 Steel

The results of force ratio (µ) as a function of lubrication condition obtained during grinding of EN 24 alloy steel are shown in Figure 6.5. The plotted data for each lubrication condition was acquired by averaging the force ratio values of 100 grinding passes from three surface grinding tests. Comparative observations were based on the mean values of 100 measurements. In Figure 6.5, base, micro, and nano refers to pure base oil (no additives), oils containing MoS_2 microparticles, and nanolubricants, respectively.

Under the investigated process conditions, flood (wet) grinding showed the highest value of force ratio (0.73). Compared to flood grinding, MQL-assisted grinding with pure base oils showed slight improvement in interfacial friction ($\mu_{para} = 0.63$, $\mu_{soy} = 0.60$,). In both the cases of paraffin and soybean-based lubricant, addition of microparticles showed slight reduction in friction ($\mu_{micropara} = 0.57$, $\mu_{microsoy} = 0.58$), over the pure base oils. Nanolubricants showed further reduction in force ratio values as a function of increase in the concentration of MoS_2 nanoparticles. Force ratio values of 0.43 and 0.41 were recorded for 8.0 wt.% loaded paraffin and soybean-based nanolubricant, respectively. These showed approximately a 32% average reduction in force ratio over pure base oils, which suggested improved lubrication capability of multicomponent nanoadditive during MQL grinding.

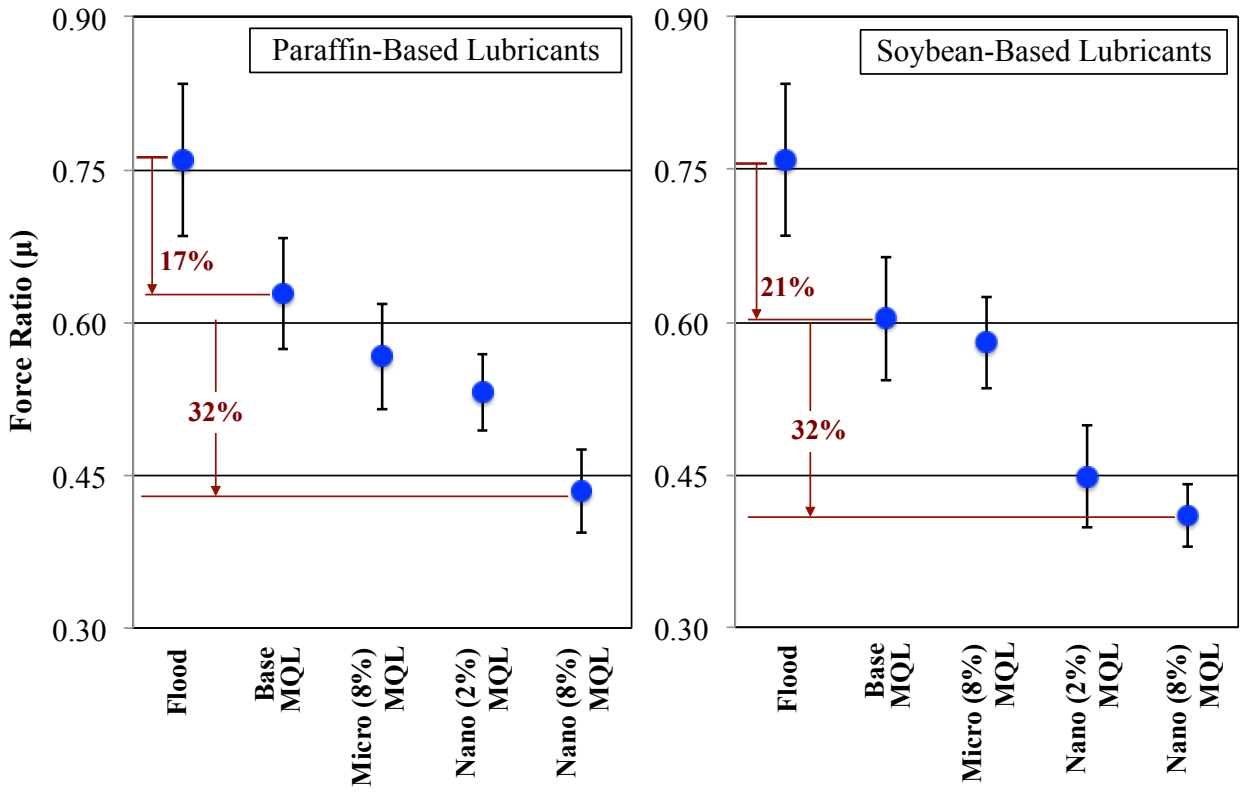

Figure 6.5 Force ratio (μ) obtained during grinding of EN 24 steel at 20 μm wheel-infeed (average values of 100 measurements, error bars represent standard deviation about the mean)

In terms of lubrication performance of the nanolubricants, MQL-assisted grinding (with 20 μm wheel infeed) of EN 24 steel yielded opposite results as compared to that of ductile iron. Soybean-based nanolubricants showed better antifriction performance during MQL grinding of EN 24 steel as compared to the paraffin-based counterparts. A plausible explanation of this workpiece-nanolubricant compositional behavior is presented in later sections.

C. G-RATIO

This section presents the results of grinding (G)-ratio obtained after 100 passes of grinding of cast iron (at 10 and 20 µm wheel infeed) and EN 24 steel (at 20 µm wheel infeed) with different lubrication conditions. The measured values of G-ratio were used as a performance index for wheel wear resistance, and hence antiwear behavior and performance of the lubricants. High values of G-ratio are representative of lower wheel wear and, hence longer wheel life.

G-Ratio - Grinding of Ductile Cast Iron

The measured values of G-ratio for different lubrication condition, obtained after 100 passes of grinding of ductile iron are shown in Figure 6.6.

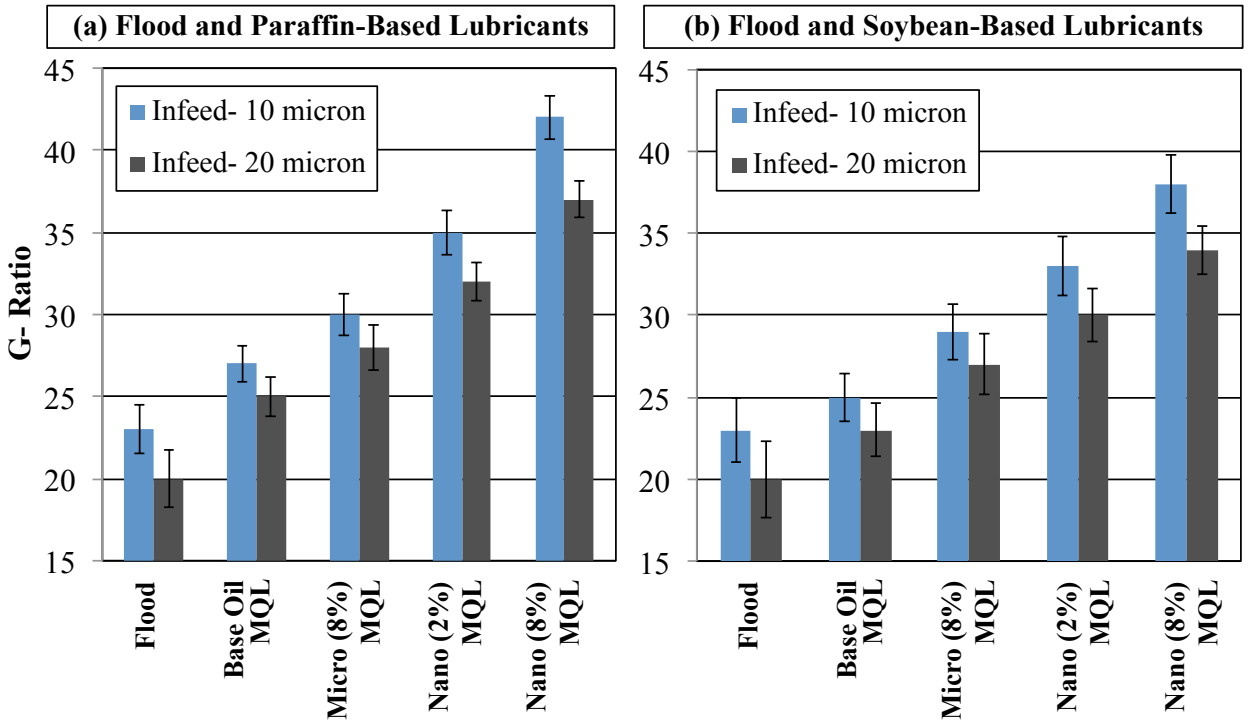

Figure 6.6 G-ratio values obtained after grinding of ductile cast iron with (a) flood and MQL with paraffin-based lubricants, and (b) Flood and MQL with soybean-based lubricants (average values of three measurements, error bars represent standard deviation about the mean)

From Figure 6.6, the lowest values of G-ratio were observed with flood (wet) grinding of ductile iron ($GR_{10\ \mu m\text{-infeed}} = 23$, $GR_{20\ \mu m\text{-infeed}} = 20$). The lowest values with flood application of water-based synthetic fluid corresponded to high-volumetric wear of the Al_2O_3 wheel during grinding. In comparison, MQL grinding with pure base oils showed slight increases in G-ratio. For 10 μm grinding infeed, paraffin and soybean oil had measured G-ratio values of 27 and 25, respectively. MQL grinding with a 20 μm wheel-infeed yielded respective G-ratio values of 25 and 23 for paraffin and soybean oil. Improvements in G-ratio values and hence, reduced wheel wear was apparent with the addition solid lubricant particles to the base oils. For a 10 μm grinding infeed, high G-ratio values of 42 and 38 were obtained with 8 wt.% loaded paraffin and soybean-based nanolubricant, respectively. The same nanolubricant compositions measured respective G-ratios of 37 and 34 with 20 μm grinding infeed. Nanoparticle-based lubricant additive exhibited better antiwear characteristics than the microparticles-based additive, corroborating with the previous antifriction results. This was evident from the 36% and 32% average increases in G-ratios with 8 wt.% nanolubricants as compared to equivalently loaded microlubricants for 10 and 20 μm grinding-infeed, respectively. On an average scale, the measured values of G-ratio with 8 wt.% loaded paraffin and soy-based nanolubricants were 18% and 14% higher than those obtained with the respective 2 wt.% loaded nanolubricants. This suggested the antiwear property of nanolubricants increased with an increase in the loading concentration of MoS_2 nanoparticles.

G-Ratio - Grinding of EN 24 Steel

Figure 6.7 shows the measured value of G-ratios for different lubrication conditions, obtained after 100 passes of grinding of EN 24 alloy steel at 20 μm depth of cut. The values of G-ratio followed a similar trend as was observed for 20 μm infeed grinding of ductile iron.

The lowest G-ratio was measured for flood grinding (GR = 23) while MQL grinding with 8 wt.% loaded soy-based nanolubricant measured the highest (GR = 39). MQL grinding with 8 wt.% loaded soybean and paraffin-based nanolubricants reduced volumetric wheel wear by 33% and 30% as compared to the respective base oils without additives. The same nanolubricant compositions measured 23% and 19% reduction in volumetric wheel wear, compared to the microparticles bearing soybean and paraffin oil, respectively. MQL grinding with 8 wt.% loaded soybean and paraffin-based nanolubricants increased G-ratios by 15% and 9%, compared to the respective 2 wt.% loaded nanolubricants. This was consistent with the earlier findings where antiwear performance of nanolubricants was strengthened by an increase in the concentration of organic-coated nanoparticles.

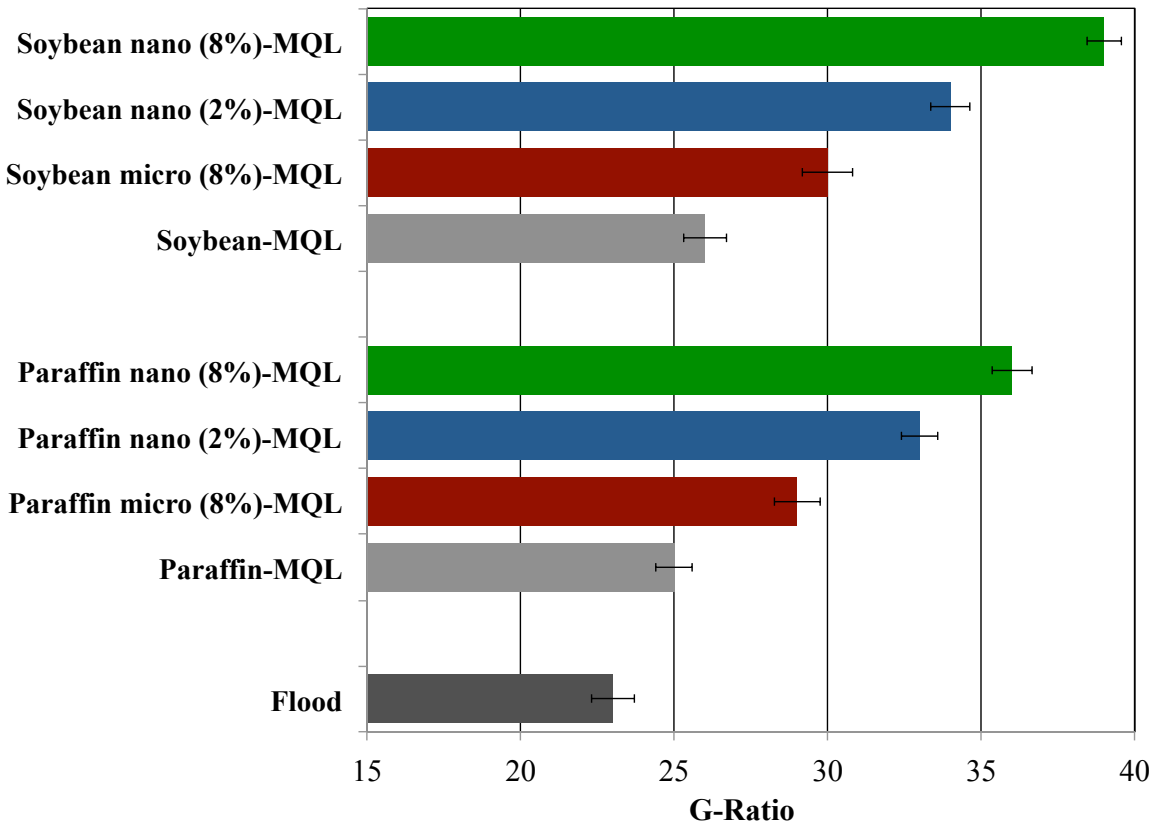

Figure 6.7 G-ratio values obtained after grinding of EN 24 alloy steel (average values of three measurements, error bars represent standard deviation about the mean)

High G-ratio values with low-friction nanolubricants were an indicative of reduction in attritious and fracture wear of abrasive grains during MQL-assisted grinding. Formation of stable low-shear strength films at the micro interfaces between grains and workpiece asperities by organic-coated MoS_2 nanoparticles was the cause of the antiwear property of nanolubricants. This antiwear property preserved the integrity of abrasive grains of the bonded Al_2O_3 wheel for increased number of grinding passes.

D. SPECIFIC GRINDING ENERGY

This section presents the results of specific energy requirements during grinding of cast iron (at 10 and 20 μm wheel infeed) and EN 24 steel (at 20 μm wheel infeed) using different lubrication conditions. A low value of specific energy represents an energy-efficient grinding process that consumes less energy for unit volume of material removal. From Equation 14, a decrease in tangential force from a reduction in friction (friction coefficient- μ) by a lubricant would yield a low value of specific energy consumption during grinding.

Specific Grinding Energy - 10 μm Infeed Grinding of Ductile Cast Iron

The results of specific energy consumption versus tangential forces obtained during grinding of ductile iron at 10 μm depth of cut are shown in Figure 6.8. The plotted values of specific energy for each lubrication condition was acquired by averaging energy measurements of 100 grinding passes from three surface grinding tests.

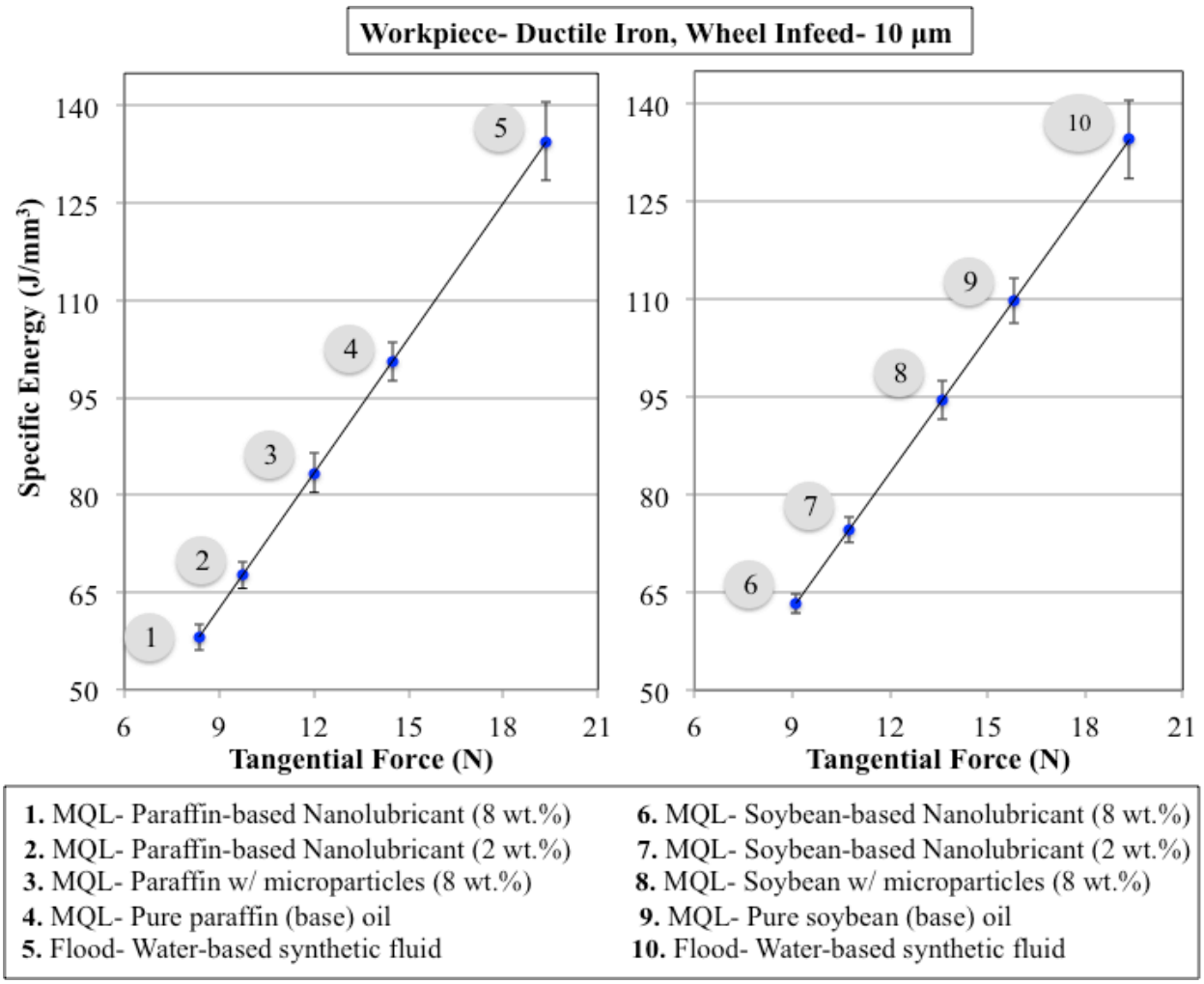

Figure 6.8 Specific energy obtained during grinding of ductile cast iron at 10 µm wheel-infeed (average values of 100 measurements, error bars represent standard deviation about the mean)

Flood (wet) grinding with a synthetic fluid showed highest energy consumption of 135 J for 1.0 mm^3 volume of material removal. MQL assisted grinding with pure soybean and paraffin oil showed 18% and 25% reductions in specific energy consumption, respectively. MQL grinding with microparticles bearing soybean and paraffin oil measured 95 J/mm^3 and 83 J/mm^3 as specific energy. Lowest energy consumption was measured during MQL-assisted grinding with 8.0 wt.% loaded paraffin nanolubricant (U= 58 J/mm^3) followed by the soybean-based counterpart (U= 63 J/mm^3). Decrements of 57%, 43%, and 30% in energy consumption were

recorded with 8 wt.% loaded paraffin nanolubricant as compared to flood cooling, MQL with pure paraffin, and MQL with paraffin-microlube, respectively. Soy-based nanolubricant (with 8 wt.% loading) reduced energy consumption by 53%, 43%, and 34%, compared to flood, MQL with pure soybean, and MQL with soybean-microlube, respectively. Energy consumptions during MQL grinding with oil-based nanolubricants were found to reduce with an increase in the loading concentration of hybrid nanoadditive.

From Figure 6.8, the effect of tangential grinding force and hence, coefficient of friction (μ) was clearly reflected in the values of specific energy consumption. Flood grinding (using synthetic MWF) with highest force and friction coefficient (F_t = 19.4 N and μ = 0.38) emerged as the largest energy consuming process. With comparatively low tangential forces, paraffin oil-based lubricants showed reduced specific energy consumption during MQL-grinding as compared to equivalent soybean-based lubricant compositions. MQL use of nanolubricants enabled grinding with reduced frictional losses and wear that yielded maximum reductions in tangential forces and hence, specific energy requirements for material removal.

Specific Grinding Energy - 20 μm Infeed Grinding of Ductile Iron and EN 24 Steel

The results of specific energy consumption obtained during grinding of ductile iron and EN 24 steel at 20 μm depth of cut are shown in Figures 6.9 and 6.10, respectively. Specific energy value for individual lubrication condition was acquired by averaging energy measurements of 100 grinding passes from three surface grinding tests. The effect of tangential grinding force and hence, coefficient of friction (μ) on specific energy consumption was plotted for the grinding cases with 20 μm infeed as well. A 52-110% higher energy consumption due to additional material removal per unit time with an increase in depth of cut was also evident in the results of specific energies measured with 10 and 20 μm infeed grinding of ductile iron.

Figure 6.9 Specific energies obtained during grinding of ductile cast iron at 20 µm wheel-infeed (average values of 100 measurements, error bars represent standard deviation about the mean)

Under the investigated grinding conditions of ductile iron, flood (wet) grinding showed the highest energy consumption of 205 J/mm^3. A corresponding high value of friction coefficient indicated the inability of the applied synthetic fluid to reduce frictional losses, and hence, energy consumption of the process. MQL-assisted grinding with pure soybean and paraffin oil measured specific energies of 195/mm^3 and 175 J/mm^3, respectively, suggesting 5% and 15% less energy consumption due to reductions in frictional losses. MoS_2 microparticles added soybean oil measured 7% reduction in energy consumption ($U_{microsoy}$ = 182 J/mm^3), whereas microparticles bearing paraffin oil showed 24% reduction in energy consumption ($U_{micropara}$ = 133 J/mm^3) over

pure base oil. In comparison, both 2.0 wt.% loaded nanolubricants in soybean and paraffin oil showed improvements in process efficiency by measuring specific energies of 157 J/mm^3 and 112 J/mm^3, respectively. MQL grinding of ductile iron with MoS_2-based soybean lubricants showed between 36-40% higher specific energy consumption as compared to the paraffin-based lubricant compositions. This was correlated with the observed 29-38% higher friction coefficients (frictional losses) with MoS_2-based soybean lubricants as compared to the paraffin-based counterparts. MQL-assisted grinding with paraffin-based nanolubricant (8.0 wt.% loaded) emerged as the most energy-efficient process by measuring 96 J/mm^3 as specific energy. These were approximately 53%, 45%, and 28% reductions in specific grinding energy as compared to flood grinding, MQL with pure paraffin oil and microparticles bearing paraffin oil, respectively. With 39% higher friction coefficient, 8.0 wt.% loaded soybean-based nanolubricant consumed more energy per unit volume of material removal (U = 133 J/mm^3).

The results of specific energy obtained during grinding of EN 24 steel showed a similar pattern as seen in the case of ductile cast iron, with flood grinding measuring the highest consumption of energy and 8.0 wt.% loaded-nanolubricants the least. MQL-assisted grinding with paraffin-based nanolubricant (8.0 wt.% loaded) measured specific energy reductions of 34%, 29%, and 22%, compared to flood, MQL with pure paraffin oil, and MQL with paraffin-microlube, respectively. Better energy efficiency was observed during MQL grinding with soy-based nanolubricant (8 wt.% loaded) that reduced specific energy by 38%, 33%, and 26% as compared to flood, MQL with pure soybean and soybean-microlubricant, respectively. Because of their enhanced antifriction and EP properties, nanolubricants consistently yielded low tangential forces that led to low-energy consumptions and hence, high process efficiencies during MQL-assisted grinding.

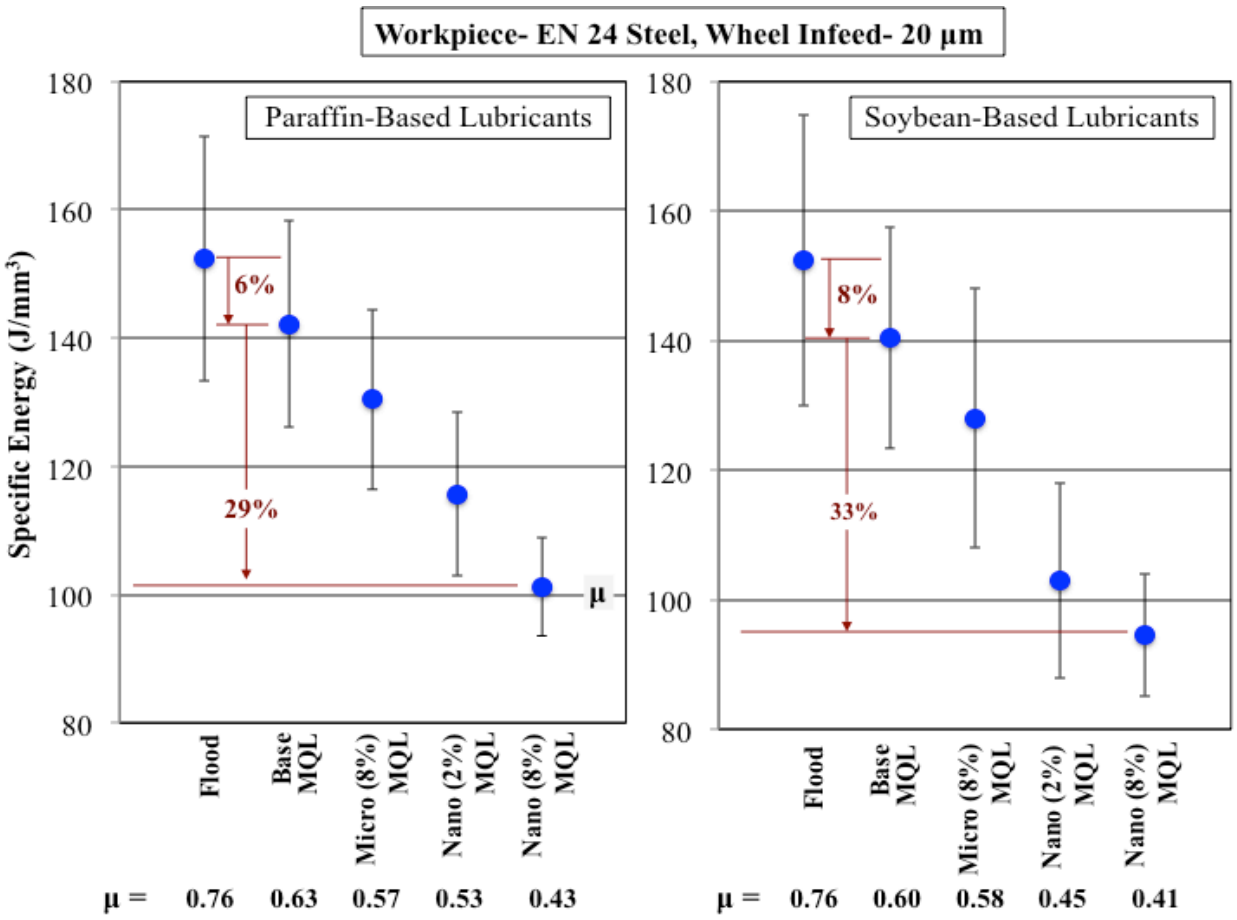

Figure 6.10 Specific energies obtained during grinding of EN 24 steel at 20 µm wheel-infeed (average values of 100 measurements, error bars represent standard deviation about the mean)

E. GRINDING TEMPERATURE AND THERMAL ANALYSIS

This section presents the results of maximum temperature rise at the grinding zone and heat flux into the workpiece during grinding of ductile cast iron with different lubrication conditions. The results of the thermal analysis of the grinding processes were used to determine the cooling behavior and performance of the lubrication conditions. Figure 6.11 show the peak or maximum temperatures at the workpiece surface (h = 0) obtained during grinding with different lubrication conditions. The surface grinding experiments were carried out on cast iron workpieces using 10 µm depth of cut.

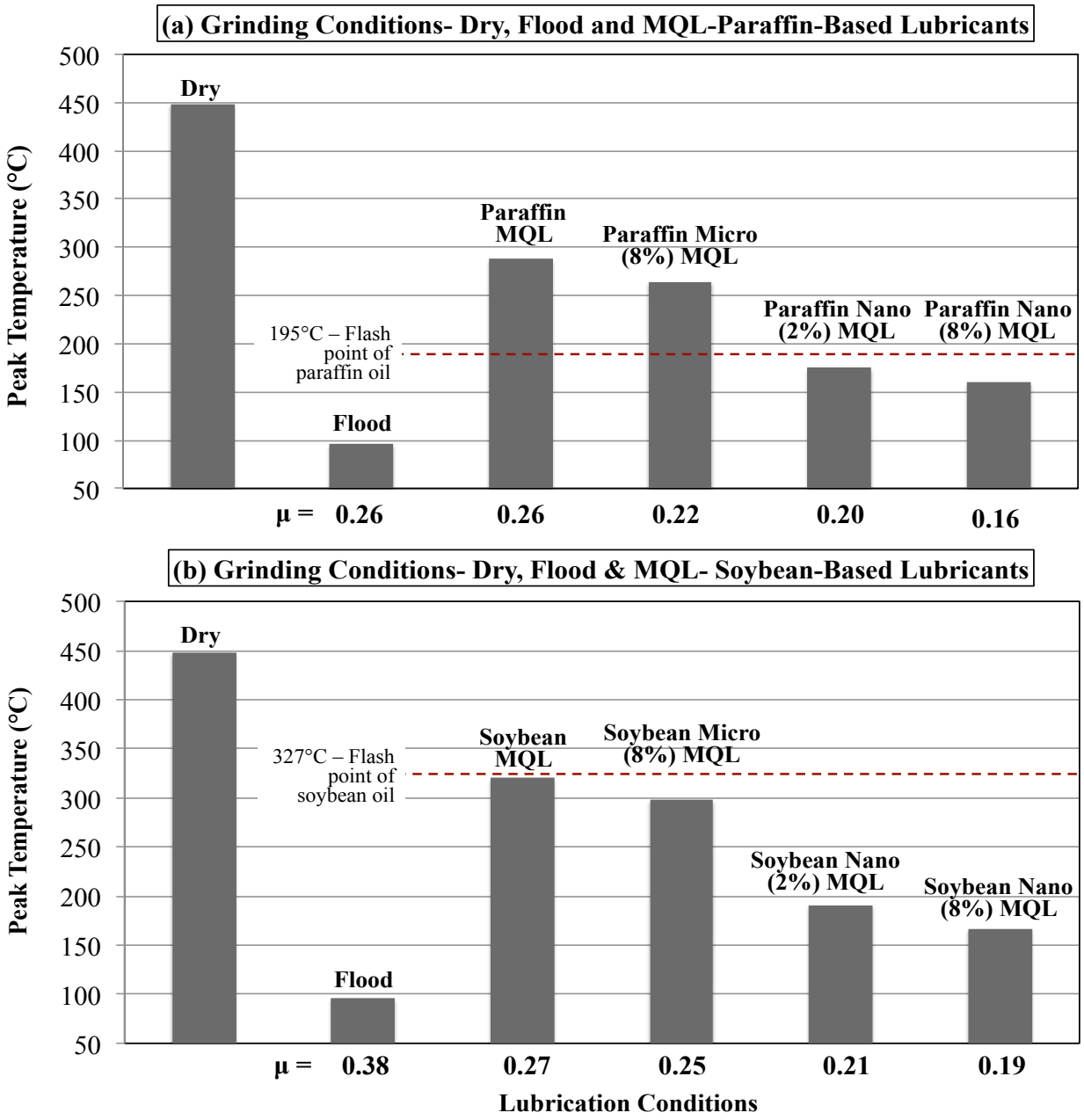

Figure 6.11 Maximum rise in grinding temperatures at the workpiece surface (z = 0) as function of lubrication conditions obtained during grinding of ductile iron at 10 μm wheel-infeed

The embedded thermocouple system measured 448˚C as the peak surface temperature for dry grinding (without any lubricant). Flood grinding with water-based synthetic MWF exhibited the lowest surface temperature of 96˚C. The surface temperature being below film boiling

temperature (100˚C) indicated that the water-based coolant provided bulk workpiece cooling by convective-heat transfer during grinding.

MQL-assisted grinding with paraffin (base) oil resulted in a maximum surface temperature of 288˚C, which was higher than its flash temperature of 195˚C. While MQL with soybean (base) oil showed a maximum surface temperature of 320˚C, which was close to its flash temperature of 327˚C. Microparticles-integrated paraffin and soybean oil exhibited maximum temperatures of 264˚C and 298˚C, respectively, showing some reduction in surface temperatures during MQL grinding. Application of 2 wt.% loaded paraffin and soybean based nanolubricants showed a steep drop in the surface temperatures by reducing the measured values to 175˚C and 191˚C, respectively. MQL grinding with 8 wt.% loaded paraffin nanolubricant exhibited the lowest surface temperature of 160˚C, followed by 167˚C with 8 wt.% loaded soybean based nanolubricant.

To understand the mode of heat transfer during grinding, thermal conductivities of base oils and nanolubricants were measured using the hot wire method, as shown earlier in Figure 4.10. The measured values of thermal conductivity of paraffin (base) oil, 2 and 8 wt.% loaded nanolubricants were 0.146, 0.150, and 0.165 W/m-K, respectively. While, for soybean (base) oil, 2 and 8 wt.% loaded nanolubricants, the values were found to be 0.155, 0.158, and 0.159 W/m-K, respectively. Thus, between 3-13% improvement in thermal conductivity were observed in the base oils due to the addition of organic-coated nanoparticles. This confirmed that the enhancement in convective heat transfer wasn’t responsible for the steep decline in the maxium surface temperatures with nanolubricants, as compared to the base oils using MQL. Albeit, reduction in friction-induced heat generation was suggested for the observed decrease in maximum surface temperature with nanolubricants.

Table 6.1 summarizes the thermal analysis of grinding processes using different lubrication conditions. The heat flux into workpiece material was calculated by matching the values of maximum temperature rise (θ_{max}) at the workpiece surface and tangential force (F_t) in Equation 14. The table also lists the specific energy and grinding power obtained during grinding with each lubrication condition.

Table 6.1 Summary of maximum temperature rise and heat transfer analysis

Lubrication Conditions	Maximum Temp. Rise above Ambient, θ_{max} (z=0), °C	Tangential Grinding Force (N)	Specific Grinding Energy (J/mm^3)	Grinding Power (W)	Heat Flux into Workpiece (W/mm^2)
Dry Grinding	423	-		-	42.05
Flood Grinding	71	19.37	135	581	20.82
MQL- Pure Paraffin	263	14.49	101	435	32.40
MQL- Pure Soybean	295	15.81	110	474	34.33
MQL- 8 wt.% Microparticles- Paraffin	239	12.00	83	360	30.95
MQL- 8 wt.% Microparticles- Soybean	273	13.61	95	408	33.00
MQL- 2 wt.% Paraffin-based Nanolubricant	150	9.73	68	292	25.58
MQL- 2 wt.% Soybean-based Nanolubricant	166	10.75	75	322	26.55
MQL- 8 wt.% Paraffin-based Nanolubricant	135	8.36	58	251	24.68
MQL- 8 wt.% Paraffin-based Nanolubricant	142	9.12	63	274	25.10

Note- Ambient temperature- 25 °C

Assisted by bulk cooling from water-based synthetic MWF, a low heat flux of 20.82 W/mm^2 was obtained for flood grinding. In comparison, MQL fluid delivery technique showed relatively high

values of heat flux due to the limited cooling capacity of MQL. The observed temperature rises at the grinding surfaces with pure base oils using MQL indicated inadequate cooling of the grinding zone, very likely due to lubricant film burn out and desorption. MQL grinding with microparticles-integrated base oils also exhibited high temperature rise and heat flux into the workpiece and hence, inadequate cooling of the grinding zone. In comparison, nanolubricants reduced temperature rise and heat flux values that indicated their effectiveness to improve the cooling performance of MQL technique. Reduced power fluxes of around 25 W/mm^2 and 26 W/mm^2 were obtained from MQL grinding with 8 wt.% and 2wt.% loaded nanolubricants, respectively. This was attributed to the effectiveness of nanolubricants in reducing coefficient of friction as shown in Figure 6.9 (x-axis). A low coefficient of friction between abrasive grains and the workpiece leads to cutting instead of ploughing by allowing dull/flattened grits to cut as well as reducing force and energy requirements for given a material removal rate. This was evident from the previous grinding results as well as from the data in summary Table 6.1 showing low tangential forces and specific grinding energy with nanolubricants. The use of nanolubricants sustained material cutting instead of ploughing and rubbing that resulted in the reduction of energy and hence, heat to be dissipated from the grinding zone through workpiece

The results of this work's studies of friction coefficient, tangential forces, grinding energy and power, maximum surface temperature, and heat flux, the lubrication and cooling behavior of the tribological system of grinding with different lubrication conditions are summed up in Figure 6.12.

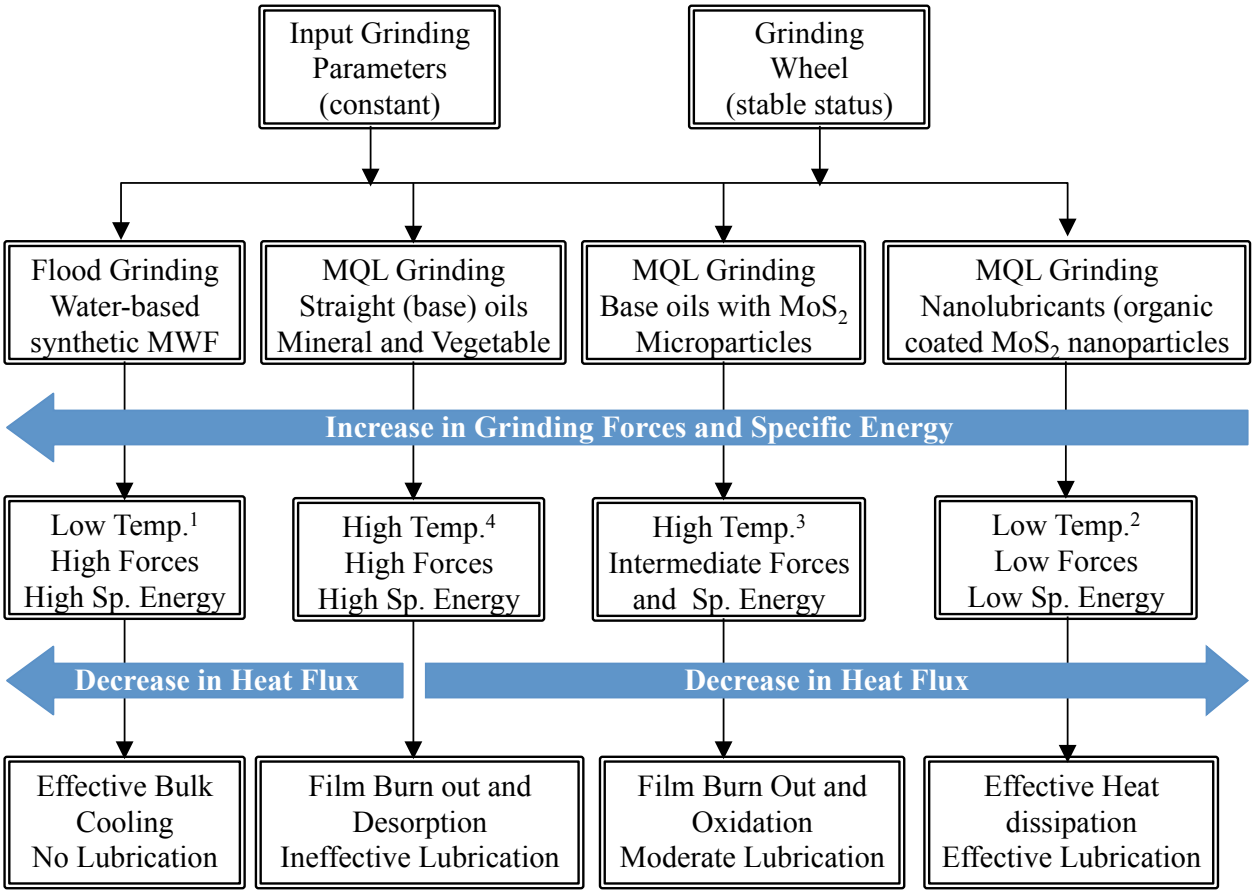

[1,2,3,4]Order of surface temperature increase 1 < 2 < 3 < 4

Figure 6.12 Lubrication and cooling behavior of the tribological system of grinding with different lubrication conditions

Also, the results of this work's experimental studies showed improvement in lubrication performance of the nanolubricants with an increase in the concentration of organic-coated nanoparticles (from 2 to 8 wt.%). For the investigated grinding conditions, the maximum concentration of organic-coated nanoparticles was kept at 8 wt.% based on the following factors:

- **Concentration dependent performance improvement** - Feasibility MQL experiments (under similar surface grinding conditions) with 5 wt.% and 20 wt.% loaded paraffin and soybean based nanolubricants at 300 ml/min flow rate produced average friction

coefficients of 0.17 and 0.16 and G-ratios of 25 and 38, respectively [28]. No improvement in superficial roughness (R_a) was observed due to an increase in nanoparticle concentration ($R_{a\_5\%\ para}$ and $R_{a\_20\%\ para}$- 0.38 μm, $R_{a\_5\%\ soy}$- 0.45 μm, and $R_{a\_20\%\ soy}$- 0.46 μm) [28]. In the current research, by adjusting the MQL parameters including, air pressure, nozzle design and placement, 8 wt.% loaded nanolubricants at 120 ml/min flow rate produced relatively lower superficial roughness (minimum R_a- 0.35 μm), higher G-ratios ($G.R_{max}$- 42), and similar values of friction coefficients (μ_{min}- 0.16).

- **Wheel loading** - In the current and the prior feasibility research on MQL grinding, nanolubricants with concentrations higher than 10 wt.% showed clogging of the grinding zone with debris that eventually led to wheel loading This was attributed to an increase in the viscosity of the base oils with an increase in the concentration of organic-coated nanoparticles. The clogging of the grinding zone showed deleterious effect on the surface quality of the ground workpieces.
- **Application cost -** An increase in the concentration of nanoparticles increases the application cost of the nanolubricants in MQL grinding. For example, based on the lab scale manufacturing of nanolubricants, per minute application cost of 20 wt.% soybean-based nanolubricant (at 300 ml/min MQL flow rate) was estimated at $ 2.44 as compared to $ 2.46 with flood coolant (at 5000 ml/min flow rate and neglecting recirculation) [28]. In comparison, application cost/min went down to $ 0.65 with 5 wt.% nanolubricant Therefore, for maintaining a balance between MQL grinding performance and application costs of lubricants, a maximum 8 wt.% loaded nanolubricants along with the adjusted MQL parameters (nozzle design and placement, air-lubricant flow rate, etc.) were selected in this research. Further cost-to-performance optimization of

nanolubricants in MQL grinding is required. This should not only consider the scale-up manufacturing and application cost of nanolubricants, but also the cost of involved MQL parameters, such as, compressed air, related energy expenditures, etc.

VII. RESULTS AND DISCUSSION - SURFACE GRINDING PRODUCTIVE OUTPUTS

This chapter presents the results and discussion of the productive outputs obtained from surface grinding tests with a conventional Al_2O_3 wheel. These results assisted in understanding the lubrication (friction and wear reduction) effectiveness of nanolubricants in maximizing the productive outputs of MQL-assisted grinding process. The chapter is divided into two sections that present the obtained results and discussion of, A) surface integrity of ground workpieces and B) grinding efficiency.

A. SURFACE INTEGRITY OF GROUND WORKPIECE

This section presents the results of the surface integrity of ground workpieces - the most important productive output of the process. The analysis of surface integrity included arithmetic average roughness (R_a). 3-D profile of surface texture, and surface microstructure of workpieces obtained after 100 passes of grinding with different lubrication conditions.

Surface Roughness of Cast Iron Workpieces

Figures 7.1 and 7.2 compare the mean values of surface roughness (R_a parameter) of ductile iron workpieces obtained after conventional (flood) grinding and MQL-assisted grinding. The values were obtained after 100 grinding passes with a vitrified bond Al_2O_3 wheel using 10 and 20 μm depth of cuts (infeed). Each value was obtained by averaging the measurements of R_a at five different surface positions equidistant from each other. The error bars represent standard deviation about the mean R_a value.

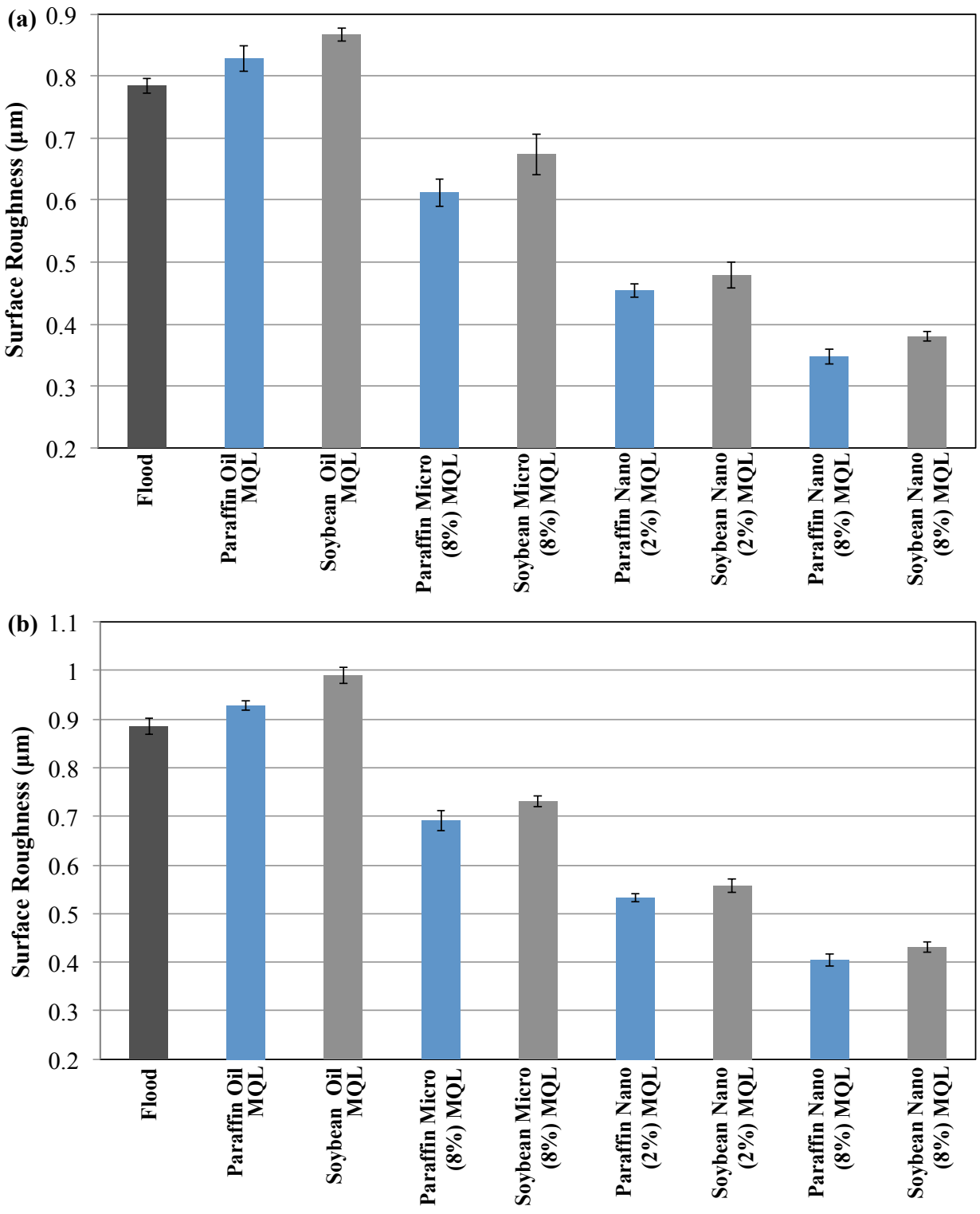

Figure 7.1 Average surface roughness (R_a) measurements of ductile iron obtained after grinding with, (a) 10 µm infeed and, (b) 20 µm feed using different lubrication conditions. Each plotted R_a value is an average of 5 measurements; error bars represent standard deviation about the mean R_a value

For 10 and 20 μm infeed conditions, the lowest superficial roughness (R_a) was found to be 0.35 μm and 0.40 μm for MQL grinding with 8 wt.% loaded paraffin-based nanolubricants. While MQL grinding with pure soybean oil resulted in the highest superficial roughness values of 0.87 μm and 0.99 μm for 10 and 20 μm infeed conditions, respectively.

For 10 μm infeed condition, flood grinding produced R_a = 0.78 μm as compared to 0.83 μm and 0.87 μm from MQL with paraffin and soybean oil, respectively. While for 20 μm infeed condition, flood grinding produced R_a = 0.88 μm as compared to R_a = 0.93 μm with paraffin oil and R_a = 0.99 μm with soybean oil. In MQL, addition of solid lubricant (MoS_2) particles showed improvements in the surface finish of ground workpieces. MQL with microparticles added paraffin and soybean oil reduced R_a values to 0.61 μm and 0.67 μm (for 10 μm wheel infeed) and 0.69 μm and 0.73 μm (for 20 μm wheel infeed), respectively. 2 wt.% loaded paraffin and soybean-based nanolubricant produced superficial roughness of 0.45 μm and 0.48 μm, respectively, after MQL grinding with 10 μm infeed/pass. The same nanolubricant compositions showed respective R_a measurements of 0.53 μm and 0.56 μm for the grinding case of 20 μm infeed/pass. On average, workpiece surfaces after finish grinding with 8 wt.% loaded nanolubricants using MQL were over two times smoother than those obtained from conventional flood condition and MQL with pure base lubricants.

Surface Roughness of EN 24 Steel Workpieces

Figure 7.2 compares the mean surface roughness (R_a) values of EN 24 steel workpieces obtained after 100 passes of conventional (flood) grinding and MQL grinding at 20 μm infeed/pass. Like ductile iron, each value was obtained by averaging the measurements of R_a at five different surface positions equidistant from each other.

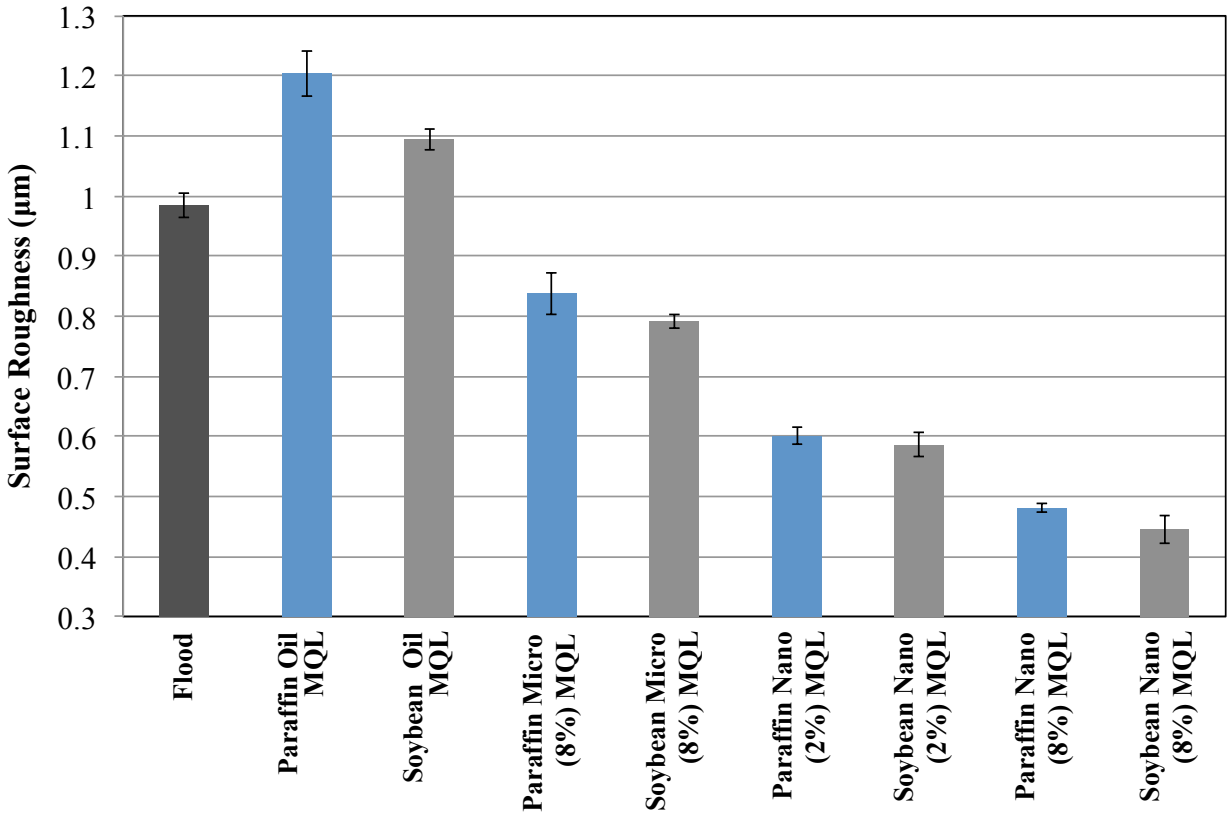

Figure 7.2 Mean surface roughness (R_a) values of EN 24 steel workpieces obtained after 100 passes of conventional (flood) grinding and MQL grinding at 20 µm infeed/pass, each plotted R_a value an average of 5 measurements; error bars represent standard deviation of the mean R_a value

Based on the analysis of the measured R_a values, MQL grinding with 8 wt.% loaded soybean-based nanolubricant produced the lowest superficial roughness of 0.45 µm. This was followed by R_a = 0.48 µm that was obtained from MQL grinding with 8 wt.% loaded paraffin-based nanolubricant. The highest R_a value of 1.20 µm was observed with pure paraffin oil, followed by R_a = 1.09 µm with pure soybean oil using MQL. In similar observations with ductile cast iron cases, flood grinding led to a better surface finish (R_a = 0.98 µm) of workpieces as compared to MQL with pure base oils (without nanoparticles). MQL with microparticle integrated soybean and paraffin oil resulted in relatively better surface finish by delivering R_a values of 0.79 µm and

0.83 μm, respectively. Respective R_a measurements of 0.59 μm and 0.60 μm from 2 wt.% loaded soybean and paraffin-based nanolubricants indicated further improvement in surface finish. These values were approximately 25% less rough than those obtained with microparticles-integrated oils. An increase in the loading concentration of nanoparticles fostered better surface finish of ground workpieces. On average, MQL with 8 wt.% nanolubricants reduced surface roughness by over 50% or two times as compared to conventional flood grinding and MQL with pure base lubricants.

Summary of Surface Roughness

From the analysis of R_a results for ductile iron and alloy steel workpieces, flood grinding with synthetic fluid led to a slightly better workpiece surface finish than MQL grinding with pure base oils, possibly by providing better bulk cooling and flushing of the accumulated chips from the machining zone. In general, MQL provide better lubrication at the grinding zone, albeit low flushing capacity of MQL system affects the surface roughness of ground workpieces. The accumulated metal chips from low MQL flushing can lead to surface degradation by scratching the ground workpieces and by re-welding on the workpiece surface due to intensive heat at the grinding zone. This was reflected in the surface roughness results obtained from the MQL-assisted grinding with pure base oils (without MoS_2 particles). The observed improvements in workpiece surface finish from MQL lubrication with solid lubricant particles can be attributed to the superior adhesion of MoS_2 to metal surfaces. The oleophilic tails of MoS_2 molecules are known to provide very good adhesion to metal surfaces including metallic chips [80]. This was evident from the chemical analysis of grinding debris/residues after MQL grinding with MoS_2-based lubricants, as discussed in the next chapter. The surface adhered low-friction MoS_2 species assisted in reducing the scuffing of workpiece surface by the accumulated chips. The metal

adhesion property of MoS_2 was further enhanced by the high-surface energy of organic coated nanoparticles that improved the surface quality of the ground workpieces with nanolubricant compositions. Reduced surface temperatures from nanolubricants during MQL-assisted grinding also contributed in improving the surface quality of workpieces by inhibiting chip re-welding.

At 20 μm depth of cut, the surface roughness of ductile iron obtained after grinding with a 46 grit size Al_2O_3 wheel was seen to be higher than those obtained at 10 μm depth of cut, using a similar lubrication condition. This was a usual effect of increasing depth of cut, or in other words, a larger cross-sectional area of the chip that increased the surface roughness of the machined parts [109]. Increase in the feed rate also affects the surface roughness of ground workpieces [109,110]. As recalled from experimental parameters, EN 24 steel was ground with a 46 grit size Al_2O_3 wheel at a higher feed rate of 0.1 m/s as compared to 0.06 m/s for ductile iron. While other lubrication conditions showed wider increments in surface roughness values, MQL grinding of EN 24 steel with nanolubricants produced surface finishes comparable to those of cast iron. Hence, a low surface roughness value with nanolubricants in MQL-assisted grinding was a significant step towards improving grinding productivity (increasing feed and depth of cut) while achieving better surface quality.

Surface Topography

Figures 7.3, 7.4, and 7.5 show the results from optical profilometry performed on representative workpieces that were obtained after grinding with different lubrication conditions. Figure 7.3 compares the surface profiles of workpieces after flood grinding and MQL grinding with pure base lubricants (without nanoparticles), while Figures 7.4 and 7.5 compares the surface profiles of workpieces obtained after MQL grinding with base oils containing MoS_2 microparticles and nanolubricants, respectively.

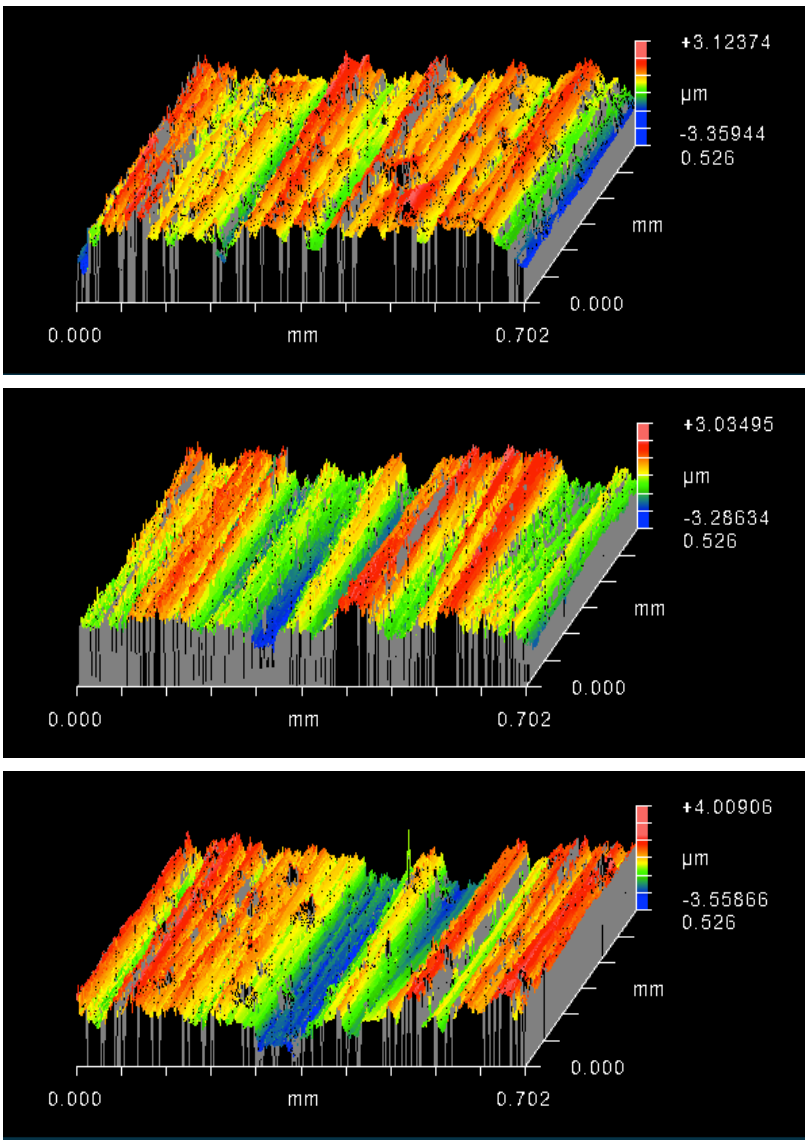

Flood Grinding- Synthetic MWF
Workpiece- Ductile Iron
Depth of Cut- 10 µm

MQL Grinding- Pure Paraffin Oil
Workpiece- Ductile Iron
Depth of Cut- 10 µm

MQL Grinding- Pure Soybean Oil
Workpiece- Ductile Iron
Depth of Cut- 10 µm

Figure 7.3 Surface profiles of ground workpiece surface obtained after 100 passes of grinding with flood application of water-soluble synthetic fluid and MQL using pure base oils

Unidirectional scratches and grooves typically characterize the work surface generated by straight plunge grinding. Grinding generated scratches and grooves in workpiece surfaces can be seen from the 3-D profiles of Figure 7.3. However, the workpiece grooves were deeper and exhibited significant sideways flow of material due to ploughing and wearflat rubbing. These surface features were indicative of high adhesion friction between the abrasive grains and the

workpiece owing to insufficient lubrication during grinding. The grinding-generated scratches and groves were rough and their peak-to-valley patterns were erratic for workpieces obtained from MQL grinding with pure base oils as compared to those obtained from flood grinding. This validated that base oils were unable to provide adequate lubrication and prevent additional scuffing of the workpiece surface by the accumulated metal chips during MQL grinding. Erratic and rough surface texture with base oils using MQL was also indicative of rapid fracture and glazing of abrasive crystals of wheel during grinding.

Figures 7.4(a) and 7.5(a) showed improvements in the surface profile of workpieces obtained from MQL grinding with microparticle-integrated oils as compared to those obtained from pure base oils. The observed improvements in surface quality were attributed to MoS_2 lubrication, however inconsistent scratches and groove patterns were still visible on the ground workpiece surface. As mentioned before, MQL with highly viscous microparticles-integrated oils showed dense clogging of the grinding zone with debris. Though MoS_2 was able to adhere and overlayer the debris particles and provide partial relief against scuffing, the overwhelming accumulation of debris persisted to deteriorate the quality of ground surface by producing third body abrasion.

Compared to all other lubrication conditions, the surface textures of ground workpieces obtained from nanolubricants showed consistent peak-to-valley patterns of grinding-generated grooves and scratches (Figures 7.4(b) and (c) and 7.5(b) and (c)). Also, the width of the valleys of the surface grooves were less as compared to those of the workpieces obtained from flood grinding and MQL with base lubricants. This indicated that during MQL grinding with nanolubricants, the geometrical integrity of the sharp abrasive points of the wheel was maintained due to reduced flattening or dulling of the abrasive grains. Reduced sideways displacement of material from the grooves and scratches was seen from the surface profiles of Figures 7.4(b) and (c) and 7.5(b) and

(c). This indicated that the low-friction nanolubricant films resulted in shear cutting of material instead of ploughing and rubbing. These collective effects that originated from MQL assisted lubrication by nanolubricants produced improvements in the surface quality of the ground workpieces.

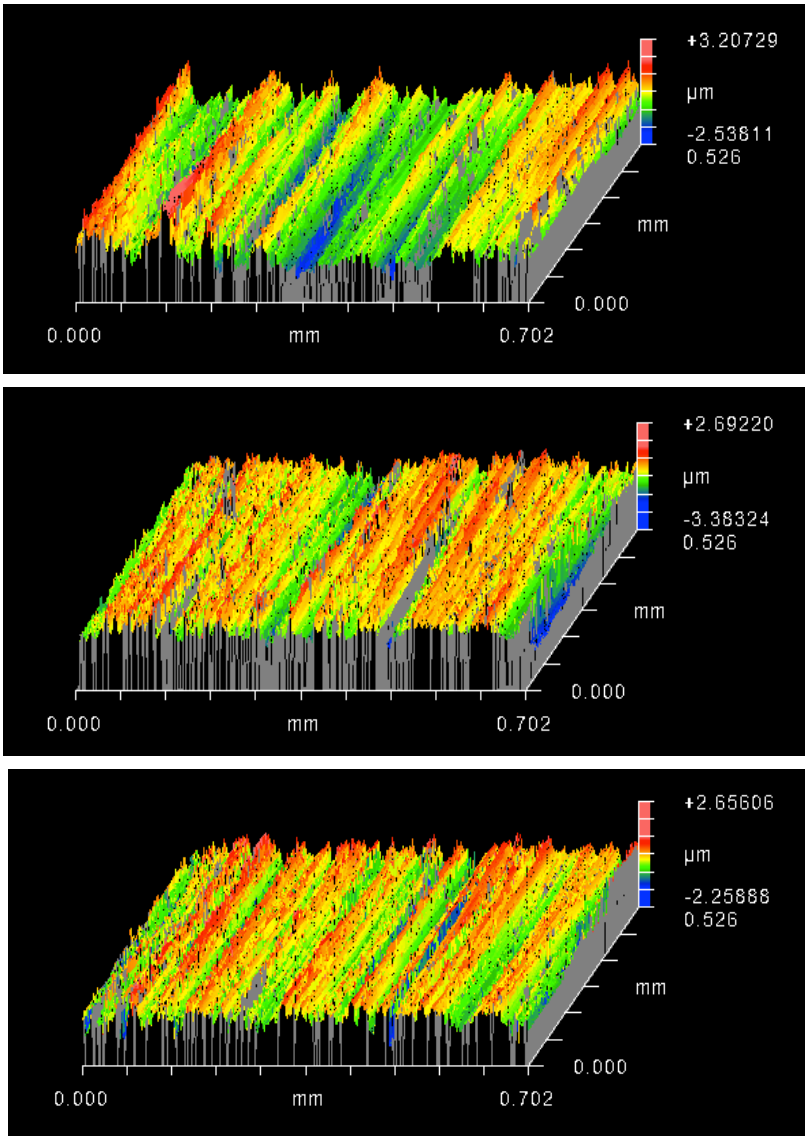

(a) MQL Grinding- Paraffin Micro (8 wt.%)
Workpiece- Ductile Iron
Depth of Cut- 10 µm

(b) MQL Grinding- Paraffin Nano (2 wt.%)
Workpiece- Ductile Iron
Depth of Cut- 10 µm

(c) MQL Grinding- Paraffin Nano (8 wt.%)
Workpiece- Ductile Iron
Depth of Cut- 10 µm

Figure 7.4 Surface profile of ground workpiece surfaces obtained after 100 passes of grinding with MQL using paraffin-based lubricants (micro- 8 wt.% and nano- 2 and 8 wt.%)

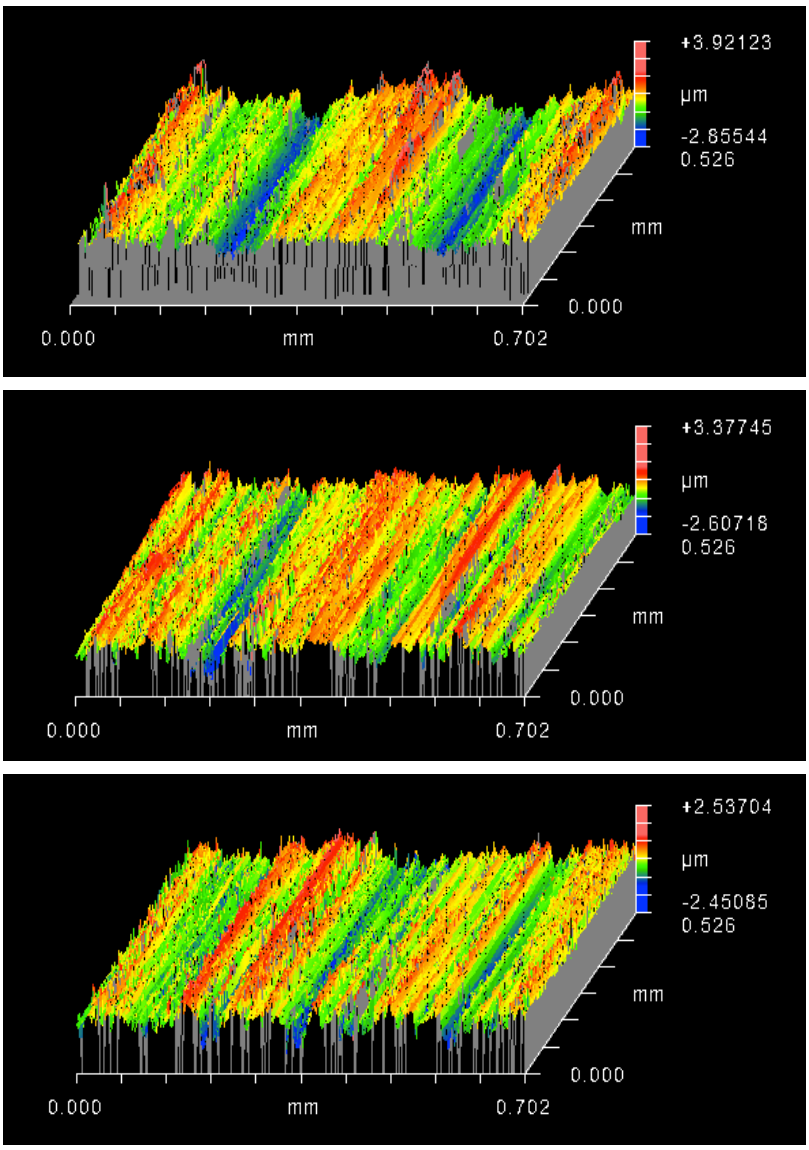

(a) MQL Grinding- Soybean Micro (8 wt.%)
Workpiece- Ductile Iron
Depth of Cut- 10 µm

(b) MQL Grinding- Soybean Nano (2 wt.%)
Workpiece- Ductile Iron
Depth of Cut- 10 µm

(c) MQL Grinding- Soybean Nano (8 wt.%)
Workpiece- Ductile Iron
Depth of Cut- 10 µm

Figure 7.5 surface profiles of ground workpiece surfaces obtained after 100 passes of grinding with MQL using soybean-based lubricants (micro- 8 wt.% and nano- 2 and 8 wt.%)

For a comprehensive analysis of surface texture, the workpieces obtained after grinding with different lubricants were examined using SEM. Representative SEM micrographs of steel surface obtained after MQL grinding with nanolubricant and pure base oil are shown in Figures 7.6a and 7.6b and c, respectively.

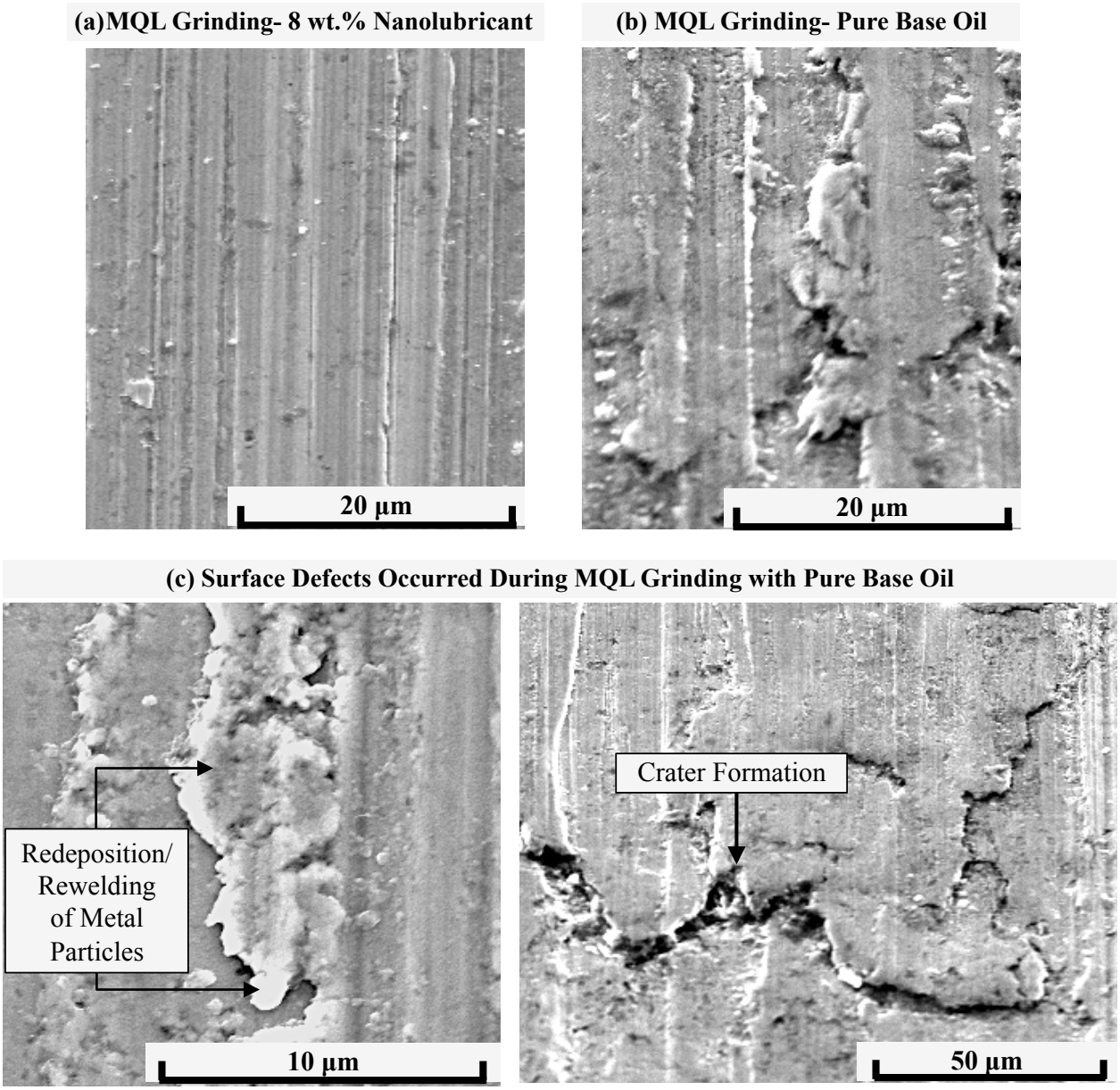

Figure 7.6 SEM micrographs of steel surface obtained after MQL grinding with nanolubricant and pure base oil

As opposed to a visually smooth surface with nanolubricant, the steel surface obtained from grinding with pure base lubricant showed visually rough scratches with high degree of sideways displacement of material from ploughing action. Other surface deteriorations included redeposition or rewelding of metal particles and crater formation on the ground surfaces are as

shown in Figure 7.6c. Crater formations occurred due to sudden interruption in material cutting action by the fracture of the abrasive grains during grinding. Many times, the fractured micro fragments are embedded in the surface craters. According to literature, many difficult to grind materials (including steel) exhibit extensive crater formation and embedding of abrasive grains [3]. Such surface defects act as potential sites of localized stress concentration that deteriorates the fatigue strength of machined parts and components.

B. GRINDING EFFICIENCY

Grinding wheel life and energy consumption are decisive factors for an economical and energy-efficient grinding process and both factors are significantly influenced by the state of lubrication during grinding. Therefore, the grinding efficiency was measured for each lubrication condition by considering both grinding wheel life and grinding energy requirement. Grinding efficiency (E) is defined as the ratio of G-ratio and specific grinding energy [111]. High values of grinding efficiency represent high grinding productivity at lower energy consumption [111]. Figures 7.7(a) and (b) show the results of grinding efficiency obtained during grinding of cast iron at 10 and 20 μm wheel infeed with different lubrication conditions. The grinding efficiency obtained during grinding of EN 24 steel at 20 μm wheel infeed is shown in Figure 7.8.

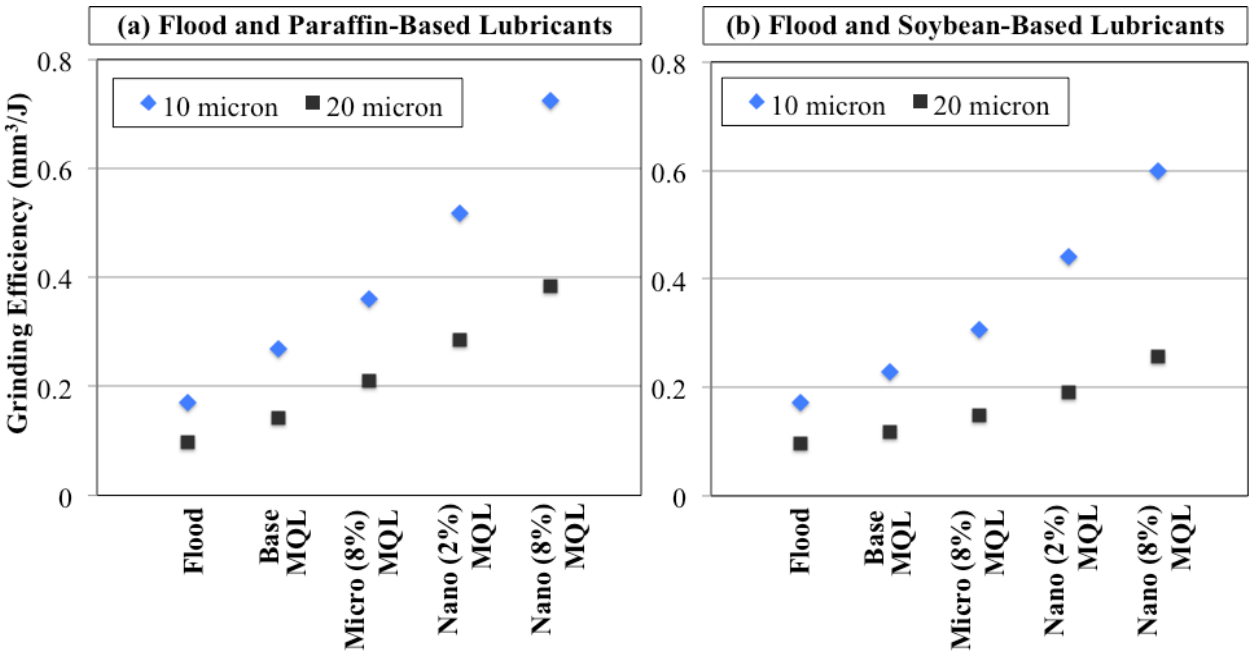

Figure 7.7 Grinding-efficiency obtained during grinding of cast iron with, (a) flood and MQL with paraffin-based lubricants and, (b) flood and MQL with soybean-based lubricants

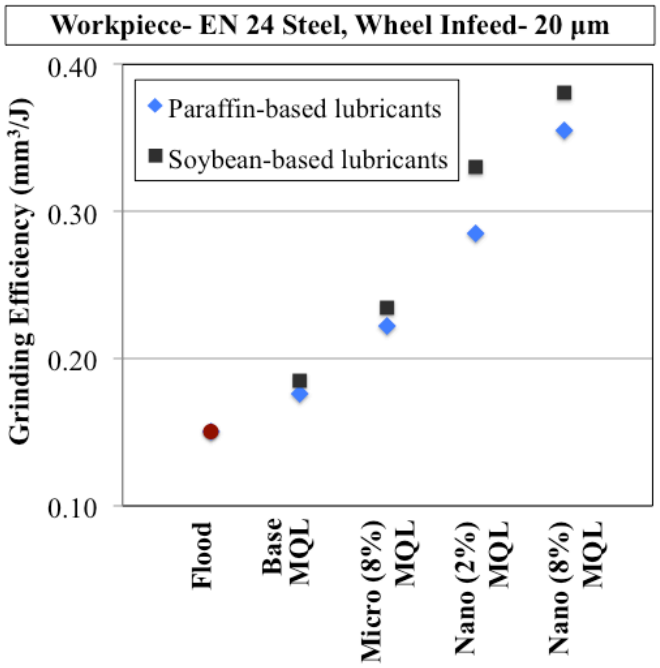

Figure 7.8 Grinding-efficiency obtained during grinding of EN 24 steel at 20 µm wheel-infeed with different lubrication conditions

Based on the measured data, MQL with 8 wt.% loaded nanolubricants demonstrated the highest grinding efficiencies for both workpiece materials and wheel-infeed conditions, while flood grinding with water-based fluid demonstrated the lowest grinding efficiencies. During grinding of cast iron with 10 and 20 μm wheel infeed, MQL with 8 wt.% paraffin-based nanolubricants produced grinding efficiencies of 0.72 and 0.38, respectively. While for the same grinding conditions, 8 wt.% soybean-based nanolubricants produced respective grinding efficiencies of 0.60 and 0.26. MQL with 8 wt.% paraffin-based nanolubricants demonstrated percentage increments of 164% and 289% in grinding efficiency as compared to MQL with pure paraffin (base) oil and flood grinding, respectively. While, MQL with 8 wt.% soybean-based nanolubricants produced respective increments of 144% and 220% in grinding efficiency over MQL grinding with pure soybean (base) oil and flood grinding.

Based on the measured data, MQL with 8 wt.% loaded nanolubricants demonstrated the highest grinding efficiencies for both workpiece materials and wheel-infeed conditions, while flood grinding with water-based fluid demonstrated the lowest grinding efficiencies. During grinding of cast iron with 10 and 20-μm wheel infeed, MQL with 8 wt.% paraffin-based nanolubricants produced grinding efficiencies of 0.72 and 0.38, respectively. While for the same grinding conditions, 8 wt.% soybean-based nanolubricants produced respective grinding efficiencies of 0.60 and 0.26. MQL with 8 wt.% paraffin-based nanolubricants demonstrated percentage increments of 164% and 289% in grinding efficiency as compared to MQL with pure paraffin (base) oil and flood grinding, respectively. While, MQL with 8 wt.% soybean-based nanolubricants produced respective increments of 144% and 220% in grinding efficiency over MQL grinding with pure soybean (base) oil and flood grinding.

In general, grinding of cast iron workpieces using paraffin-based lubricants produced better grinding efficiencies as compared to soybean-based lubricants. For grinding of EN 24 steel, MQL with 8 wt.% loaded nanolubricants demonstrated the highest grinding efficiencies (G.E = 0.36-0.38). The second best grinding efficiencies were obtained MQL grinding with 2 wt.% nanolubricants (G.E = 0.29-0.33). In terms of percentage increments, MQL with 8 wt.% nanolubricants produced 147% and 100% average increase in grinding efficiency over flood grinding with water-based synthetic fluid and MQL grinding with pure base oils, respectively. Based on the overall data analysis, MQL use of nanolubricants demonstrated excellent grinding productivity by yielding longer wheel life, low energy consumption, and superior work surface quality.

VIII. RESULTS AND DISCUSSION- MECHANISMS OF LUBRICATION DURING GRINDING

This chapter presents the results of electro-optical characterization analysis that were used to study and understand the lubrication mechanisms at the abrasive grain-workpiece contact surfaces of the grinding zone. This was accomplished by analyzing A) the tribolayers on the ground workpiece surface and abrasive grains of the grinding wheel, B) chemical integrity of nanolubricant-derived tribochemical films and, C) mechanisms of formation and deformation of tribolayers, as discussed below.

A. TRIBOLAYERS ON WORKPIECE SURFACE AND ABRASIVE GRAINS

This section discusses the structural and chemical microanalysis of tribolayers derived from the processes of physisorption, chemisorption, and tribochemical reactions between lubricant (oil and additive) molecules and the surfaces of ground workpiece and Al_2O_3 grains of the grinding wheel.

Tribolayers on Ground Workpiece Surface

Representative SEM micrographs of ground workpiece (ductile iron) surfaces lubricated with synthetic fluid (flood grinding) and pure base oil (MQL grinding) are shown in Figure 8.1. While representative SEM micrographs of ground ductile iron surfaces lubricated with 2 and 8 wt.% loaded nanolubricants are shown in Figure 8.2. Corresponding EDS microanalyses returned the elemental distribution of lubricant-derived layers formed on the ground surfaces. The investigated work surfaces were obtained after 100 grinding passes at 10 μm infeed/pass.

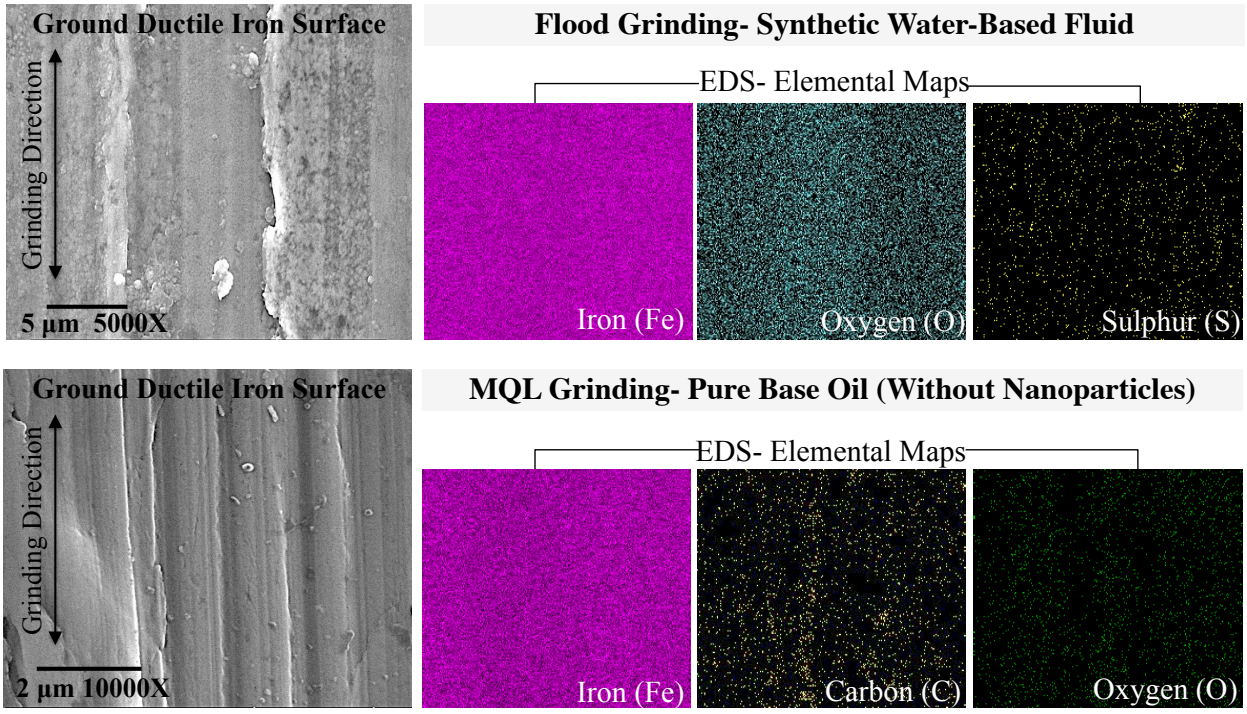

Figure 8.1 SEM-EDS microanalysis of workpiece surface after 100 passes of flood grinding with synthetic MWF and MQL-assisted grinding with pure base oil (without nanoparticles)

In Figure 8.1, elemental distributions of Sulphur (S) and Oxygen (O) on the flood-lubricated metal surface indicated the presence of weak sulphide and iron oxide species. Sulphur present in the formulated lubricants and MWFs reacted with metal oxides on the metal surface to form soft metal sulphide films (here iron sulphide) that possessed good antifriction and antiwear properties. However, the weak elemental signatures of Sulphur suggested either the inability of flood (wet) grinding to form stable physisorbed-sulphide films or desorption of physisorbed layers due to temperature and contact pressure (loading) effects at the grinding zone. EDS elemental distributions of Carbon-Oxygen confirmed the presence of a weak oil film on the base oil-lubricated metal surface. Physisorbed oil films can provide effective lubrication in low-load conditions and operating temperatures of upto 100 °C [7]. However, lubrication effectiveness of such films diminishes in high-load asperity contact conditions, like MQL grinding.

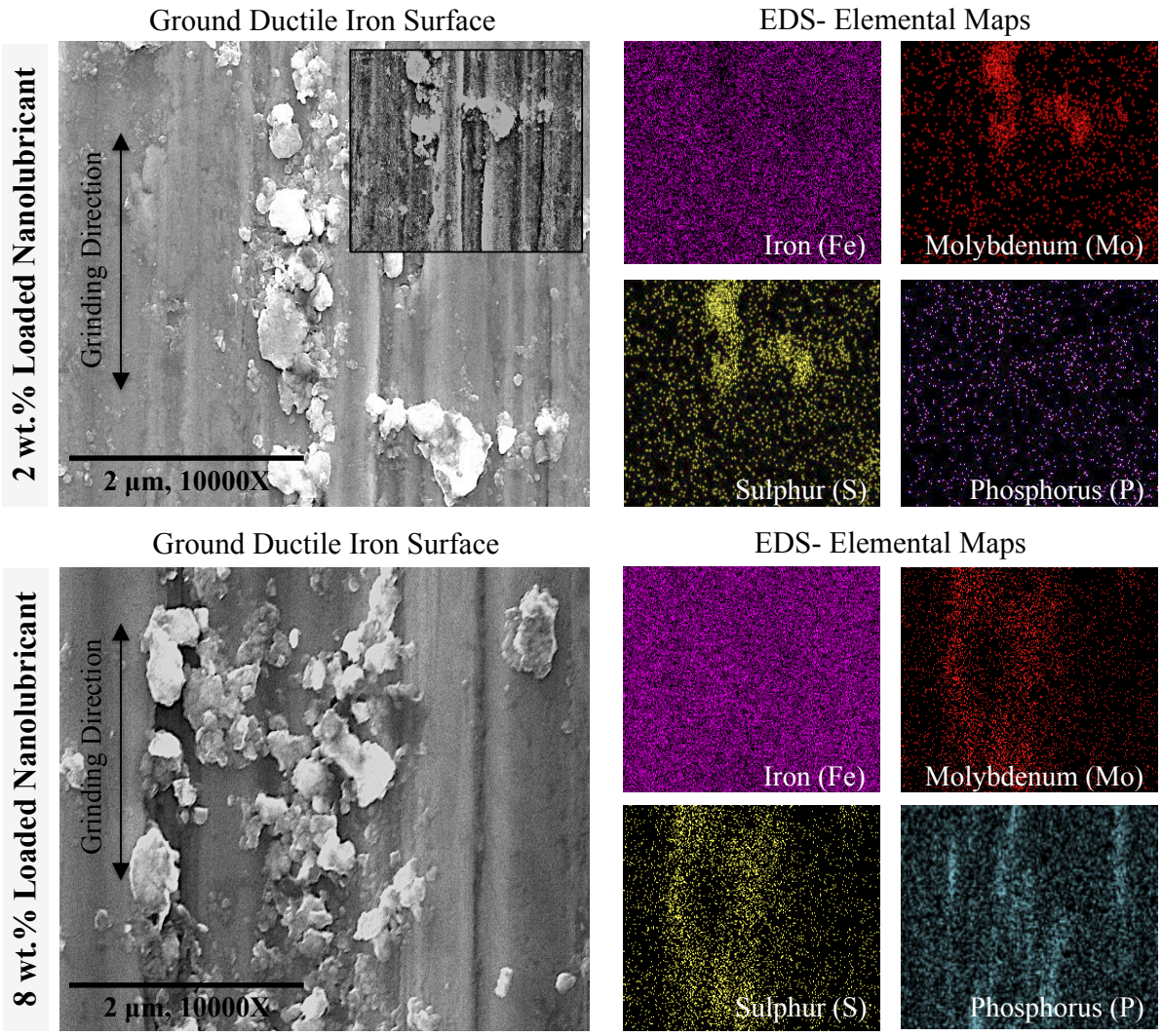

Figure 8.2 SEM-EDS microanalysis of ground workpiece (ductile iron) surfaces lubricated with 2 wt.% and 8 wt.% loaded nanolubricants [46]

In addition, high temperature at the friction surfaces and strong shear due to intensive seizure at the tool-workpiece interface cause film burn out and desorption of oil films from the metal surface, respectively. All these effects eventually result in absolute loss of lubrication and hence, an increase in friction and wear as witnessed in the results of grinding force and G-ratios with MQL application of base paraffin and soybean oil. The SEM micrographs in Figure 8.2 of nanolubricant-lubricated metal surfaces showed evolution of sliding-oriented platelet-like

structures. EDS analysis of the platelets confirmed the presence of Molybdenum (Mo), Sulphur (S), and Phosphorus (P), indicating their origin from organic-coated MoS_2 nanoparticles. Mo-S-P-Fe-O chemical complex of platelet-like tribolayers suggested sulphide and phosphate layers that are known to have excellent antifriction (low shear strength) and antiwear (extreme-pressure) properties [112-114]. The low shear strength tribolayers derived from the nanolubricant sacrificed itself at the grain-workpiece interface in lieu of wearing the harder abrasive grains and their adhesion friction with relatively soft metal surface. This was correlated with the observed results of low friction coefficients and high G-ratios during MQL grinding with nanolubricants.

High accumulation of grinding debris over the workpiece and its surroundings was observed during MQL grinding of cast iron with soy-based nanolubricants, as shown in Figure 8.3.

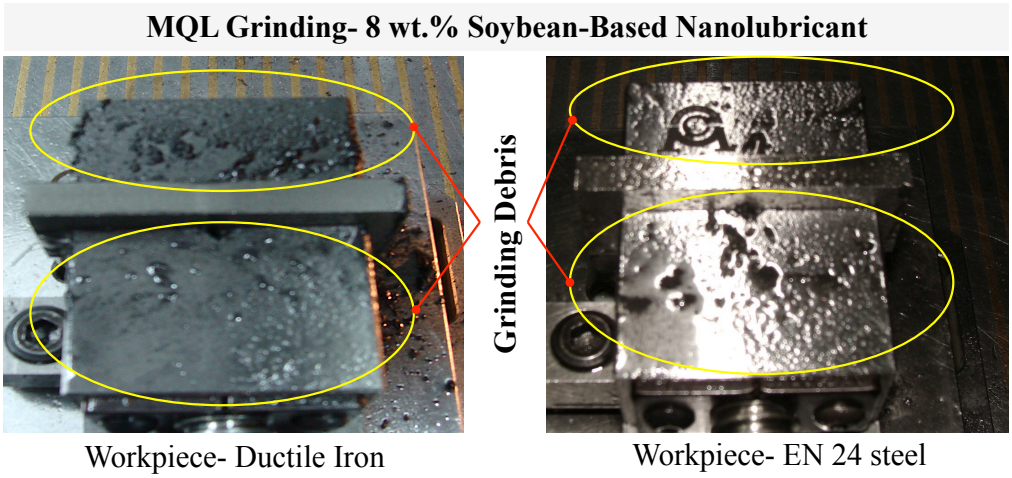

Figure 8.3 Debris accumulations over workpiece and its surroundings during MQL grinding of ductile cast iron and EN 24 steel with soybean-based nanolubricant; grinding of ductile iron accumulated more debris as compared to that of EN 24 steel

As recalled from previous grinding results, soybean and paraffin based nanolubricants showed better performances during MQL grinding of EN 24 steel and ductile iron, respectively. The

observed variation in the performance of lubricants during MQL grinding can be explained based on:

- Generation and accumulation of debris during cast iron machining (Figure 8.3)
- Strong polarity of sulphurized-triglyceride molecules of soybean-based nanolubricant

Machining of cast iron is known to generate fine particles (ranging 25 pm in size) in addition to the metal chips. Due to their size, the particles become suspended in the liquid lubricant to create sludge-like debris. The polarity of sulfurized-triglyceride molecules of soybean-based nanolubricant generated a strong affinity for metal workpiece surface. This strong polar attraction may have resulted in the surface deposition of sludge particles (trapped in the lubricant films) and eventually clogging the grinding zone to cause an increase in friction. This was evident from Figure 8.3 that showed relatively high accumulation of debris during MQL grinding of ductile iron. Mineral-based paraffin oil has no polarity and therefore, less affinity to ductile iron surface and less clogging of the grinding zone.

While grinding EN 24 steel, the observed performance variations were a direct result of the properties of the base oils. The polarity of soybean-based nanolubricants provided a strong affinity for steel surfaces and hence, more effective lubricant film protection at the grain-workpiece interface during grinding. More in depth study is required to understand the plausible relationship mechanisms between the workpiece materials and functionalized lubricant compositions of varying base chemistries.

Tribolayers on Abrasive Grains of Grinding Wheel

Optical images of a section of the vitrified-bond Al_2O_3 wheel used during MQL-assisted grinding with nanolubricant are shown in Figure 8.4. Localized retention of entrapped nanolubricant can be seen in the networks of natural microporosity and cavities in between the abrasive grains. This supported the idea of a readily available delivery of organic-coated MoS_2 nanoparticles at the grinding zone through the microporosity and the capillary networks of the grinding wheel.

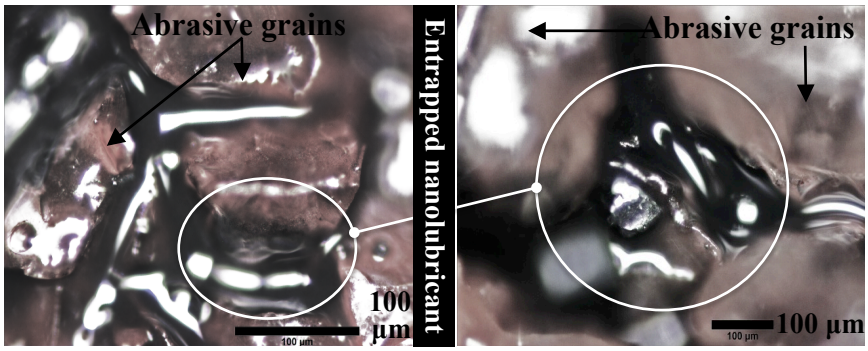

Figure 8.4 Optical images of nanolubricant-lubricated vitrified-bond Al_2O_3 wheel showing retention and entrapment of nanolubricant in the wheel porosity [46]

The structure and chemistry of nanolubricant-derived tribolayers that evolved and deposited in the micro cavities and the surface of abrasive grains during grinding were investigated using SEM-EDS microanalysis. Figure 8.5a and b shows the SEM-EDS analysis of two grains (and its immediate surroundings) from the same vitrified-bond Al_2O_3 wheel, one before grinding and the other after MQL assisted grinding of cast iron with nanolubricant. Deposition of micro sized metal debris was detected on the surface of the Al_2O_3 grain after grinding, as shown in Figure 8.5(b).

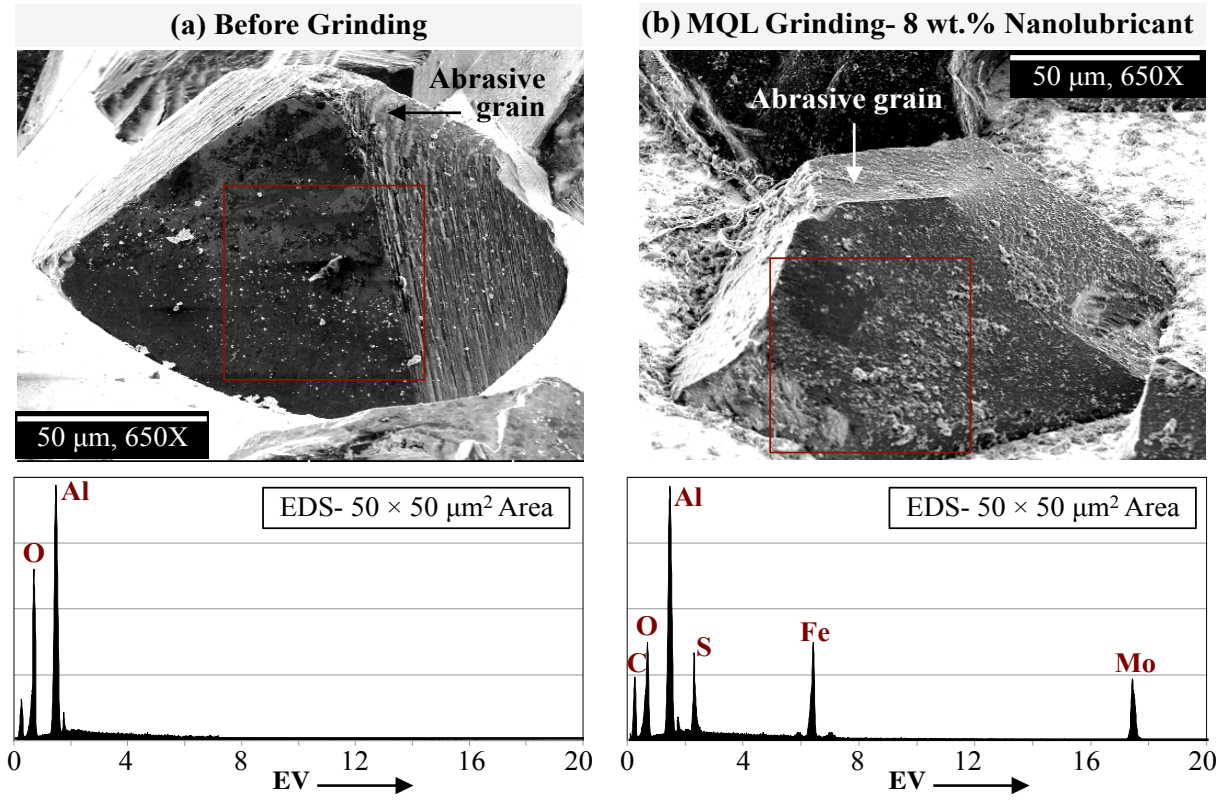

Figure 8.5 SEM-EDS microanalysis of abrasive grains from vitrified-bond Al_2O_3 wheel, (a) before grinding and (b) after MQL grinding of ductile iron with nanolubricant [46]

No serious mechanical loading of wheel porosity with metal debris was observed during MQL grinding. This is not unusual with Al_2O_3 wheels that are less prone to loading due to their faster rate of wear as compared to the CBN wheels. During grinding, an Al_2O_3 wheel wears or dresses out before loading of metal chips/debris can accumulate to levels that deter the cutting action of the abrasive grains [115]. EDS spectrum of the debris retained on the abrasive grain (Figure 8.5(b)) confirmed the presence of elemental Mo and S that suggests two possibilities, both being beneficial to the grinding process:

- Penetration and retention of organic coated MoS_2 nanoparticles in the wheel porosity and eventually yielding at the grinding zone to form friction-reducing tribolayers.

- Overlayering of the metal chips/debris with low-friction metal sulphide species, aiding to reduce work surface abrasion by the trapped debris.

B. CHEMICAL INTEGRITY OF TRIBOCHEMICAL FILMS

This section presents the chemical integrity of nanolubricant-derived tribochemical films evolved on the workpiece surface during MQL grinding. These analyses were carried out using Raman spectroscopy to identify the unique chemical species responsible for tribological behavior and lubricating mechanisms of the nanolubricant compositions during MQL-assisted grinding. Figure 8.6 shows the Raman spectra of three samples, a tribofilm overlayered workpiece surface obtained from MQL grinding with 8 wt.% loaded soybean, a workpiece after MQL grinding with 8 wt.% paraffin-based nanolubricant, and a ground workpiece after cleaning the adhering tribochemical films.

Raman spectra of tribofilms derived from soybean and paraffin-based nanolubricant revealed distinct MoS_2 peaks located at 408 cm^{-1} (A_{1g}). This A_{1g} (408 cm^{-1}) first order Raman active mode is an outcome of an out-of-plane vibrational mode within S-Mo-S layers [116,117]. In this out-of-plane mode, Sulphur atoms of MoS_2 vibrate out-of-plane in opposite directions [116]. The tribofilms also revealed MoS_2 peaks centered around 383 cm^{-1} (E^1_{2g}). This E^1_{2g} (383 cm^{-1}) first order Raman active mode corresponds to in-plane opposite vibrations of two Sulphur atoms with respect to a Molybdenum atom [116]. The peaks centered at 365 cm^{-1} and 224 cm^{-1} corresponded to MoO_2 and Fe_2O_3 species, formed by the oxidation of MoS_2 and ferrous substrate, respectively. Low-intensity peaks identified at 372 cm^{-1} were consistent with phonon vibrations of pyrite FeS_2 [118], suggesting the presence of FeS_2 species in the nanolubricant tribofilms. In addition, the identified peaks at 988 cm^{-1} were from the phosphate tribofilms [119]. This confirmed the

presence of phosphate layers in the tribofilms that were derived from the phospholipid molecules of nanolubricant. The Raman spectra of the ground workpiece (after cleaning the adhering tribochemical films) showed low-intensity MoS_2 peaks at 408 cm^{-1}. This suggested there was negligible surface contamination of workpiece from nanolubricant additives during MQL-assisted grinding.

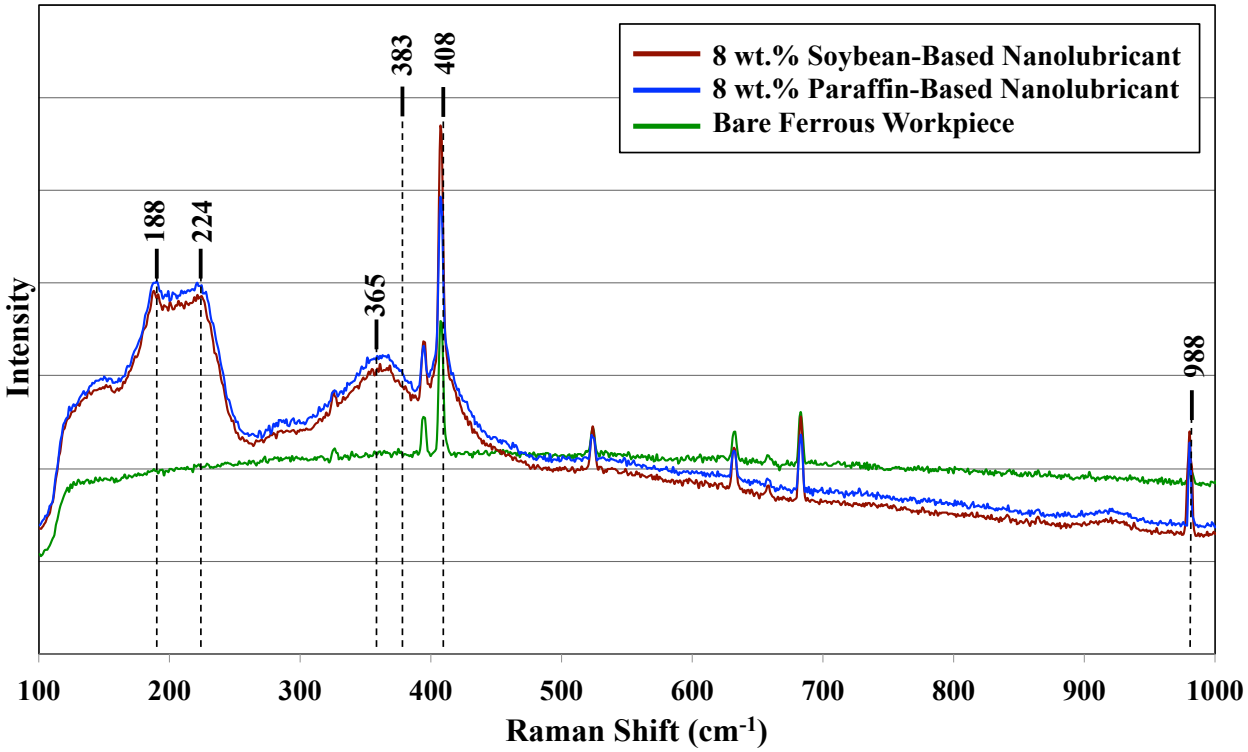

Figure 8.6 Raman characterizations of tribochemical films derived from 8 wt.%- loaded soybean and paraffin-based nanolubricant during MQL grinding of ferrous workpiece. Location and designation of the prominent lines have been adapted from [116-123]

In Figure 8.6, similar Raman spectral patterns of the two nanolubricant-derived tribofilms suggested that the chemistry of base oil (mineral vs. vegetable) had little influence on the output composition of the tribochemical films. Their influence was more pronounced on the physical

activity and properties of nanolubricant tribofilms including metal adhesion, surface density and distribution, and thermal stability.

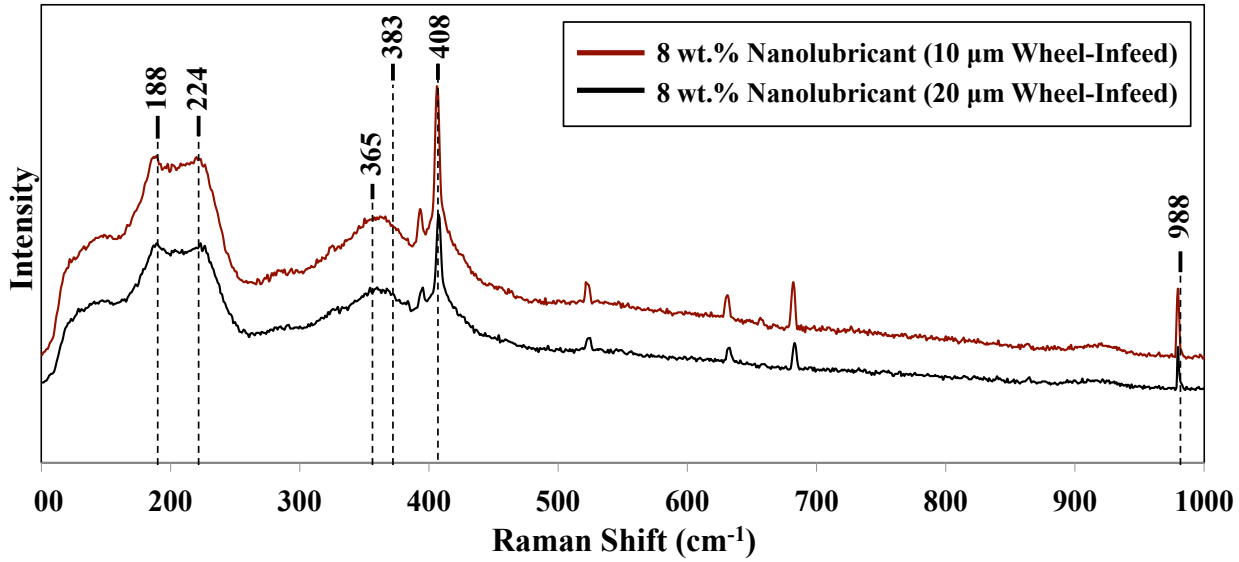

Figure 8.7 Raman characterization of tribochemical films derived from 8 wt.%- loaded nanolubricant during MQL grinding of ferrous workpiece at 10 and 20 µm depth of cut. Location and designation of the prominent lines have been adapted from [116-123]

Figure 8.7 compares the Raman spectra of two workpiece samples (ground with 10 and 20 µm wheel infeed) using the same nanolubricant composition. Similar characteristic peaks as revealed in Figure 8.6, were also seen for nanolubricant tribofilms formed on the metal surface during 20 µm wheel infeed MQL grinding. The characteristic peaks include those of MoS_2 (408 cm^{-1} and 383 cm^{-1}), metal oxide species (365 cm^{-1} and 224 cm^{-1}), and phosphate species (988 cm^{-1}). However, compared to 10 µm depth of cut case, the intensity (counts) of the characteristic peaks of the tribofilm were low with the 20 µm infeed condition. The low intensity of tribofilm species suggested reduced evolution of tribolayers due to incremental effect of higher depth of cut on grain-workpiece seizure leading to film desorption.

Hence, Raman characterization results have confirmed that the nanolubricant tribochemical films consisted of low shear strength (antifriction) and load carrying (antiwear) chemical species. These intermediate species were derived from organic-inorganic molecular friction-polymer precursors of nanolubricant during MQL grinding.

C. FORMATION AND DEFORMATION MECHANISMS OF TRIBOLAYERS

This section studied of the physical formation and deformation of nanolubricant-derived tribolayers at the abrasive grain-workpiece contact interfaces and their correlation with the tribological behavior of nanolubricants during MQL grinding.

Figures 8.8 (a, b) and (c, d) shows the representative SEM micrographs of 8 wt.% loaded nanolubricant-derived tribofilms formed during MQL grinding of ductile iron at 10 and 20 μm wheel infeed, respectively. The repeatable evolution of plate-like tribofilms was observed on the workpiece surfaces, as shown by Figure 8.8(a) and (c). However, a low surface density of plate-like films on the metal surface was observed with 20 μm wheel infeed as compared to the grinding condition with 10bμm wheel infeed. These physical observations confirmed the chemical results of the previous section that indicated a serious impact of increased grinding thrust forces on the lubrication, where intensive grain-metal seizures tend to desorb lubricant films from the metal surface. This study also suggested the potential challenges of deep feed grinding on the tribological performance of MQL based lubrication systems.

SEM micrographs in Figure 8.8(b) and (d) presented a closer view of the microstructure of the composite tribofilms derived from nanolubricant additives during MQL-assisted grinding. Elongated and sliding-oriented tribolayers can be observed in the micrographs for both the grinding conditions of 10 and 20 μm wheel infeed.

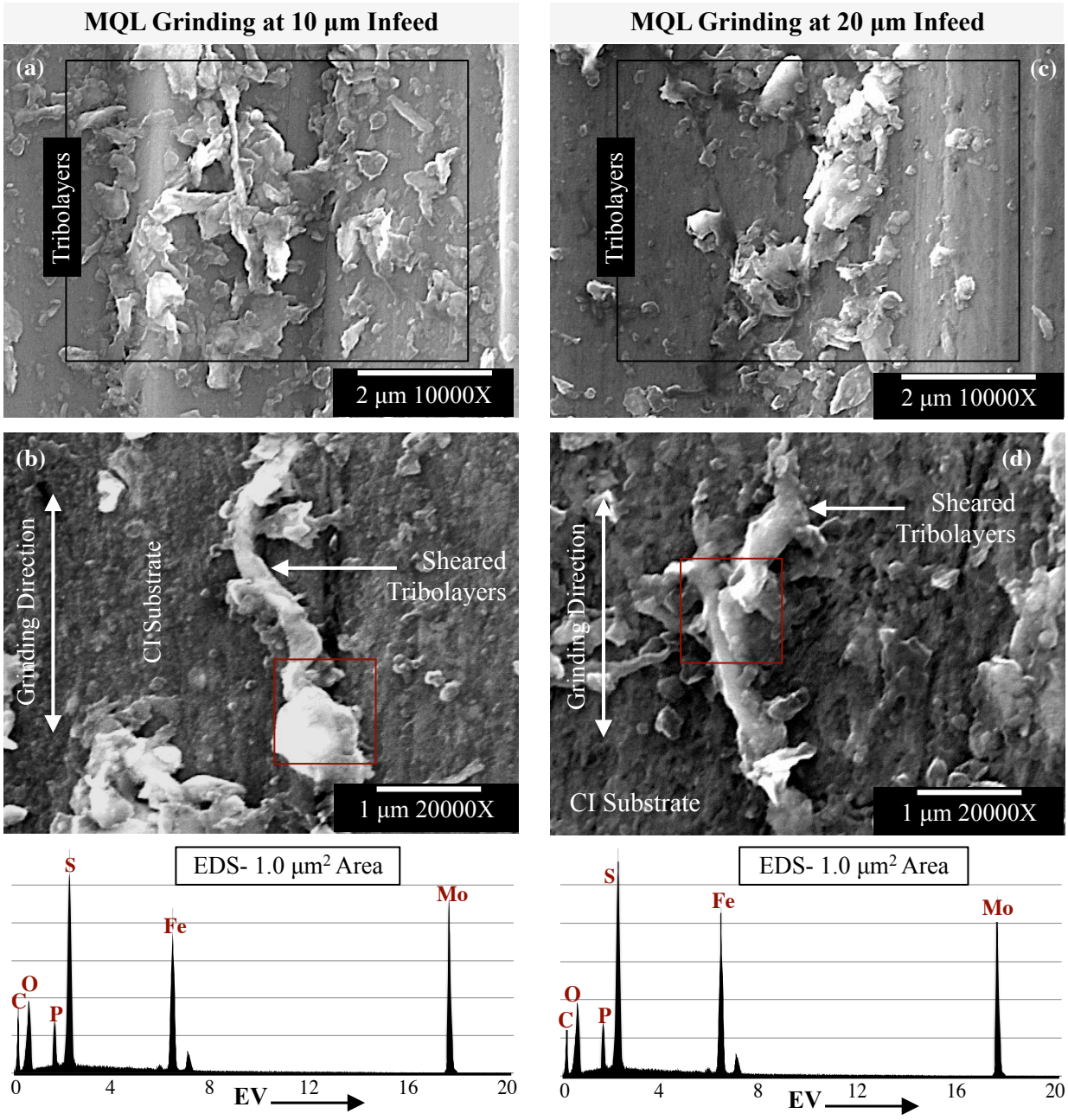

Figure 8.8 SEM-EDS microanalysis of 8 wt.%-loaded nanolubricant tribofilms formed during MQL grinding at (a, b) 10 and, (c, d) 20 µm wheel-infeed; (CI- cast iron substrate) [46]

These observations established correspondence with plastic deformation and alignment as the mechanisms of formation and deformation of the tribolayers at the grain-workpiece contact interfaces during grinding. Sheared between the high-strength abrasive grains and relatively low-

strength workpiece, the MoS_2 lamellas underwent continuous plastic deformation and the resultant plate-like tribolayers were aligned in the direction of sliding motion. The low coefficient of friction was attributed to the favorable orientation of the MoS_2 tribolayers derived from nanolubricants. Studies have reported that favorable orientation MoS_2 sheets occur upon reaching sufficiently high contact pressure ranging between 1.5-3 GPa [114]. Such high contact pressures were attained when phospholipids additive was used along with MoS_2 nanoparticles. The formation of antiwear phosphate layers from phospholipids increased the load carrying capacity of nanolubricant tribofilms, thus accommodating the high contact pressures for favorable orientation of MoS_2 layers.

To further understand the lubrication mechanism, the FIB milled cross-section of a nanolubricant tribofilm was studied using SEM-EDS. The cross-section of a nanolubricant-derived tribofilm is shown in Figure 8.9, which showed numerous sheared tribolayers gliding simultaneously or separately above one another. The gliding tribolayers were of different sizes and thickness. This sacrificial (easy shearing) action of tribolayers allowed low resistance sliding of grain wearflats against the workpiece and reduced interfacial stress on the abrasive grains as well as adhesion friction with the metal surface.

These mechanisms (sliding-induced plastic deformation, orientation of MoS_2 layers, and sacrificial yielding of load-carrying nanolubricant-tribolayers) were collectively responsible for the observed friction, energy, and wheel-wear reductions during the MQL-assisted grinding investigations.

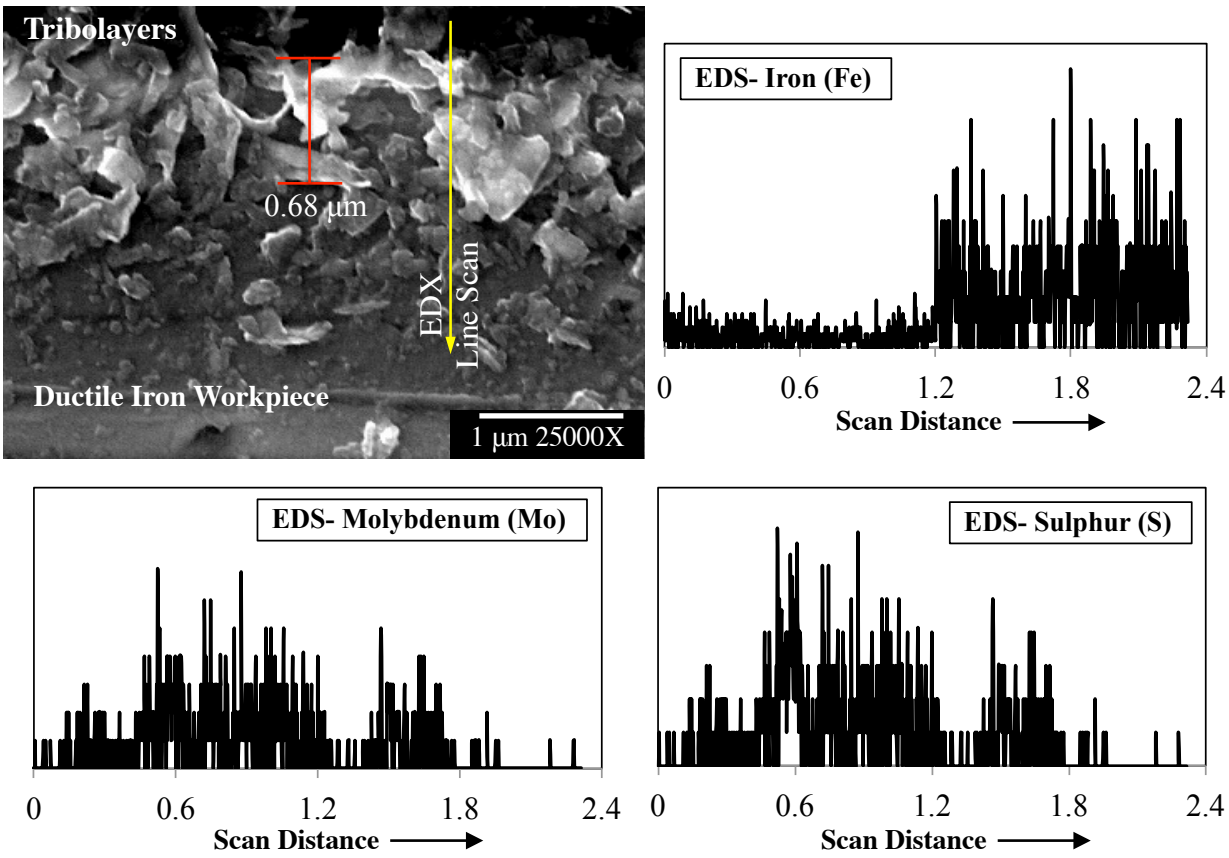

Figure 8.9 Cross-sectional microstructure of nanolubricant tribofilm; EDS line scan confirms the presence of Molybdenum and Sulphur especially in zones where no iron debris was detected [46]

IX. RESULTS AND DISCUSSION - TRIBOLOGICAL TESTING

The chapter discusses the results of wear and friction analyses in the tribosystem of nanolubricant-lubricated cubic boron nitride (cBN) superabrasives-1045 steel sliding pairs that were carried out on a reciprocating tribotest rig resembling the tool-lubricant-workpiece interactions of MQL assisted grinding. Tribological assessment of nanolubricant compositions was used to understand antifriction and antiwear behavior as a function of cBN grain-workpiece sliding time, and to validate the results with those obtained from MQL grinding. The chapter is divided into five sections that discusses the tribological attributes of the nanolubricants, A) coefficient of friction, B) surface topography of workpieces and cBN grains, C) tribochemical films formed at the grain-workpiece contact interfaces, D) effect of nanolubricant films on material removal, and E) evolution and lubrication mechanisms of nanolubricant films.

A. COEFFICIENT OF FRICTION (COF)

The variations in coefficient of friction (μ) as a function of sliding time (t) was studied to quantify the time-dependent friction behavior of nanolubricant lubricated cBN superabrasives-1045 steel sliding pairs and compare the μ-t behavior with base lubricants without nanoparticles.

The results of COF (μ) as a function of sliding time (t), obtained during simulated tribological testing with pure base fluids and MoS_2 nanoparticles-based lubricants are shown in Figure 9.1 a and b, respectively. The bar graph in Figure 9.2 summarizes the mean values of friction coefficient obtained with different lubricants.

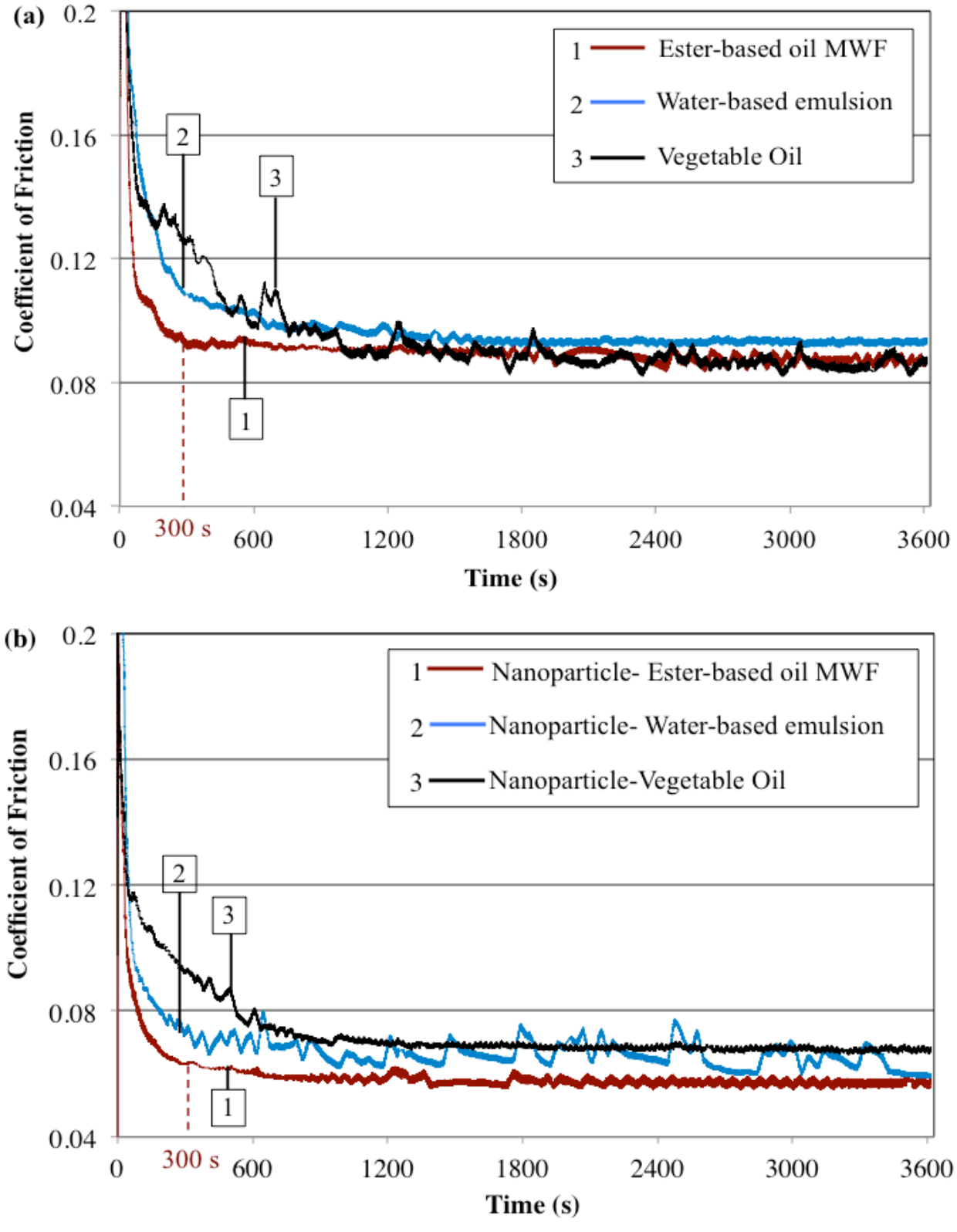

Figure 9.1 Coefficient of friction vs. sliding time plots for (a) base oils and (b) MoS_2 nanoparticles-based lubricants

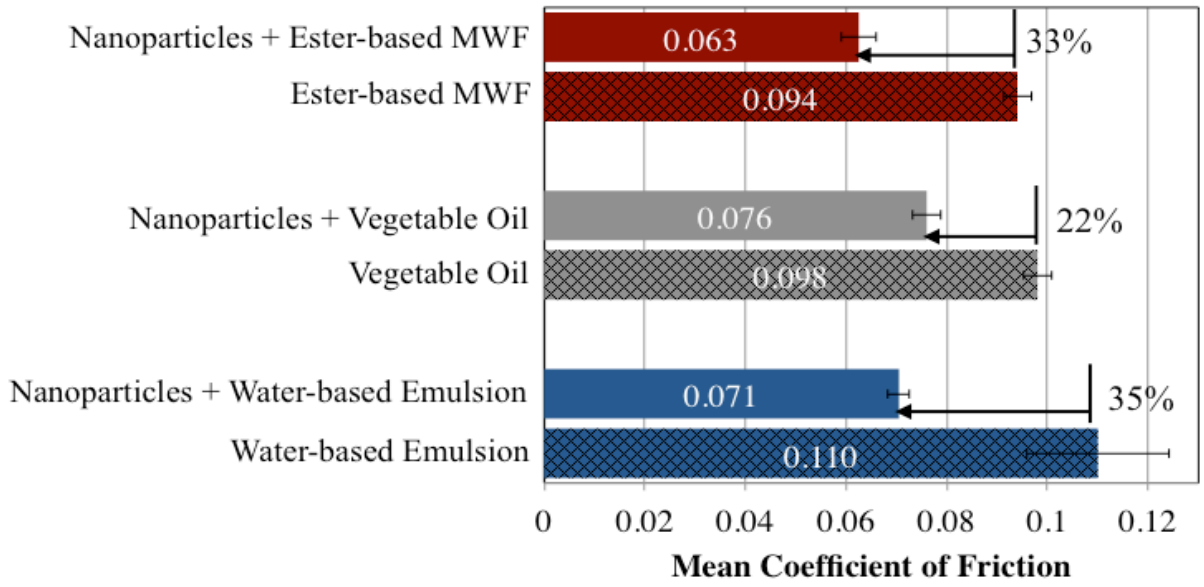

Figure 9.2 Average values of friction coefficient obtained after 1 h tribotest or 6070 sliding cycles with different lubrication conditions (error bars represent standard error of the mean COF obtained from three sliding tests

In Figure 9.1(a) and (b), a similar trend in μ-t curves can be seen for every lubrication condition. The COFs started with high values and gradually decreased to an average steady state value in the run-in-period. The sliding time corresponding to the start of the steady state of μ is the time required for the formation of stable tribochemical films in the contact zone. The time required for attaining stability in the values of μ, or in other words, the time required for the formation of stable tribochemical films was found to be distinctive for different lubricants. An early evolution of tribochemical films reduces adhesion friction as the films undergo continuous shear-deformation between the sliding facets of the abrasive grains and the workpiece. The COFs for ester-based oil (with and without MoS_2 nanoparticles) decreased to a steady value at approximately 300 s of sliding time. As compared to other lubricants, it was the shortest recorded time period for the growth of tribochemical films. This indicated excellent film forming capacity of the ester-based MWF in the sliding zone. However, at 300 s of sliding time, ester-

based MWF with MoS_2 nanoparticles showed an additional reduction in the COF value (μ = 0.065) as compared to 0.09 without nanoparticles. This was suggestive of the superior antifriction property of organic-coated MoS_2 nanoparticles. The improvement in antifriction property was further confirmed by the observed trends in the μ-t curves of nanoparticles integrated vegetable oil and water-based emulsion. The addition of nanoparticles not only shortened the run-in-time-period for attaining stability in the values of μ, but also reduced friction as compared to the pure base fluids.

The overall antifriction performance of the lubricants was analyzed using the average COF values as shown in Figure 9.2. Under the investigated process conditions, water-based emulsion (without nanoparticles) showed the highest value of μ =0.11, while the lowest value of μ was recorded with nanoparticles integrated ester-based MWF ($\mu_{avg.}$ = 0.063). Reductions in the values of μ were observed with the addition of MoS_2 nanoparticles to the base fluids. Nanoparticles integrated ester-based MWF, vegetable oil, and water-based emulsion showed COF decrements of 33%, 22%, and 35%, respectively, as compared to the respective base fluids. With 30% average reduction in COF over pure base fluids, nanoparticle-based formulations showed improvement in the lubrication capability under the representative tribological conditions of MQL grinding. The results also suggested a reduction in tool-workpiece frictional loss by MoS_2-based nanolubricants in real-time MQL grinding involving cBN superabrasives.

B. SURFACE TOPOGRAPHY

2-D surface profiles of the worn surfaces of workpieces obtained after 6070 sliding cycles of simulated tribological testing with pure base fluids and MoS_2 nanoparticles-based lubricants are shown in Figure 9.3. While SEM micrographs of the worn surfaces of cBN pins and steel

workpieces after 6070 sliding cycles with different lubricants can be seen in Figures 9.4 and 9.5, respectively.

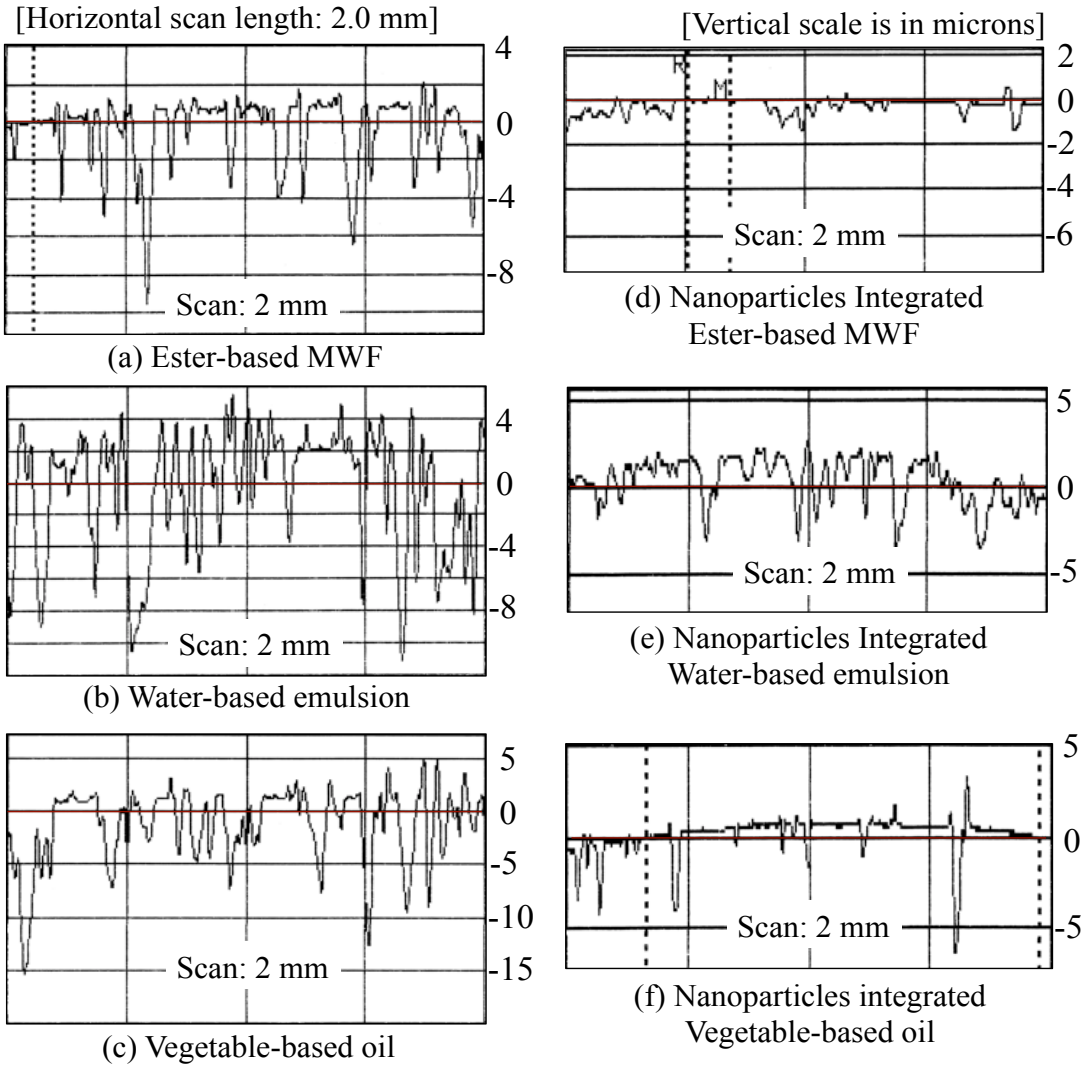

Figure 9.3 Surface profiles of workpieces, obtained after 1-hour tribotest or 6070 sliding cycles with different lubrication conditions

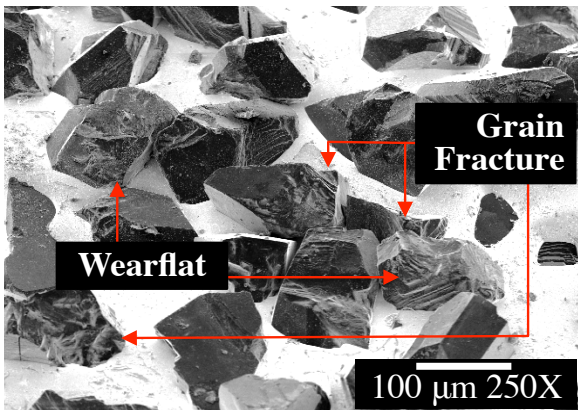

(a) Ester-based MWF

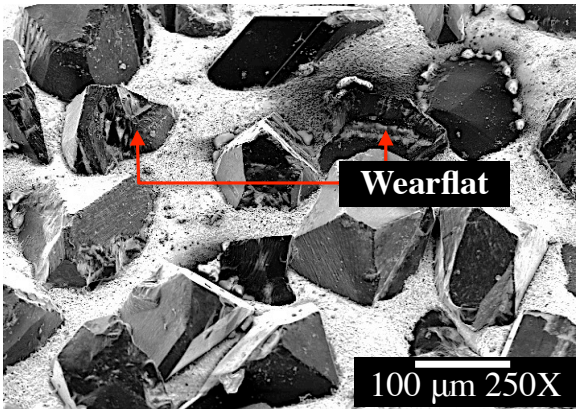

(d) Nanoparticles + Ester-based MWF

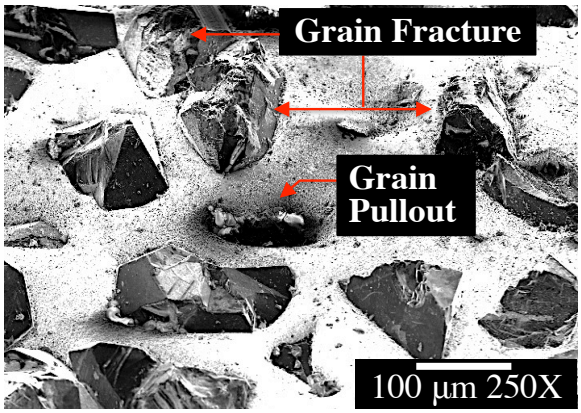

(b) Water-based emulsion

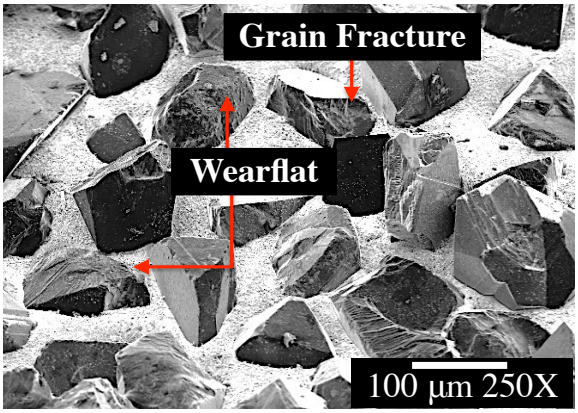

(e) Nanoparticles + Water-based emulsion

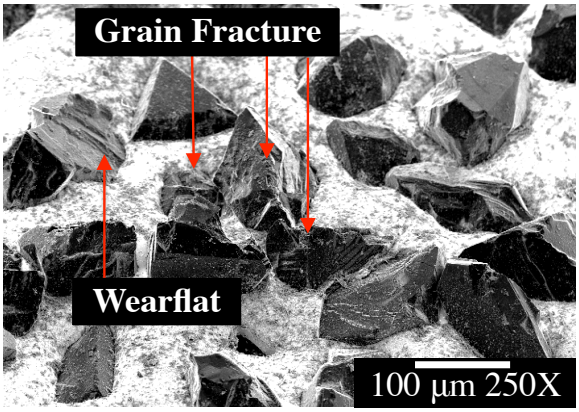

(c) Vegetable-based oil

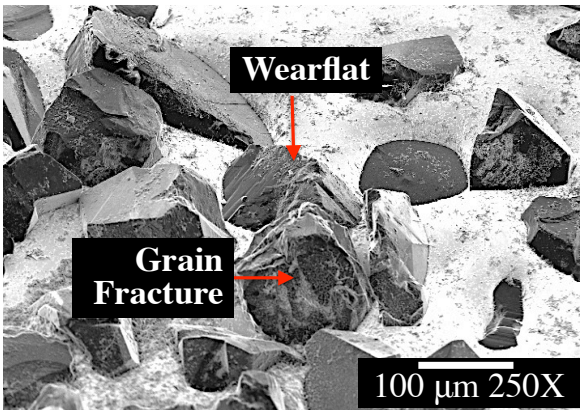

(f) Nanoparticles +Vegetable-based oil

Figure 9.4 SEM micrographs of cBN pin surfaces, obtained after 1 h tribotest or 6070 sliding cycles with different lubrication conditions

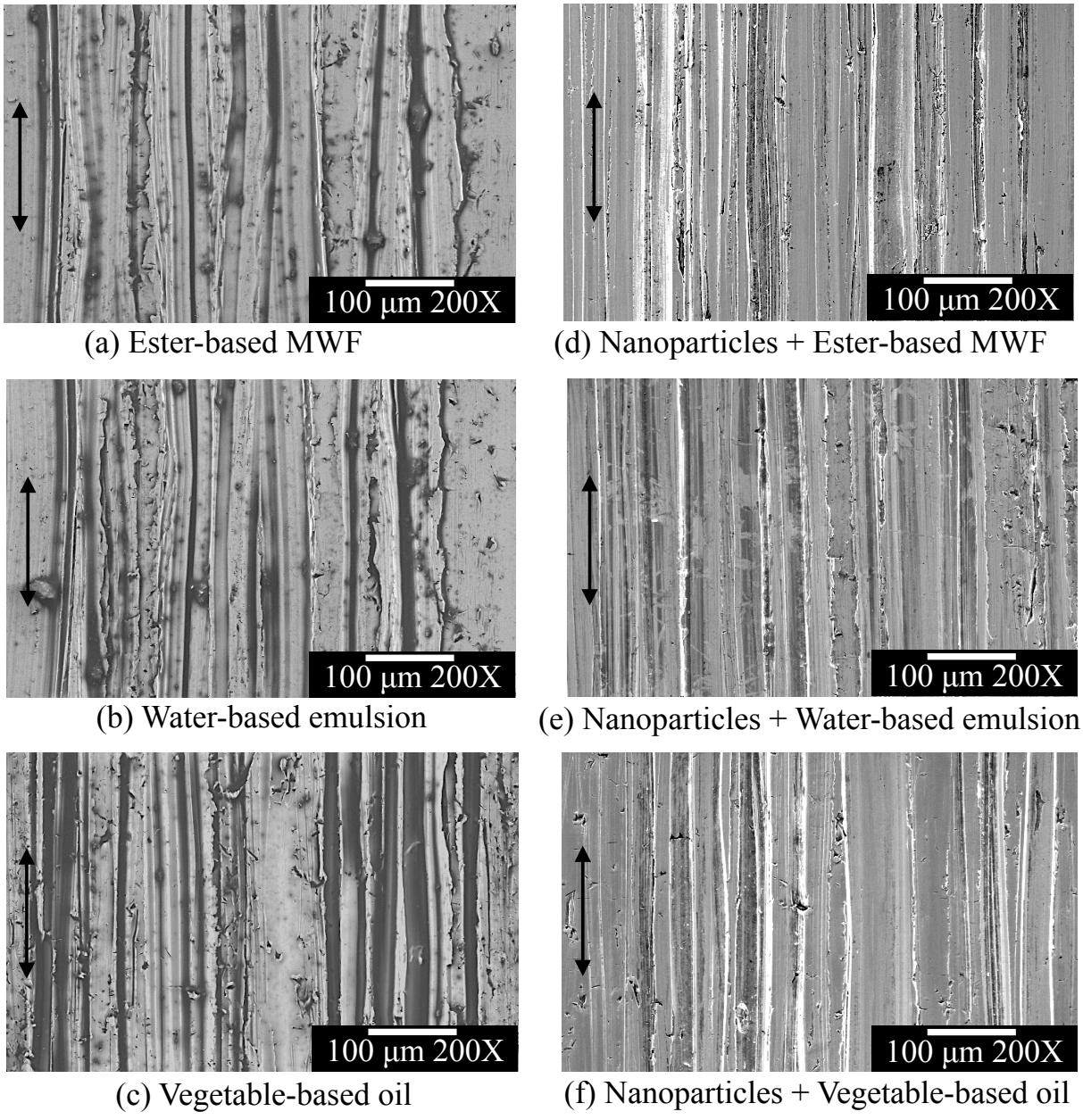

Figure 9.5 SEM micrographs of workpieces, obtained after 1 h tribotest or 6070 sliding cycles with different lubrication conditions; arrows indicate sliding direction, surface density of rough weartracks on the workpiece surfaces decreased with nanoparticles-based lubricants

From Figure 9.3(a)-(c), no qualitative difference in the surface characteristics of workpieces was observed with pure base fluids (without nanoparticles). Surface profiles revealed the erratic nature of material removal, while SEM micrographs demonstrated a high surface density of

rough and deep weartracks on the workpiece surfaces. Erratic surface patterns and rough surface textures were an indicative of glazing and rapid in-process dressing/fracture of abrasive crystals, which adversely affected the cutting process of the work material. These traits were seen in the corresponding SEM micrographs of worn surfaces of cBN pins (Figure 9.4). Wearflats, fractured grains at the tip and at the bond posts, and grain pull out were apparent on the sliding surfaces of the abrasive pins.

On the contrary, after comparable abrasion cycles the topographical characteristics of workpiece surfaces and cBN abrasive grains were found to be in better condition with lubricants containing MoS_2 nanoparticles. Relatively consistent peak and valley patterns of the workpiece surface profiles indicated a more uniform material removal. This was further confirmed by the apparent reduction in the surface density of rough weartracks on the workpiece surfaces, as can be seen in Figure 9.5. Wearflats were visible on the cBN grains, but the surface density of fractured abrasive grains was reduced with nanoparticles-based lubricants as compared to the base fluids. This was attributed to the continuous growth of sacrificial (low shear strength) tribolayers by MoS_2 nanoparticles in-between the cBN-1045 steel sliding counterfaces. Weakly bonded (by van der Waals forces) crystalline layers of MoS_2 are responsible for the sacrificial mechanism. The sacrificial tribolayers deformed plastically to reduce interfacial stress on the individual abrasives, which in turn, reduced the rapid fragmentation of cBN grains during sliding and rubbing against the workpiece material. This suggested that the antifriction and antiwear property of organic-coated MoS_2 nanoparticles could significantly increase cBN wheel life by preserving the grain geometry for prolonged machining cycle times.

C. TRIBOCHEMICAL FILMS

Figure 9.6 shows the SEM micrographic observations of the tribochemical films that were formed on the workpiece weartracks after 6070 abrasion cycles. Corresponding EDS spectra provided the elemental composition of the tribofilms.

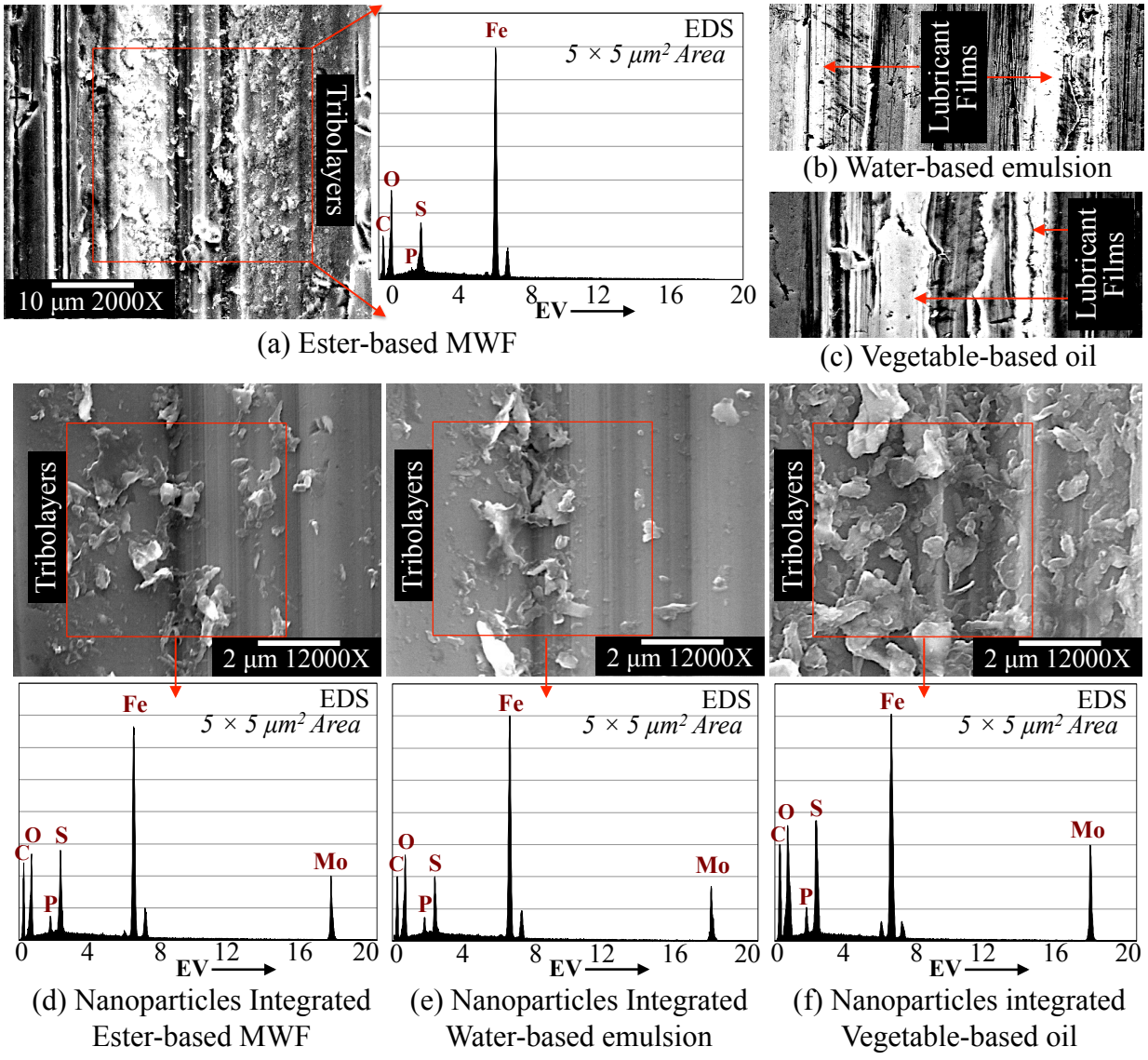

Figure 9.6 SEM-EDS microanalyses of tribochemical films formed on workpiece weartracks after 1 h (6070 sliding cycles) of tribotest

Formation of patchy tribofilms was observed with pure ester-based oil (without nanoparticles). While for pure vegetable oil and water-based emulsion, formation of tribofilm was limited to smeared oil traces on the workpiece weartracks. Elemental peaks of Sulphur (S) in addition to Iron (Fe) in the EDS spectrum suggested metal sulphide as the dominant chemical species in the tribofilms derived from ester-based MWF. The formation of patchy tribofilms was held responsible for the observed reduction in frictional losses with ester-based MWF as compared to the other base fluids. The tribochemical films derived from the nanoparticles integrated lubricants consisted of interspersed pad-like structures on the weartracks and were oriented along the sliding-direction. Corresponding EDS analysis indicated an organic-inorganic composite nature of the films comprising of Molybdenum (Mo), Sulphur (S), Phosphorus (P), Carbon (C) and Oxygen (O) as the primary elements along with Iron (Fe). The growth of low-friction sulphide species from the reaction of organic coated MoS_2 nanoparticles with metal surface was responsible for the excellent tribological performance of nanolubricants.

The surface density of the tribofilms derived from nanoparticle-based formulations was found to be dependent on the viscosity and chemistry of the base fluids. Accumulation density of the tribofilms showed amplification with an increase in the viscosity (ν) of the base fluids ($\nu_{\text{vegetable oil}} > \nu_{\text{ester-based MWF}} > \nu_{\text{water-based emulsion}}$). Heavy tribofilm build-up was observed with nanoparticles integrated vegetable oil, while nanoparticles integrated water-based emulsion showed the least tribofilm build-up (Figures 9.6(e) and (f), respectively). The polarity of sulphurized-triglyceride molecules of nanoparticles integrated vegetable oil was believed to be responsible for such heavy deposition of tribofilms. This data suggested that a strong affinity between the lubricant additives and the metal surface developed due to the polarity of the molecules, which in turn, caused heavy deposition of lubricant films on the workpiece surface. Potential deleterious effects of such

conditions in MQL grinding include significant trapping and accumulation of machining debris/sludge in the grinding zone. The presence of debris/sludge particles introduces a third-body abrasion effect, which tends to amplify interfacial friction and wear as discussed in Ref. [124]. This was reflected in the results of coefficient of friction measurements in this work, where nanoparticles integrated into vegetable oil showed the highest value of friction coefficient compared to the other base formulations containing MoS_2 nanoparticles. Based on these observations, it was asserted that the MQL performance of solid lubricant integrated MWFs was demonstrated to be highly dependent on the chemo-physical properties of the base fluids. Application and function-specific selection of base fluids is vital for optimizing the tribological performance of MoS_2 nanoparticles in MQL-assisted grinding.

D. EFFECT OF NANOLUBRICANT FILMS ON MATERIAL REMOVAL

To study any potential affect on the workpiece material removal from tribofilm formation at the grain-workpiece interface by nanolubricants, the mass of material removed was measured after each tribological test. This was accomplished by repeatedly measuring the dry mass of the workpiece before and after the tribological test in an electronic balance with a resolution of 0.1 mg. Before measurements of mass, the post-test steel specimens were carefully cleaned to remove all organic and metallic residues/debris.

The reduction in sliding friction due to the formation of antifriction tribofilms by nanoparticle-based lubricants was not achieved at the cost of material removal volume. This was confirmed by the results of workpiece material loss after successive 6070 sliding cycles, as shown in Figure 9.7. A workpiece material loss of 0.07 g was measured after the tribological testing with

lubricants with and without MoS_2 nanoparticles. This demonstrated < 1% effect of the formation of low-friction tribofilms by MoS_2 nanoparticles on material removal.

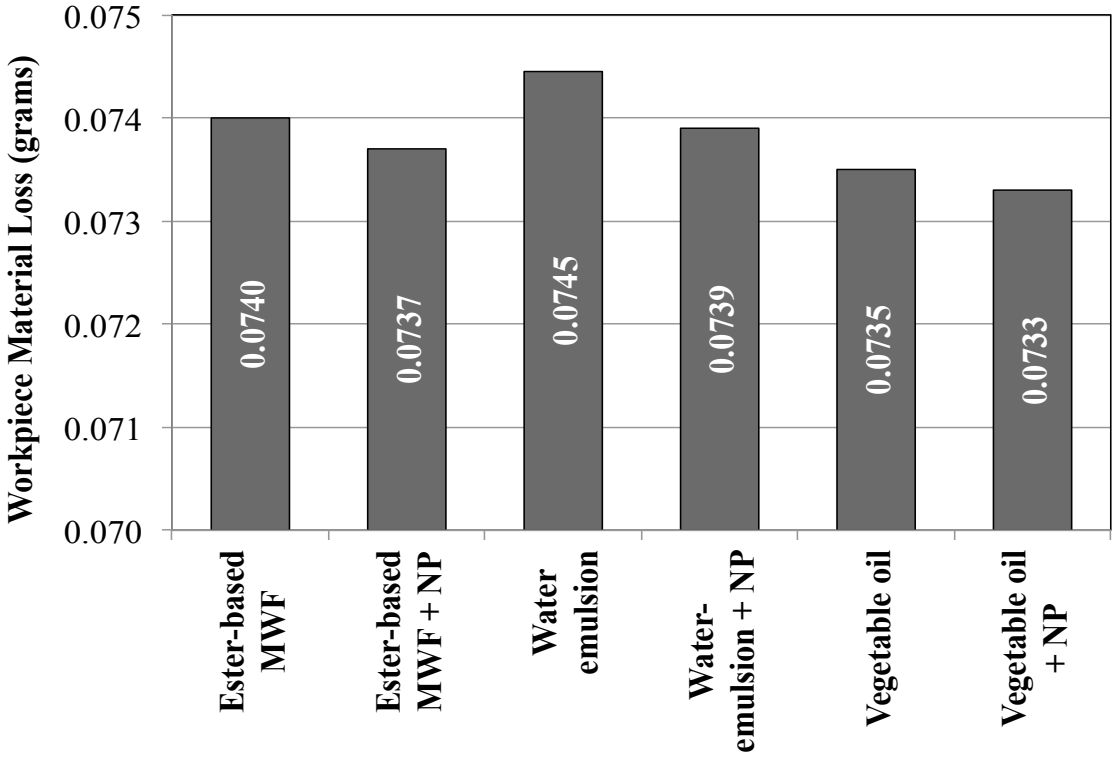

Figure 9.7 Workpiece material loss (in grams) vs. lubrication condition, NP refers to MoS_2 nanoparticles

Negligible effect of interfacial lubricating films on material removal was not contrary to abrasive machining. This was explained based on the structure of lubricant-derived tribofilms that evolved during abrasive machining and the in-process influence of the geometry of abrasive contact on the shearing of the evolved films. During machining, the contacting abrasive grains were subjected to small elastic deformation as compared to large plastic deformation of workpiece material. This was due to the differences in their structural strength and hardness (E_{cBN} = 706 GPa, H_{cBN} =40-50 GPa, E_{steel} = 201 GPa, H_{steel} =1.7 GPa). The prevalence of large

plastic deformation resulted in the formation of lacunous tribochemical films between the sliding surfaces that provided lubrication in critical areas of the abrasive grain-workpiece contact [8]. This was apparent in the microstructural analysis of tribofilms derived from the nanoparticles based lubricants, as discussed in Section IX.C. In terms of structural and tribofunctional characteristics, this type of film was completely different from a hydrodynamic or separating film that is formed between the moving parts under boundary lubrication condition. During abrasive machining, on-site lubrication by the shearing of tribofilms was favored in the regions of blunt asperity contact that did not contribute in material cutting. The sliding facets of abrasive grains and wearflats in contact with the workpiece surface were characterized as blunt asperity contact. However, high stresses at sharp asperity contact (contact between sharp abrasive points and workpiece material) resulted in material cutting without any impact from changes in the lubricant film. Further details on the shear deformation of lubricant films in blunt and sharp asperity contacts can be found elsewhere in [7,60].

E. EVOLUTION AND LUBRICATION MECHANISM OF NANOLUBRICANT FILMS

Figure 9.8 shows the SEM micrographs of nanolubricant-derived tribofilms formed on the workpiece surface during two tribological tests. The areas of high-contrast topography represent the tribofilms, whereas the low area (dark grey) represents the underlying steel (workpiece) surface.

Repeatable evolution of smooth pad-like structure of tribofilms was seen in the SEM micrographs. The pad-like structure of tribofilms derived from the MoS_2-based nanolubricant showed some resemblance to the post-deformed structure of ZDDP (zinc

dialkyldithiophosphates) antiwear films and MoDTC (molybdenum dialkyldithiocarbamate) friction modifying films under boundary lubrication conditions as reported in Ref. [101,125].

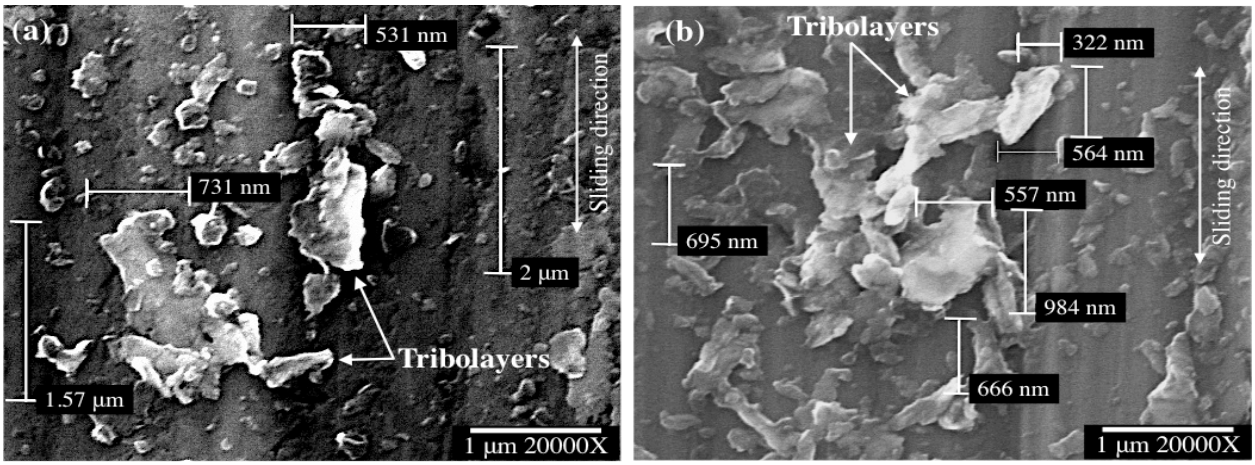

Figure 9.8 SEM micrographs of tribochemical films derived from nanoparticles integrated lubricant

However, as compared to ZDDP and MoDTC boundary films, nanolubricant derived tribofilms were lacunous and widely interspersed in the weartracks. From approximate dimensions of the pad-like structures, it was clear that the interspersed tribofilms were elongated along the sliding direction. This indicated continuous shearing of large-sized tribofilms into smaller pads in the sliding interfaces of cBN grains and workpiece. A closer topographical observation of a cluster of pads in Figure 9.9 illustrated multiple tribolayers gliding simultaneously or separately along the sliding direction. The sliding oriented multilayer architecture implied a continuous formation and deformation of sacrificial tribofilms by the shear motions of the grain-workpiece sliding surfaces.

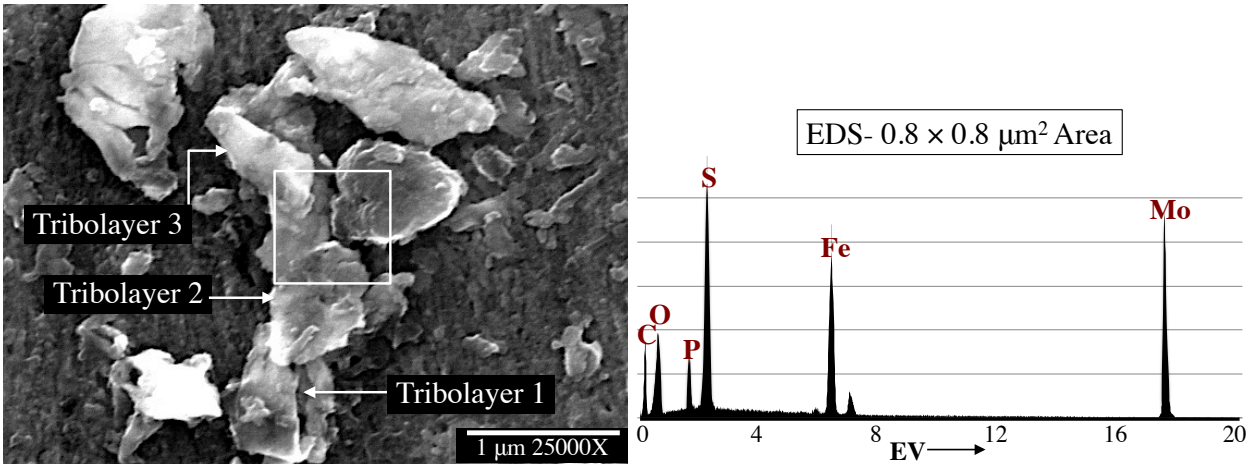

Figure 9.9 SEM micrograph showing multi-layer structure of tribofilm derived from organic-coated MoS_2 nanoparticles

Based on these observations, the lubricating mechanisms of fluids containing MoS_2 nanoparticles was summarized as follows:

1. **Continuous delivery** - Targeted lubricant delivery through MQL and high surface energy of MoS_2 nanoparticles triggered the absorption of nanolubricants into the porous abrasive tool (in this case, it is cBN mounted pin). This resulted in a continuous delivery and replenishment of lubricant additives into the machining zone.
2. **Friction-induced surface reactions** - Polar organic ligands overcoating the MoS_2 nanoparticles were physisorbed as well as chemisorbed onto the reactive abrasion-exposed metal surface. Redox reactions of the organic-inorganic additives with the friction surfaces led to the evolution of tribochemical films of organometallic chemistry.
3. **Sliding-induced shearing and alignment of MoS_2 layer -** Inorganic MoS_2 nanoparticles endowed a sacrificial mechanism to the tribochemical films and functioned as a friction modifier. Guided by sliding-induced mechanical stress, MoS_2 lamellas underwent shearing deformation, displacement, and deposition to form sacrificial tribolayers at the

grain-workpiece interface. With the sliding process, the lamellas of MoS_2 were continually deformed and aligned along the sliding direction. The sacrificial tribolayers that appeared as elongated pad-like structures reduced interfacial friction and wear of cBN grains.

X. CONCLUSION AND FUTURE WORK

A. CONCLUSION

This research advanced the composition, application and, fundamental understanding of MoS_2 based nanolubricants, consisting of organic molecules with phospholipid intercalated-MoS_2 nanoparticles (≈ 200 nm), in minimum quantity lubrication (MQL) grinding. For the first time, tribological efficiency and mechanisms of lubrication of MoS_2 based nanolubricants were established to address the extreme friction and thermal environments of MQL grinding.

The tribological behavior and lubrication efficiency of MoS_2 additized paraffin and soybean-based nanolubricants were investigated in MQL assisted surface grinding of ductile cast iron and EN 24 alloy steel with Al_2O_3 wheel at different infeed conditions. The surface grinding tests were carried out with nanolubricants of varying compositional chemistry and concentration of MoS_2 nanoparticles, their performance was compared to MQL grinding with base oils w/o nanoparticles, with MoS_2 microparticles (> 3 μm), and to flood grinding with a water-based synthetic coolant.

Based on the experimental findings, nanolubricants were found to enhance process productivity by improving surface quality by over two times (R_a as low as 0.35 μm) and increasing the functional life of grinding wheel (G-ratio- 42, > 50% increment over other MQL cases and flood grinding). Lubrication by nanolubricants reduced frictional losses (lowest friction coefficient-0.22) at the grain-workpiece contact interfaces by 45% that stimulated material cutting instead of rubbing and ploughing leading to reduction in energy and power requirements (upto 53% reduction). Measurement of grinding temperatures showed nanolubricants to compensate their inability of convective bulk cooling by reducing friction-induced heat generation for easy

dissipation through the workpiece. MQL with oil-based nanolubricants (120 ml/min flow) yielded 25 W/mm^2 as heat flux into workpiece as compared to 21 W/mm^2 with flood cooling (8400 ml/min flow).

Surface examination of grinding interfaces indicated continuous delivery of organic-coated MoS_2 nanoparticles through the microporosity networks of the grinding wheel and formation of sacrificial tribolayers by shear-induced plastic deformation and alignment at the grinding zone. Chemical examinations of reaction surfaces showed low-friction sulphide species and antiwear phosphate layers in nanolubricant-derived tribochemical films. Load carrying tribolayers sustained the intensive grain-workpiece contact seizure during grinding, while the low shear strength tribolayers sacrificed themselves at the grain-workpiece interface in lieu of wearing the harder abrasive grains through their adhesion friction with relatively soft metal surface. These tribological mechanisms were correlated with friction, energy, and wheel wear reduction efficacy of nanolubricants during MQL assisted grinding.

In conclusion, the suitability and excellent grinding productivity of nanolubricants in MQL grinding was established under the investigated process conditions by addressing frictional losses, energy consumption, tool life, surface temperatures, and surface quality.

B. RECOMMENDATIONS FOR FUTURE STUDY

This research has identified several future directions for the advancement of nanolubricants in MQL grinding. They are discussed below:

1. Further enhancement in the tribological properties of nanolubricants needs to be explored. One area would be the selection of appropriate base oil/ fluid chemistry. While grinding different workpiece material, base oil chemistry showed a significant influence in the tribological mechanisms of the nanolubricants. A synergistic base oil chemistry of nanolubricants would facilitate its application and performance in grinding different workpiece materials, including difficult to grind adhesive metals such as titanium and nickel alloys. Along with the base chemistry of nanolubricants, the dependence of size and shape of MoS_2 nanoparticles in the tribological properties of nanolubricant compositions and machining characteristics should also be investigated.
2. For optimization of cooling behavior of nanolubricants during MQL grinding, following studies are recommended:
    - Studies on the flash temperatures of base oils in the presence and variation in mist (compressed air) parameters, such as air temperature, pressure, and flow rates.
    - Studies on the oxidation temperatures and behavior of nanolubricants as a function of variation in the size and concentration of MoS_2 nanoparticles.
    - Studies on water-based nanolubricant emulsions for achieving optimum thermal and tribological performance during MQL grinding.
3. The effect of MQL use of nanolubricants on the compressive residual stress of ground parts and workpieces should be studied. Residual compressive stress is an important component of surface integrity that improves the fatigue and fracture strength and hence,

the working life of the ground parts and components.

4. Further enhancement in the design and material composition of nanolubricants along with an optimization of design and process parameters of the MQL system is required to expand its application in creep-feed grinding and high-efficiency deep grinding.
5. Tribological tests with cBN superabrasives demonstrated excellent antifriction and antiwear performance of oil-based nanolubricants. Therefore, the MQL application of nanolubricants should be studied and optimized for high-productivity grinding with vitrified cBN wheels.
6. Fundamental research needs to be continued to understand the tribological mechanisms of nanolubricant in MQL grinding. This includes the study of workpiece chip morphology formed during MQL grinding with nanolubricants to assess their lubrication effect on the mode of chip formation (shearing, fracturing, rubbing, or ploughing). Another fundamental research could be exploration of nanomechanical properties of nanolubricant-derived tribofilms during grinding. This includes, single point abrasive scratching of tribofilm-covered workpiece to determine the interfacial shear strength and adhesion of the films and nanoindentation studies to determine the elastic modulus and hardness of the tribofilms. These data would help in better functionalization of nanolubricants to improve their lubricating and load carrying capacity.

REFERENCES

1. Grinding, http://www.oocities.org/venkatej/mech/grinding/grinding.html, Information accessed on 04/15/2013.

2. Basics of Grinding, http://manufacturing.stanford.edu/processes/Grinding.pdf, Information accessed on 04/15/2013.

3. Malkin, S., (1989), "Theory and Applications of Machining with Abrasives", Ellis Horwood, Chichester, and John Wiley & Sons, New York.

4. Grinding, http://www.leechind.com/grinding.html, Information accessed on 04/15/2013.

5. Bhushan, B., (1999), "Principles and Applications of Tribology", John Wiley & Sons, New York.

6. Brinksmeier, E., Heinzel, C., Wittmann, M., (1999) "Friction, Cooling and Lubrication in Grinding", CIRP Annals - Manufacturing Technology, 48 (2), 581–598.

7. Shen, B., Xiao, G., Guo, C., Malkin, S., Shih, A.J., (2008), "Thermocouple Fixation Method for Grinding Temperature Measurement", Journal of Manufacturing Science and Engineering, 130, 051014-1-8.

8. Marinescu, L.D., Rowe, W.B., Dimitrov, B., and Inasaki, I., (2004), "Tribology of Abrasive Machining Processes", William Andrew, Inc., New York.

9. Li, C.H., Hou, Y.L. Xiu, S.C., Cai, G.Q., (2008), "Application of Lubrication Theory to Near-Dry-Green Grinding – Feasibility Analysis", Advanced Materials Research, 44-46, 135-142.

10. Whittaker, S.G., (1997), "Metalworking Fluids: A Resource for Employers and Health & Safety Personnel in Washington State", Safety & Health Assessment & Research for Prevention (SHARP) Program.

11. Dhar, N.R., Hossain, M.,Kamruzzaman, M., (2005), "MQL Applications in Grinding of 16MnCr5 Steel: A Comparison With Wet And Dry Grinding", ICME05-AM-33, 1-5.

12. Understanding Grinding Fluid, http://www.cimindustry.com/article/grinding/understanding- grinding-fluid, Information accessed on 04/15/2013.

13. Carter, N., (2010), "What is Green, Tribology and Lubrication Technology", Tribology and Lubrication Technology, STLE, 50-58.

14. Adler, D.P., Hii, W. W. S., Michalek, D. J., Sutherland, J. W., (2006), " Examining the Role of Cutting Fluids in Machining and Efforts to Address Associated

Environmental/Health Concerns", Machining Science and Technology: An International Journal, 10(1), 23-58.

15. Sanchez, J.A., Pombo, I., Alberdi, R., Izquierdo, B., Ortega, N., Plaza, S., Martinez-Toledano, J., (2010) "Machining Evaluation of a Hybrid MQL-CO_2 Grinding Technology", Journal of Cleaner Production, 18(18), 1840–1849.

16. Shen, C., (1996), "The Importance of Diamond Coated Tools for Agile Manufacturing and Dry Machining", Surface and Coatings Technology, 86–87, 672.

17. Klocke, F., and Eisenblätter, G., (1997), "Dry Cutting", Annals of the CIRP, 46(2), 519-526.

18. Machado, A., and Wallbank, J., (1997), "The Effect of Extremely Low Lubricant Volumes in Machining," Wear, 210 (1-2), 76 – 82.

19. Nouari, M., List, G., Girot, F., and Coupard, D., (2003), "Experimental Analysis and Optimisation of Tool Wear in Dry Machining of Aluminum Alloys", Wear, 255, 1359–1368.

20. Kobayashi, S., Ohgoe, Y., Ozeki, K., Sato, K., Sumiya, T., Hirakuri, K., and Aoki, H., (2005), "Diamond-like Carbon Coatings on Orthodontic Archwire", Diamond and Related Materials, 14, 1094-1097.

21. Reddy, N., and Rao, P., (2006), "Selection of an Optimal Parametric Combination for Achieving a Better Surface Finish in Dry Milling Using Genetic Algorithms", International Journal of Advanced Manufacturing Technology, 28 (6), 463-473.

22. Su, Y.L., Y., Liu, T., Su, C., Yao, S., Kao W., and Cheng, K., (2006), "Wear of CrC-Coated Carbide Tools in Dry Machining", Journal of Materials Processing Technology, 171(1), 108- 117.

23. Arumugam, P., Malshe, A.P, and Batzer, S., (2006), "Dry Machining of Aluminum-Silicon Alloy using Polished CVD Diamond-Coated Cutting Tools Inserts", Surface Coating and Technologies, 200, 3399-3403.

24. Sun, J., Wong, Y., Rahman, M., Wang, Z., Neo, K., Tan, C., and Onozuka, H., (2006), "Effects of Coolant Supply Methods and Cutting Conditions on Tool Life in End Milling Titanium Alloy", Machining Science and Technology, 10, 355-370.

25. Davim, J., Sreejith, P., Gomes, R., and Peixoto, C., (2006), "Experimental Studies on Drilling of Aluminum (AA1050) under Dry, Minimum Quantity of Lubricant, and Flood-lubricated Conditions", J. Engineering Manufacture, 220, 1605-1611.

26. Heinemann, R., Hinduja, S., Barrow, G., and Petuelli, G., (2006), "Effect of MQL on the Tool Life of Small Twist Drills in Deep-hole Drilling", International Journal of Machine Tools and Manufacture, 46, 1-6.

27. Shen, B., Kalita, P., Malshe, A. P., Shih, A. J., (2008), "Performance and Behavior of Novel MoS_2 Nanoparticles based Grinding Fluids in Minimum Quantity Lubrication Grinding", Transactions of NAMRI/SME, 36, 357-364.

28. Kalita, P., (2009), "Testing of Nano-Engineered Lubricants for Minimum Quantity Lubrication (MQL) Grinding: Performance Testing and Fundamental Understanding", University of Arkansas, Fayetteville, Masters Thesis.

29. Wakabayashi, T., Sato, H., and Inasaki, I., (1998), "Turning using Extremely Small Amounts of Cutting Fluids", JSME International Journal, 41, 143-148.

30. Dhar, N., Islam, M., Islam, S., and Mithu, M., (2006), "The Influence of Minimum Quantity of Lubrication (MQL) on Cutting Temperature, Chip and Dimensional Accuracy in Turning AISI-1040 Steel", Journal of Materials Processing Technology, 171, 93-99.

31. Davim, J. Paulo, Sreejith, P., and Silva, J., (2007), "Turning of Brasses using Minimum Quantity of Lubricant and Flood Lubricant Conditions", Materials and Manufacturing Processes, 22, 45-50.

32. Kamata, Y., and Obikawa, T., (2007), "High Speed MQL Finish-turning of Inconel 718 with Different Coated Tools", Journal of Materials Processing Technology, 281-286.

33. Autret, R., and Liang, S. (2003), "Minimum Quantity Lubrication in Finish Hard Turning", HNICEM '03.

34. Rahman, M., Senthil Kumar, A., and Salam, M., (2001), "Evaluation of Minimal Quantitiesof Lubricant in End Milling", International Journal of Advanced Manufacturing Technology, 18(4), 235-241.

35. Rahman, M., Senthil Kumar, A., and Salam, M., (2002), "Experimental Evaluation on the Effect of Minimal Quantities of Lubricant in Milling", International Journal of Machine Tools and Manufacture, 42(5), 539-547.

36. Lopez de Lacalle, L., Angulo, C., Lamikiz, A., and Sanchez, J. A., (2006), "Experimental and Numerical Investigation of the Effect of Spray Cutting Fluids in High Speed Milling", Journal of Materials Processing Technology, 172, 11-15.

37. Su, Y.L., Y., Liu, T., Su, C., Yao, S., Kao W., and Cheng, K., (2006), "Wear of CrC-Coated Carbide Tools in Dry Machining", Journal of Materials Processing Technology, 171(1), 108- 117.

38. Liao, Y., and Lin, H., (2007), "Mechanism of Minimum Quantity Lubrication in High-speed Milling of Hardened Steel", International Journal of Machine Tools and Manufacture, 47, 1660-1666.

39. Filipovic, A., and Stephenson, D., (2006), "Minimum Quantity Lubrication (MQL) Applications in Automotive Power-Train Machining", Machining Science and Technology, 10, 3–22.

40. Braga, D., Diniz, A., Miranda, G., and Coppini, N. (2002), "Using a Minimum Quantity of Lubricant (MQL) and a Diamond Coated Tool in the Drilling of Aluminum-Silicon Alloys", Journal of Materials Processing Technology, 122, 127-138.

41. Heinemann, R., Hinduja, S., Barrow, G., and Petuelli, G., (2006), "Effect of MQL on the Tool Life of Small Twist Drills in Deep-hole Drilling", International Journal of Machine Tools and Manufacture, 46, 1-6.

42. Kristopher S., "Sustainable Powertrain Operations Save Money, Boost Quality, Protect The Environment", http://media.ford.com/article_display.cfm?article_id=24107, Ford motor company, Information accessed on 04/15/2013.

43. Surface Grinding Services, http://www.es-engineering.co.uk/machinery/manual/surface-grinding-telford-shropshire/, Information accessed on 04/15/2013.

44. Introduction to grinding, http://www.nitc.ac.in/dept/me/jagadeesha/mev402/Chapter1_Introduction_to_Grinding.pdf, Information accessed on 04/15/2013.

45. Dzebo, S., (2009) "Investigation of Methods to Improve Process Performance in Centerless Grinding of Inconel 718 and Ti-6Al-4V superalloys", Georgia Institute of Technology, Masters Thesis.

46. Kalita, P., Malshe, A.P, Rajurkar, K.P., (2012), "Study of Tribochemical Lubricant Film Formation During Application of Nanolubricants in Minimum Quantity Lubrication (MQL) Grinding", CIRP Annals - Manufacturing Technology, 61(1), 327–330.

47. Abrasive process (grinding), Version 2 ME, IIT Kharagpur, http://nptel.iitm.ac.in/courses/Webcoursecontents/IIT%20Kharagpur/Manuf%20Proc%20II/pdf/LM-27.pdf, Information accessed on 04/15/2013.

48. Tian, W., (2009), "Signature Analysis of OD Grinding Processes with Applications in Monitoring and Diagnosis", M.S. Thesis, Worcester Polytechnic Institute.

49. Marinescu, I.D., Hitchiner, M., Uhlmann, E., Rowe, W.B., Insaki, I., (2006), "Handbook of Machining with Grinding Wheel", CRC Press.

50. Hadad, M.J., Tawakoli, T., Sadeghi, M.H., Sadeghi, B., (2012), "Temperature and energy partition in minimum quantity lubrication-MQL grinding process", International Journal of Machine Tools and Manufacture, 54–55, 10–17.

51. Silva, L., Bianchi, E., Catai, R., Fusse, R., França, R., and Aguiar, P., (2005), "Study on the Behavior of the Minimum Quantity Lubricant – MQL Technique under Different Lubricating and Cooling Conditions when Grinding ABNT 4340 steel", Journal of the Brazilian Society of Mechanical Sciences and Engineering, 17(2), 193-198.

52. Cutting fluid management for small machining operations, Iowa Waste Reduction Center, University of Northern Iowa, http://cedarfallsoil.com/_IWRC_mirror/cfm.pdf , Information accessed on 04/15/2013.

53. Da Silva, E.J., Bianchi, E.C., De Aguiar, P.R., (2001), "A Review of Grinding Fluids – Performances and Management", Revista De Ciência & Tecnologia, 8(18), 67-77.

54. Byers, J.P., (2006), "Metalworking Fluids, Second Edition", CRC Press.

55. Sluhan, C.A., (1994), "Selecting the Right Cutting and Grinding Fluids", Tooling & Production, 60(2).

56. Brinksmeier, E., Garbrecht, M., Heinzel, C., Koch, T. Eckebrecht, J., (2009), "Current Approaches in Design and Supply of Metalworking Fluids", Tribology Transactions 52(5).

57. Passman, F.J., (2004), "Microbial Problems in Metalworking Fluids", Tribology & Lubrication Technology, 24-27.

58. Setti, D., Ghosh, S., Rao, P.V., (2012), "Application of Nano Cutting Fluid under Minimum Quantity Lubrication (MQL) Technique to Improve Grinding of Ti – 6Al – 4V", World Academy of Science, Engineering and Technology, 70, 512-516.

59. Tawakoli, T., Hadad, M.J., Sadeghi, M.H., Daneshi, A., Stöckert, S., Rasifard, A., (2009), "An Experimental Investigation of the Effects of Workpiece and Grinding Parameters on Minimum Quantity Lubrication—MQL Grinding", International Journal of Machine Tools and Manufacture, 49 (12–13), 924–932.

60. Kalita, P., Malshe, A.P., Arun Kumar, S., Yoganath, V.G., Gurumurthy, T., (2012), "Study of Specific Energy and Friction Coefficient in Minimum Quantity Lubrication Grinding Using Oil-Based Nanolubricants", Journal of Manufacturing Processes, 14(2), 160–166.

61. Hafenbraedl, D., and Malkin, S., (2000), "Environmentally-Conscious Minimum Quantity Lubrication (MQL) for Internal Cylindrical Grinding", Transactions of NAMRI/SME, 28, 149 – 154.

62. Sadeghi, M. H., Haddad, M. J., Tawakoli, T., Emami, M., (2008), "Minimal Quantity Lubrication-MQL in Grinding of Ti–6Al–4V Titanium Alloy", International Journal of Advanced Manufacturing Technology.

63. Tawakoli, T., Hadad, M.J., Sadeghi, M.H., (2010), "Influence of Oil Mist Parameters on Minimum Quantity Lubrication – MQL Grinding Process", International Journal of Machine Tools and Manufacture, 50(6), 521–531.

64. Tawakoli, T., Hadad, M.J., Sadeghi, M.H., (2010), "Investigation on Minimum Quantity Lubricant-MQL Grinding of 100Cr6 Hardened Steel Using Different Abrasive and Coolant–Lubricant Types", International Journal of Machine Tools and Manufacture, 50(8), 698–708

65. Islam, M.A., Dhar, N.R., (2008), "Effects of Minimum Quantity Lubrication by Vegetable Oil-Based Cutting Fluid on Temperature, Chip Morphology, and Surface Finish in Grinding AISI 1060 Steel", Proceedings of the 4th BSME-ASME International Conference on Thermal Engineering, 861-865.

66. Haddad, M. J., Sadeghi, B., (2012), "Thermal Analysis of Minimum Quantity Lubrication-MQL Grinding Process", International Journal of Machine Tools and Manufacture, 63, 1–15.

67. Shen, B., Shih, A.J., and Tung, S., (2008), "Application of Nanofluids in Minimum Quantity Lubrication Grinding", STLE Tribology Transactions 51, 730-737

68. Srivastava, A., (2006), "The ABCs of CBN Grinding", "http://www.gearsolutions.com/article/detail/5427/the-abcs-of-cbn-grinding", Information accessed on 04/15/2013.

69. Alves, J.A.C, Fernandes, U.B., da Silva Júnior, C.E., Bianchi, E.C., de Aguiar, P.R., da Silva, E.J., (2009), "Application of the Minimum Quantity Lubrication (MQL) Technique in the Plunge Cylindrical Grinding Operation", J. Braz. Soc. Mech. Sci. & Eng., 31(1).

70. Oliveira, D.J., Guermandi, L.G., Bianchi, E.C., Diniz, A.O., de Aguiar, P.R., Canarim, R.C., (2012), "Improving Minimum Quantity Lubrication in CBN Grinding Using Compressed Air Wheel Cleaning", Journal of Materials Processing Technology, 212(12), 2559–2568.

71. Sanchez, J.A Pombo, I., Alberdi, R., Izquierdo, B., Ortega, N., Plaza, S., Toledano, J. M., (2010), "Machining Evaluation of a Hybrid MQL-CO_2 Grinding Technology", Journal of Cleaner Production, 18(18), 1840–1849.

72. Shen, B., Shih, A.J., (2009), "Minimum Quantity Lubrication (MQL) Grinding Using Vitrified CBN Wheels, Transactions of NAMRI/SME, 37, 129-136.

73. Hadad, M.J., Tawakoli, T., Sadeghi, M.H., Sadeghi, B., (2012), "Temperature and Energy Partition in Minimum Quantity Lubrication-MQL Grinding Process", International Journal of Machine Tools and Manufacture, 54–55, 10–17.

74. Rudnick, L.R., (2009), "Lubricant Additives: Chemistry and Applications", II Edition, CRC Press.

75. Shaji, S., Radhakrishnan, V., (2002), "An Investigation on Surface Grinding Using Graphite as Lubricant", International Journal of Machine Tools and Manufacture, 42(6), 733–740.

76. Vemula, V.V., Khan, T.A., (2012), "Study on Grindability of Ti-6Al-4V Using Solid Lubricants, International Journal on Emerging Technologies", 3(1), 109-114

77. Shaji S., Radhakrishnan, V., (2003), "Application of Solid Lubricants in Grinding: Investigations on Graphite Sandwiched Grinding Wheels", Machining Science and Technology, 7(1), 137–155.

78. Alberts, A., Kalaitzidou, K., Melkote, S., (2009), "An Investigation of Graphite Nanoplatelets as Lubricant in Grinding, International Journal of Machine Tools and Manufacture", 49(12–13), 966–970.

79. Malshe, A.P., and Verma, A., (2006), "Nanoparticle Compositions and Methods for Making and Using the Same", International Application No. PCT/US07/60506.

80. Basic Details on Molybdenum Disulphide, High Temperature Grease, "http://htgrease.blogspot.com/ ", Information accessed on 04/15/2013.

81. Rosentsveig, R., Margolin, A., Gorodnev, A., Popovitz-Biro, R., Feldman, Y., Rapoport, L., Novema , Y., Naveh, G., Tenne, R., (2009), "Synthesis of Fullerene-Like MoS_2 Nanoparticles and Their Tribological Behavior", J. Mater. Chem., 19, 4368-4374.

82. Verma, A., Jiang, W., Abu-Safe, H.H., and Malshe, A.P., (2008), "Tribological Behavior of the Deagglomerated Active Inorganic Nanoparticles for Advanced Lubrication", Tribology Transactions, 51(5), 673-678.

83. Rapoport, L. Leshchinsky, V., Volovik, Y., Lvovsky, M., Nepomnyashchy, O., Feldman, Y., Popovitz-Biro, R., Tenne, R., (2003), "Modification of Contact Surfaces by Fullerene-Like Solid Lubricant Nanoparticles", Surface And Coatings Technology, 163–164, 405–412.

84. Zhu, Y.Q., Sekine,T., Li, Y.H., Fay, M.W., Zhao, M.Y., Patrick, C. H., Wang, W.X., Roe, M.J., Brown, P.D., Fleischer, N., Tenne, R., (2005), "Shock-Absorbing and Failure Mechanisms of WS_2 and MoS_2 Nanoparticles with Fullerene-like Structures under Shock Wave Pressure", Journal of the American Chemical Society, 127(46), 16263-16272.

85. Rapoport, L., Fleischer, N., and Tenne R., (2005), "Applications of WS_2 (MoS_2) Inorganic Nanotubes and Fullerene-Like Nanoparticles for Solid Lubrication and for Structural Nanocomposites", Journal of Materials Chemistry, 15,1782-1788.

86. Verma, A., (2008), "Fundamental Understanding of the Synthesis and Tribological Behavior of Organic-Inorganic Nanoparticles", Doctoral Dissertation.

87. Le, C.G., Delcroix, P., Bégin-Colin, S., Ziller, T., (2002), "High-Energy Ball-Milling of Alloys and Compounds", Hyperfine Interactions 141-142, 63–72.

88. Koch, C.C., (1992), Material Science Forum, 88-90, 243.

89. Suryanarayana, C., (2001), "Mechanical Alloying and Milling", Progress in Materials Science, 46, 1-184.

90. Huot, J., Balema, V., (2011), "Mechanochemical Effect of Severe Plastic Deformations: Metal Alloys, Hydrides and Molecular Solids", Material Matters, 5 (4), 1-9.

91. Smoke Point of different Cooking Oils, http://chartsbin.com/view/1962, Information accessed on 04/15/2013.

92. Caldwell, M., Properties of Mineral Oil, "http://www.ehow.com/about_5445558_properties-mineral-oil.html", Information accessed on 04/15/2013.

93. Shen, B., (2008), "Minimum Quantity Lubrication Grinding Using Nanofluids", University Of Michigan, Doctoral Dissertation.

94. Kalita, P., Malshe, A.P., Arun Kumar, S., Yoganath, V.G., Gurumurthy, T., (2012), "Study of Specific Energy and Friction Coefficient in Minimum Quantity Lubrication Grinding Using Oil-Based Nanolubricants", Journal of Manufacturing Processes, 14(2), 160–166.

95. Tawakoli, T., Hadad, M.J., Sadeghi, M.H., (2010), "Influence of Oil Mist Parameters on Minimum Quantity Lubrication – MQL Grinding Process", International Journal of Machine Tools and Manufacture, 50(6), 521–531.

96. Jackson, M.J., Hitchiner, M. P., (2013), "High Performance Grinding and Advanced Cutting Tools", Springer.

97. Davies, M.A., Ueda, T., M'Saoubi, R., Mullany, B., Cooke, A.L., (2007), "On The Measurement of Temperature in Material Removal Processes", CIRP Annals - Manufacturing Technology, 56(2), 2007, 581–604

98. Guo, C., and Malkin, S., 1992, "Heat Transfer in Grinding," J. Mater. Process. Manuf. Sci., 1, 16–27.

99. Surface roughness produced by common production processes, http://icrank.com/cgi-bin/pageman/pageout.cgi?path=/data/surface_finish.htm&t=2, Information accessed on 04/15/2013.

100. Badger J., "Grinding: A Pictorial Odyssey", http://www.abrasiveengineering.com/semgrind.pdf, Information accessed on 04/15/2013.

101. Zhang, Z., Yamaguchi, E.S., Kasrai, M., and Bancroft, G.M., (2005), "Tribofilms Generated from ZDDP and DDP on Steel Surfaces: Part 1, Growth, Wear and Morphology", Tribology Letters, 19(3), 211-220.

102. Malkin, S., (1985), "Current trend in CBN grinding technology", Annals of the CIRP. 43(2), 557.

103. Kohli, P., Guo, C., Malkin, S., (1995), "Energy Partition for Grinding with Aluminum Oxide and CBN Abrasive Wheels", J. Eng. Ind.-Trans. ASME, 117, 160-168.

104. Guo, C., Wu, Y., Varghese, V., Malkin, S., (1999), "Temperatures and Energy Partition for Grinding with Vitrified CBN Wheels", Annals of the CIRP, 48, 247-250.

105. Upadhyaya, R.P., Malkin, S., (2004), "Thermal Aspects of Grinding With Electroplated CBN Wheels", J. Manuf. Sci. Eng.-Trans. ASME, 126, 117-124.

106. Fusse, R.Y., Franca, T.V., Catai, R.E., Silva, L.R., Aguiar, P.R., Bianchi, E.C., (2004), "Analysis of The Cutting Fluid Influence on The Deep Grinding Process with a CBN Grinding Wheel", Mater. Res., 7(3), 451-457.

107. Oliveira, J.F.G., Alves, S.M., (2006), "Development of Environmentally Friendly Fluid for CBN Grinding", Annals of the CIRP, 55(1), 343.

108. Alves, S.M., Bianchi, E.C., Aguiar, P.R., (2008), "Grinding of Hardened Steels Using Optimized Cooling", Ingeniare. Rev. chil. Ing., 16, 195-202.

109. Rowe, W.B., (2009), "Principles of Modern Grinding Technology", Elsevier.

110. Kuttolamadom, M.A., Hamzehlouia, S., Mears, M.L., (2010), "Effect of Machining Feed on Surface Roughness in Cutting 6061 Aluminum", SAE International, 1-19.

111. Krueger, M.K., Yoon, S.C., Gong, D., McSpadden Jr., S.B., O'Rourke, L.J., and Parten, R.J., (2000), "New Technology in Metalworking Fluids and Grinding Wheels Achieves Tenfold Improvement in Grinding Performance", Coolants/Lubricants for Metal Cutting and Grinding Conference, Session 5.

112. Liu, Y.D., Wang, C.B., Yuan, J.J., Liu, J.J., (2010), "The Effect of FeS Solid Lubricant on the Tribological Properties of Bearing Steel under Grease Lubrication", Tribology Transactions, 53(5), 667-677.

113. Wang, H.D., Zhuang, D.M., Wang, K.L., Liu, J.J., Cui, Y., Cui, Z.P., (2003), "Study on Tribological Properties of Iron Sulfide Coatings Prepared by a Sol-Gel Method", Journal of Materials Science Letters, 22 (14), 1043.

114. Bec, S., Tonck, A., Georges, J.M., Roper, G.W., "Synergistic Effects of MoDTC and ZDTP on Frictional Behavior of Tribofilms at the Nanometer Scale", Condensed Mater, Material Science, arXiv.org.

115. Badger, J.A., (2009), "Grinding: A Pictorial Odyssey, Cutting Tool Engineering", 61(2).

116. Li, H., Zhang, Q., Yap, C.C.R., Tay, B.K., Edwin, T.H.T., Olivier, A., Baillargeat, D., (2012), "From Bulk to Monolayer MoS_2: Evolution of Raman Scattering", Advanced Functional Materials, 22(7), 1385–1390.

117. Windom, B.C., Sawyer, W.G., Hahn, D.W., (2011), "A Raman Spectroscopic Study of MoS_2 and MoO_3: Applications to Tribological Systems", Tribol Lett., 42, 301–310.

118. Webber, T.E., “Synthesis of Iron Pyrite and Tin (VI) Sulfide Nanoparticles for Potential Application in Solar Cells”, University of Nebraska at Kearney.

119. Gangopadhyay, A., Sinha, K., Uy, D., Mcwatt, D.G., Zdrodowski, R.J., Simko, S.J., (2011), “Friction, Wear, and Surface Film Formation Characteristics of Diamond-Like Carbon Thin Coating in Valvetrain Application”, Tribology Transactions, 54, 104-114.

120. Frey, G.L, Tenne, R., Matthews, M.J., Dresselhaus, M.S., Dresselhaus, G., (1999), “Raman and Resonance Raman investigation of MoS_2 nanoparticles”, Physical Review B, 60(4), 2883-2892.

121. Smudde, G.H. Jr., Stair, P.C., (1994), “The Oxidation of Mo (100) Studied by XPS and Surface Raman Spectroscopy: the Onset of MoO_2 Formation and the Formation of Surface Polymolybdate,” Surf. Sci., 317(1-2), 65-72.

122. Zhang. W., Jahan, M.P, Malshe, A.P., (2012), “Chemical Understanding of Friction Polymer Based Tribochemical Films Derived from Nanolubricant”, Proceedings of the ASME/STLE, IJTC2012.

123. Lewis, I.R., Edwards, H., (2001), “Handbook of Raman Spectroscopy”, CRC Press.

124. Singer, I.L., (1998), “How Third Body Processes Affect Friction and Wear”, MRS Bull., 23, 37-40.

125. Miklozic, K.T., Spikes, H.A., (2005), “Application of Atomic Force Microscopy to the Study of Lubricant Additive Films”, J. Tribol., 127, 405-415.

APPENDICES

APPENDIX A: TRIBOLOGICAL PERFORMANCE COMPARISON OF SOLID LUBRICANTS

Favored by the excellent tribological properties, Molybdenum Disulphide (MoS_2) nanoparticles were used as solid lubricant in this research. As a part of the selection process of solid lubricant candidate, the tribological performance of MoS_2 nanoparticles was compared with that of hexagonal boron nitride (hBN) and graphite nanoparticles. Coefficient of friction results from the comparative tribological testing was used as an important selection criterion of solid lubricant additive for formulating nanolubricants for MQL grinding.

Tribological Properties of Solid Lubricants - Graphite and hBN

Like MoS_2, hBN and graphite are widely used as solid lubricants and belongs to the class of lamellar structured inorganic lubricants. Their intrinsic self-lubricating properties are due to their characteristic layered crystal structure as shown in Figure 1.1. The parallel crystalline planes are bonded to each other by weak van der Waals forces that impart low shear strength in the direction of sliding motion. As a result, the parallel planes readily glide over each other virtually without any shear resistance to provide excellent low-friction performance. However, the crystal structures have high compressive strength in the direction perpendicular to the sliding motion. These anisotropical properties provide low-friction and high load carrying capacity to graphite and hBN.

When smeared between sliding contact surfaces, the shear (friction) forces causes sliding induced orientation of the particles of MoS_2, graphite, and hBN in a direction parallel to the substrate or motion. Due to their strong adherence to metallic substrates, the deformed or sheared

particles form lubricating films at the contacting interfaces. Many tribological studies have reported low-friction, antiwear, and anti-seizure performance of such solid lubricant films. Compared to graphite and hBN, the metal adhesion of MoS_2 films have been reported stronger due to the presence of large number of oleophilic tails [1]. Tables 1.1 and 1.2 compare the friction and wear properties of MoS_2 with those of graphite and hBN. These findings were obtained from [2].

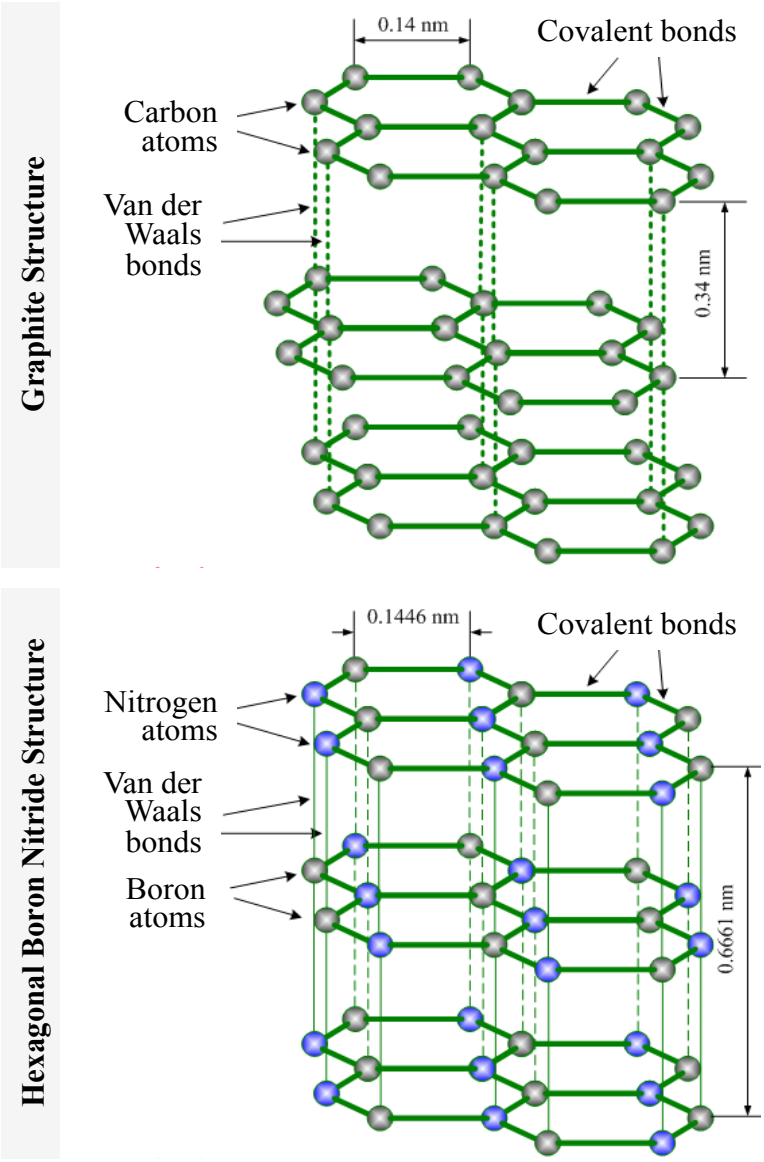

Figure 1.1 Crystal structures of Graphite and Hexagonal Boron Nitride (hBN) [3]

Table 1.1 Bench lubrication test results [2]

	Four Ball lubrication test				Falex Lubrication test		
	Wear ASTM D-4172		Extreme-pressure ASTM D-2783		Wear ASTM D-2670	EP ASTM D-3233	Coefficient of friction
	20 kg mm	40 kg mm	Weld (kg)	Load Wear Index (kg)	Teeth	lb. to failure	Calculated
Base oil	0.678	1.060	126	17.20	Fail	875	0.1590
With 1% colloidal graphite	0.695	0.855	160	18.70	78	1000	0.1320
With 1% colloidal MoS_2	0.680	0.805	200	24.30	8	4375	0.0770
With 1% colloidal BN	0.370	0.720	126	19.90	Fail	500	0.1602

Table 1.2 Solid lubricant selection comparison and rating [2]

Criteria	Graphite	MoS_2	BN
Normal atmospheres	1	1	1
Vacuum atmospheres	3	1	1
Ambient Temperature	1	1	1
Continuous service temperature to 260 ^{o}C in air	1	1	1
Continuous service temperature to 400 ^{o}C in air	1	1	1
Continuous service temperature to 450 ^{o}C in air	2	3	1
Burnishing capability	1	1	2
Hydrolytic stability	1	2	1
Thermal conductivity	2	3	1
Load-carrying lubrication	2	1	2
Friction reduction	2	2	3
Dispersibility	1	1	2
Color	Black	Gray	White
Relative cost	1	2	3
Note: 1 = best, 2 = good, 3 = ok			

Energy-intensive grinding processes involve severe friction and seizure between the abrasive grains and the workpiece. Hence, antifriction, load carrying capacity (extreme-pressure/antiwear), and thermal stability are vital properties of an effective grinding lubricant. From the results of Tables 1.1 and 1.2, MoS_2 has higher load-carrying capacity and lower friction coefficient as compared to graphite and hBN. Hence, based on these results, MoS_2 appeared to be the most suitable solid lubricant additive for grinding application despite its limited high-temperature performance.

Since the proposed nanolubricant compositions were designed for MQL grinding, base lubricants containing nanoparticles of MoS_2, graphite, and hBN were tested on a tribotest rig that simulated the friction and wear mechanisms of MQL-assisted grinding. The experimental details of tribological testing are explained below.

Experimental Conditions

The test lubricants were synthesized by homogenizing 2 wt.% of nanoparticles (≈ 200 nm) of MoS_2, graphite, and hBN in three base lubricants. The base lubricants included, vegetable-based oil, water-based emulsion, and biodegradable ester-based cutting fluid. The details of the base fluids are given in section B of Chapter 5. The lubricant compositions used for tribological testing are listed in Table 1.3. The friction characteristics of cubic boron nitride (cBN) superabrasives-1045 steel sliding pairs lubricated with pure base fluids and nanoparticle-based fluids were investigated on a reciprocating (sliding) tribotest rig, as explained in section B of chapter 5. The test setup simulated the tool-lubricant-workpiece interaction of MQL technique as well as the material removal mechanisms of reciprocating surface grinding (no cross feed) where the workpiece traverses in contact with the rotary abrasive wheel.

Table 1.3 List of lubricants

Test Lubricants	
Group 1 Nanoparticle-based lubricants	MoS_2 nanoparticles (2 wt.%) + Ester-based MWF
	MoS_2 nanoparticles (2 wt.%) + Vegetable oil
	Graphite nanoparticles (2 wt.%) + Water-based emulsion
	Graphite nanoparticles (2 wt.%) + Ester-based MWF
	Graphite nanoparticles (2 wt.%) + Vegetable oil
	Graphite nanoparticles (2 wt.%) + Water-based emulsion
	hBN nanoparticles (2 wt.%) + Ester-based MWF
	hBN nanoparticles (2 wt.%) + Vegetable oil
	hBN nanoparticles (2 wt.%) + Water-based emulsion
Group 2 Base lubricants	Ester-based MWF (pure base fluid)
	Vegetable oil (pure base fluid)
	Water-based emulsion (pure base fluid)

Mirror-polished AISI 1045 carbon steel and electroplated cBN-superabrasive mounted pins (Saint Gobain/Norton abrasives, average grit size- 150 μm) were used as the workpiece substrate and static partner (abrasive tool), respectively, during tribological testing. The test parameters were kept constant during all tribotests and are listed in Table 1.4.

Table 1.4 Pin-on-Flat Tribological Test Parameters

Tribotest Parameters	Values
Normal Load	10 N
Linear speed	200 mm/s
Test duration	60 min
Linear passes	6070
Sliding distance/pass	24 mm

Coefficient of Friction Results

The results of COF (μ) as a function of sliding time (t), obtained during simulated tribological testing with ester-based lubricants, water-based fluids, and vegetable-based lubricants w/ and w/o nanoparticles are shown in Figure 1.2, 1.3 and 1.4, respectively.

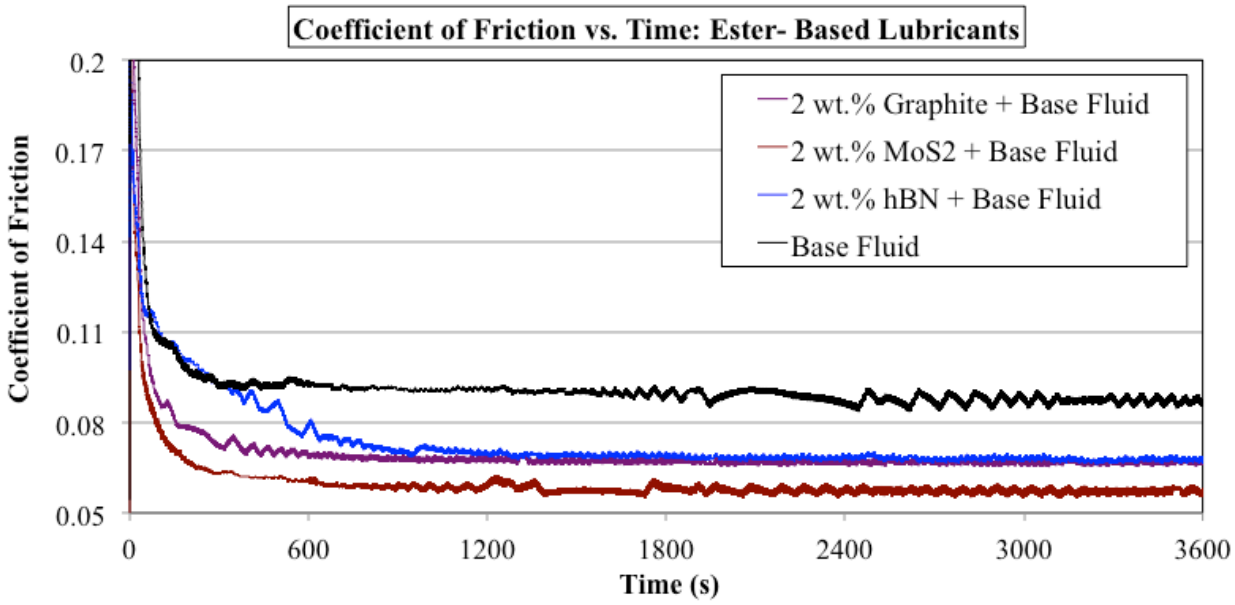

Figure 1.2 COF (μ) vs. sliding time (t) plots for ester-based MWF w/ and w/o nanoparticles

In Figures 1.2, 1.3 and 1.4, similar trends in μ-t curves were observed for each lubrication condition. The COFs started with high values and gradually decreased to an average steady state value in the run-in-period. The sliding time corresponding to the start of the steady state of μ represents the time period of formation of stable tribochemical films in the contact zone. Among all nanoparticles added fluids, MoS_2 nanoparticle-based lubricants yielded the lowest friction coefficient values throughout the 3600 s sliding period. In comparison, hBN nanoparticles added fluids showed the highest values of friction coefficient while graphite nanoparticles yielded intermediate results.

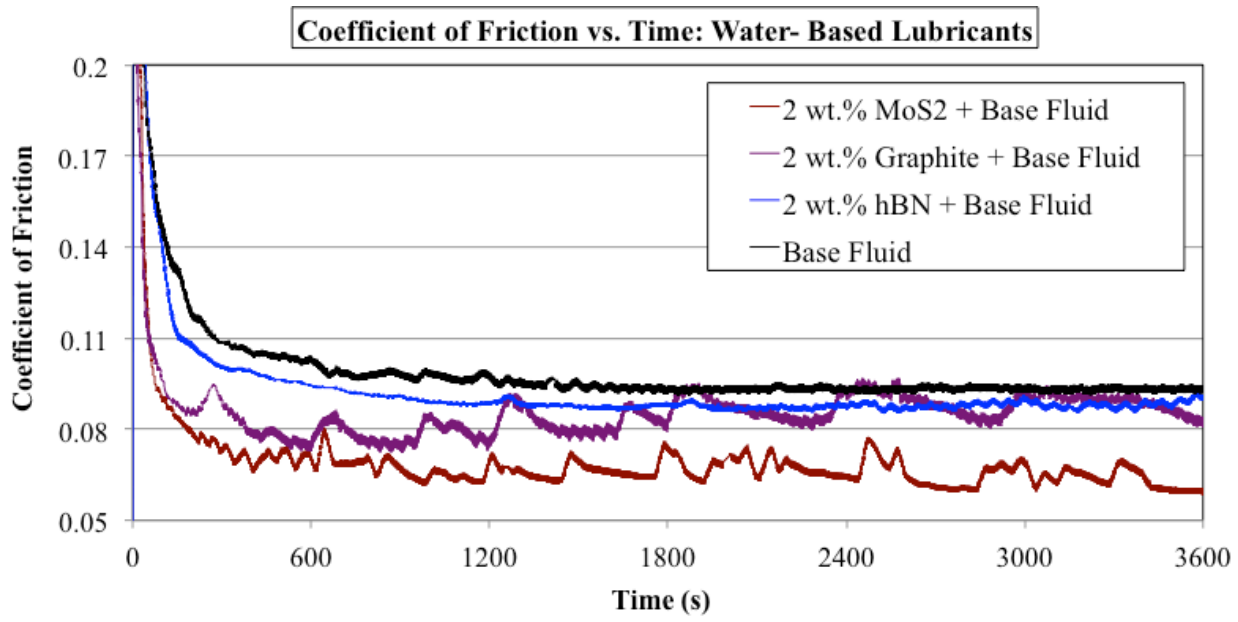

Figure 1.3 COF (μ) vs. sliding time (t) plots for water-based emulsions w/ and w/o nanoparticles

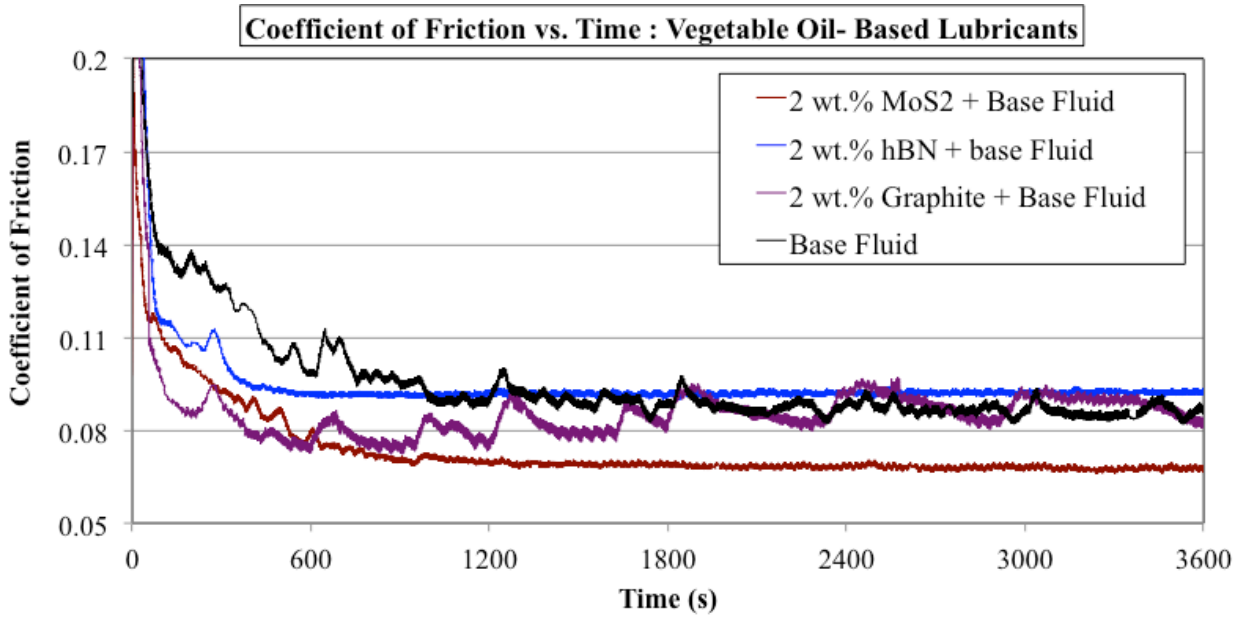

Figure 1.4 COF (μ) vs. sliding time (t) plots for vegetable-based oils w/ and w/o nanoparticles

Based on overall μ-t results, MoS_2 nanoparticles added lubricants also exhibited shortest time periods for evolution of stable tribochemical films in the grain-workpiece sliding zone.

The overall antifriction performance of the lubricants was analyzed using the average COF values as shown in Figure 1.5.

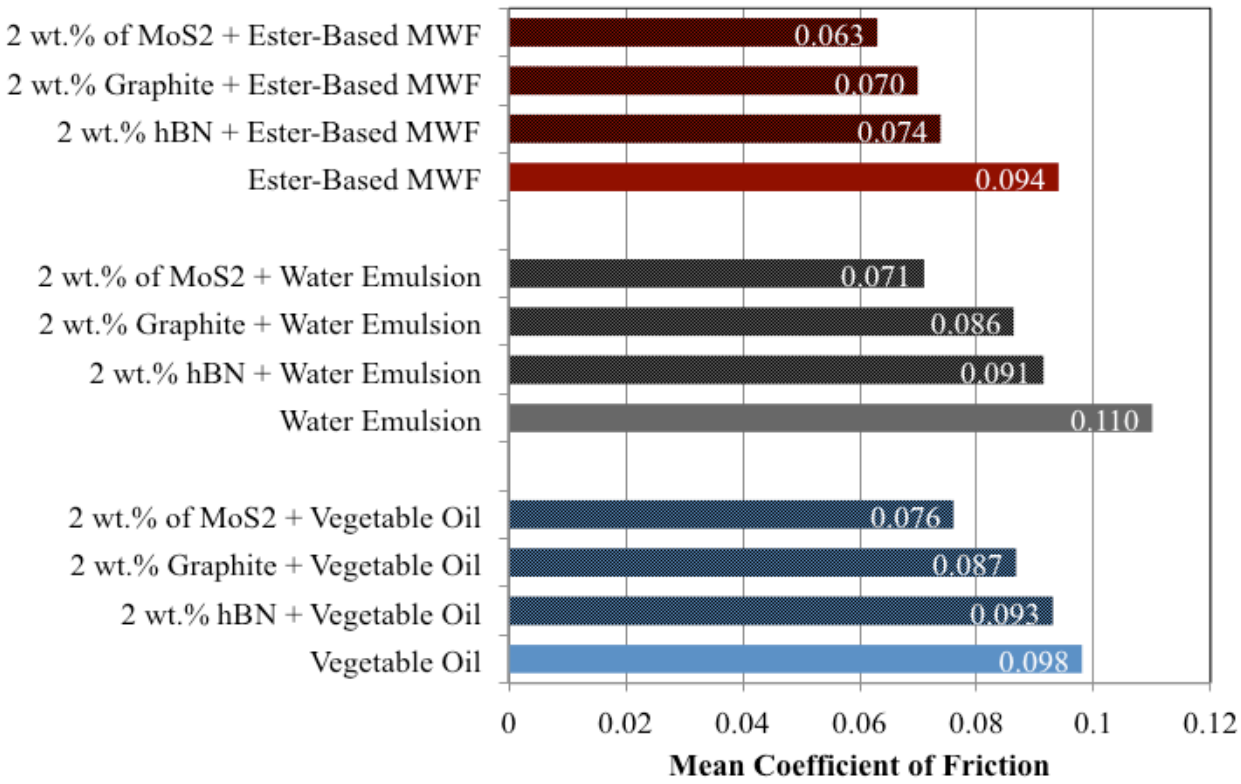

Figure 1.5 Average values of coefficient of friction for different lubrication conditions

Under the investigated process conditions, addition of nanoparticles to base fluids showed reductions in coefficient of sliding friction between cBN superabrasives and 1045 steel substrates. Ester-based MWF, water-based emulsion, and vegetable oil containing MoS_2 nanoparticles showed μ values of 0.063, 0.071, and 0.076, respectively. MoS_2 nanoparticle-based formulations showed 30% average reduction in COF over pure base fluids, as compared to 20% and 14% reductions with graphite and hBN nanoparticle-based lubricants, respectively. Using similar tribological test conditions, comparable reductions in friction coefficients were also observed between Al_2O_3-cast iron sliding pairs lubricated with MoS_2 nanoparticle-based

compositions [4]. Due to their excellent lubrication under representative tribological conditions of MQL-assisted surface grinding, nanoparticulate MoS_2 was selected over graphite and hBN as solid lubricant additive for the proposed nanolubricant compositions.

References

1. Basic Details on Molybdenum Disulphide, High Temperature Grease, "http://htgrease.blogspot.com/ ", Information accessed on 04/15/2013.

2. Rudnick, L.R., (2009), "Lubricant Additives: Chemistry and Applications", II Edition, CRC Press.

3. Kopeliovich, D., "Solid lubricants", "http://www.substech.com/dokuwiki/doku.php?id=solid_lubricants", Information accessed on 04/15/2013.

4. Kalita, P., (2009) Testing of Nano-Engineered Lubricants for Minimum Quantity Lubrication (MQL) Grinding: Performance Testing and Fundamental Understanding, University of Arkansas, Fayetteville, Masters Thesis.

APPENDIX B: DESCRIPTION OF RESEARCH FOR POPULAR PUBLICATION

Sustainable Machining Through Nanotechnology Developments and Innovations

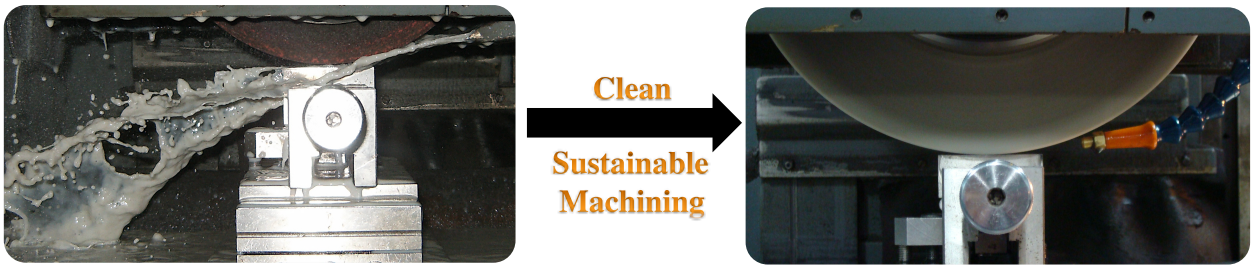

Sustainable or environmentally conscious machining is an ongoing trend in manufacturing sector. In machining, this process is driven by tighter restrictions with demands of increasing productivity and quality of machined parts and components. Mr. Parash Kalita, PhD student of Microelectronics-Photonics program at the University of Arkansas has studied this under Dr. Ajay P. Malshe, Professor in Mechanical Engineering at the University of Arkansas.

An important objective of researchers in this field has been to reduce the consumption levels of metalworking fluids (MWFs) during machining operations. Over thousands of gallons of various chemically activated oils or water-based MWFs are used in daily manufacturing operations worldwide. These fluids play an important role in reducing the ill effects of heat generated during machining on the quality of the final parts and components. However, heavy use of such fluids generates significant levels of aerosol mist and pollutants (including carcinogens) that are extremely hazardous to millions of people that work in close proximity to machining operations on a daily basis throughout the world. Mr. Kalita noted, “This is terrible!”

Traditional approach of using high volumes of fluid are ineffective in yielding desired machining outputs and significantly increases energy requirements and costs, upto 22% of total production

cost. U.S alone consumes about 2.7 billion gallons of metal working fluids annually. Dr. Malshe noted, “There is an opportunity in this problem!”

Dr. Malshe realized that technological innovations that reduce the consumption and use of fluids while maintaining or increasing productivity goals would foster sustainable and safe manufacturing. He also realized that cost and energy savings through such innovations would increase competitiveness of the US manufacturing industries to come out of the current economic slump and allow growth.

Mr. Kalita’s research developed a unique nanoengineered-based metalworking fluid system through advanced material design and nanomanufacturing methods that cuts the fluid use by 3-4 orders of magnitude as compared to traditional methods while amplifying the productivity and efficiency of the machining processes. The nanoengineered fluid system was established as a potential technology to reduce airborne aerosols and wastes from traditional machining fluids, thereby improving both the safety of workers and significantly increase the overall manufacturing efficiency (including twice as better energy saving, extended tool life, output quality of parts, and cost saving with reduced use of metalworking fluids). The proven innovative fluid solution would facilitate the replacement of traditional recirculating fluids systems, which are sources of variation and significant waste streams, with sustainable and high-productivity techniques in even the most demanding and aggressive machining applications. This successful research has immediate applications and would provide sustainable machining solution to a range of key manufacturing industries including, automotive, heavy machinery, aerospace, railways, electric motor casings, etc.

Dr. Malshe proudly notes, “This research is an unique example of how recent investment in

nanomanufacturing in U.S could help in developing sustainable technology platform to increase productivity and benefit traditional machining and manufacturing industries, and eventual job creation".

APPENDIX C: EXECUTIVE SUMMARY OF INTELLECTUAL PROPERTY AND POTENTIAL PATENT AND COMMERCIALIZATION ASPECTS

Executive Summary of Intellectual Property

Novel compositions of mineral and vegetable oil-based metalworking fluids containing an organic-inorganic additive package were developed and tested in the course of this research. The nanoengineered fluid compositions were named nanolubricants.

Potential Patent and Commercialization Aspects

The composition of oil-based nanolubricants as metalworking fluid should be patented. However, the design and synthesis process organic-organic additive used in the nanolubricant formulations cannot be patented*.

(*Patent pending: Malshe, A.P., and Verma, A., (2006), "Nanoparticle Compositions and Methods for Making and Using the Same", International Application No. PCT/US07/60506)

APPENDIX D: MICROSOFT PROJECT FOR PhD MICREP DEGREE PLAN

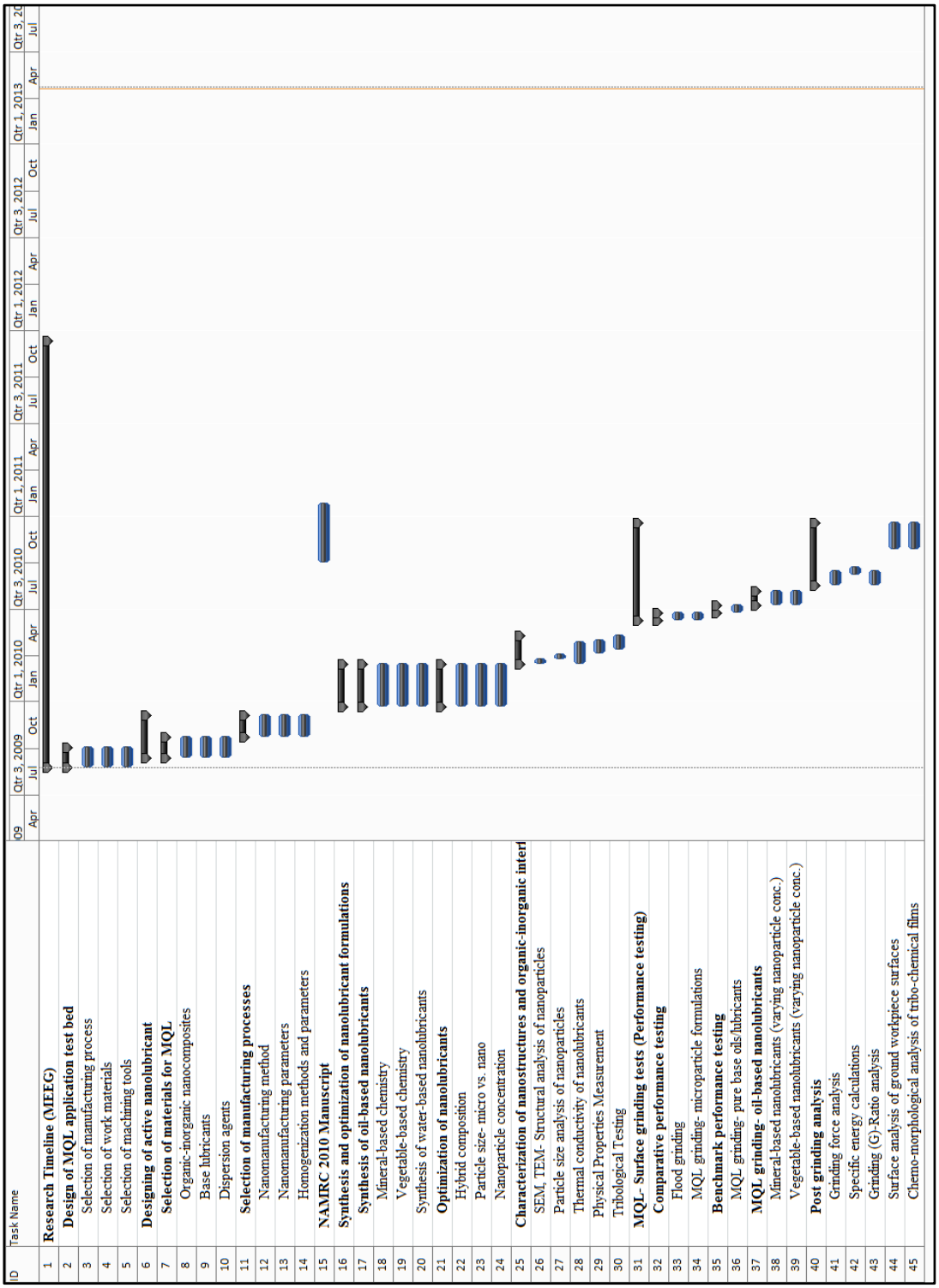

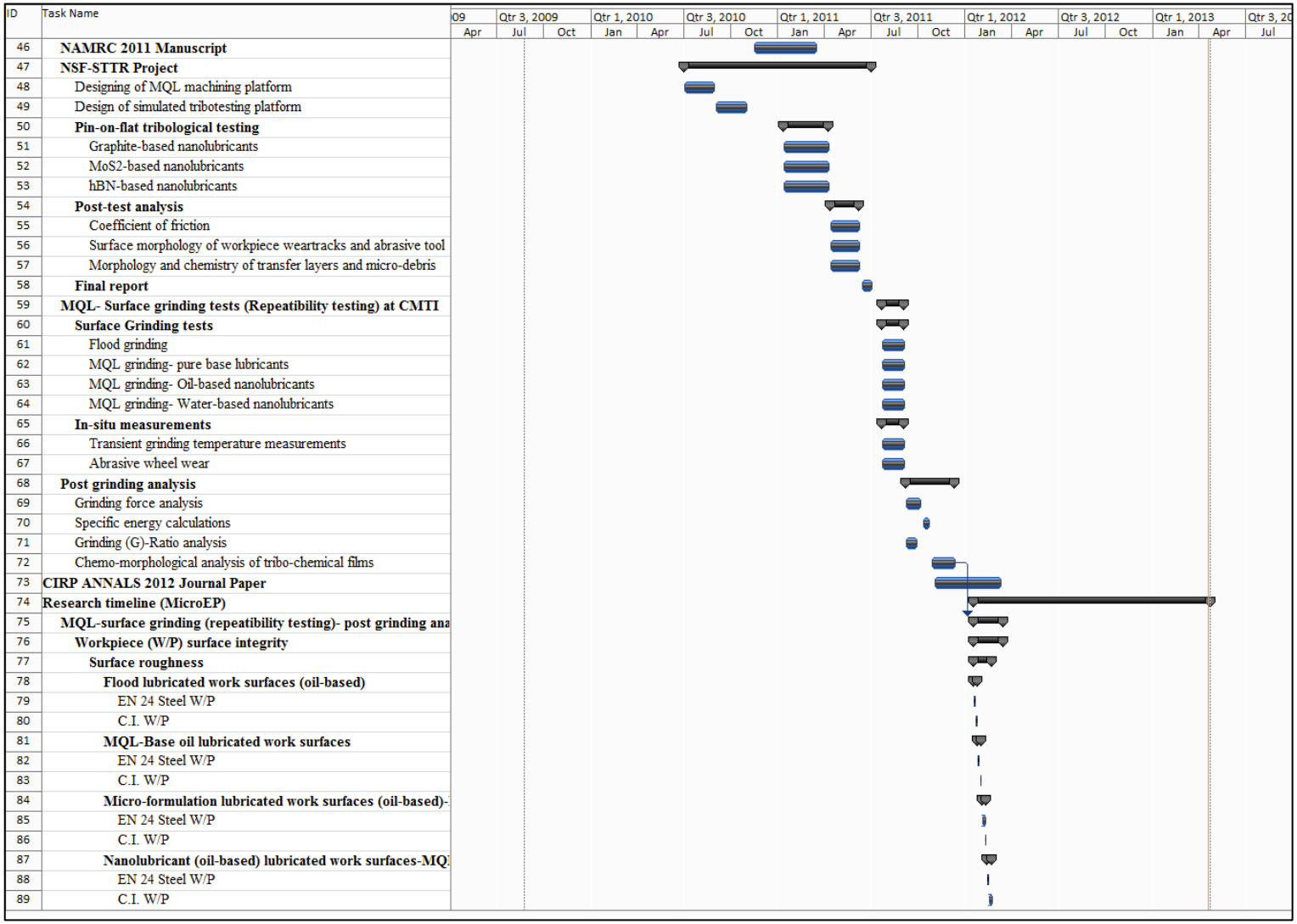
ID
Task Name
09
Qtr 3, 2009
Qtr 1, 2010
Qtr 3, 2010
Qtr 1, 2011
Qtr 3, 2011
Qtr 1, 2012
Qtr 3, 2012
Qtr 1, 2013
Qtr 3, 20
Apr
Jul
Oct
Jan
Apr
Jul
Oct
Jan
Apr
Jul
Oct
Jan
Apr
Jul
Oct
Jan
Apr
Jul
46 NAMRC 2011 Manuscript
47 NSF-STTR Project
48 Designing of MQL machining platform
49 Design of simulated tribotesting platform
50 Pin-on-flat tribological testing
51 Graphite-based nanolubricants
52 MoS2-based nanolubricants
53 hBN-based nanolubricants
54 Post-test analysis
55 Coefficient of friction
56 Surface morphology of workpiece weartracks and abrasive tool
57 Morphology and chemistry of transfer layers and micro-debris
58 Final report
59 MQL- Surface grinding tests (Repeatibility testing) at CMTI
60 Surface Grinding tests
61 Flood grinding
62 MQL grinding- pure base lubricants
63 MQL grinding- Oil-based nanolubricants
64 MQL grinding- Water-based nanolubricants
65 In-situ measurements
66 Transient grinding temperature measurements
67 Abrasive wheel wear
68 Post grinding analysis
69 Grinding force analysis
70 Specific energy calculations
71 Grinding (G)-Ratio analysis
72 Chemo-morphological analysis of tribo-chemical films
73 CIRP ANNALS 2012 Journal Paper
74 Research timeline (MicroEP)
75 MQL-surface grinding (repeatibility testing)- post grinding ana
76 Workpiece (W/P) surface integrity
77 Surface roughness
78 Flood lubricated work surfaces (oil-based)
79 EN 24 Steel W/P
80 C.I. W/P
81 MQL-Base oil lubricated work surfaces
82 EN 24 Steel W/P
83 C.I. W/P
84 Micro-formulation lubricated work surfaces (oil-based)-
85 EN 24 Steel W/P
86 C.I. W/P
87 Nanolubricant (oil-based) lubricated work surfaces-MQ
88 EN 24 Steel W/P
89 C.I. W/P

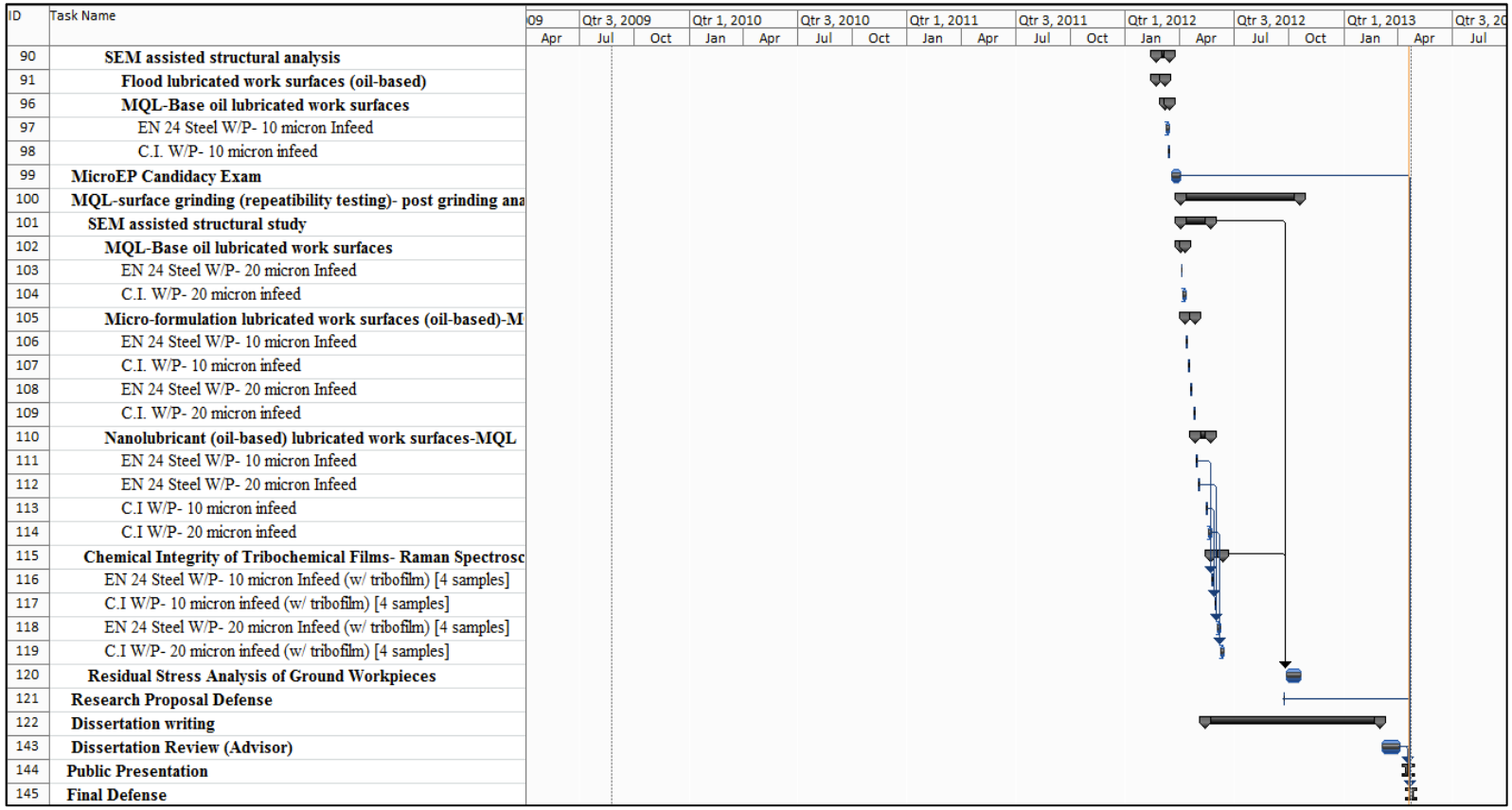

ID	Task Name
90	**SEM assisted structural analysis**
91	**Flood lubricated work surfaces (oil-based)**
96	**MQL-Base oil lubricated work surfaces**
97	EN 24 Steel W/P- 10 micron Infeed
98	C.I. W/P- 10 micron infeed
99	**MicroEP Candidacy Exam**
100	**MQL-surface grinding (repeatibility testing)- post grinding ana**
101	**SEM assisted structural study**
102	**MQL-Base oil lubricated work surfaces**
103	EN 24 Steel W/P- 20 micron Infeed
104	C.I. W/P- 20 micron infeed
105	**Micro-formulation lubricated work surfaces (oil-based)-M**
106	EN 24 Steel W/P- 10 micron Infeed
107	C.I. W/P- 10 micron infeed
108	EN 24 Steel W/P- 20 micron Infeed
109	C.I. W/P- 20 micron infeed
110	**Nanolubricant (oil-based) lubricated work surfaces-MQL**
111	EN 24 Steel W/P- 10 micron Infeed
112	EN 24 Steel W/P- 20 micron Infeed
113	C.I W/P- 10 micron infeed
114	C.I W/P- 20 micron infeed
115	**Chemical Integrity of Tribochemical Films- Raman Spectrosc**
116	EN 24 Steel W/P- 10 micron Infeed (w/ tribofilm) [4 samples]
117	C.I W/P- 10 micron infeed (w/ tribofilm) [4 samples]
118	EN 24 Steel W/P- 20 micron Infeed (w/ tribofilm) [4 samples]
119	C.I W/P- 20 micron infeed (w/ tribofilm) [4 samples]
120	**Residual Stress Analysis of Ground Workpieces**
121	**Research Proposal Defense**
122	**Dissertation writing**
143	**Dissertation Review (Advisor)**
144	**Public Presentation**
145	**Final Defense**

APPENDIX E: IDENTIFICATION OF ALL SOFTWARE USED IN RESEARCH AND DISSERTATION GENERATION

Computer 1:

Model: MacBook Pro
Serial number: C1MJ4DWSDTY3
Owner: Parash Kalita

Software 1:

Name: Microsoft Office 2011
Purchased by: Parash Kalita
License (product) id: 03314-042-1233237-02752

Software 2:

Name: Microsoft Project 2010
Purchased by: Parash Kalita
Free Microsoft software under College of Engineering license, University of Arkansas
License owned by the University of Arkansas

Computer 2:

Model: Dell desktop, Windows XP Professional
Serial number: 249YQ61
Location: Nano 222
Owner: Mechanical Engineering, University of Arkansas

Software 1:

Adobe acrobat professional
License owned by: Mechanical Engineering, University of Arkansas

Computer 3:

Model: Dell desktop, Windows XP professional
Serial number: 43B043J
Location: Nano 222
Owner: Mechanical Engineering, University of Arkansas

Software 1:

TriboX (CSM Tribometer)
License owned by: Mechanical Engineering, University of Arkansas

Computer 4:

Model: HP Pavilion, Windows 7
Serial number: 4CE14106ZT
Location: Nano 222
Owner: Mechanical Engineering, University of Arkansas

Software 1:

WiRe3.3 (Renishaw InVia Raman spectrometer)
License owned by: Mechanical Engineering, University of Arkansas

APPENDIX F. LIST OF PUBLICATIONS

1. Kalita, P., Malshe, A.P, Rajurkar, K.P., (2012), Study of tribochemical lubricant film formation during application of nanolubricants in minimum quantity lubrication (MQL) grinding, CIRP Annals - Manufacturing Technology, 61(1), 327–330.

2. Kalita, P., Malshe, A.P., Arun Kumar, S., Yoganath, V.G., Gurumurthy, T., (2012), Study of specific energy and friction coefficient in minimum quantity lubrication grinding using oil-based nanolubricants, Journal of Manufacturing Processes, 14(2), 160–166.

3. Kalita, P., Malshe, A.P., (2010) Tribological Study of Nano Lubricant Integrated Soybean Oil for Minimum Quantity Lubrication (MQL) Grinding, Transactions of NAMRI/SME, 38, 137-144